Influence of electrolytes on liquid-liquid equilibria for extraction processes

Dissertation

zur Erlangung des Doktorgrades der Naturwissenschaften

(Dr. rer. nat.)

der Fakultät für Chemie und Pharmazie

der Universität Regensburg

vorgelegt von

Gabriel Grundl

aus Deggendorf

2020

Official Registration:	
Defense:	
PhD Supervisor:	Prof. Dr. Werner Kunz
Adjudicators:	Prof. Dr. Werner Kunz
	Prof. Dr. Rainer Müller
	Prof. Dr. Frank-Michael Matysik
Chair:	PD Dr. Axel Dürkop

Acknowledgement

This thesis was made at the Institute of Physical and Theoretical Chemistry (Faculty of Natural Sciences IV) of the University of Regensburg between February 2014 and April 2020 under the supervision of Prof. Dr. Werner Kunz. Some results, which are presented in this work, were gained through several stays at the research group of Prof. Dr. Gabriele Sadowski (Thermodynamics, Faculty of Bio- and Chemical Engineering) of the Technical University of Dortmund in 2015 and 2016.

At first, I want to thank Prof. Dr. Werner Kunz for his support and for providing me the opportunity to do my PhD at his chair. I thank him for the interesting topic and for the continuing discussions during my research. His friendly attitude and impressive way of teaching raised my enthusiasm for natural sciences in particular for research topics at his chair.

I would like to show my gratitude to Prof. Dr. Rainer Müller for being a great help in planning analytics, assessing different methods, providing me access to his laboratory equipment and for his support while accompanying the AiF-project.

Further thanks goes to Dr. Didier Touraud for his great ideas, positive attitude and for supporting my research projects. I want to thank Dr. Roland Neueder and Dr. Jelena Tsurko for discussions in the field of thermodynamics, especially about osmotic coefficients and electrolyte solutions.

I also want to thank the workgroup of Prof. Dr. Richard Buchner for providing access to measuring devices and technical introduction. Special thanks, at this point, is owed to Andreas Nazeth. Furthermore, I want to thank Dr. Matthias Hofmann for introducing me to pendant drop tensiometry.

The technical stuff is indispensable and I want to express my gratitude to Barbara Widera for being a great help for vapour pressure osmometry measurements, Helmuth Schönsteiner for introducing me to gas chromatography and in general for his support in any kind of technical problem and Franziska Wolf for ordering and receiving chemicals. Special thanks goes to all members of the “Kaffeerunde” and in particular to Georg Berger for IT aid.

Not to forget to thank the secretaries Rosi, Sonja and Bianca for help in organisational issues and for their friendly attitude.

I would like to thank all collegues I have spent time with at the chair: Martina Müller, Tatjana Leibßle, Dr. Alexander Wollinger, Julian Rieder, Andreas Schneider, Dr. Auriane Freyburger, Dr. Julien Marcus, Dr. Veronika Fischer, Dr. Stefan Wolfrum, Dr. Sebastian Krickl, Dr. Damian Brock, Dr. Theresa Höß, Dr. Marcel Flemming, Dr. Lydia Braun, Dominik Zahnweh, Dr. Katharina Häckl, Dr. Sergej Friesen, Tobias Lange, Alexander Dietz, Pierre Degot, Jutta Lehnfeld, Franz Schermer, Manuel Rothe, Evamaria Hofmann and Johannes Ramsauer.

Additional thanks is expressed to the workgroup of Prof. Dr. Gabriele Sadowski. In particular to Dr. Ing. Christoph Held, as leader of the AiF-project, for the organisation of the stays at the TU-Dortmund and giving advice for any problems I had. The hospitality at the Faculty of Bio- and Chemical Engineering (BCI) in Dortmund was outstanding. Not less appreciation is expressed to Dr. Mohammad Sultan (project partner) for his technical advices, especially for introducing me to ion-exchange chromatography and further fruitful discussions about the determination of liquid-liquid equilibria.

Further thanks goes to Dr. Ing. Christoph Brandenbusch for introducing and providing me access to the gas chromatograph of the laboratory at the TU-Dortmund. The opportunity for a research stay at the BCI is highly appreciated from my side, for which I want to express my gratitude to Prof. Dr. Gabriele Sadowski.

I want to thank all PhD students I met at the BCI for introducing me into the “Kreuzviertel” of Dortmund where many pleasant restaurants are located. All these things considered, the research visit to the TU-Dortmund resulted in a very pleasant stay with a lot of positive impressions coupled with effective work in a very modern laboratory.

I further want to thank Dr. Ulrich Westhaus (Dechema) for providing me access to the *detherm* data base.

This thesis was possible due to financial support of the IGF-project 17114/N of the Dechema e.V. research association. The project was realised by the AiF and supported from the BMWi. The AiF is the German Federation of Industrial Research Associations “Otto von Guericke” (Arbeitsgemeinschaft industrieller Forschungsvereinigungen “Otto von Guericke” e.V.).

Finally sincerest thanks goes to my parents Gabriele-Johanna and Lothar as well as to all my sisters and brothers: Martin, Miriam, Florian, Magdalena, Lucia and Marie. Last but not least, loving thanks goes to Caroline for being partner in life and always on my side during writing this thesis.

Table of content

Structure of the thesis

The thesis is organised in six chapters. Chapter I gives a general introduction with motivation, important organic molecules for white biotechnology and the aim of research in the field of biotechnology and related processes. Chapter II provides the fundamental knowledge about liquid-liquid extraction (LLEx), effects of salts, hydrotropy, thermodynamic modelling, and contains the characterisation and analytical methods used in this work. Chapter III deals with properties and characterisations of aqueous HMF mixtures. The focus lies on osmotic and activity coefficients of binary and ternary mixtures inferred from vapour pressure osmometry (VPO) and the solubiliser properties of HMF investigated by solubilisation and surface tension measurements. Chapter IV is about salting-in and salting-out effects studied on the binary model system water/dipropylene glycol n-propyl ether (DPnP), which exhibits a lower solution temperature (LST). Besides inorganic salts, several organic compounds were added to the mixed solvent system water/DPnP, while salting-in and salting-out effects were detected by means of decreasing or increasing LST, respectively. In addition, a liquid-liquid separation of ethanol from water induced by the addition of different salts was considered. Chapter V includes the results of experimental liquid-liquid equilibrium (LLE) data of ternary systems with and without salt and quaternary systems with salt. The LLEx of two product molecules (HMF, glycerol) from water with n-butanol as extracting solvent, supported by salt addition, was investigated. Chapter VI provides a summary of the gained results and includes some comments on supporting or prospective experiments.

Chapter I

Introduction

I.1 Motivation

The global energy consumption increased by 2.9% in 2018, which represents the strongest since 2010. Primary energy was provided by oil (34%), coal (27%), natural gas (24%), hydroelectricity (7%), nuclear energy (4%) and renewables (4%). Thus, 85% of the worldwide energy was produced from fossil fuel. Nevertheless, a strong growth of the energy share of renewables has been noticed from 2010 to 2018[1]. The industrial production of organic compounds from biomass feedstocks, also called 'white biotechnology'[2–6], has gained increasing attention from chemical industries aiming to find methods to replace products, which are usually derived from petroleum. In this branch of biotechnology, living cells (from yeast, moulds, bacteria and plants), enzymes and basic chemical processes are applied to synthesize organic compounds[3]. In some segments, white biotechnology has already captured leading market positions, e.g. biotechnological production of amino acids exceeds one million tons annually, the trend from chemical to biotechnological production of vitamins is increasing, strong growth in the market volume for enzymes[6] has been noticed and the success of polylactid has helped white biotechnology to settle down in the field of polymers[5]. Reasons for the demand of bio-based products are the increasing global need for resources, sustainable processes and environmental aspects above all, the climate protection. Biomass is the most important alternative feedstock, because it is a highly available carbon source besides oil and coal. It consists of carbohydrates, lignin, fatty acids, lipids, proteins and others. By far the most abundant natural source of carbon is presented by carbohydrates (75% of plant biomass, with 40% cellulose and 25% hemicellulose)[7,8]. The development of a robust biorefining industry requires economic incentives to support biomass as feedstock, which is coupled to efforts on research and technology for the realisation of final products on commercial scale. As fuel is a low value product, its displacement by bio-fuels does not present an attractive strategy for biorefining industry, whereas the combination of bio-fuel production with the production of high value-added chemicals (integrated biorefinery) can meet economic goals. In addition, bio-fuel production leads to a certain indepenence on crude oil imports[9], concurrently supporting the use of domestic renewable raw material[10]. Challenges accompanied with the production of chemicals from renewable carbon sources are first, the conversion technology, which is the least developed and most complicated of all biorefinery operations and secondly, the rational selection of core groups of primary chemicals and secondary intermediates. A fundamental difference between fuel and chemical production lies in the fact that in case of bio-fuels mainly single product operations by fermentation to ethanol or biodiesel are considered. This means, different technologies can be applied for the production of single targets (biofuel production is *convergent*). In contrast, if the production of chemicals is integrated to biorefinery, a single technology leads to numerous outputs (chemicals production is *divergent*). This leads to difficulties for techno-economic process analysis, as each product has its own process cost and selling price. Here, the focus lies on the *choice of technology*, which leads to product identification and realisation, whereas for biofuels the focus on *product identification* dictates the applied/available technology[11]. As pointed out by Bozell, the technology development is the main issue for realisation of the bio-based chemical industry[10–12] with high value-added products as economic driver supporting also the low value-added but high-volume fuel sector. Petroleum as feedstock presents a resource with a low extent of chemical functionalities (e.g. -OH, -C=O, -COOH) and thus is directly applicable for processing (cracking, isomerisation) to obtain fuels. For the production of chemical intermediates, it is then neccessary to introduce such chemical functional groups e.g. by selective oxidation. In the very contrast to petrochemicals, biomass feedstocks contain a large proportion of oxygen, which makes them inappropriate for direct use as fuels or chemicals. The task here is to control these functionalities in the final product[13]. Ways to reduce the high oxygen content in carbohydrates are the removal of CO_2 by fermentation to ethanol or butanol, the removal of oxygen by hydrogenolysis and the removal of water by dehydration of carbohydrates to furans and levulinic acid (LA)[14]. Reports from the US Department of Energy (DOE)[15,16] and review papers[10,17] summarise top value-added chemicals attainable by biomass feesdstocks (carbohydrates and lignin). In 2010, Bozell[10] has updated the original list (2004)[15] of the “top 10” chemicals from carbohydrates by removing some with a less growing market and adding some with high potential in industries, among them ethanol, 5-hydroxymethylfurfural (HMF) and furfural (FF). Criteria used for the evaluation of products from renewable carbohydrates are its attention in literature, the technology applicability to multiple products, the direct substitution for existing petrochemicals, the volume of production, its potential as platform chemical, the viability of upscaling, the commercial potential, its suitability as primary building block and the established commercial production. These criteria, however, may change by time because biorefining industry is in developing stage coupled with rapid changes in markets and technology. HMF is considered to be one of the most promising platform molecules that provide access to a lot of building blocks for chemical industry. Further interesting compounds are glycerol, n-butanol and ethanol. These four compounds are adressed in this thesis with the focus on their separation from aqueous solutions with the help of electrolytes.

I.2 5-Hydroxymethylfurfural (HMF)

5-Hydroxymethylfurfural (HMF), 5-(hydroxymethyl)-2-furaldehyde or 5-(hydroxymethyl)furan-2-carbaldehyde, the latter being the preferred IUPAC name, is an organic aromatic compound consisting of a furan ring, which exhibits an aldehyde and an alcohol functional group in position 2 and 5, respectively, see Figure I.1. HMF can be derived from renewable biomass by dehydration of hexoses (glucose, fructose). The highly functionalised molecule paves the way for various reactions and a huge number of chemical derivatives, see Figure I.2 for some examples, which reveals its high potential as platform compound[14,18]. Such derivatives can be used for the production of polymers[18–24], liquid fuels[25,26], pharmaceuticals, food additives[27], chemicals and solvents[14,28].

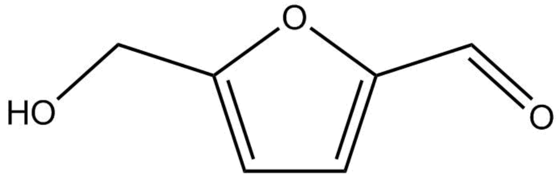

Figure I.1.Chemical structure of 5-hydroxymethylfurfural (HMF)

I.2.1 HMF in Diet and Toxicological Aspects

HMF is formed during the thermal decomposition of sugar-containing foods or beverages like honey, dried fruits, coffee, wine, fruit juices and baking products etc[27,29,30]. The *Maillard* reaction can also be a reason for HMF formation *via* Amadori compounds during the first steps of reaction. These reactions were first studied and termed by the french scientist Louis Camille Maillard, who studied the non-enzymatic reactions of amino acids and carbohydrates[31]. Products from caramelisation and *Maillard* reactions are known to be responsible for the flavour and browning of certain foods and in some cases, HMF is even added to foods as a flavouring agent. Due to the widespread occurrence of HMF in foods, it is almost impossible not to take up HMF as a human who values balanced and healthy nutrition. Estimated intakes range between 5 and 150 mg per person and day[14]. Different studies have stated different daily intake ranges. A maximum HMF content (1022.1 mg/kg) was reported for beverages made from dried plums. But, even long-term daily consumption does not lead to any concrete health risk. The concentration of HMF in fresh foods is usually very low, but increases rapidly during drying and heating[27]. Detection of HMF in foods is well established, as it is an indicator for possible deterioration of the goods due to wrong storage conditions or other treatments. As an example, the HMF content in fresh honey is less than 15 mg/kg, which increases by 2-3 mg/kg per year at correct storage conditions. In the EU, the maximum limit for the HMF content in honey is 40 mg/kg, while the seal of approval for german honey ("Echter Deutscher Honig") allows at most 15 mg/kg[32].

Due to the occurrence of HMF in foods, toxicological effects of HMF and its derivatives and metabolites have been investigated by several *in vivo* and *in vitro* assays. Ames tests were performed and no mutagenic effect was found for HMF[33]. However, it was demonstrated that HMF is an indirect mutagen, because it can be converted *in vitro* to 5-sulfoxymethylfurfural (SMF), which has genotoxic and mutagenic properties[34]. The formation of SMF was found *in vivo* in the FVB/N mouse, but there was no evidence for SMF formation in humans. SMF has either not been detected in human urine, which is plausible due to its instability[27,30,35]. Short-term and long-term carcinogenicity studies lead to the conclusion that the possible risk of carcinogenic effects, if present at all, are not currently identifiable or only to be estimated as extremely low. So far, there is no reliable evidence that HMF induces tumours in the colon or small intestine. The remaining toxic potential is rather low. Animal experiments have shown that there are no negative effects in range of 80-100 mg/kg body weight and day. The consumption of HMF-containing foods is therefore regarded to be harmless[27]. It is known that HMF is cytotoxic at high concentrations and causes irritation to eyes, the upper respiratory tract, the skin and mucous membranes in general[36].

I.2.2 HMF Derivatives and some Applications

The aldyhyde group of HMF can be oxidised to a carboxyl group and the hydroxyl group can be subjected to etherification, esterification and oxididation to an aldehyde or a carboxyl group. By oxidation of HMF, chemicals like 5-formylfuran-2-carboxylic acid, 2,5-diformylfuran and 2,5-furandicarboxylic acid (FDCA) can be obtained. Aldeyde functions allow for C-C coupling, which makes it possible to synthesise linear polymers containing furan rings[37]. FDCA is an important renewable building block due to its similar properties to terephtalic acid (TPA), which is a commodity chemical used as precursor for polyethylene terephthalate (PET) for the production of plastics. Kröger et al.[20] demonstrated direct production of FDCA by dehydration of fructose and subsequent oxidation of HMF to FDCA. Synthesis of FDCA from HMF oxidation and from carbohydrates by one-pot reactions was reviewed by Zhang and Deng[38]. Besides chemical oxidation, FDCA can also be produced *via* fermentation involving two types of bacteria. With this approach even higher product purity can be achieved[39]. The replacement of TPA with FDCA for polymer production envisages polyethylene furanoate (PEF) as candidate for a bio-based polymer[40]. A consortium (*Synvina*) between *BASF* and *Avantium* aimed the commercial production of FDCA and PEF in 2024 but at the end of 2018, *BASF* pulled out the consortium due to disagreements. *Avantium* continues under the name *Avantium Renewable Polymers* and plans the production to start in 2023 in cooperation with the engineering company *Worley*[41]. PET can be produced based on renewables as well[42]. *Gevo* has produced *para*-xylene from isobutanol, which is obtained by fermentation of sugars from cellulose. By oxidation of *para*-xylene, TPA is accessible, which can be polymerised with ethylene glycol to PET[43]. Thus, there may be a competition between both bio-based polymer markets. PEF exhibits some properties superior to those of PET: higher barrier for O_2 and CO_2, lower melting point, higher glass transition temperature, higher tensile strength and less required feedstock for production. On the other hand, the existing PET infrastructure (converting, tooling, recycling) could be maintained without changes, using bio-based PET. Further important products like 2,5-bishydroxymethylfuran (BHMF) and 2,5-dimethylfuran (2,5-DMF) are accessible *via* reduction of HMF. BHMF can be used as building block for polymers as well and for polyurethane foams[39]. 2,5-DMF shows similar physico-chemical properties to petroleum-based gasoline, which are more favourable than those of ethanol for fuel applications. These are, among others, an advantageous boiling point, the low water solubility of 2,5-DMF, which prevents undesired blending, the high energy density of 2,5-DMF (30 kJ/cm^3, close to that of gasoline) and the octane number of 2,5-DMF, which is even higher than that of gasoline[26,44,45]. Great attention to this molecule was induced by the publication of Román-Leshkov et al.[26] in *nature*, in which the production of 2,5-DMF from fructose was demonstrated in two steps (dehydration to HMF and hydrogenolysis to 2,5-DMF). Other potential fuel candidates are 5-ethoxymethylfurfural (EMF), ethyl levulinate and γ-valerolactone (GVL)[46]. In a patent assigned to *GF Biochemicals*, the large-sacle production of LA *via* HMF is described[47].

The potential substitution of toxic and volatile formaldehyde by HMF, e.g. for the production of textiles, resins, pharmaceuticals and cosmetics, presents another interesting application[39]. Besides negative effects on health, it was found that HMF has also some positive pharmacological functions like antioxidant activity[48–50] and activity against sickle cell desease[51]. Hepatoprotective effects of HMF were detected and related to restisting apoptosis and thus to protective effects against chemical liver cell damage[52–54]. Thus, HMF is also a conceivable Active Pharmaceutical Ingredient[39].

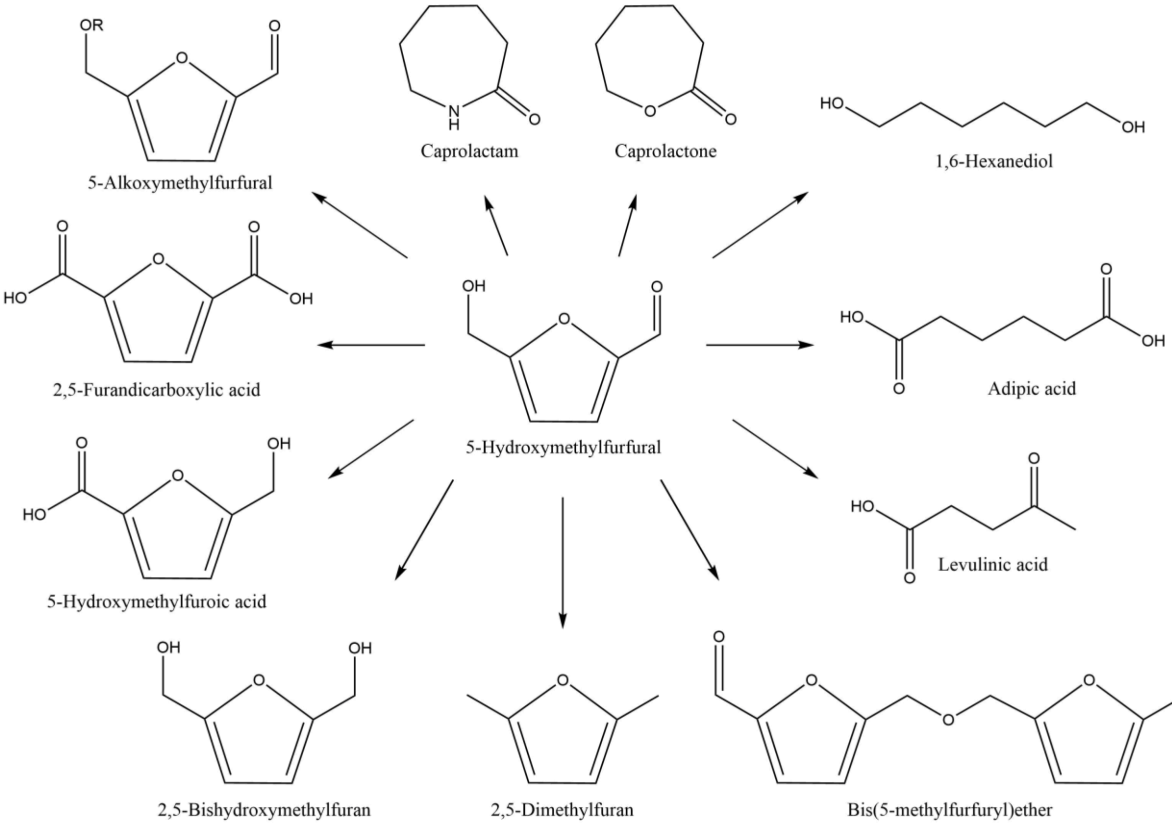

Figure I.2. HMF as a platform chemical providing access to various important compounds. The figure was reproduced from literature[14].

I.2.3 HMF-Synthesis

The first publications of HMF synthesis from Düll and Kiermayer date back to 1895. HMF is formally accessible from each hexose or hexulose. The basic chemical transformations to HMF include the hydrolysis of disaccharides or polysaccharides (sucrose, cellobiose, inulin or cellulose) to glucose and/or fructose followed by the acid-catalysed dehydration, see Figure I.3. The selective dehydration of hexoses to HMF involves the removal of three water molecules. Glucose reactivity is lower than that of fructose (ketose), which is explained by the stable ring structure of glucose. Thus, the enolistaion rate in solution is lower compared to fructose. Since the enolisation step is rate-determining, fructose will react more readily and faster to HMF than glucose[55]. Fructose forms di-fructose and di-anhydrides in an equilibrium reaction while the most reactive groups are internally blocked, which is favourable for the selectivity of the reaction due to less by-product formation. In contrast, glucose forms true oligosaccharides with active reactive groups presenting a risk for cross-polymerisation[55,56]. Although glucose is cheaper than fructose, the most convenient way to synthesise HMF is the dehydration of fructose[18]. To obtain the fructose, acid-catalysed hydrolysis of sucrose and inulin or the selective isomerization of glucose to fructose can be applied[57]. A lot of catalysts have been used for the dehydration of carbohydrates, among them, organic acids, inorganic acids, organic and inorganic salts, Lewis acids and others (ion-exchange resins and zeolites)[58]. A large progress in catalytic conversion of carbohydrates from biomass can be noticed during the 21th century.

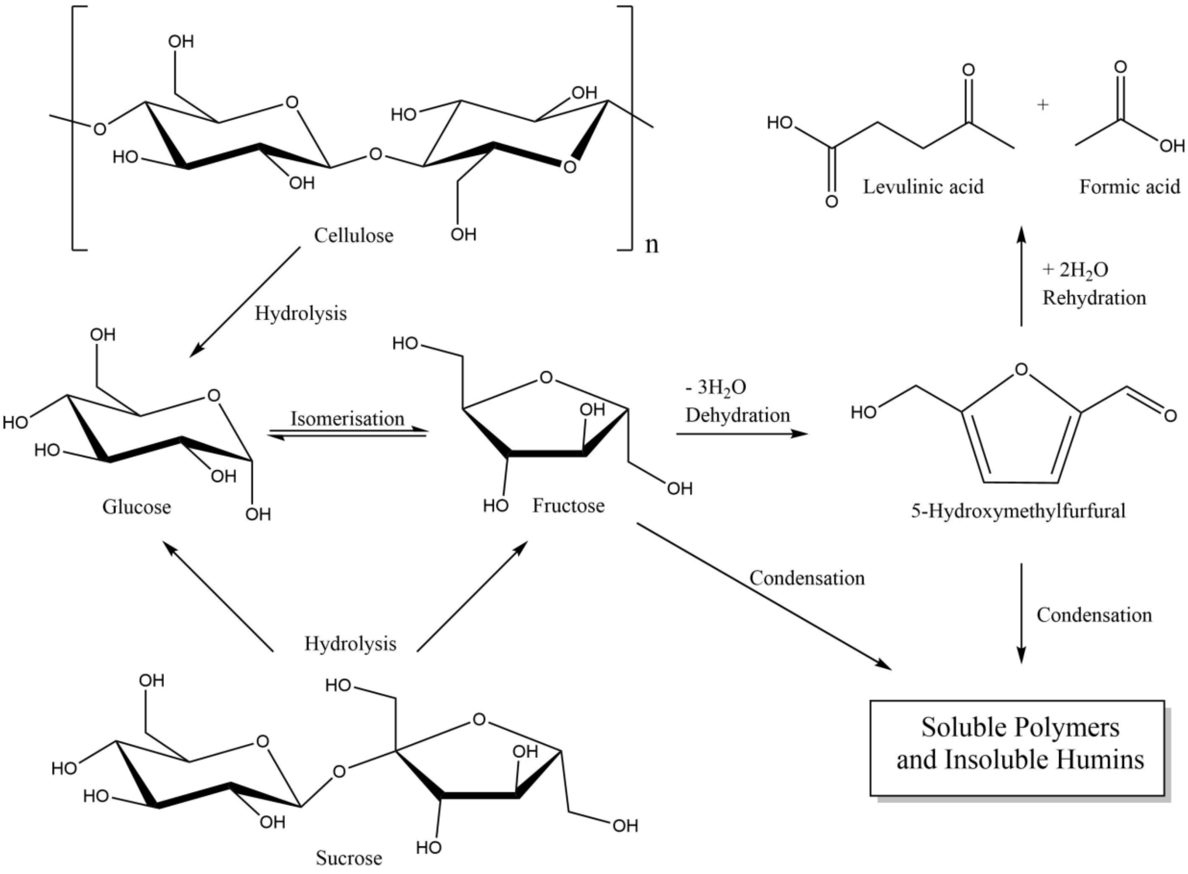

Figure I.3. Schematic representation of the HMF production starting from carbohydrates (celluslose, sucrose) *via* hydrolysis and acid-catalysed dehydration of fructose to HMF and side-product formation by rehydration and condensation. The figure was created, inspired by pictures viewed in literature[59,60].

I.2.4 Solvent Systems for HMF-Synthesis

Aqueous processes are ecologically convenient but they lack in efficiency, which is due to non-selective fructose dehydration leading to many side-products, e.g. by rehydration of HMF to LA and formic acid or by condensation to insoluble humins (undefined polymer structures of sugar derivatives). Side-product formation by decomposition of fructose in water at high temperatures by isomerisation, dehydration, fragemtation and condensation was reported by Antal et al.[61], who studied the mechanism for the HMF formation from D-fructose and sucrose. However, patents of the *Südzucker AG*[62,63] describe the HMF synthesis with high purity (> 99%) using water as solvent, solely. Here, the products are separated and fractionated *via* chromatography on ion exchange resins.

The rehydration of HMF can be supressed in nonaqueous systems, provided that the solubility of the carbohydrate (starting material) is high enough in the organic solvent. **Low-boiling solvents** (bp < 150°C) like acetonitrile (ACN)[64], ethyl acetate[64], methanol[65,66], ethanol[66], acetic acid[65,67] and dioxane[68–70] have been applied. For alcohols with a low carbon number and acetic acid, reactions of the OH-group of HMF with the solvents were observed, leading to the according ethers 5-methoxymethylfurfural (MMF) and EMF, and esters 5-acetoxymethylfurfural (AMF) as main products. These *in situ* conversions of HMF were patented by *Furanix* (a division of *Avantium*)[66,71] (for further patents, see references 201f in[14]).

High-boiling solvents like dimethylsulfoxide (DMSO)[64,68,72–75], *N*,*N*-dimethylformamide (DMF)[64], *N*-methyl-2-pyrrolidone (NMP)[76], sulfolane[64], dimethylacetamid and a dimethylacetamid-LiCl combination[77] (the combination allows for the HMF production from untreated lignocellulosic biomass), GVL and γ-hexalactone were used for the HMF synthesis. The latter two solvents are bio-based[78]. Various catalysts have been applied and high product yields were achieved. The furanoid form of fructose is best stabilised by DMSO, which is why highest selectivities and yields are observed for that solvent. The problem with these solvents is their energy-intensive separation (distillation) from HMF. In addition, HMF is temperature sensitive, which is why high temperatures should be avoided. DMSO also posses risk for the environment and health[14,18,28,55,64,79]. The intermolecular interactions between DMSO and HMF are stronger than those between water and HMF, which was confirmed by Henry coefficients of HMF in both solvents obtained from COnductor-like Screening MOdel for Real Solvation (COSMO-RS)[80], which means that the extraction of HMF from DMSO is even more diffcult than from water[81].

A combination of a **low- and a high-boiling solvent** for catalytic (ion exchange resin) dehydration of fructose to HMF with microwave heating was studied by the mixed organic solvent system acetone/DMSO. Promoted HMF formation, more efficient separation and less environmental risk was achieved by acetone addition to DMSO[82]. Another example for such a solvent combination is the methyl isobutyl ketone (MIBK)/DMSO system. Here, MIBK served as extracting solvent in continuously countercurrent principle[83].

Single phase aqueous-organic solvent mixtures were found to improve the dehydration and to diminish HMF hydrolysis. A certain amount of water in the reaction medium provides the sufficient solubility of sugar molecules. Monophasic water/organic solvent mixtures with DMSO[84], acetone[85–87], butyl acetate[64], 1,2-dimethoxyethane[88] and polyethylene glycol (PEG-600)[89] as organic solvent, were applied. Acetone at sub- and supercritical conditions with sulfuric acid as catalyst leads to promising HMF selectivities up to 75% at 95% fructose conversion[86]. Recently, catalytic dehydration of fructose to HMF in a mixture of water and the low-boiling point solvent hexafluoroisopropanol (bp = 58°C) was demonstrated. High yields, comparable to those obtained using high-boiling point solvents, were achieved and the advantage of easier solvent separation by distillation was stated[90,91]. Similarly, high HMF recovery (96%) and purity (~99%) was recently reported by using the inexpensive water/acetone solvent system[87].

Ionic liquids (ILs) have excellent dissolution properties, as they are capable to dissolve cellulose and lignocellulosic biomass, which may be useful for the HMF production from non-digestable feedstocks (cellulose, hemicellulose, lignin and inulin)[92,93]. High HMF selectivities and yields have been observed by IL-assisted dehydration of carbohydrates. But, the high prices for ILs combined with difficult product isolation from reaction media results in uneconomic processes[94,95]. Since ILs have extremely low vapour pressures and HMF is heat sensitive, distillation cannot be applied and solvent extraction is the remaining possibility to recover HMF from the reaction medium. Due to strong interactions between ILs and HMF, large amounts of solvent are required for separation.

Besides the search for efficient synthesis methods (e.g. by using ILs), the crucial issue for large-scale HMF production is a proper isolation and purification method[14]. Further chemical engineering aspects are design of process equipment, recycling of the catalyst, environmental safety of the process, cost of the raw material (carbohydrates) and the catalytic system[96]. Considering the fact that 3 moles of water are released during the dehydration of sugars, water is always present, and the use of DMSO or ILs as reaction solvent complicates the system by an additional compound to be handled. To use water as reaction solvent only, keeps the reaction mixture as simple as possible[81].

Respecting all these criteria, HMF synthesis in **biphasic reactors**[55,59,97], applying an acidic aqueous reaction medium and an organic extracting solvent, seems to be a straight forward method. The concurrent HMF removal from the aqueous phase into the organic solvent leads to a higher HMF yield and selectivity by shifting the reaction equilibrium to the product side and by the reduction of side-product formation in the aqueous phase. In addition, HMF can be produced with good selectivity from polysaccharides (inulin, sucrose, starch, cellubiose) with high feed concentrations (10 - 30wt %). This allows for inexpensive and abundantly available feedstocks without the need of fructose as starting material, which has to be provided in a separated processing step (acid hydrolysis)[84,98]. Although relatively large volumes of extracting solvent would be/are required, this method is suitable for upscaling[14]. HMF production in aqueous-organic biphasic reactor systems, providing *in situ* LLEx, has already been presented for several solvents. A lot of them are tabulated in the detailed review of van Putten et al.[14], the review of Saha and Abu-Omar[59] and in the very recent review of Esteban et al.[99].

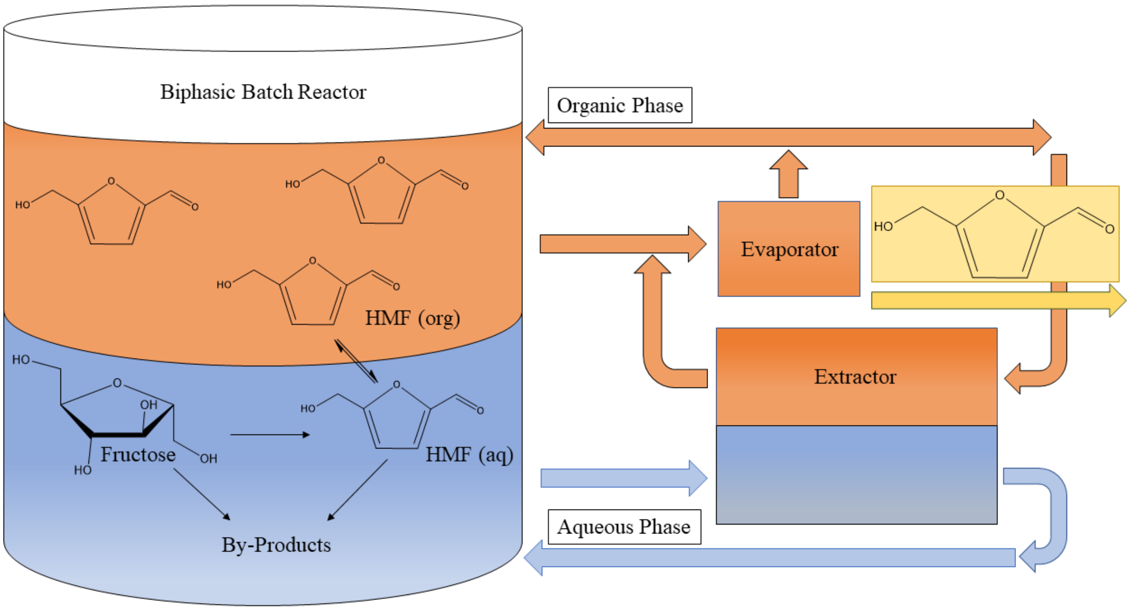

Figure I.4. Scheme for a biphasic reactor for HMF production with *in situ* extraction and a following solvent evaporation step. The aqueous phase contains fructose and the catalyst, and the organic phase is an extracting solvent. The scheme was recreated after reference[79].

The solvents are subdivided concerning the dehydration to HMF in biphasic solvent systems from different starting materials (fructose, glucose, di- and polysaccharides) and concerning the used catalysts (homogeneous or heterogeneous). Some important solvents are n-butanol[60,81,100–102], 2-butanol[81,103], 2-pentanol[60], 2-butanone[60], MIBK[81,97,101,104–106], dichloromethane[84], 2-methyltetrahydrofuran (MTHF)[60,81], tetrahydropyran[60], *o*-propylphenol[81], *o*-isopropylphenol[81], dimethyl carbonate[107], ethyl acetate[108], 2-heptanone[108] and toluene[109]. Using n-butanol as extracting solvent and a porous titania (TiO_2) catalyst for the conversion glucose, fructose and sucrose lead to low HMF yields. This observation was explained by the increasing mutual solubilty of water and n-butanol at the reaction conditions ($T \geq 180°C$, $p = 2000$ psi)), nullifying the ability of n-butanol to act as an extracting solvent. This was proofed by use of shorter water miscible alcohols, which lead also to low yields[101].

Modifications of the aqueous and the organic phases have been tested to enhance conversion and extraction performance. The extracting solvent was modified by addition of co-solvents like 2-butanol[79,101] and 4-methyl-2-pentanol[101] to MIBK. Aqueous phase modifiers were DMSO and/or poly(1-vinyl-2-pyrrolidone) (PVP)[79]. Different compositions of the biphasic systems were tested for the acid-catalised dehydration of fructose. In the *science* paper of Román-Leshkov et al.[79], an optimum composition was reported for the organic phase to be MIBK:2-butanol (7:3) together with the aqueous phase (water/DMSO (8:2)):PVP (7:3) and HCl as catalyst. For both feed concentrations, 30 and 50 wt% fructose to water, high conversions (89%, 92%) and selectivities (85%, 77%) have been achieved, respectively. NMP was also used for the aqueous phase modification and generated 68% HMF selectivity at 80% conversion. NMP and DMSO are both polar aprotic solvents and it appeared that similar mechanisms have driven to enhanced HMF selectivities. But due to a higher distribution of NMP to the organic MIBK phase compared to DMSO, subsequent separation of HMF from the organic solvent was less favourable[79].

Addition of inorganic salts to the reactive aqueous phase (30wt% fructose on salt free basis) being in contact with an organic extracting solvent was performed due to poor partitioning of HMF into most of the extracting solvents[26,60,110]. In the *nature* paper of Román-Leshkov et al.[26], the tested systems contained the organic solvents n-butanol, 2-butanol, n-hexanol, MIBK, or a toluene/2-butanol mixture as organic phase. Although other extracting solvents lead to high selectivities (e.g. 2-butanol), n-butanol showed some advantages for further processing of being inert in the hydrogenolysis step to produce 2,5-DMF and being available from biomass *via* fermentation. The added salts were NaCl, KCl, NaBr, KBr, $NaNO_3$, Na_2SO_4, Na_2HPO_4, $CaCl_2$, CsCl or $MgCl_2$, which lead to higher HMF yields and selectivities due to an increased distribution behaviour of HMF towards the organic phase by means of the salting-out effect. Except for $NaNO_3$, Na_2SO_4 and Na_2HPO_4, for which low reactivity and solid formation was observed. NaCl induced the largest HMF partition ratios (linked to HMF selectivity) of all tested salts. It was stated that the primary role of added NaCl is to change the solvent properties while remaining inert to the fructose dehydration[26]. In a following paper[60], further solvents for fructose dehydration to HMF in biphasic systems with and without added salt were studied; among them primary and secondary alcohols, ketones and cyclic ethers. Results (conversions, selectivities, partition ratios (R)) for n-butanol at 453 K are summarised in Table I-1. Similarly to the described result of the previous publication, higher HMF selectivities and partition ratios are a consequence of salt addition to the reactive aqueous phase. The increase of the distribution ratio is not only dependent on the salt but also on the nature of the solvent. In the system with n-butanol, the increase is two-fold (from 1.6 to 3.2) and for 2-butanone the increase is three-fold (from 1.8 to 5.4) at a salt saturated aqueous phase and 423 K.

Another useful effect of salt-addition is the generation of an aqueous organic two-phase system with water miscible solvents. This allows for the usage of solvents like n-propanol, 2-propanol, acetone and tetrahydrofuran (THF) for solvent extraction purposes. In this context, THF is a prominent example, because the water-miscible solvent leads to the best combination of HMF selectivity (83%) and distribution ratio (7.1) supported by NaCl addition at 423K. The binary system water/n-butanol exhibits an upper critical solubility temperature (UCST) at 398.2 K, which increases in the presence of salts. Thus, through salt addition, a biphasic system is still provided at temperatures above the UCST of the binary mixture without salt (water/n-butanol). It is known that higher HMF selectivities are achieved at lower fructose concentrations[55,97]. But, even higher HMF selectivities (80%) were realised in biphasic systems with added NaCl compared to the corresponding monophasic water/n-butanol system (69%) without salt, in which fructose is evidently more diluted. This highlights the positive effect of salt addition to biphasic systems.

Highest HMF selectivities were reported for C_4 solvents within each solvent class, which decrease in the following order: 2-butanol (85%) > THF (83%) > 2-butanone (82%) > n-butanol (80%). HMF selectivity was also found to increase with increasing temperature.

For the 2-butanol system, raising the temperature from 423 to 453 K improved HMF selectivity from 85 to 90% and for the THF system, HMF selectivities of 83 and 89% were detected at 423 and 433 K, respectively. To find the optimal process temperature for HMF formation, a compromise between activation energy for reaction and degradation temperature of the applied solvents has to be found. The observed salting-out effects (measured by the R values in Table I-1) reveled that among the chloride salts, NaCl and KCl caused the highest distribution ratios but if Cl^- is replaced by Br^-, for both salts only a small effect on R was detected. Na_2SO_4 did not lead to phase separation if C_3 alcohols, acetone or THF were used as organic solvent but it induced the highest partition ratio ($R = 8.1$) for the n-butanol system. On the other hand, lower selectivities were achieved by Na_2SO_4, which indicates that Na_2SO_4 is not inert to the dehydration reaction in the n-butanol system. This was related to hydrate or other complex formation of the salt[60].

Table I-1. Fructose (30 wt%) dehydration results using different salts to saturate the aqueous phase of biphasic systems using n-butanol as extracting solvent at T = 453K, $V_{org}/V_{aq} = 3.2$ and pH = 0.6. The table was adapted from reference[60].

Salt	Conversion (%)	Selectivity (%)	R
No salt	77	69	1.7
LiCl	71	72	2.2
KCl	89	84	2.7
NaCl	87	82	3.1
CsCl	92	80	2.5
$CaCl_2$	77	73	2.2
$MgCl_2$	78	74	2.3
KBr	77	71	1.7
NaBr	90	73	1.9
Na_2SO_4	62	71	8.1

Further studied biphasic systems for HMF production with added salt are published for MIBK and NaCl[111,112], n-butanol and NaCl, KCl, $MgCl_2$ or KBr[102], 2-butanol or THF plus NaCl[102] (here the coversion of glucose to fructose using Sn-Beta as catalyst was described), n-butanol and NaCl[113], THF and NaCl[114–117], *o*-sec-butylphenol and NaCl[118–120], dioxane and NaCl[121] (in their process, higher HMF yields were obtained with dioxane than with THF) and hexafluoroisopropanol plus NaCl[122]. Many organic solvents and salts for microwave enhanced dehydration of fructose to HMF in biphasic systems were studied by

Wrigstedt et al.[123]. They found that, if KBr is used in combination with GVL or ACN as extracting solvent, excellent HMF yields (up to 91%) were achieved. The reaction was also scalable up to 50 wt% fructose while the decrease of HMF selectivities was small. With the help of an isomerisation catalyst, glucose, various disaccharides and cellulose can also be converted by their process. A comparison with the extracting solvents like MIBK/2-butanol, THF, DMF, 2-butanol or *i*-propanol, which were also tested in the study, revealed that faster fructose conversion rates and higher HMF selectivities and yields were observed with the ACN/KBr and GVL/KBr systems. The high HMF yields are comparable to those obtained in ILs and high boiling organic solvents and of course better than those from aqueous processes.

In most of the mentioned studies, different catalysts were applied for the dehydration of sugar to HMF and/or the conversion of glucose to fructose, to which no further attention is payed within this thesis. For the above-mentioned solvent systems, many articles can be found in the literature. Here, it was attempted to name a few important ones. Especially for ILs, there can be found many more publications but this is off the topic of this thesis.

It was stated by Blumenthal et al.[81] that the addition of salts leads also to further problems like increased corrosion under reaction conditions, which rises the cost for equipment, energy demand for salt separation from waste-water and cost for the salt itself and its disposal. They also stated that high concentrations of sugar can have an enhancing effect on the partition ratio similar to that of salts by means of the salting-out effect. Accordingly, **the effect of added sugar** is called “sugaring-out”. Such an effect was observed, as phase separation occured in the binary ACN/water system[124,125] and as an increased LA distribution ratio in the water/GVL system[126] was found by sugar addition. Similarly, increasing HMF distribution ratios were determined with increasing fructose concentration in biphasic systems with MTHF, n-butanol, 2-butanol and MIBK as extracting solvent. As already stated for the salting-out effect, the effect of fructose addition is also dependent on the nature of the solvent, e.g. for MIBK the effect was less pronounced. Fructose addition also induced two-phases in the ternary water/2-butanol/HMF mixture at high HMF concentrations, at which the ternary mixture alone is monophasic. The ability of HMF to close the miscibility gap between water and 2-butanol is attributed to co-solvency or hydrotropy, which is counteracted by fructose in this case.

HMF distribution ratios in ternary water/solvent/HMF mixtures were predicted applying COSMO-RS and determined experimentally for MTHF, n-butanol, 2-butanol and MIBK as solvent. A comparison of the results showed that COSMO-RS overpredicts the distribution ratios (within the expected error of COSMO-RS), but clearly represents the trend of the HMF distribution ratios within the biphasic systems. In a continous flow setup, it was shown that the influence of temperature on the HMF distribution ratio is small. The successful prediction of the trend of distribution ratios validated COSMOS-RS as tool for solvent selection of the discussed extraction problem. Over 6000 solvents were screened for the LLEx of HMF. Among this large number of solvents, the highest partition ratio was observed for 2-phenyl-1,1,1,3,3,3-hexafluoro-2-propanol (R = 110.67). The number of solvents was reduced to 110 by checking their commercial availability. Respecting also the ability of the solvents to extract fructose, short-chain-alkylated phenols provide a compromise between high and low distribution ratios for HMF and fructose, respectively. If a reasonable price is also respected, *o*-propylphenol and *o*-isopropylphenol were short-listed and chosen for further experimental verification. At an HMF content of 1 wt%, high distribution ratios for *o*-propylphenol (11.468) and *o*-isopropylphenol (11.971) have been detected at 25°C. At the same conditions, COSMO-RS predictions give distribution ratios equal to 9.47 and 9.29 and at infinite dilution 10.02 and 9.82, respectively. Results at infinite dilution deviate from experimental results (at 1 wt% HMF) within the expected error of the method. The distribution ratios obtained by use of the latter two solvents for HMF separation from the aqueous phase are approximately 5 times higher than previous found distribution ratios detected experimentally e.g. for MTHF (R = 2).

In the very recent review of Esteban et al.[99], solvent selection for HMF extraction was conducted with a focus on the rational selection of green solvents for the biphasic dehydration of sugars. They stated that the two identified solvents by Blumenthal et al.[81] are not in accordance with the environmental, health and safety (EHS) parameters. In addition, *o*-propylphenol and *o*-isopropylphenol have boiling points of 220 and 230°C, respectively, which is less favourable for solvent separation as already stated for high-boiling solvents. Another critic statement was subjected to halogenated solvents, which allow for very good partition behaviour of HMF towards the organic phase, but exhibit unfavourable EHS profiles. In this context, they proposed to start the solvent screening from preselected candidates (which agree with EHS parameters) using solvent selection guides from *Pfizer*, *GlaxoSmithKline*, *Sanofi*, *ACS Green Chemistry-Pharmaceutical Roundtable* and *CHEM21* in combination with COSMO-RS. In the work of Moity et al.[127], a panorama of sustainable solvents has been created using COSMO-RS. The panorama is an overview of the physico-chemical properties of the solvents, which is useful for the comparison of green and classical organic solvents. Esteban et al. also included this list of bio-based solvents to their solvent selection for a rational screening implying the check for miscibility gaps with water, the solubility of the furan compound in the solvent, LLE and distribution ratio calculations and finally the ranking of the solvents. As a result, they identified ethyl acetate and methyl propionate as promising solvents for the *in-situ* extraction of HMF and furfural from the aqueous phase. These solvents exhibit good extraction performance (high distribution ratios), score well concerning EHS parameter (considered as green solvents) and are recommended by the solvent selection guides.

I.2.5 HMF Isolation and Purification Strategies

As described in the previous sections, the HMF synthesis can occur in aqueous or nonaqueous medium. In case of an aqueous medium, the product is isolated in the following sequence: 1. Filtration of solids (humins), 2. Neutralization, 3. HMF isolation *via* solvent extraction or chromatographic separation and 4. HMF purification *via* distillation or crystallization. Typically, the aqueous mixture in a chemical HMF production process contains about 10wt% HMF[14]. For nonaqueous reaction systems, e.g. in DMSO or ILs, the HMF yields are generally high but HMF then is still not isolated. A solvent extraction step with DCM and water was reported for HMF isolation from DMSO. After solvent removal, purification of HMF was performed by crystallization. Another route was presented *via* the intermediate AMF and subsequent hydrolysis to HMF in methanol and crystallization from MTBE[14]. Extracting solvents employed for HMF separation from a biphasic reactive ILs systems ([BMIM]Cl, $CrCl_3$) were THF, glycol dimethyl ether, methyl tertiary butyl ether and MIBK[128].

An elegant method to bypass the challenging isolation process of HMF is the direct conversion of sugars into biofuels such as 2,5-DMF[26,129] or chemicals such as

2,5-diformylfuran[130], FDCA[20,38], the ethers[66] and esters[71] of HMF (MMF, EMF, AMF) with HMF as intermediate.

I.2.6 Developments of Industrial HMF Production

Although difficulties of HMF production exist in terms of the isolation procedure and feedstock costs, the first industrial production of HMF was realised by the swiss company *AVA Biochem* in 2014. The modified hydrothermal carbonisation (HTC) process was developed by *AVA Biochem*'s parent company, *AVA-CO2*, in cooperation with the *Karlsruher Institute of Technology*[39]. They produced high purity HMF primarly for the research and the specialty chemical markets and technical-grade HMF for bulk applications. Biomass or sugars are converted into bio-coal under high pressure and elevated temperature *via* the modified HTC, while process water, containing HMF, is precipitated. It is described that if lignocelluslosic material is used as feedstock for the HTC process, at first conversion to glucose occurs followed by fructose and finally HMF. The conversions are supported by citric or acetic acid. After conversion, the slurry is filtered and separation methods like adsorption, crystallisation or extraction can be applied. If solvent extraction is applied supercritical CO_2 is preferred[131].

AVALON Industries has taken over all bio-based chemistry activities from *AVA-CO2* and aims for worldwide future large-scale production of HMF[132]. *AVA-CO2* also sold the HTC technology to the *International Power Invest AG* (IPI), which invested in the "Innovationspark Vorpommern" in Relzow Germany.

In 2020, *AVA Biochem* (a subsidiary of *AVALON Industries*) teamed up with the *Michelin Group* to establish the world's first commercial-scale production plant of 5-HMF. The collaboration with an industrial partner (*Michelin Group*) allows to introduce novel products to the market.

I.3 Glycerol

Glycerol was listed in the in the “top 10” biomass derived chemicals due to its potential as a primary building block for biorefinery, its biodegradeabillity and non-toxicity[10,17]. It was already commercialised at the time of the first report of the top value-added chemicals from biomass in 2004[15]. Glycerol is abundantly available due to the production of biodiesel and through saponification[133]. Biodiesel is a blend of fatty acid alkyl esters, which is industrially produced by transesterification. Here, vegetable oils or fats (triglycerides) react with an alcohol (methanol or ethanol) catalised by a strong base, which yields fatty acid esters and glycerol as a main by-product (~10 wt%)[134]. From the 70s to 2004, the glycerol price was relatively stable, but the strong increase of biodiesel production has led to a surplus of glycerol, which flooded the market with excessive crude glycerol. Consequently, the price dumped and reached the lowest historical value ($0.05/pound). At such a low price, glycerol combustion or feedstuff for animals are options to reduce the large amount of “waste” glycerol arising from biodiesel production. *Dow Chemicals* closed its 60000 tons/year glycerol plant (the worlds largest) in Texas in 2006 similarly, *Procter & Gamble* shut down its 12500 tonnes/year plant near London. Also, *Solvay* closed its glycerol plant in Tavaux, France. In Germany, *Dow* still produces glycerol with high purity (> 99.7%) for pharmaceutical applications. These developments have led to a reduced share of synthetic glycerol (<5000 tons of 2 million tonnes). In 2012, the global bio-glycerol production has exceeded 2 million tons[135] and for 2025 a production of over 6 million tons was forecasted[136]. Thus, the supply is entirely independent on the market demand. New uses for glycerol were required, which initiated researchers to develop methods for crude glycerol conversion into value-added chemicals. Conventional catalysis and biotransformations are two main routes for conversion of crude glycerol into many different compounds. 1,3-propandiol (1,3-PDO), citric acid, succinic acid, poly (hydroxyalkanoates), butanol, hydrogen monoglycerides, lipids and syngas from glycerol are some candidates. But operation feasibility and costs are issues of many available technologies[137].

A large proportion of crude glycerol is refined before its further use. The main uses (64%) for refined glycerol are products for food and cosmetics[134]. The problem with crude glycerol from biodiesel is its contamination with methanol/ethanol, water, soap, fatty acid methyl esters (FAMEs) glycerides, free fatty acids and ash. The proportion of the contaminats can vary significantly with the methods and feedstocks used to produce biodiesel. Because in most cases, crude glycerol cannot be used directly in catalytic conversion or fermentation processes due to the risk of catalyst deactivation or inhibition of microbes through impurities, purification steps are thus required for further processing into value-added compounds. A universal procedure for crude glycerol purification was reported by Xiao et al.[138]. This included the following steps: initial microfiltration of the crude glycerol, saponification, acidification, phase separation and biphasic extraction of upper- and lower-layer products.

Several processes including reduction, dehydration and fermentation have been considered to convert glycerol into higher value chemicals[10]. Catalytic hydrogenolysis converts glycerol to ethylene glycol, propylene glycol, acetol, lactid acid and propandiols. The production of 1,3-PDO *via* hydrogenolysis of bio-based glycerol has been commercialised by *Archer Daniel Midlands* (ADM), *Dow Chemicals* and *Ashland and Cargill*. Propandiols and ethylene glycol are common solvents, for which the bio-based production is competitive to that of petroleum-based route[139]. Catalytic and thermal dehydration of glycerol leads to hydroxypropionaldehyde (reuterin), acetol or acrolein. The latter compound is a precursor for acrylic acid, which is used for polymer production[10,17].

Glycerol carbonate can be prepared directly in high yields by carbonation of glycerol and can be used for cosmetics personal care and medicinal applications due to its low toxicity and low flammability. It can also be used to replace dimethyl carbonate for polycarbonate and polyurethane production, as bio-based solvent, to make lithium batteries and surfactants. Cyclic glycerol acetals and ketals as bio-based solvents were reported and positioned in Hansen and COSMO-RS spaces, among them glycerol carbonate[10,17,139].

Another important commodity, which can be derived by chlorination of glycerol is epichlorohydrin (used for epoxy resins). This is a good example for a high-volume industrial product derived from a biobased building block. Several improvements to the conventional method *via* propylene hydrochlorination are a better regioselectivity of the chlorination step, reduction of by-product formation and a decreased waste. *Solvay* and *Dow Chemicals* have developed processes for epichlorhydrin production[10,17].

A market analysis revealed that the glycerol market is expected to grow again due to high demand on personal care products especially in Asia. The fact that glycerol holds potential as a platform for renewable production of chemicals provides economic and environmental incentives and motivates manufactures for intermediates, especially in China. Increasing demand for glycerol can be noticed in Europe for the production of epichlorohydrin and propylene glycol. With the increasing demand on pharmaceutical and and cosmetic products containing glycerol, the global glycerol market will experience significant growth[140].

I.4 n-Butanol

Bio-butanol has a potential to play a significant role in a sustainable industrial system. It contributes with 20% to the total n-butanol market and has two primary commercial applications, which are the automotive fuel market and the use as an industrial solvent or co-solvent (mainly for surface coatings). As a fuel, n-butanol offers some benefits compared to lower alcohols like methanol, ethanol or propanol. First, it has been shown that n-butanol is suitable for original equipment manufacturer (OEM) gasoline engines without futher modifications and with similar performance to gasoline (net heat of combustion ~ 83%)[141,142]. The existing pipeline infrastructure can be used as well. A very important aspect is that n-butanol is less hazardous than gasoline (less flammable due to a lower vapour pressure and higher flash point). It is also non-hygroscopic, non-corrosive and bears only low order of toxicity[143]. In addition, it is not fully miscible with water, which reduces the risk of unintentional blending, but it is fully miscible with gasoline and diesel fuel, which allows for alcohol-blended fuels. Besides its direct use, derivatives of n-butanol are widely used in industry. The solvent sector is attended by n-butanol itself as well as by esters and ethers of n-butanol. E.g. butylacetate (inks, surface coatings, perfumery and synthetic flavours share 16% of the total butanol market), di-n-butyl ether (extractant and solvent for resins, fats and oils), butyl glycol ethers (largest volume derivative of n-butanol in the solvent sector) and n-butyl propionate, which can replace hazardous solvents like xylenes. Further applications of derivatives of n-butanol are the production of polymers, plasticisers and others[143].

Industrially, n-butanol is produced by hydroformylation of propene to butyraldehyde and hydrogenation in second step to obtaine the primary alcohol (see Figure I.5).

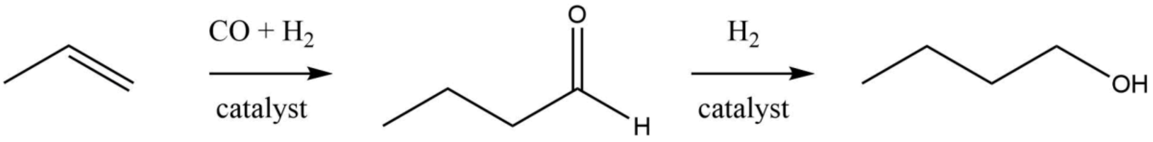

Figure I.5. Industrial production of n-butanol from propene *via* butyraldehyde.

Alternatively, n-butanol can be derived *via* the acetone-butanol-ethanol (ABE) fermentation process. This method was established in the early 20th century mainly for the production of ethanol. In the 1950s, economic factors and new petrochemical methods led to a reduction of this industry. New attention to this method emerged due to increasing oil prices and the increasing trend to use renewable feedstocks[144].

It has been reported that the most effective strains for the ABE process are *Clostridium beijerinckii* and *Clostridium acetobutylicum*[145]. These microorganisms are able to ferment un-hydrolised starch and a wide range of simple sugars and are promising species for commercial application. The main problem of bio-butanol production is that the product is toxic for the engaged microorganisms, which leads to low final butanol content at the end of the fermentation process. If sugars from lignocellulose are used for fermentation (financial reasons), even further limitations appear due to compounds within the lignocellulose hydrolysate, which are toxic for the strains intended to ferment the sugars and produce the bio-solvents. Such inhibitory compounds are HMF, FF and lignin derivates[146]. Therefore, a pretreatment of the feedstock material is required to remove lignin and the comounds formed during hydrolysis[147].

Due to these negative effects on the efficiency and economics of bio-butanol recovery, a main research goal in this field is to improve the ability of microorganisms to tolerate higher butanol concentrations and the efficient separation after fermentation or *in-situ*, during the process. The integration of the product recovery to the fermentation process is desirebale concerning economics and the relief of toxic butanol[148,149]. The feed material used for fermenations contains mostly carbohydrates. Salts are added as nutrient and by controlling the pH through acid and base dosing, further electrolytes are introduced. Thus, electrolytes are present in the process and the knowledge of their effects on the phase behaviour is crucial, e.g. for the separation of n-butanol from the aqueous phase *via* liquid-liquid demixing[150]. Solvent recovery by distillation is robust and proven but energy intensive. Several separation techniques like adsorption, gas stripping, LLEx, perstraction, reverse osmosis and pervaporation were evaluated[144,151]. Both studies reported that pervaporation and adsorption-based techniques are preferable. More recently, Abdehagh et al.[152] showed that combined gas stripping and adsorption could be an effective separation method for bio-butanol.

I.5 Ethanol

Ethanol is the most produced compound through biochemical transformations in the bio-fuel sector. It is considered as a so-called supercommodity and did not appear in the original "top 10" list of value-added chemicals from biomass[15]. The potential of ethanol as a platform chemical was raised through technology develpoments and commercial partnerships and therefore it was picked up to the revised list of 2010[10]. Bio-ethanol is mostly produced through established fermentation technologies from first generation biomass (sugar or starch essentially from corn and sugar cane). From a total market size of 86 million tons/year, only 18% have been used for non-fuel applications. These are ethanol conversions like dehydration for ethylene production (used for diverse polymers), esterification to ethyl lactate and ethyl acetate (green solvents), oxidation to acetic acid or acetaldehyde and conversion to butadiene[17,153].

In fermentation processes, an ethanol concentration of 8 to 10 mol% in ethanol/water mixtures is usually obtained. With improved methods even 15 mol% of ethanol are achievable. Distillation is conducted for purification while a maximum purity of 90 mol% of ethanol is possible. To use ethanol as an additive for gasoline, higher purity is necessary. The difficulty of separartion of these two liquids lies in fact that they form an azeotrope at 90.37 mol% of ethanol, 1 bar and 78.16°C. Preferred methods at the industrial scale to obtain absolute ethanol are azeotropic distillation, extractive distillation with solvents and adsorption. To avoid the usage of hazardous solvents, a renewed interest for salt extractive distillation emerged. Salts are a green alternative to break the azeotrope and help to purify ethanol. It was stated that this method is advantageous due to energy saving, reduced equipment size and cost, high product purity and the scaleability of the production[154]. Calcium chloride ($CaCl_2$) has been used for salt extractive distillation due to its favourable effect on the vapour-liquid phase equilibrium of the ethanol/water system, which was already determined experimentally[155].

I.6 Aim of the Thesis

Beside the studies on the synthesis of chemicals derived from biomass, the investigation of the separation and isolation processes by means of thermodynamic properties of the involved liquid mixtures is important. Distribution ratios of the desired compounds and especially LLE are essentially for the design of separation units.

Main focus of this work lies on the experimental determination of the influence of electrolytes on LLE for extraction processes. The hetereogenous mixtures of interest comprise an organic substance (product molecule) in a binary water/organic solvent system. This implies the determination of LLEs of ternary and quaternary systems in presence and absence of electrolytes.

The ternary systems with electrolytes include water, n-butanol and one type of salt. Here, the influence of the electrolytes on the mutual solubility of water and n-butanol is of interest. The salting-out effect of electrolytes on n-butanol from the aqueous phase and a modified *Setchenov*-type correlation are applied for the evaluation. These systems represent the extraction systems used for the product molecules. The obtained LLE data can also serve as basis for the LLEx of n-butanol from the aqueous phase (e.g. ABE-fermentation broths). Other ternary systems are composed of water, n-butanol and a product molecule (HMF, glycerol), which distributes between both liquid layers. Here, the distribution ratio of the product molecule between the liquid phases and the influence of the product molecules on the phase behaviour of the binary water/n-butanol system are major aspects.

The quaternary systems include water, n-butanol, electrolytes and a product molecule and can be subdivided regarding the investigated product molecule HMF or glycerol. Here, the influence of the product molecule concentration at a constant salt concentration and of the salt concentration at constant product molecule concentration on the product molecule distribution ratios is investigated.

The gained LLE data in combination to binary water/HMF data (osmotic coefficients and density, determined by co-workers at the TU Dortmund) served as a basis for thermodynamic modelling using the Pertubed-Chain Statistical Association Fluid Theory (PC-SAFT) and the electrolyte PC-SAFT (ePC-SAFT) equations of state (performed by co-workers Mohammad Sultan and Christoph Held at the TU Dortmund).

Further characterisations of binary water/HMF and ternary water/HMF/salt mixtures by means of osmotic coefficients are conducted at higher HMF concentrations. Activity coefficients of HMF in binary and ternary as well as mean activity coefficients of salts in ternary mixtures are calculated from osmotic data using a procedure according to Robinson and Bower. The investigation of the binary water/HMF system is extended to density measurements at high HMF concentrations and to the ability of HMF to act as a solubiliser by means of solubilisation experiments and surface tension measurements.

The general interest on salting-in and salting-out effects is ensued by the addition of charged and uncharged compounds to the model system water/DPnP, while monitoring LST variations depending on the additive´s nature and concentration. Following the concept of salt extractive distillation, salting-out effects in water/ethanol mixtures are studied.

Chapter II

Fundamentals

II.1 Liquid-Liquid Extraction (LLEx)

LLEx is the process of transferring one solute or more from one liquid phase to another immiscible or partially miscible liquid phase in contact. It is a common separation technique in industrial and laboratory scale, besides distillation. Whereas distillation is based on different volalitilies of the mixture components, LLEx is based on different solubilities of a solute in the two liquid phases. The mass streams in an extractor are pictured in Figure II.1, schematically. In most cases, the initially stream (feed), which contains the solute is an aqueous phase, whereas the other liquid phase is usually an organic extractive solvent (extractant). In an extractor, both liquids get in contact and equilibrate, while mass transfer from the feed to the extractant occurs. The organic solvent stream, which is enriched with the desired solute (extract), leaves the extractor for further operations, like solvent distillation and recovery. The depleted stream (raffinate) may be recycled to the feed stream after other eventual separation processes[156].

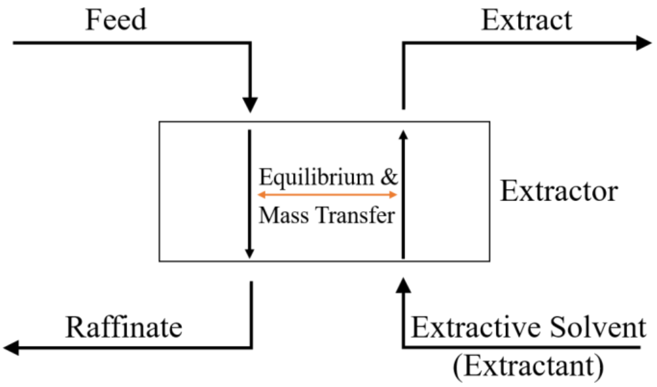

Figure II.1. Scheme of the mass streams in an extraction unit.

The method is preferred to distillation-based separations if:

- the substance to be separated is heat-sensitive
- the components in the present mixture are close-boiling or form azeotropes
- the desired substance is present only in small amounts and is higher boiling than the solvent, which would require vaporisation of large amounts of solvents, usually connected to a high energy demand (depending on the heat of vaporisation (ΔH_{vap}) of the solvent)

As the product is still not purified after LLEx but in another mixture, secondary separation steps like distillation, evaporation, crystallisation or others are conducted. The overall process cost has to be respected, if LLEx is taken into consideration. Benefits of LLEx are resulting e.g. for diluted aqueous feed streams due to the relative high value of ΔH_{vap}(water) = 40.65 kJ/mol. In case of temperature sensitive compounds, separation from the organic extractive solvent in the secondary step is feasible by e.g. gentle distillation. Generally, LLEx processes can be performed in different operation modes: single stage, multistage crosscurrent or countercurrent. Single stage mode in a laboratory is presented by LLEx using a separation funnel. It allows well mixing and easy phase separation and can be repeated, if one extraction step (discontinuous) is not enough. Typically, the organic solvent is the upper layer and water is the lower layer (depending on density). For industrial scale application, LLEx is performed in a continuous manner using mixer settler units in crosscurrent or countercurrent arrays. In crosscurrent mode, fresh extractive solvent is added to each individual stage, while in countercurrent mode, the extract phase of one stage is the extractant for a previous stage. In both modes, the raffinate of one stage is the feed stream for the next stage. In the last stage of the countercurrent mode, the most depleted raffinate gets in contact with fresh solvent and in the first stage the most enriched extract phase gets in contact with the maximum loaded feed stream. Generally, the countercurrent mode provides best extraction resuslts coupled with minimum solvent consumption[157]. Countercurrent LLEx can also be performed using a column, in which both liquids get in contact due to density differences. Furthermore, there are devices for LLEx based on centrifugal forces for the separation.

The field of application is huge ranging from the standard separation method in analytical and organic chemistry in lab scale to separations in chemical process industry including petrochemical, food, pharmaceutical and metal industries[158]. The biggest application field is in the production of aromatic compounds (BTX = benzene, toluene, xylenes)[157]. Other important application areas are waste-water treatment[159] and the recovery of biotechnology-derived chemicals like alcohols from fermentation broths. The most useful alcohols obtainable from fermentation are ethanol and n-butanol[160].

II.1.1 Nernst Distribution Law

Considering two liquid phases α and β; a solute 1, which is distributed between these two liquid phases and the assumption of ideal dilute solutions, i.e. the mole fractions of solute 1 in both liquids are very low, the fugacities of solute 1 in phase α and β can be written as:

$$f_1^{\alpha} = H_{1,\alpha} x_1^{\alpha} \tag{II-1}$$

$$f_1^{\beta} = H_{1,\beta} x_1^{\beta} \tag{II-2}$$

where $H_{1,\alpha}$ is Henry´s constant for solute 1 in phase α and $H_{1,\beta}$ is Henry´s constant for solute 1 in phase β. Both fugacities are equal at equilibrium and a constant K is obtained at constant temperature and pressure for sufficiently dilute solutions. K is called the partition or distribution coefficient and reads:

$$K = \frac{x_1^{\alpha}}{x_1^{\beta}} = \frac{H_{1,\beta}}{H_{1,\alpha}} \tag{II-3}$$

Equation (II-3) is named the *Nernst distribution law*. Deviations from this law may stem from chemical effects like molecular association in solution. An example for such a case is the distribution of benzoic acid between water and benzene. The latter two solvents can be considered as immiscible. Due to the strong tendency of benzoic acid to dimerize in the benzene layer, the distribution coefficient is not constant[161]. The concentration distribution of a solute between two immiscible solvents without the assumption of ideal solution is generally termed as “distribution ratio” and preferred to the term “partition coefficient”, the latter one is not recommended. Precise terminology is discussed in the next section.

II.1.2 Extraction Parameter and Terminology

The terms “distribution” or “partition” are frequently used in replacement of the term “extraction”. If the substance to be extracted is initially present as solute in a liquid phase, the term “solvent extraction” is also a synonym to LLEx. Many different terms are spread in the literature, which is why the IUPAC made an attempt to clarify the terminology and symbols, which should be used related to this discipline[162].

For instance, the quantity, which describes the concentration distribution of the solute between the two liquids has received many names by the permutation of the words: “distribution”, “partition” and “extraction” with the words: “constant”, “ratio” and “coefficient”; and even more. The recommended term for the ratio of the concentration of a substance in a single definite form, A, in the extract phase (mostly organic phase) to its concentration in the same form in the other phase (feed, aqueous or raffinate phase) at equilibrium is the “partition ratio” (K_D). “Distribution constant” can be used as a synonym.

The difference to the term “distribution ratio” is that the latter one describes the distribution of a solute in a two-phase system, which is not necessarily in equilibrium and the species of the solute is not necessarily identical. The suggestion of the reviser of this IUPAC publication is to use the term “distribution”, if the total amount of related species is considered and “partition” if only one single chemical species is considered. The term “constant” should be used for fixed thermodynamic true constants, otherwise the term “ratio” should be used. The term “partition coefficient” is not recommended at all, although it is often preferred e.g. by chromatographers[163]. The translation of this recommended terminology by IUPAC applied to this work dictates the usage of the term “partition ratio” as all experiments in this work are performed at thermodynamic equilibrium and the products or solutes under investigation are not involved in a chemical reaction nor ionisable in the used two-phase liquid systems. On the other hand, a synonym for the term “partition ratio” is “distribution constant”, which implies that the quantity is invariant and that the activity coefficient of the solute is constant. As activity coefficients highly depend on the concentration and deviate more pronouncedly at high concentrations, due to chemical effects like molecular association, discrepancies appear with the term “constant” and with the term “partition”, if molecular association is seen as a chemical reaction in terms of complexation. To avoid any conflicts with terminology and to be more general, the ratio of the concentrations of the product or solute in both phases is named “distribution ratio” in this work with the add-on: “at thermodynamic equilibrium”, abbreviated by “distribution ratio” $D^w(solute)$ solely, which is calculated by the following equation:

$$D^{w}_{solute} = w^{org}_{solute} / \, w^{aq}_{solute} \tag{II-4}$$

where $w^{org}(solute)$ and $w^{aq}(solute)$ are the concentrations of the solute in the organic and aqueous phase, respectively. The superscript w within the symbol $D^w(solute)$ indicates that the distribution ratios are based on weight fractions. Another important measure for the quality of the separation of component A (solute) and C (water) by LLEx is the separation factor $\alpha^w(solute,water)$, which is defined by the following equation[164–166].

$$\alpha^{w}_{solute,water} = \frac{w^{org}_{solute} w^{aq}_{water}}{w^{aq}_{solute} w^{org}_{water}} = \frac{D^{w}_{solute}}{D^{w}_{water}} \tag{II-5}$$

The separation factor is equal to the ratio of the distribution ratios of the solute and water. With the equilibrium condition that the activities of both components are equal in both phases:

$$x^{aq}_{solute}\gamma^{aq}_{solute} = x^{org}_{solute}\gamma^{org}_{solute} \tag{II-6}$$

$$x^{aq}_{water}\gamma^{aq}_{water} = x^{org}_{water}\gamma^{org}_{water} \tag{II-7}$$

the separation factor can be written as:

$$\alpha_{solute,water} = \frac{\gamma^{aq}_{solute}\gamma^{org}_{water}}{\gamma^{org}_{solute}\gamma^{aq}_{water}} \tag{II-8}$$

where γ_i^{phase} is the activity coefficient of the component i (water or solute) in the corresponding liquid phases (aqueous or organic). The separation factor is kind of a measure for the selectivity of the extracting solvent. Other definitions for the selectivity $S^w(solute,water)$ are also found in the literature[167,168]:

$$S^{w}_{\text{solute,water}} = \frac{w^{\text{org}}_{\text{solute}} / (w^{\text{org}}_{\text{solute}} + w^{org}_{water})}{w^{aq}_{\text{solute}} / (w^{aq}_{\text{solute}} + w^{aq}_{water})} \tag{II-9}$$

The higher the selectivity of a solvent in an extraction, the lower the number of required extraction steps for compound separation and thus, less required volume of organic solvent.

The distribution of a compound between n-octanol and water in thermodynamic equilibrium is termed the octanol/water partition coefficient (K_{ow}), which is against the IUPAC recommendation, but, as it is such an important parameter and frequently used in literature, the term has become established. Because K_{ow} values can range over many orders of magnitude, they are usually presented in logarithmic form ($\log K_{ow}$)[169]. The value provides a measure for the hydrophilic and lipophilic balance (HLB) of a substance and is also indicated as $\log P$. Compounds with negative $\log P$ values are considered to be hydrophilic whereas lipophilic compounds exhibit positive $\log P$ values. This partition coefficient serves as a physico-chemical parameter in ecotoxicology for the environmental risk assessment of organic chemicals and in pharmacy for the distribution of a drug within the body[170–172]. The lipophilicity of a compound determines its bioaccumulation in living organisms, its soil adsorption as well as its occurrence in groundwater[173]. In pharmaceutical science, the $\log P$ value plays a crucial role, because it determines the ADMET (absorption, distribution, metabolism, excretion, and toxicity) properties and helps for the assessment of drug candidates[174].

II.1.3 Ternary Phase Diagram

A LLEx system is typically pictured in a ternary phase diagram as shown in Figure II.2. The carrier substance or raffinate phase (C) contains the solute (A) to be separated from the feed stream with the help of the extractive solvent (S). The closed miscibility gap (2-phase region) within the ternary system represents the operational area for LLEx. It dictates the maximum concentration of A in the feed stream (mixture of C and A). The solubility of S in R_n is the attendant solvent loss. Tie-lines connect the equilibrium concentrations of the extract (E_n) and raffinate (R_n) phase and pass through the mixture points (M_n). Depending on the course of the binodal curve and the distribution ratio $D^w(A)$ (Eq. (II-4)), the tie-lines will have a certain length and slope. The tie-line length (TLL) and the tie-line slope (TLS) at different compositions (weight fractions) can be calculated according to Eq. (II-10) and (II-11), respectively. Liquid-liquid phase separation is no longer possible at the critical or plait point (CP), because at this point the composition of E_n equals that of R_n.

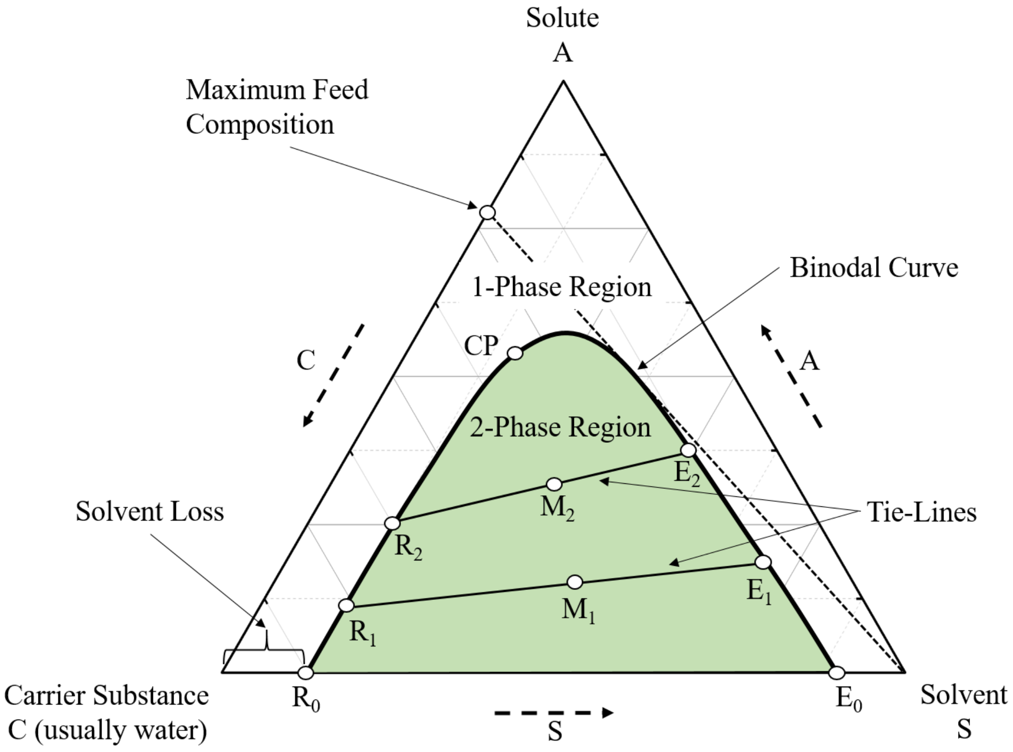

Figure II.2. Scheme of a ternary phase diagram of a LLEx system composed of the carrier substance C, the extracting solvent S (extractant) and the solute A. The raffinate (R_n) and extract (E_n) phases located on the binodal curve are in equilibrium and connected by the tie-lines. The critical point (CP) defines the point, at which the composition of E_n equals R_n.

$$TLL = \sqrt{\left[\left(w_S^{E_n} - w_S^{R_n}\right)^2 + \left(w_A^{E_n} - w_A^{R_n}\right)^2\right]} \quad \text{(II-10)}$$

$$TLS = \frac{\left(w_A^{E_n} - w_A^{R_n}\right)}{\left(w_S^{E_n} - w_S^{R_n}\right)} \quad \text{(II-11)}$$

In Eq. (II-10) and (II-11), w_S^{En}, w_S^{Rn}, w_A^{En} and w_A^{Rn} are the equilibrium concentrations of the extractant (S) and the solute (A) in the extract (E_n) and the raffinate (R_n) phases, respectively. If the slope is positive, the affinity of the solute towards the organic phase (extractant) is higher compared to that towards the aqueous phase (carrier substance), which is beneficial for solute separation by LLEx. Once the equilibrium concentrations or LLE data are obtained, the distances from the equilibrium concentrations (R_n, E_n) to the mixture point (M_n) can be determined, similar to Eq. (II-10). With the known total mass $M_{total,n}$, the masses of the extract and the raffinate phases can be determined *via* the lever-rule:

$$m^{R_n} \cdot \overline{R_n M_n} = m^{E_n} \cdot \overline{M_n E_n} \quad \text{(II-12)}$$

$$M_{total,n} = m^{R_n} + m^{E_n} \quad \text{(II-13)}$$

The ternary system in Figure II.2 is an example of a *Class I* ternary mixture with one pair of components bearing a miscibility gap. Accordingly, *Class II* and *III* contain two and three partially miscible liquid component pairs, respectively. In *Class IV* ternary systems, a solid phase is formed in equilibrium with liquid phases and *Class 0* refers to an island type (all binary component pairs are miscible but certain mixtures of all three components separate in two liquid phase). This classification of different types of ternary systems was made by Treybal[175]. The ternary systems water/n-butanol/HMF and water/n-butanol/glycerol studied in this work belong to *Class I*, whereas systems containing a salt belong to *Class IV*. However, only LLE tie-lines were studied independently of the type of the multicomponent system.

The LLE of the multicomponent system is the thermodynamic basis for LLEx processes. Several methods for tie-line correlations (Campbell[176], Brancker-Hunter-Nash[177], Bachmann[178], Othmer-Tobias[179], Hand[180] and Eisen-Joffe[181] (for salts)) exist, which are useful, if only a small amount (3 or 4) of tie-lines are known.

II.1.4 Solvent Selection

The choice of solvent is most important to realise LLEx processes and following purification steps (e.g. distillation). The existence of a miscibility gap between the solvent and the carrier substance (mostly an aqueous phase) is a precondition. A large miscibility gap leads to a better extraction performance in terms of higher separation factors and less solvent loss. In addition, the larger the closed biphasic region in the ternary system, the higher is the possible concentration of (A) in the feed stream, see Figure II.2. The lower the solvent loss, the lower are the purification costs of the raffinate and the lower is the required amount of (S) for extraction. An estimate of the solvent loss (solubility of (S) in (R_n)) can be made by the inverse activity coefficient of (S) at infinite dilution ($1/\gamma_{S,R_n}^{\infty}$) in ($R_n$).

The extractive solvent (S) should provide sufficient high solubility for the solute (A) to be short-listed for extraction applications. High solubility of (A) in the extractant (S) has positive effects on the $D^w(A)$ value (Eq.(II-4)), which is a measure of the solvent´s capacity. The solvent capacity (solubility of (A) in (E_n)) can be expressed as the inverse activity coefficient of (A) at infinite dilution ($1/\gamma_{A,S}^{\infty}$) in (S).

In addition, the solvent (S) should exhibit high selectivity to reduce the number of theoretical stages for extraction and to avoid coextraction of possible contaminants. High selectivity also reduces the costs for solvent regeneration (distillation) after the extraction process.The selectivity can be estimated by the ratio of the activity coefficient of the solute (A) to that of the carrier substance (C) both at infinite dilution ($\gamma_{A,S}^{\infty}/\gamma_{C,S}^{\infty}$) in solvent (S). Another measure for the selectivity is the separation factor α^w*(solute, water)* according to Eq. (II-5). Further physico-chemical properties of the extractive solvent should be respected:

- azeotropic behaviour between (S) and (A) should be avoided to allow solvent recovery from the extract and raffinate by simple distillation
- separation factors in the distillation columns
- density difference between both liquids
- melting point
- viscosity
- surface tension

As already mentioned in section I.2.4, further important factors are environmental, health and safety aspects (EHS parameter), which include toxicity, flammability (high flashpoint) and the environmental impact like the water hazard class. The extractive solvent (S) must also be chemically inert, temperature stable and of low corrosiveness. And, evidently, the solvent must be of low cost to allow economic feasability[164,166,182].

Physico-chemical properties and separation factors of the components can be obtained from databases like the Dortmunder Datenbank (DDB)[183], the Design Institute for Physical Properties (DIPPR)[184] and Reaxys[185]. For the prediction of phase equilibria the key quantitiy is the chemical potential of the components in the phases, which are connected to the corresponding activity coefficients. These properties can be calculated using PC-SAFT[186], COSMO-RS[80,187] or the group contribution method UNIFAC[188]. Thus, solvent selection tools to calculate thermodynamic properties, like the above mentioned ones, are highly demanded.

The first approach to estimate the solubility in different solvents was suggested by Hildebrand[189]. He introduced the Hildebrand solubility parameter δ ($\delta = (E_{coh}/V_m)^{0.5}$). The cohesion energy E_{coh} is the difference between the enthalpy of evaporation ΔH_{vap} and the energy of the ideal gas RT and thus, E_{coh} ($E_{coh} = \Delta H_{vap} - RT$) is easy to determine. Two substances are miscible if the δ values of both components are similar, in line with the principle “like extracts like”. This simple concept can be extended to multicomponent systems but works in practice only for substances, which form regular mixtures. For systems, in which strong intermolecular interactions like hydrogen bonding are present, this method is not recommended. This approach was further developed by Hansen who introduced the Hansen solubility parameters (HSPs)[190] by splitting δ ($\delta^2 = \delta_d^2 + \delta_p^2 + \delta_{hb}^2$) and E_{coh} ($E_{coh} = E_d + E_p + E_{hb}$) into three contributions. The indices *d, p and hb* stand for the dispersive, the polar and the hydrogen-bond contribution, respectively. If the three paramerters are similar the compounds are estimated to be soluble or even fully miscible. With the three parameters a three dimensional space (*Hansen Space*) can be defined. The ratio (R_a/R_0) of the distance between HSPs (R_a) in the *Hansen Space* and a certain interaction radius (R_0) is the relative energy difference (RED). For RED < 1, RED = 1 and RED > 1 the compounds are fully miscible, partially miscible and non-soluble, respectively.

A problem with this model is apparent if one considers a solvent, which is more likely dissolved in another solvent than in itself. Because, in this situation negative distances would appear, which is not possible. The model is based on experimental data with no theory behind, which is why the Hansen solubility parameter are hardly to predict.

The huge advantage of COSMO-RS in this context is its predictive power without the need for experimental data or at least a few. Although the predictions are not precise, the method is very useful to screen many solvents and based on the obtained distribution ratios or Henry coefficients, the number of considered solvents for application can be reduced. The promising candidates can be added to the closer solvent selection, for which experimental investigations can be planned and executed. In this field of application, the COSMO-RS method is most useful leading to a decreased experimental effort and thus to savings of money and time[182].

The solvent used in this work for LLEx of HMF from aqueous solution is n-butanol. This decision is based on relatively high distribution ratios reported in studies of HMF production by sugar dehydration in biphasic systems with n-butanol as extractive solvent[26,60]. In addition, the solvent of choice is bio-based and appears in the list of green solvents classified by Moity et al.[127]. Evaporation of n-butanol for solvent recovery and HMF purification after the LLEx process is feasible without risk of HMF decomposition. Although the miscibility gap between n-butanol and water is not that large as that between MIBK (classical extractive solvent) and water, the addition of salts to the water/n-butanol mixture will increase the gap in favour of LLEx application.

II.2 Effects of Salts

II.2.1 Hofmeister Series

During 1880 and 1890, the pharmacologist Franz Hofmeister and co-workers published a series of 7 papers in the "*Archiv fuer experimentelle Pathologie und Pharmakologie"* with the title *"Zur Lehre der Wirkung der Salze"* (about the science of the effect of salts). These extended investigations on salt effects considered the precipitation of different substances like proteins (e.g. purified egg white)[191], colloidal ferric oxide, collagen (isinglass) and sodium oleate from electrolyte solutions. The first systematic studies on specific ion effects were probably done by Poiseuille in 1847, who studied the influence of salts on the viscosity of water[192]. However, based on the protein precipitation studies, Hofmeister was the first to draw general conclusions about specific ion effects beyond the effect of different charges. The main conclusion was that salts with a high ability to withdraw water are effective in protein precipitation and Hofmeister classified the salts regarding their capability to decrease (salting-out) or to increase (salting-in) the solubility of proteins in water. He proposed the series only for salts and not for individual ions. Anyway, by tabulating and comparing salts of equal cations or anions, he was able to construct more or less the separated series of cations and anions[193,194]. The typical ordering of the ions known as the *"Hofmeister series"* or the *"lyotropic series"* appeared only many years later and is shown in Figure II.3. It reflects the relative effectiveness of ions on the precipitation (salting-out) or, the other way round, on the stabilisation (salting-in) of standard proteins (globular protein with net negative charge)[195] in solution. Many physico-chemical properties or phenomena like the water-air surface tension, the solubility of non-electrolytes, gases or colloids, the catalysis of chemical reactions and enzyme activities are influenced by the presence of ions according to the Hofmeister series[196–198]. Thus, the influences of salts are relevant for a wide range of application from molecular biology to chemical engineering and are ubiquitous in physical and biochemistry. The ion sequence in the Hofmeister series is often referred to as specific ion effects, which appear at relatively high concentrations (> 0.1 mol/kg), where long-range electrostatics are screened, and short-range interactions begin to be dominant.

The scheme in Figure II.3 is regarded as the *direct order*, which differs for the cations from Hofmeister´s original work[191,193], because his protein precipitation studies involved complex mixtures of proteins bearing different net charges (egg white). And thus, the original found cation Hofmeister series corresponds to what we call today the *indirect order*, which is representative for neutral or positively charged proteins. It is important to note that the Hofmeister series is not universally applicable to all systems. Reversal or partly alterations of the anion and/or the cation series depending on parameters like surface charge and polarity[195,199] of the solute, temperature and salt concentration[200,201], pH[202–205] and buffer system[206] are observed in many systems, which is highlighted by a title of a recent review of Nadine Schwierz et. al: "Reversed Hofmeister series - The rule rather than the exception"[207].

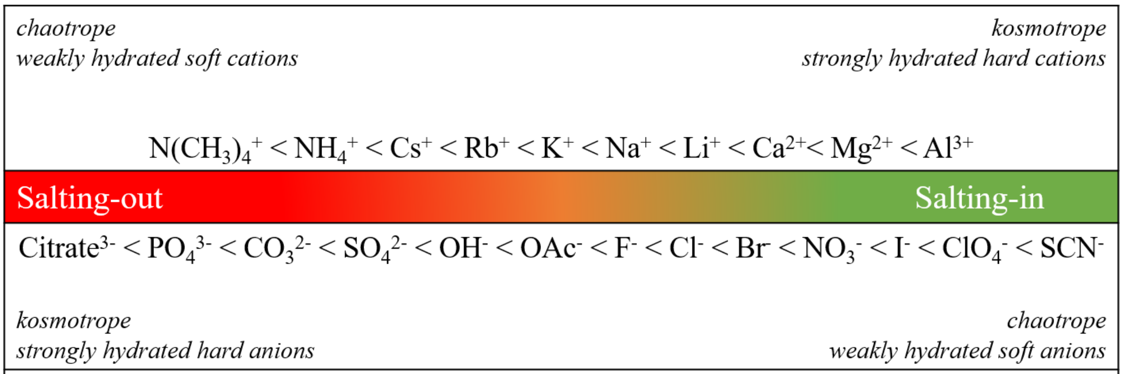

$N(CH_3)_4^+ < NH_4^+ < Cs^+ < Rb^+ < K^+ < Na^+ < Li^+ < Ca^{2+} < Mg^{2+} < Al^{3+}$

$Citrate^{3-} < PO_4^{3-} < CO_3^{2-} < SO_4^{2-} < OH^- < OAc^- < F^- < Cl^- < Br^- < NO_3^- < I^- < ClO_4^- < SCN^-$

	Properties and Effects of Anions	
↓	*protein denaturation*	↑
↑	*protein stability*	↓
↑	*surface tension*	↓
↓	*solubility of hydrocarbons*	↑

Figure II.3. Direct Hofmeister series for anions and cations based on precipitation studies of negatively charged proteins and some important properties and effects of the anions.

Regarding the *direct order*, ions on the left are effective in protein precipitation (salting-out) and prevent protein unfolding (structure stabilisers), while ions on the right are less efficient in salting-out proteins or may even increase the solubility of proteins in water (salting-in) and promote the denaturation of proteins (structure destabilisers). The border between both effects is usually drawn at the chloride anion and the sodium cation. Specific anion effects are generally more pronounced compared to specific cation effects if the ion-water interactions are dominant. This is due to stronger interactions of water with anions compared to cations with the same size and absolute charge density[208]. In many publications, dealing with specific ion effects, only the anion series is displayed[209,210]. At a first glance, the ion effects seem to correlate with the polarisability or charge density of the ions. In case of anions, the polarisability increases from left to right. That means, salting-out anions are unpolarisable, hard anions and the salting-in anions are polarisable, soft anions. Regarding the halide ions, the series is directly related to the ion size, with the large I^- as the least effective halide ion in precipitating proteins from aqueous solution. For the cations, the ordering is just the opposite. Here, the salting-out cations are polarisable, soft cations and the salting-in cations are unpolarisable, hard cations. As an example, the alkali ions are more effective in protein precipitation (more salting-out) as the ion size increases. The polarisability of the cations decreases from left to right. This asymmetry between anions and cations is generally attributed to different charged and nonpolar groups on the surface of proteins, with which the ions interact in different ways[208], which will be explained in a following paragraph.

II.2.2 Water Structure

The interaction of ions with water results in the formation of hydration shells, within the water molecules are rearranged around the ions with a different structure compared to that of water in the bulk. Small ions with high charge density remain highly hydrated in the bulk whereas large ions with low charge density are weakly hydrated. This structured water around the ions is definite and undisputed[211]. A long-time accepted picture for the origin of specific ion effects (salting-in and salting-out) was that of ions affecting the hydrogen-bond network of liquid water throughout the entire solution. Indication for such long-range alterations of the water structure is given by viscosity measurements of aqueous electrolyte solutions[212,213]. The influence of ions on the water viscosity, which is described by the Jones-Dole expression[214] (Eq.(II-14)), lead to the conclusion that some ions enhance the structure of water (positive viscosity B coefficients, “water structure makers”) and others disrupt the structure of water (negative viscosity B coefficients, “water structure breakers”)[215]:

$$\left(\frac{\eta}{\eta^*}\right) = 1 + A\sqrt{c} + Bc \qquad \text{(II-14)}$$

with η being the viscosity of the solution, η^* being the viscosity of pure water, c being the ion concentration and A as well as B being constants. A is related to electrostatic interactions, whereby B is attributed to the influence of ions on the hydrogen-bond structure. In Table II-1, Jones-Dole viscosity B coefficients of some cations and anions are presented.

Table II-1. Jones-Dole viscosity *B* coefficients. Values for phosphate, formate and perchlorate stem from reference[216]. All others values stem from reference[217].

Cations	*B*	Anions	*B*
Mg^+	0.385	PO_4^{3-}	0.590
Ca^+	0.285	$CH_3CO_2^-$	0.250
Ba^+	0.22	SO_4^{2-}	0.208
Li^+	0.150	F^-	0.10
Na^+	0.086	HCO_2^-	0.052
K^+	−0.007	Cl^-	−0.007
NH_4^+	−0.007	Br^-	−0.032
Rb^+	−0.030	NO_3^-	−0.046
Cs^+	−0.045	ClO_4^-	−0.061
		I^-	−0.068
		SCN^-	−0.103

Further experimental indication is given by different mobilities of the ions in water observed by conductivity measurements. The ionic mobility in water can be described by the Zwanzig equation[218,219], which accounts for the hydrodynamic size of ions and the polarisability of the solvent. Ions with low charge density (loosely bound hydration shell, less hindered) have a higher mobility than ions with a high charge density (strongly hydrated), predicted by the Zwanzig equation[220]. This is a second argument for enhancing or breaking the hydrogen-bond network in water induced by ions. However, the two previous mentioned observations are based on macroscopic properties (viscosity and conductivity), which do not allow to distinct between water in the hydration shell and water in bulk. The current view of the large influence of ions on the water viscosity is rather the formation of rigid (long lifetime) hydration shells and not the change of the bulk hydrogen-bond network. Thus, in the context of viscosity, the hydrated ions are seen as more or less charge neutral colloid particles in pure liquid water, which can be rationalised by the Einstein equation for suspended particles in a liquid[221].

The terms "kosmotrope" (strongly hydrated hard ion) and "chaotrope" (weakly hydrated soft ion) were designated to "water structure makers" and "water structure breakers", respectively[197,211]. Due to the water withdrawing effect, kosmotropes are enclosed by water molecules with a higher density compared to bulk water and were assigned rather to be salting-out. The opposite holds for chaotropes (less water withdrawing), which were assigned rather to be salting-in due to their tendency to nonpolar surfaces and the resulting solubilisation effect. This simple concept is appealing but can be very misleading, which is why it is quite controversial[222]. First, because it is the chaotropic cations, which are on the salting-out side in the *direct* Hofmeister series and the kosmotropic cations are salting-in[223]. Second, serious experimental[224–227] and computational[228] evidence showed that there is no significant water structure-making or water structure breaking effect for kosmotropes nor for chaotropes beyond the first hydration shell of the ions. Thus, the effect of ions on the hydrogen-bond structure in water was identified to be negligible[224]. However, the dynamic nature of liquid water presents a significant challenge in determining long-range structural effects beyond the first hydration shell[229]. The hydrogen-bond network, the water molecule reorientation time or the residence time of water in the hydration shells are aspects of an ongoing discussion about ordering or disordering the water structure and are frequently debated, e.g. by Yizhak Marcus[211,230,231]. He argued that the high salt concentrations, at which the femtosecond pump-probe spectroscopy[224,225,232] experiments were carried out, are not appropriate to gain information about the structure of water in electrolyte solutions. At such high concentrations of electrolytes (3M $Mg(ClO_4)_2$, 6M $NaClO_4$, 6M KF, NaCl, NaBr, NaI), there is no free bulk water left[230], to which a comparison of water in the hydration shells could be done. Hence, the conclusions drawn from femtosecond pump-probe spectroscopy cannot be directly transferred to dilute solutions. In addition, only the effects of ions on the reorientation dynamics of water were considered and thus only a limited insight to the general problem was given. Yizhak Marcus pointed out that the structure of water should be described by the extent of the hydrogen-bonding network instead of its strength or its dynamics[211]. He is still adamant about the classification of ions into water structure-makers and water structure-breakers as a guide to order the ions following their effects on macroscopic properties (e.g. viscosity) in dilute solutions. Although there are similarities to the Hofmeister series, ion effects in dilute solutions should not be directly related to ion effects near surfaces like in protein solutions[231]. Thus, the prediction of whether a particular ion will induce salting-in or salting-out on a macromolecule cannot be done on the basis of the properties of the salt/water solution alone[222,233]. So, it is unlikely that the Hofmeister series originates solely from structuring effects of water induced by ions.

The expressions kosmotrope and chaotrope are favoured in biophysical literature and are of historical importance, which is why they are still often used, also in this manuscript. Originally, chaotropicity had nothing to do with the water structure, but rather with the structure of macromolecules, like proteins or DNA, in solution[233,234]. The meaning of the ion classification into kosmotropes and chaotropes is no longer related to long-range "water structure" but rather to the degree of ion hydration.

Another, more recent study by Tielrooij et al.[235] showed that certain salts can indeed change water reorientation dynamics at a longer distance. The hydration structure of a strongly hydrated ion depends crucially on the counterion. If the counterion is weakly hydrated, the hydration shell of the strongly hydrated ion can be described as semi-rigid (reorientation of water is restricted only in a certain direction). In contrast, if the counterion is strongly hydrated, cooperative effects lead to rigid hydration structures and the reorientation dynamics of water molecules are affected well beyond the first hydration shell, e.g. for salts like $MgSO_4$ and Na_2SO_4. In case of the combination of two weakly hydrated ions, the local water dynamics appear to be unaffected and thus, no structure-breaking effect was found, e.g. for the salt CsI. These results show that the effect of ions and counterions on water dynamics can be strongly interdependent and nonadditive[235,236].

II.2.3 Collins Concept of Matching Water Affinities

A relatively simple concept to rationalise ion-specific phenomena and ion pairing was proposed by Collins, which allows to qualitatively understand multiple experimental findings in biology and colloidal science, including the Hofmeister series[208]. The "*law of matching water affinities*" (LMWA) is based on the relative strength of water-water and water-ion interactions in aqueous solutions[237–241]. Some experimental findings about ion hydration, which lead to the development of Collins ideas are given in the following paragraph.

Chromatography experiments on Sephadex G-10 (beads of crosslinked dextran with non-polar surface and small pore size) showed that protein stabilising (protein precipitants) anions are cleanly separated from protein destabilising (protein denaturants) anions. The sequence of halide ion elution follows directly the trend of their ion size (charge density). Meaning, the interaction of the bigger iodide ions (chaotrope) with the stationary phase is more pronounced compared to that of small fluoride ions (kosmotrope). The driving force for this adsorption is the release of weakly bound water from the hydration shell around chaotropes and the formation of strong water-water interactions in the bulk. Kosmotropes do not adsorb onto the stationary phase due to their stronger interaction with water molecules in their hydration shell compared to the water-water interactions[242,243]. The separation of the same two groups of ions is observed by the Jones-Dole viscosity B-coefficients, with positive B-coefficients for kosmotropes and negative B-coefficients for chaotropes, see Table II-1. In addition, negative charges on proteins (carboxylates) are strongly hydrated in contrast to positive charges on proteins (ammonium), which are weakly hydrated. The major intracellular anions (carboxylates and phosphates) are strongly hydrated, whereas the major intracellular cations (K^+ and positively charged amino acid side chains) are weakly hydrated. These different water affinities of ions are most import to ensure the proteins carrying charges within the living cells. The charged macromolecules will stay in solution and will not precipitate by the influence of the soft counter-ions[237]. High resolution X-ray crystallographic studies of protein-water interactions confirmed the hydration properties of simple ions analogue to the Jones-Dole viscosity B-coefficients. Aspartate and glutamate side chains, both carrying two carboxylate groups, are found to be most extensively hydrated within grooves of the proteins’ surface[244]. Neutron and X-ray diffraction of ions in aqueous solution further supports the relation between ion hydration and ion surface charge density[245].

In Collins model, the ions are considered as spheres with a point charge in its centre and water is considered as a zwitterion with ideal cation and anion size (no preferential interactions with nearby water molecules). In Figure II.4 a), the water zwitterion is drawn on the level of the strength of the water-water interactions, which separates kosmotropes (Na^+, F^-..) from chaotropes (K^+, Cl^-..). An ion is defined as chaotrope or kosmotrope, respectively, if the water-ion interactions are weaker or stronger compared to the water-water interactions. The water-ion interaction is decreasing with increasing ion size due to the larger distance between the point charge of the ion and the oppositely charged portion of a surrounding water molecule. Thus, the chaotropic ions are referred to as "big" ions compared to the "medium" sized water zwitterion. Accordingly, kosmotropes are referred to as "small" ions[238].

The LMWA states that oppositely charged ions will only form inner sphere ion pairs, if their respective hydration energies (considered to be a measure of water affinities) are similar. In simple terms, a kosmotropic (small) cation likes a kosmotropic (small) anion and a chaotropic (big) cation likes a chaotropic (big) anion[237,246], see Figure II.4 b).

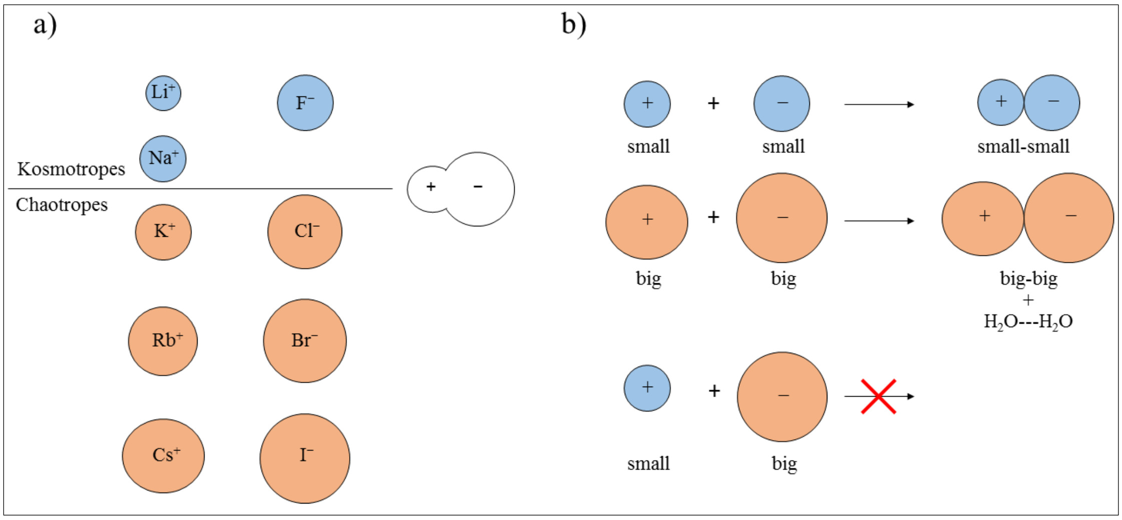

Figure II.4. a) Division of the alkali cations and the halide anions into strongly hydrated kosmotropes and weakly hydrated chaotropes. Ion sizes are approximately to scale. Water is shown as a zwitterion of ideal cation and anion size (no preferential interactions). The separation line between kosmotropes and chaotropes represents the strength of water-water interactions. b) Ion size determines the formation of inner sphere ion pairs.

In the following, the different scenarios of ion pair formation pictured in Figure II.4 b) are treated separately for convenience with a focus on water-water and water-ion interactions. In general, the strength of the interactions is decreasing in the order: kosmotrope-kosmotrope > kosmotrope-water > water-water (reference energy of interaction) > chaotrope-water > chaotrope-chaotrope.

Kosmotrope-Kosmotrope

The combination of two kosmotropes to ion pairs is energetically favourable, because their strong electrostatic mutual attraction overcompensates the energy cost of ion dehydration. This is due to the closer approach of the point charges of two small kosmotropic ions compared to the approach of the point charge of one small kosmotropic ion and the medium sized oppositely charged portion of a water molecule.

Chaotrope-Chaotrope

The combination of two chaotropes to ion pairs is also energetically favourable, although the interaction between two big chaotropic ions is weak. The reason for the energy gain is the release of loosely bound water molecules from the hydration shells of big chaotropic ions, which leads to the formation of new strong water-water interactions in the bulk phase.

Kosmotrope-Chaotrope

The combination of a kosmotropic and a chaotropic ion will not result in the formation of an ion pair because the interaction of a small kosmotropic ion with a charged portion of the medium sized water molecule is stronger (closer approach of point charges) than that of a small kosmotrope with a big chaotrope. In other words, the energy gain by breaking the chaotrope-water bond (imply new water-water bonds) and the formation of an ion pair does not compensate the energy cost of breaking the strong kosmotrope-water bond. Thus, the kosmotrope will not lose its hydration shell and the two ions will stay separated by water molecules.

The volcano plot, shown in Figure II.5 (A), is a presentation of the standard heat of solution of crystalline alkali halides at infinite dilution versus the difference between the absolute heats of hydration of the corresponding gaseous cations and anions. The correlation of thermodynamic properties of salts and single ions at infinite dilution lead to the development of Collins´ concept of matching water affinities. Salts with comparable heats of ion hydration are located above the zero line of enthalpy of solution. Those salts are identified in Figure II.5 (B) as chaotrope-chaotrope or kosmotrope-kosmotrope combinations, which produce cold solutions upon dissolution. The oppositely charged ions of the salts will tend to form ion pairs as described in the scenarios above. If the difference of water affinities of the constituent ions is larger, the salts are located below the zero line of enthalpy of solution. In this case (chaotrope-kosmotrope or kosmotrope-chaotrope combination, see Figure II.5 (B)), hot solutions are often produced, which indicates strong interaction between the small kosmotropic ion and water. The oppositely charged ions of the salts will stay separated upon dissolution. For an exothermic heat of solution (hot solution), it requires the dissolution of a salt constituent of ions with mismatched water affinities, since the hydration of the kosmotrope (from large chaotropic partner to medium sized water) and chaotrope (from small kosmotropic partner to medium sized water) will generate or take up heat, respectively. The net effect of the ion hydration processes then is decisive to obtain a hot or cold solution. An example for a salt composed of ions of mismatched water affinities, which leads to cold solutions upon dissolution is ammonium sulphate (chaotrope-kosmotrope combination)[237,238,240,241].

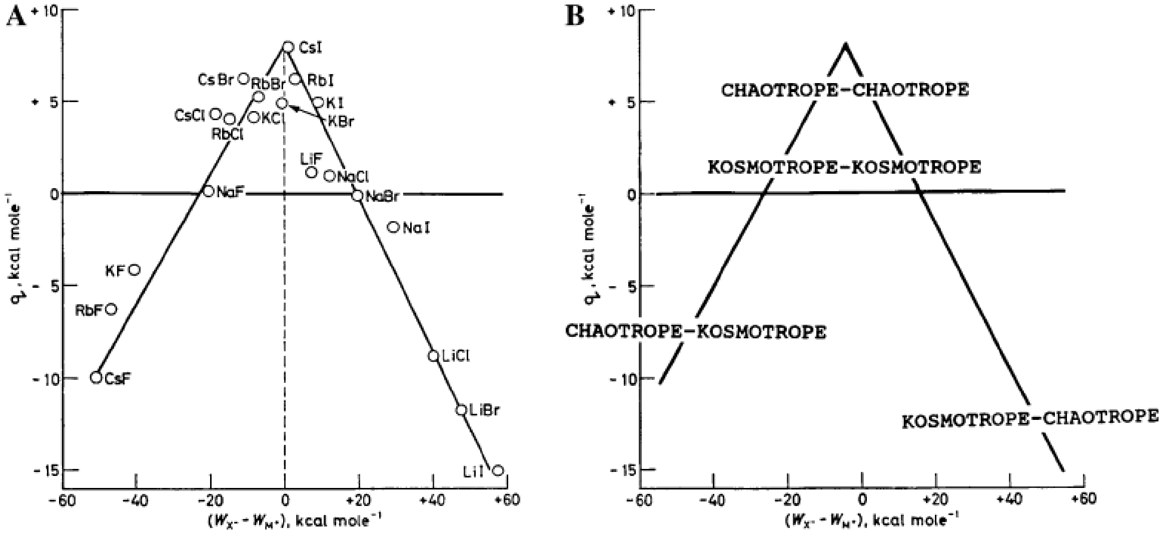

Figure II.5. (A) Relationship between the standard heat of solution of a crystalline alkali halide (at infinite dilution) in kcal^{-1} and the difference between the absolute heats of hydration of the corresponding gaseous aqueous anion and cation, also in kcal^{-1}. (B) Identification of ions as chaotropes or kosmotropes. The enthalpy of solution of chaotrope-chaotrope and kosmotrope-kosmotrope salts is positive, whereas the enthalpy of solution of chaotrope-kosmotrope and kosmotrope-chaotrope salts is either negative (gives off heat) or positive (takes up heat). The figure was taken from ref.[238] after Morris[247].

In Table II-2, the water solubilities of alkali halides are presented and the least soluble halides in each column are underlined. Salts composed of two small or two big ions show least water solubilities, whereas the combination of a small and a big ion results in high water solubility. If lattice enthalpies are ignored, the tendency of ions to form inner sphere ion pairs in solution according to the LMWA show a notable relationship to the salt solubilities[237].

Table II-2. Water solubilities of alkali halides in molarity [mol/L]. The table was adapted from ref[237] after Lee[248].

M	MF	MCl	MBr	MI
Li	0.1	19.6	20.4	8.8
Na	1.0	6.2	8.8	11.9
K	15.9	4.8	7.6	8.7
Rb	12.5	7.5	6.7	7.2
Cs	24.2	11.0	5.1	3.0

This model is somewhat an extension of the general rule “like dissolves like” or “like seeks like”, which every chemist is familiar with[203,237].

A strong reinforcement of Collins LMWA is given by the qualitative explanation of the reversal of the mean activity coefficients of simple electrolyte solutions[194,208,249] and by the different affinity of charged headgroups of surfactants for different counter ions[194,208,250].

The mean activity coefficients of alkali metal salts follow a reversed cation order with a change of anions. At a given concentration, the mean activity coefficients of bromide or iodide salts increase with increasing charge density of the cations $Cs^+ < Rb^+ < K^+ < Na^+ < Li^+$ while for acetates, hydroxides or fluorides the mean activity coefficients decrease with increasing charge density of the cations $Cs^+ > Rb^+ > K^+ > Na^+ > Li^+$. As low mean activity coefficients indicate ion association, the hard acetate, hydroxide or fluoride anions interact stronger with hard cations (Li^+) and the soft bromide or iodide anions interact stronger with soft cations (Cs^+), which is in line with the LMWA[194,208,246].

In a series of experiments, Vlachy et al. studied the influence of added alkali chlorides on the micelle-to-vesicle transition in aqueous mixtures of anionic and cationic surfactants[250–252]. In general, the addition of all salts induced vesicle formation by increasing the packing parameter (screened electrostatics and headgroup dehydration) and the aggregate size increased with increasing salt concentration. Due to the negatively charged aggregate surface in surfactant mixtures of sodium dodecylsulphate (SDS) and dodecyltrimethylammonium bromide with SDS in excess, no significant anion specificity was found for the vesicle growth. In contrast, a strong cation influence on the hydrodynamic radii of the catanionic aggregates was expected and confirmed. As the critical salt concentration for vesicle formation decreased in the order LiCl > NaCl > KCl ~ RbCl ~ CsCl, the ability of cations to increase the hydrodynamic radii follows a direct Hofmeister series: $Cs^+ \sim Rb^+ \gtrsim K^+ > Na^+ > Li^+$ [251]. If SDS was replaced by sodium dodecyl carboxylate (SL), similarly no anionic specificity was found, but the cation series appeared to be inverted. The ability of cations to increase the hydrodynamic radii followed the order: $Li^+ > Na^+ > K^+ \sim Cs^+$, which is a reversed Hofmeister series[252]. Again, the LMWA provides a qualitative explanation for this reversal. The single charged alkyl sulphate headgroup possesses rather chaotropic character in contrast to the doubly charged sulphate anion[251]. Thus, chaotropic cations like Cs^+ come into closer vicinity to alkyl sulphate headgroups compared to kosmotropic cations like Li^+ and screen more effectively the negative charge of the headgroup. Consequently, the headgroup will be less hydrated (increase of the packing parameter) and the formation of bigger aggregates is promoted. The carboxylate headgroup exhibit higher charge density than the alkyl sulphate headgroup and interacts more strongly with kosmotropic cations, which was observed by the increased aggregate radii resulting from the addition of alkali chlorides comprising kosmotropic cations[252]. With the identification of carboxylate headgroups being of kosmotropic nature, the reversed order of cations in the Hofmeister series (Figure II.3) is also explained. The combination of computational results and the LMWA allowed a general description of ion-headgroup interactions for many systems and applications. The proposed ordering of headgroups is carboxylate > phosphate > sulphate ≈ sulfonate with the most kosmotropic one on the right and most chaotropic one on the left[250]. Similarly, an ordering of cationic headgroups (alkyl ammonium cations) exist for interactions with counter anions[253].

II.2.4 Ion-Surface Binding Affinities

The idea that kosmotropes and chaotropes provoke structural changes in the water network beyond the first hydration shell of the ions, as described in section 2.3.1.2, and in turn affects the physico-chemical properties of the substances in solution was set aside due to serious experimental and theoretical evidence against long-range water structure alterations. Additionally, a diverse spectrum of direct, altered and reversed Hofmeister series have been discovered, which are not always in line with the modification of the bulk properties. Consequently, direct ion-macromolecule interactions as well as interactions between ions and the water molecules from the first hydration shell of the macromolecule were set into the focus of researchers investigating specific ion effects[208,210,254].

An important insight concerning the behaviour of ions near surfaces was presented by Jungwirth et al.[255,256]. Usually, salts increase the surface tension of water[257,258], which was interpreted by ion depletion at the interface[259]. However, the simulations of halide ions at the air-water interface by Jungwirth et al. have shown that the small halide ion F^- is repelled from the interface, while the bigger halide ions like Cl^- and Br^- are slightly present at the interface and I^- is even attracted to the hydrophobic water-air interface. These predictions have been confirmed by electron spectroscopy measurements[260] and by grazing incidence x-ray fluorescence[261]. Enrichment of the big polarisable thiocyanate anion at the water-air interface was also verified experimentally *via* vibrational sum frequency spectroscopy[262]. With these findings the direct anion Hofmeister series can be easily explained. Hard (small, unpolarizable) ions (F^-), which are strongly repelled from hydrophobic surfaces, raise the interfacial tension and cause proteins to minimize their surface area exposed to the surrounding solvent by folding into compact structures (native protein structure stabilizer). These ions will also promote the adhesion of hydrophobic surface patches resulting in the precipitation of the macromolecules by aggregation (strong precipitators). By contrast soft (large, polarizable) ions (I^-, SCN^-), which are less repelled or even attracted to hydrophobic surfaces, decrease the interfacial tension and promote protein unfolding (denaturant) by hydrophobic solvation. The adsorbing ions will also give an effective negative charge to the hydrophobic surfaces, which leads to surface-surface repulsion and thus inhibit precipitation and may even enhance the solubility (salting-in) of the protein[195].

In a series of papers, Schwierz et al.[195,199,204] studied the influence of surface properties such as polarity, charge and chemical structure on the adsorption behaviour of halide anions and alkali cations by applying a two-step modelling approach. In a first step, they used molecular dynamics (MD) simulations to calculate the free energy profile or potential mean force (PMF) accompanied by ion adsorption at different surfaces (hydrophobic or hydrophilic). In the simulations, self-assembled monolayers (SAM) with different terminal groups were used. The hydrophobic surface was represented by a SAM with methyl (CH_3) end groups while the hydrophilic surface was represented by SAMs with hydroxyl (C_2OH), carboxyl (COOH) and charged carboxylate (COO^-) end groups. Correct ion-water and ion-ion interactions were ensured by optimized force field parameters for anions and cations, which reproduced thermodynamic solvation properties[263]. The calculated PMFs of ion-surface adsorption imply contributions of ion hydration and direct ion-surface interactions. In a second step, the interaction potentials were incorporated to the Poisson-Boltzmann theory to quantify long-range electrostatic forces, which stabilize solutes against precipitation (salting-in). With this information, orderings of ions analogue to the Hofmeister series or its reversal were constructed.

These studies were motivated by former experimental evidence of Hofmeister alterations in a wide variety of colloidal systems with different hydrophobic or hydrophilic surface character and a pH-dependent charge sign. The colloidal stability, depending on the surface properties and the present electrolyte, was used to classify the involved ions according to the Hofmeister series. Typical Hofmeister series inversions from direct to indirect were found by the change of surface charge from negative to positive as well as and more noteworthy, by the change of the surface nature from hydrophobic to hydrophilic, respectively[264].

Anion Adsorption

The investigations of Schwierz et al. concerning the specific anion (F^-, Cl^-, I^-) adsorption at surfaces of varying charge and polarity revealed that a direct anion Hofmeister series is obtained at negatively charged nonpolar surfaces and at positively charged polar surfaces. In contrast, a reversed anion Hofmeister series is obtained if the charge of the nonpolar surface is changed from negative to positive or if the polarity of the negative charged surface is changed from hydrophobic to hydrophilic[199]. These theoretical considerations and calculations are supporting the previous found experimental results[264].

In detail, at **hydrophobic** surfaces (methyl end-group), large anions are attracted, which results in negative surface potentials leading to surface-surface repulsion and salting-in behaviour. Even though the nonpolar surface is negatively charged, and electrostatic repulsion will reduce the adsorption of anions, the direct Hofmeister series will retain because large anions are less repelled compared to small anions. Thus, a higher negative surface potential will result in NaI solutions than in NaF solutions. Simulated snapshots of anions near the nonpolar surface at the distance of minimum PMF for I^- show that the hydration shell of the iodide ion is partially stripped off in contrast to the smaller anions. This behaviour is connected to a hydrophobic effect or to hydrophobic solvation theory and is best described as surface modified ion hydration, which is also found at the water-air interface[265,266]. For hydrophobic cationic surfaces, the decrease of the surface potential will be more pronounced by strongly adsorbing I^- ions than by weakly adsorbing F^- ions. In this case, I^- will be salting-out and F^- will be salting-in, reflecting a reversed anion Hofmeister series. Partially Hofmeister alterations occur with the transition from negative to positive charged hydrophobic surfaces.

At **hydrophilic** surfaces (hydroxyl end-group), the surface affinity decreases with increasing anion size: $F^- > Cl^- > I^-$. In this case, the anion specificity is less pronounced but a reversed Hofmeister series can be detected. Simulated snapshots of anions near the polar surface show that F^- forms two hydrogen bonds with surface OH-groups. The preferential adsorption of small anions of high charge density to the small hydrogen on the OH-group of high charged density resembles to the LMWA of Collins[237,238]. The formation of ion pairs between small anions and surface hydrogen atoms counterbalances the dehydration of kosmotropic anions.

Cation Adsorption

The investigations of Schwierz et al. were extended to mixed surfaces with polar and nonpolar groups and the effect of surface charge and surface polarity were considered for both anions and cations[195]. At neutral **hydrophobic** surfaces (methyl end-group), the cation surface affinity correlates with the ion size and follows the series $Cs^+ > K^+ > Na^+$, which agrees with experimental observations of cation adsorption on silica surfaces[267,268]. Similar to the behaviour of anions, large cations like Cs^+ adsorb strongly on nonpolar surfaces and increase the surface potential of neutral and cationic surfaces. In this case, large cations are salting-in and small cations like Na^+ (repelled from nonpolar surface) are salting-out, which is the reversed Hofmeister series. For anionic surfaces (usual the case for most proteins), large cations will reduce the surface potential more than small cations and thus large cations like Cs^+ will be salting-out and small cations like Na^+ will be salting-in, resulting in the direct Hofmeister series. This is the reason for the asymmetry of cations and anions in the Hofmeister series. There is one exception in the cation series as Li^+ is less repelled from hydrophobic surfaces than Na^+ and K^+. This behaviour is explained by the strong binding of the first hydration shell around the lithium cation, which makes it appear larger. Simulated snapshots of cations near the nonpolar surface at the distance of minimum PMF for Cs^+ show that the first hydration layer of all cations remains intact at separations larger than this distance.

If the surface is **hydrophilic** (hydroxyl end group), the situation is more complex in particular for cations. The oxygen atom of the OH-terminated surface has an intermediate surface charge density and the cation affinity decreases in the order: $Li^+ > Cs^+ > Na^+ > K^+$, which is a partially altered series. At large salt concentrations or large positive surface charge, an indirect order is found with Cs^+ as most salting-in and Na^+ as most salting-out cation. A direct series is never observed. Generally, the ordering of the cations is less pronounced compared to that of anions, which is due to the smaller size of ordinary cations and a smaller ion-size difference compared to anions. In addition, the complexity of ion adsorption at hydrophilic surfaces by means of the interplay between ion and surface hydration, the surface group geometry and the ion size, leads to multiple alterations of the cation series depending on surface charge and salt concentration. Thus, the cation series at hydrophilic surfaces do not follow that clear ordering as for anions.

The picture of the specific ion effects gained from the studies of Nadine Schwierz et. al. contributes to a more general explanation of the Hofmeister series. A relatively simple and almost symmetrical pattern can be extracted, as presented in Figure II.6. The only odd boxes in the pattern are those for cations at hydrophilic surfaces. In this situation, a direct series is never obtained, and the effects are generally less pronounced and less defined compared to the other scenarios.

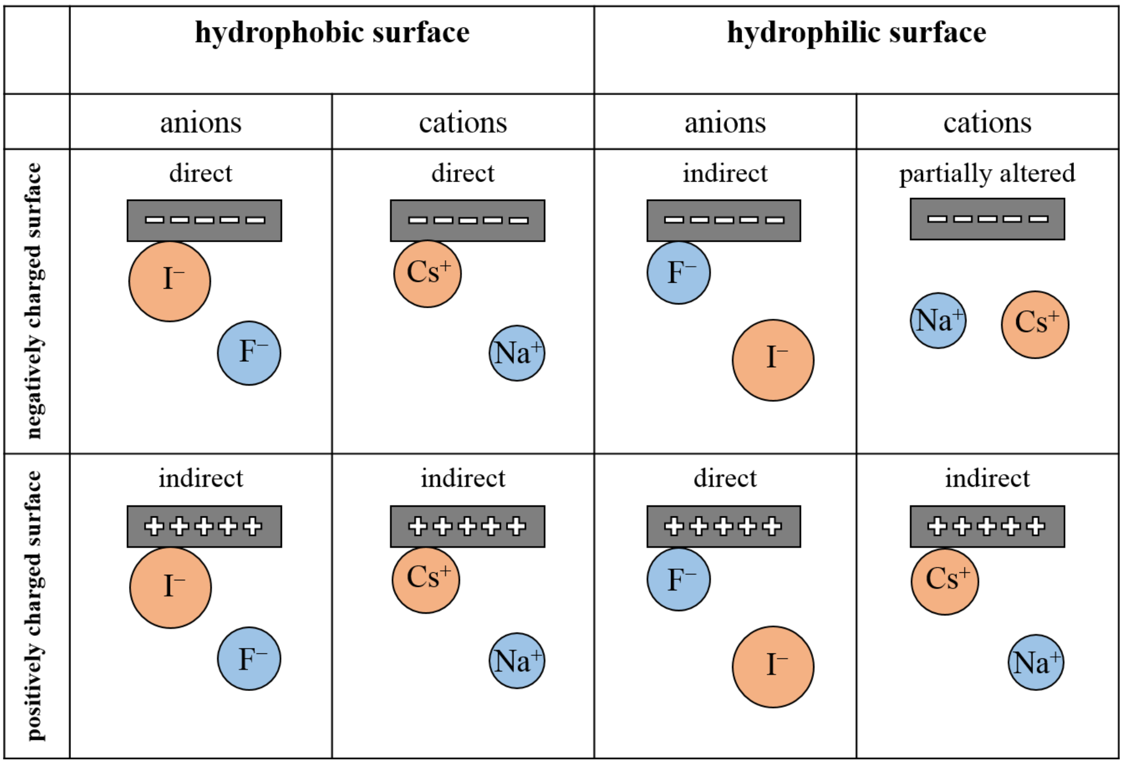

Figure II.6. Schematic representation of different affinities of small (blue) and big (orange) ions for surfaces with varying polarity and charge. Big ions preferentially adsorb at hydrophobic surfaces and small anions are more attracted to hydrophilic surfaces. Depending on the charge of the ion and the surface, either an increase or a decrease of the surface potential results. A direct Hofmeister series for anions and cations is obtained at negatively charged hydrophobic surfaces and for anions at positively charged hydrophilic surfaces. Indirect Hofmeister series for anions and cations are found at positively charged hydrophobic surfaces, for anions at negatively charged hydrophilic surfaces and for cations at positively charged hydrophilic surfaces. For cations at negatively charged surfaces the series is partially altered.

II.2.5 Solubility of Non-Electrolytes in Aqueous Electrolyte Solutions

Although the salting-in and salting-out effects are originally related to protein solutions represented by the Hofmeister Series, the salt effects were also found to be of great importance for small organic molecules in solution. Concerning the water solubility of small non-polar solutes like benzene in presence of electrolytes, the salt effect is nearly consistent with the original found Hofmeister Series (*indirect order*). That is, highly charged and hard (SO_4^{2-}) ions show a significant salting-out effect, while bigger, polarisable (Cs^+, I^-, ClO_4^-) and organic ($(CH_3)_4N^+$) ions are salting-in, independently of the sign of ion charge. Nevertheless, inconsistency remains, because lithium chloride shows a smaller salting-out effect on benzene than potassium or sodium chloride[194,195,208,269]. This feature is due to the pronounced hydration of Li^+ cations leading to a large hydrated ion of lower charge density[270]. Note that in the case of small non-polar organic molecules, the cation series is reversed to the commonly known cation series of the Hofmeister series. This is evident due the carboxylate or ammonium functional groups, which are present in protein chemical structures, but absent in non-polar organic molecules.

Many non-electrolytes are less soluble in a salt solution than in the corresponding pure solvent, which is the salting-out effect. The solubility of a non-electrolyte in water has been found to be dependent on the concentration and the type of salt in the mixture. At low non-electrolyte concentrations, self-interactions of the non-electrolyte can be neglected and the classical *Setchenov*[271] equation results, which relates the alteration of non-electrolyte solubility to the salt concentration:

$$\log\frac{S_0}{S} = k_s c_s = \log\gamma \tag{II-15}$$

where S_0 is the solubility of the non-electrolyte in water and S is the solubility of the non-electrolyte in the salt solution. The molar salt concentration is denoted by c_s, whereby k_s is the empirical *Setchenov* constant and γ is the molar activity coefficient of the non-electrolyte. In the review of Long and Mc Devit[269] about activity coefficients of non-electrolytes in aqueous salt solutions, several polar and unpolar non-electrolytes have been evaluted. Salting-out and salting-in are generally used to denote an increase and a decrease in the activity coefficient of the non-electrolyte with increasing concentration of the electrolyte[272]. Accordingly, positive values for k_s refer to salting-out and negative values to salting-in. Absolute k_s values are higher for salting-out than for salting-in effects. Salts composed of large ions (large partial molar volume) like the tetramethylammonium or naphtalenesulfonate ion, induce salting-in, while smaller ions usually induce salting-out. The trend of salting-out parameters k_s is the same for all nonpolar solutes. For alkali metal cations the order of increased salting-out is generally: Cs < Rb ≈ Li < K < Na. For halide anions a similar series holds: I < Br < Cl. For polar non-electrolytes, the strength of the salt effects depends strongly on the size and polarity of the neutral solute molecules. E.g. the salting-out effect from a given salt solution increases with size and decreases with polarity of the non-electrolyte[273]. A higher cation specifity compared to nonpolar solutes is commonly observed for acidic non-electrolytes, whereas for basic non-electrolytes theres is a higher sensitivity towards the anions (as it is also observed for the Hofmeister series). For acids the cation series changes to: K < Na < Li and for bases to: Li < Na < K. The salt effects are additive to relatively high salt concentrations. Molecular interactions between all species within the solution play a role if salting-out or salting-in effects are considered[269,274–276]. Among them the ion hydration and the interaction of the hydrated ions and the non-electrolyte. Interactions between the ions and the solute are partly shielded by the hydration shell[277].

Theoretical approaches for the prediction of *Setchenov* parameters have been presented by Debye and McAulay (electrostatic theory)[278], Long and Mc Devit (internal pressure/electrostriction theory)[269], Conway et al. (modified electrostriction theory)[279], Masterton and Lee (scaled particle theory)[280], Xie and Yang (modified scaled particle theory)[281] and Xie et al. (modified internal pressure theory)[282]. Solubilties of benzene, toluene, o-, m- and p-xylenes and naphthalene in water and in electrolyte solutions were measured at 25°C for 25 salts. The relation between log γ and c_s was found to be linear, according to Eq. (II-15). The above mentioned theories were applied to calculate the salting-constants k_s, whereby values obtained from the modified internal pressure approach agreed best with the experimental values[276].

Ni and Yalkowsky[283] provided *Setchenov* constants for 101 organic compounds in NaCl solution. They used the molar volume, the water solubility and log K_{ow} values as parameters for their correlations. The best correlation was observed between k_s and log K_{ow}, which was explained by the fact that log K_{ow} is a descriptor for the polarity of the solute.

Görgényi et al.[277] presented experimental Henry`s law constants for the non-electrolytes chloroform, benzene, chlorobenzene and anisole at 30°C for 28 electrolytes. Henry`s law constants were used to express the solubility changes, which were then correlated with Eq. (II-15) to obtain *Setchenov* constants. With the assumption of additivity for the ions *Setchenov* constants have also been determined for individual cations and anions. Cl^- was selected as reference for the calculation of the constants of the other ions. For all cations, a salting-out effect has been found, which depends strongly on the kind of cation but poorly on the counter anion and the organic solute. Most anions also showed a salting-out effect except the nitrate anions, which showed a salting-in effect. The effects of the anions were found to be more dependent on the counter cations than vice versa.

One important application of the salting-out phenomenon is the separation of very hydrophilic compounds like diols and organic acids from aqueous solution (salting-out extraction)[284].

As already pointed out in previous sections, a salting-out effect is caused by ions with high charge density (kosmotropes) and is dominated by the anions. The cation series is less defined and sensitive to the surface functional groups[207,269,285]. Anions have much larger ionic radii[286] and larger, more polarisable electron clouds than cations. On the other hand cations have more polarising power[277]. Salting-out of non-polar solutes is caused by the combination of electronic repulsion, ion hydration[269] and enhancement of the hydrophobic effect[287–289]. The latter leads to solute aggregation associated with a decrease in water accessible surface area and a gain in entropy for water molecules and ions. Thus, hydrated solutes are adverse and the solute aggregates leave the aqueous phase in favour of extraction, see Figure II.7 (left side). In case of highly polar solutes, molecular interactions are more complex and the described effects may be more specific.

The salting-in effects are two-fold. Ions with low charge density (chaotropes) cause a weakening of hydrophobic interaction due to preferential binding to the surface (through undirected attractive dispersion forces), see Figure II.7 (top on the right side). The charged surfaces lead then to solute-solute repulsion and thus to an increased water solubility (salting-in effect), see also section II.2.4. Chaotropic cations include Cs^+, NR_4^+, Ph_4P^+, pyridinium and guanidinium and chaotropic anions include BPh_4^-, SCN^-, BF_4^-, ClO_4^-, PF_6^-, I^- and ClO_4^- amongst others. Specific ion-surface binding is illustrated in Figure II.7 (bottom on the right side) and is the reason for variations of the cation series depending on the functional groups of the solute or protein[207,269,285]. Examples for a salting-in effect induced by cation binding to the carbonyl oxygen of the amide group is the removal of DMF from the organic phase using aqueous LiCl mixtures[290]. Specific cation binding is also generally observed in complex formations, e.g. during removal of pyridines from organic phases applying aqueous $CuSO_4$ solutions[291]. Typical metal cations, which show such behaviour are: Li^+, Mg^{2+}, Cu^{2+} and Al^{3+}. The salting-in effect caused by specfic binding is less pronounced compared to that attributed to chaotropic ions and dispersion forces. This is evident due to stoichiometric binding in the former case while multiple chaotropic ions can adsorb to the surface of the solute. The general guideline is that kosmotropes are salting-out and chaotropes are salting-in. Ion combinations of both types will have intermediate effects with chaotropic ions being dominant[292].

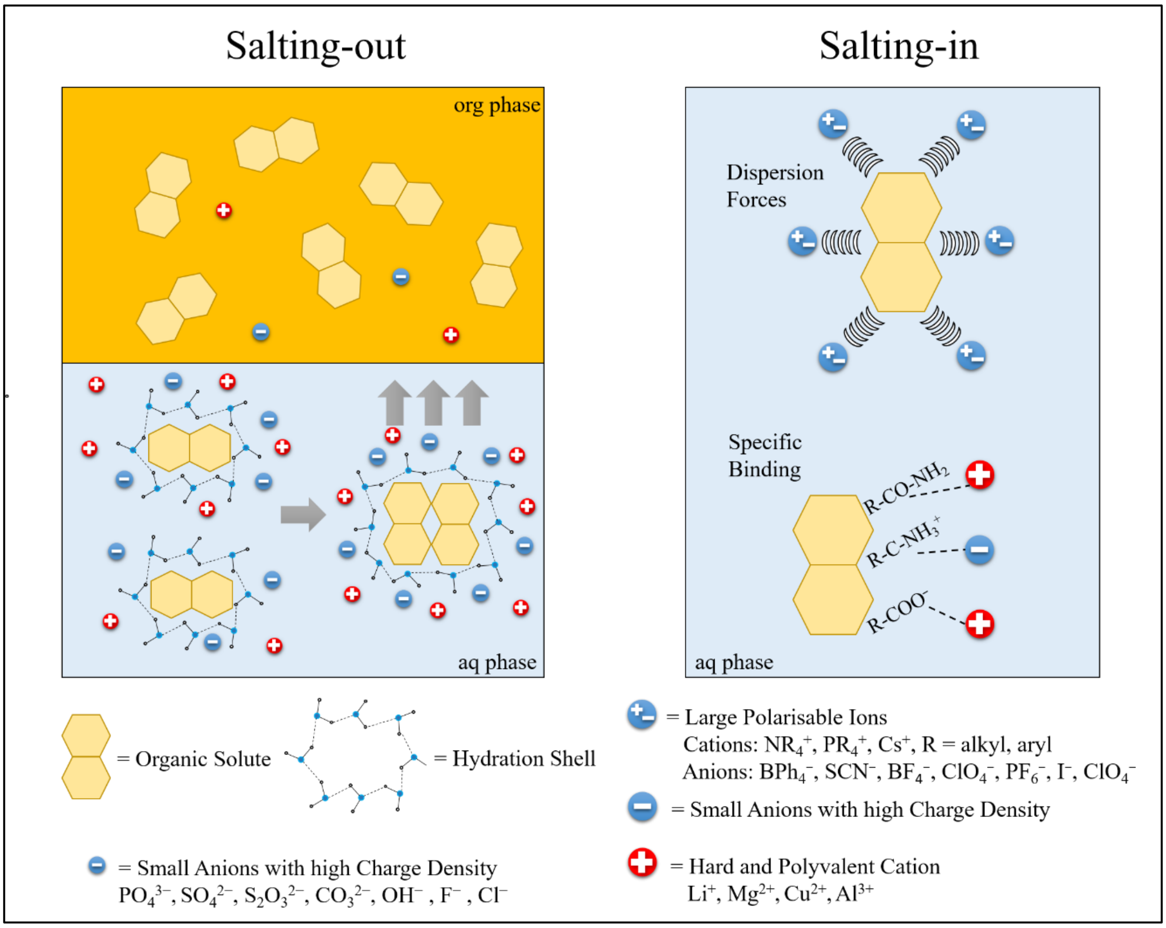

Figure II.7. Scheme of the salting machanisms. On the left: salting-out effect for LLEx induced by hydration and on the right: salting-in effect induced by dispersion forces and/or specific bindings to surface functional groups (right side). The figure was recreated from reference[292].

The salting-out effect leads to the enhanced distribution of a product between water and the organic solvent and also to a reduction of the mutual solubility of water and organic solvents, which improves LLEx performance. A big solubility gap between water and the extractive solvent is needed for a successful separation of the desired product from the aqueous phase. Solvent regeneration in a following distillation step is facilitated due to less residual water in the organic layer. Similarly, the solvent removal from the raffinate phase is less cost intensive due to a reduced solvent loss induced by the salt, see also section II.1.4. For very hydrophilic compounds, aqueous-two phase systems are frequently applied for the separation of extremely water soluble compounds. A prominent example is the system composed of water, PEG and salt. Such aqueous systems are safe, nontoxic and non-flammable and thus considered as environmental benign. The salting-out effect is apparent by the cloud-point lowering of the PEG solution[293].

In principle, organic solvents, which are completely miscible with water like THF, GVL, acetone, short-chain alcohols up to tert-butyl alcohol are also conceivable for LLEx, because, by the addition of salts, two liquid phases can be generated. Thomas Gerlach and Irina Smirnova[294] presented LLE data of quaternary systems composed of water, 1,3-PDO, a salt (K_2HPO_4, K_2CO_3, or Na_2CO_3) and a short-chain alcohol (ethanol, 1-propanol or 2-propanol), which were measured experimentally and predicted with an electrolyte extension of COSMO-RS developed by Ingram et al.[295]. $D^w(1,3\text{-}PDO)$ values were overpredicted by the model but a qualitative agreement was reached at lower salt contents. However, in cases of LLEx processes coupled to a subsequent distillation step for product purifiaction, the use an extraction solvent, which is at least partially miscible with water may be preferred in favour of the separation factor and less energy requirement for the distillation step. Very polar compounds like HMF or short-chain alcohols can act as co-solvent leading to higher mutual solubility of water and the extracting solvent. This decreases then the biphasic region for LLEx, which can be counteracted for by the addition of electrolytes. Unfortunately, the ion effects are very specific, which is why the predetermination of the influence of the electrolytes on the phase equilibrium of extraction system is very difficult without supporting experimental data.

Besides for the salting-in and salting-out effects in extraction and distillation, there are many more industrial and natural processes, for which the information on phase equilibria of electrolyte solutions is important. Some examples are: partitioning processes in biochemical systems; precipitation and crystallization processes in geothermal-energy systems or drilling muds; desalination of water; water-pollution control (waste-water treatment); production of natural gas from high pressure aquifiers where natural gas is in equilibrium with brines; food processing; and production of fertilizers[161].

To study the infuence of electrolytes on LLE is of scientific (molecular interactions between solvent, solutes and ions), ecologic and economic (energy and cost savings) interest.

II.3 Hydrotropy

Hydrotropy is the action of certain water-soluble organic molecules at high concentrations causing a significant increase in water solubility of hydrophobic molecules such as alcohols, aldehydes, ketones, hydrocarbons, esters, lipids and fats. The designation of the solubility enhancers to "*Hydrotropes*" was introduced by Carl Neuberg in 1916. According to Neuberg, hydrotropes consist of a hydrophilic anionic part and a hydrophobic aromatic ring or ring system, whereby the type of the anion and the counter cation are less important as long as they provide high water solubility[296]. The anionic part is usually a sulphate, sulfonate or carboxylate group and prominent representatives of anionic hydrotropes are sodium xylene sulfonate (SXS), sodium cumene sulfonate (SCS) or sodium benzoate (SB). The field of hydrotropes was extended to neutral and cationic species with a planar hydrophobic part by Saleh and El-Khordagui in 1989. The increase in water solubility of sparingly soluble organic molecules was explained by a stack-type aggregation (π-π stacking) of the planar hydrophobic parts of the hydrotropes and similar associative mechanisms with the solute to be solubilized. It was shown that the hydrophilic part of hydrotropes is not limited to bear anionic character[297].

In the studies of Balasubramanian, solubilisation experiments of the hydrophobic solute fluorescein diacetate in water using different hydrotropes have shown that the course of the solubility enhancement is not linear to hydrotrope concentration but rather sigmoidal shaped. This means that below a certain threshold concentration the solubilisation of the hydrophobic compound is very low or does not occur, but above this concentration, increasing solubilisation can be observed until the hydrotropic effect is depleted to a level-off plateau. The concentration, at which the hydrotrope gets effective is called minimum hydrotrope concentration (MHC) and differs for different hydrotropes used for the solubilisation of one hydrophobic compound. In contrast, similar values of the MHC are detected for one hydrotrope solubilising different hydrophobic solutes. Even sodium butylmonoglycol sulphate shows properties, which are characteristic for hydrotropes, which lead to the conclusion that hydrotropes are not limited to molecules with a planar hydrophobic moiety. Thus, hydrotropy is also attributed to short-chain aliphatic molecules with a hydrophilic group or more general to small amphiphilic molecules. The idea of the cooperative action of hydrotropes was supported by the comparison of the solubilising curves of perylene using the hydrotrope sodium p-toluene sulfonate, the salting-in compound guanidinium thiocyanate and the co-solvent or phase-mixing agent polyethylene glycol (PEG-6000). In case of the hydrotrope, the typical sigmoidal shaped curve was observed, while for the salting-in and the phase-mixing agent, the increase in solubilisation was monotonic. Thus, hydrotropy was also differentiated from co-solvency and the salting-in process[298].

P. Bauduin[299] criticised this differentiation of hydrotropy and co-solvency based on the solubilisation curve using PEG-6000. He argued that Balasubramanian et al.[298] made up their conclusions based on the investigation of one single co-solvent (PEG-6000) only, which is not even a good representative one for water. In his experiments solubilisation curves of the hydrophobic dye, Disperse Red 13 (DR-13), using the classical hydrotrope SXS, the co-solvents 1-propanol and acetone as well as the short amphiphiles propylene glycol monoalkyl ethers and 1-propoxy-2-ethanol (solvosurfactants) showed all an exponential increase (no sudden increase) and thus no hydrotropic efficiency, indicated by the MHC, could be precisely determined. Generally, the solubilisation of a hydrophobic compound increases slightly and monotonically at low and moderate co-solvent concentration and increases exponentially at very high concentrations[300]. However, in the PhD thesis of Bauduin[301], the MHC of the solubilisers was approximated by the intersection of the abscissa with the tangent at the linear part of the solubility plot where solubilsation becomes significant. SDS was also tested to show that DR-13 behaves like a classical hydrophobic compound and in this case the solubilisation curve has the sigmoidal shape as expected. The fact that no sigmoidal profile could be observed for the co-solvents, solvosurfactants and in particular not even for SXS lead to doubts concerning the concept of the MHC. The author proposed a more general method to determine the hydrotropic efficiency by the comparison of the slopes of the linear part in the log-linear graphical presentation of solubility against the solubiliser concentration. In addition, the volume of the hydrophobic part of the hydrotropes was attributed to the hydrotropic efficiency. In this manner, it was shown that the extent of the hydrophobic parts, following the order: SXS > C_3PO_1 > C_3EO_1 > 1-propanol ≈ acetone, correlates with the efficiency to dissolve hydrophobic compounds[299,301], surface tension measurements[302,303] and the lowering of the critical micelle concentration (CMC) of surfactants in water[304]. The occurrence of an aromatic ring in a hydrotrope (e.g. SXS) may enhance hydrotropy by special attractions between the rings, but it is not crucial nor a precondition for the hydrotropic effect[299].

The appearance of a MHC resembles to the more prominent cooperative behaviour of surfactants in aqueous solution by the formation of micelles above a certain concentration named CMC. In case of hydrotropes, this cooperative behaviour is not the aggregation to defined ordered structures like micelles but rather an association in consecutive steps to from dimers, trimers etc.[305]. The interactions within the described non-covalent assembled complexes are weak, but the formed assemblies provide a microenvironment of lowered polarity, which helps to solubilise hydrophobic solutes in water[306]. The most distinctive difference between surfactants and hydrotropes is the concentration, at which the cooperative actions are appearing. Typically, CMC values are in the millimolar range or less whereas MHC values are in the molar range[299]. This is evident due to their different chemical structures. Hydrotropes bear a higher hydrophile-lipophile balance compared to surfactants, which leads to a higher water solubility and a less pronounced self-aggregation or cooperative behaviour driven by the hydrophobic effect. As a consequence, hydrotropes show its aggregating tendency at much higher concentrations but provide in turn a higher and more selective solubilisation of hydrophobic compounds[307,308]. However, without a third hydrophobic compound the self-aggregation of hydrotropes in water is weak[309].

The surface activities of hydrotropes and surfactants are in line with their solubilisation and aggregation behaviour as the decrease of the surface tension appears at much higher concentrations for hydrotropes than for surfactants. The characteristic kink in the plot of surface tension against surfactant concentration is related to the CMC, similarly for hydrotropes to the MHC. However, the MHC and the concentration, at which the surface tension levels-off are similar, but not always identical[298,308,310–313]. Short amphiphiles show relatively high critical aggregation concentrations (CACs) or minimum aggregation concentrations (MACs) corresponding to the course of the surface tension against molar concentrations. For hydrotropes, the terminations CAC or MAC are preferred to CMC to distinguish the different association phenomena[314]. It was shown that in order to correctly evaluate and interpret the surface tension data, the activity must be used instead of the molar concentration. The characteristic break in the surface tension indicating the CAC may then disappear[313]. Although high hydrotrope concentrations are required to reach the minimum surface tension, a decreased value for the surface tension (27 mN/m) comparable to common surfactant solutions has already been detected[315].

There are many studies about the hydrotropic effect of nicotinamide (NA) and its association behaviour derived by several techniques like freezing point depression, light scattering, VPO and solubilisation experiments[316–319]. E.g. the solubilisation of riboflavin (RBF) with NA was investigated at different temperatures to get information about the influence of the self-association mechanism of NA on the increase of RBF solubility. With increasing temperature, the solubilisation of RBF decreased, which is consonant with the self-association hypothesis, because increased temperature leads to a decrease in self-association and thus to a decrease in RBF solubility[318]. Molecular dynamics simulations revealed that the self-aggregation of NA may be at least a major contributor to its hydrotropic effect. The non-stoichiometric aggregation of NA by stacking of the planar aromatic rings helps to segregate the hydrophobic solute from water[320]. Studies on the hydrotropic solubilisation of RBF induced by caffeine (CAF) were made by the same author[321] and have shown that the self-stacking of CAF is the primary effect and the incorporation of RBF is the secondary effect. Basically, the same driving force for the solubilisation of RBF was found for NA and CAF that is the restoration of normal water structure followed after cluster formation. But the mechanisms of the aggregation in both systems were described to be different. While the clustering mechanism in the water/CAF/RBF systems was attributed to parallel stacking of CAF and RBF, the clustering in the system with NA is due to the formation of molecular NA aggregates. Thus, two different hypotheses for the hydrotropic origin are designated to the two systems: self-assembly of hydrotrope molecules for the NA system and formation of solute-hydrotrope complexes for the CAF system.

Although self-aggregation of small amphiphilic molecules (or the pre-structuring in aqueous hydrotrope solution) serves a nice and conceivable picture to describe the origin of hydrotropy, the hydrotropic effect is more complex and still under debate. Giving a general explanation for the formation of colloidal structures based on a single mechanism, like the appearance of a MHC, solely and relating thereto hydrotrope-hydrotrope cluster formation as the origin of the hydrotrope phenomenon is questionable and not satisfactory[311].

Shimizu and co-workers have challenged the traditional views on the hydrotropic action by appliying exact statistical thermodynamics. They employed the Kirkwood Buff Integrals (KBI) to describe hydrotropic solubilisation theoretically[322–324]. In general, the three different traditional hypotheses, which are considered as the origins for the hydrotropic effect are:

(1) formation of hydrotrope-hydrotrope complexes

As already described in the paragraphs above, it is assumed that hydrotrope self-aggregation (e.g. SXS[298], SCS[325] or NA[316,317,319]) leads to clusters, in which the solute can be incorporated. This mechanism is parallel to that of micelle formation. For small amphiphilic molecules with short chains or no chains e.g. urea, doubts exist whether self-aggragtion is the driving force for hydrotropy. Urea behaves almost ideal in aqueous solution.

(2) disruption of the water structure by the hydrotrope

The change of the water structure induced by the hydrotrope is a hypothesis for an indirect mechanism of hydrotropy. It is assumed that the hydrotropes do not bind directy to the solutes but break the water structure around it[326]. Consequently, the hydrogen bonding network around the hydrophobic compound would be less pronounced as well (entropy increase), which weakens the hydrophobic effect[327] and thus increases the solubility of the hydrophobic compound. The idea of water structure breaking abilities of hydrotropes stem from Frank and Franks[327]. However, problems with this hypothesis occur as the water structure itself is ambiguous. And it is not clear if the structure of the solvent is really related to solubilisation phenomena. It has been found that the water structure is thermodynamically irrelevant for the solubilsation mechanism[328].

(3) formation of solute-hydrotrope complexes

It is assumed that the formation of low stoichiometric complexes (1:1 or 1:2) between the solute and the hydrotrope is the reason for hydrotropic solubilisation. The water/CAF/RBF system is one example, for which solute-hydrotrope complexes were found[321,326]. Solute-hydrotrope complexes were also found for several sparingly soluble drugs with NA as hydrotrope[329]. The lack of a change in the RBF UV/VIS-spectrum by the addition of NA, however, contradicts this hypothesis[318].

Booth et al.[324] analysed experimental data of the solubilisation of butyl acetate (BA) and benzyl benzoate (BB) with urea, SB or sodium salicylate (ss) as hydrotropes in terms of the transfer free energy ΔG of the solutes depending on hydrotrope concentration and the water (1) activity. The task here, was to understand the decrease of hydration-free energy of the solute (2), μ_2^*, upon the addition of hydrotrope (3), n_3:

$$\left(\frac{\partial \mu_2^*}{\partial n_3}\right)_{T,p,n_2\to 0} = \left[-\left(\frac{\partial \mu_2^*}{\partial \mu_1}\right)_{T,p,n_2\to 0}\right]\left[-\left(\frac{\partial \mu_1^*}{\partial \mu_3}\right)_{T,p,n_2\to 0}\right] \tag{II-16}$$

The differential on the right side of Eq. (II-16) is termed the ΔG gradient, which can be splitted in two contributions. The first contribution to the ΔG gradient is the preferential hydration parameter ν_{21}, which is negative for all systems when the solute solubility increases.

$$\nu_{21} \equiv -\left(\frac{\partial \mu_2^*}{\partial \mu_1}\right)_{T,p,n_2\to 0} = n_1(G_{21} - G_{23}) \tag{II-17}$$

where n_1 is the molarity of water. G_{ij} are the Kirkwood-Buff (KB) parameters, which are defined with the help of the radial distribution function, g_{ij}:

$$G_{ij} = 4\pi \int_{\infty}^{0} \left[g_{ij}(r) - 1\right] r^2 dr \tag{II-18}$$

with the distance r between the centers of the molecular species i and j. The meaning of the preferential hydration parameter ν_{21} (Eq. (II-17)) is the net excess solute-water distribution G_{21} accompanied with the solute-hydrotrope interaction G_{23}. The KB parameter were determined from experimental data like solubility, density and water activity. To do so, a set of equations including Eq. (II-17) and a relationship, independent of Eq. (II-17), which connects G_{21} and G_{23} are required and must be solved simultaneously. Such a relationship is the partial molar volume of the solute, V_2:

$$V_2 = -V_1 n_1 G_{21} - V_3 n_3 G_{23} + RT\kappa_T \tag{II-19}$$

where R is the gas constant and κ_T is the isothermal compressibility of the bulk solution. The second contribution to the ΔG gradient in Eq. (II-16) is the water activity depression upon hydrotrope addition.

$$-\left(\frac{\partial \mu_1^*}{\partial \mu_3}\right)_{T,p,n_2\to 0} = \frac{RT}{n_1(1+n_3G_{33}-n_3G_{13})} \qquad \text{(II-20)}$$

Therefore, the water activity depression is related to hydrotrope-hydrotrope G_{33} and hydrotrope-water G_{13} interactions. The KB parameters can be determined entirely from experimental data (density, solubility and osmometric data). For ionic hydrotropes, cations and anions are treated as single species, which is taken into account by a dissociation factor in Eq. (II-16).

Different solubilisation behaviour of BA with urea, sb and ss has been observed, but similar solubilisation behaviour of BB was detected with the same hydrotropes. This observation is not in line with a hydrotropic mechansim based on bulk properties like hydrotrope self-aggregation or water structure alteration, because according to these mechanisms the solubilisation of BA and BB should be similar using the same hydrotropes[324]. The two major driving forces for solubilisation *via* hydrotropes have been identified: (1) the solute-hydrotrope binding and (2) the water activity depression.

The latter one is influenced by further two contributions. If the hydrotrope is ionic, the dissociation increasingly diminishes water activity (doubled for a 1:1 electrolyte), due to the increasing number of species. In contrast, the self-aggregation of the hydrotropes reduces the water activity depression. The hydrotropic mechanism was explained by a combination of these two contributions. In contrast to the prior adoption of enhanced solubilisation due to hydrotrope self-aggregation, the analysis of Booth et al.[324] revealed the opposite, that is self-aggregation leads to a less efficient solubilising power due to the less pronounced water activity depression. No significant effect on the solubilisation was noted by the change of water structure nor by the change of hydration of the solute.

It has been demonstrated that co-solvent accumulation around the solute, rather than stoichiometric binding can increase solubility[324,330]. Thus, it is the structure of the water-hydrotrope mixture around the solute (ternary mixture) and not the structure of the aqueous hydrotrope solutions (binary mixture), which is decisive.

In a recent review about hydrotropes, Kunz et al.[309] provided an up to date definition of hydrotropes, which is based on the structuring of ternary water/hydrotrope/hydrophobic compound mixtures. It is stated as follows: *"a hydrotrope is a substance that shows property A and/or B and does not form a microemulsion or lytropic liquid crystals"*, with property A: *"a hydrotrope is a substance whose structuring in water is enforced by the presence of a third, water-immiscible compound"* and property B: *"a hydrotrope is a substance whose structuring in the organic solvent is enforced by the presence of water"*. Property A is accompanied by an enhanced solubility of the hydrophobic compound in water and the consequence of property B is the enhanced solubility of water in the organic solvent. Substances bearing only those two properties A and/or B would refer to all surfactants or detergents and the distinction to hydrotropes is made by the important additional property that hydrotropes do not form microemulsion or lytropic liquid crystals (mesophases). Hydrotropes are often used in cleaning formulations to prevent the formation of liquid crystals[331].

Property B can be referred to solvotropy or "lipotropy", which is described as the action of a hydrotrope or "lipotrope" to increase the solubility of water in an organic solvent. This mechanism was studies by Bauduin et al.[332] by transposing the common properties of hydrotropes to non-aqueous apolar systems. They studied the solubilisation curves of water and hydrophilic dye in dodecane by addition of lipotropes (n-alcohols (n = 2-4 and 7)), the low microstructure adopted by alcohol molecules in dodecane by small angle X-ray scattering and the ability of breaking ordered phases such as hexagonal or lamellar phases. The latter part of the studies was projected to the industrial application of LLEx of minor actinides from the aqueous phase. It was shown that the addition of n-alcohols efficiently avoids the phase splitting of the organic phase into a third one, which may be caused by the transition of spherical to cylindrical micellar aggregates of the extractant molecules[333]. Thus, the n-alcohols meet the lipotropic requirement of breaking ordered aggregates and the influence of the chain length of the n-alcohols on its structure breaking ability follows the same trend, which was observed for the water solubilisation experiments. Similarly, a correlation between the aggregation of alcohols in dodecane and the solubilisation was made. It should be mentioned that the term "lipotrope" has a different meaning in biology and confusing terminology should be avoided.

In the review of Kunz et al.[309], the differentiation between a hydrotrope and a co-solvent was explained on nanoscale and macroscopic scale. Concerning the nano-structuring, the addition of an organic compound to a water/co-solvent system does not lead to structuring of the solution or at least only to a minor extent. On macroscopic scale, there is no minimum co-solvent concentration, at which the solubilisation starts significantly, but the solubilisation increases slowly at low co-solvent concentration and exponentially at high concentrations as already stated above[300]. In this context, acetone and ethanol are representative for the group of co-solvents and SXS and SCS belong to the group of hydrotropes. As it was described in different solubilisation experiments, the distinction between the solubilisers is sometimes hard because a continuous transition from co-solvents to hydrotropes and from hydrotropes to surfactants[308,334,335] exist. Thus, hydrotropes lie in between co-solvents and surfactants.

If the composition in a ternary water/co-solvent/hydrophobic compound mixture is near the phase splitting area (near the plait point) in the monophasic region, highly fluctuating structures are appearing. This phenomenon is exploited to design surfactant-free microemulsions (SFME) and is discussed for the system water/ethanol/n-octanol by Schöttl and Horinek[336] using molecular dynamics (MD). The area in the ternary phase diagram where such effects were found, is called the *pre-ouzo* regime[337]. In this case, the ethanol shows hydrotropic properties and accumulates slightly in the interface between a water-rich and an octanol-rich pseudo-phase[338]. Further studies were made by introducing antagonistic salts (one hydrophobic and one hydrophilic ion, e.g. $(C_6H_5)_4NBr$ or $(C_6H_5)_4BNa$)), which lead to a more rigid interface by electrostatic repulsion between the pseudo-phases in the presence of a co-solvent. In this way, the combination of an antagonistic salt and a co-solvent within the *pre-ouzo* regime showed X-ray and neutron signals resembling to those of SDS micelles[339]. Such well-defined aggregates were distinguished from critical density fluctuation, which are always present near the critical phase separation area (critical or plait point). Such behaviour, but less pronounced, is also seen with classical salting-in salts like NaSCN. It was also shown that antagonistic salts in absence of co-solvents already can have solubilising properties[340,341].

Like hydrotropes and surfactants, co-solvents can be neutral or charged as well. Ethanol and acetone are neutral co-solvents and charged co-solvents are assigned to salting-in salts like NaSCN, CsI, $NaClO_4$ and $HClO_4$. To combine both in one category, the term “co-solubiliser” is proposed. In all cases of the co-solubilising action of charged or uncharged hydrotropic species, the self-assembly is not important but the modification of the solvent properties such as the dielectric constant is crucial.

A generalized picture of the solubilisation process is drawn, whereby a crucial role in the hydrotropic mechanism was assigned to the presence of the third hydrophobic compound and the resulting nano-structuring in the so-called pre-Ouzo regime of ternary solutions.

Thomas Buchecker and Sebastian Krickl et al.[342] investigated the impact of structuring of hydrotropes (ethanol, n-propanol, 2-propanol and *tert*-butanol) in water on the solubilisation of a hydrophobic compound (benzyl alcohol, limonene and DR-13). Weak pre-structuring was found for water/ethanol and water/2-propanol mixtures, while for water/n-propanol and water/*tert*-butanol pronounced pre-structuring was observed. Significant structuring was induced upon addition of limonene or benzyl alcohol to a weak pre-structred mixture. The lower the pre-structuring, the less hydrotrope was required to solubilise benzyl alcohol (bulk + interface solubilisation), which is in line with Booth et al.[324,330] and Kunz et al.[309]. In case of limonene and DR-13, pronounced pre-structuring led to reduced amount hydrotrope required for solubilisation (pseudo-bulk solubilisation), which is the inverse relation. Thus, the selection of the short-chain alcohol used as solubiliser for a hydrophobic compound in water depends strongly on the nature of the hydrophobic compound. For a more hydrophilic solute, weak pre-structuring in the binary (water/ethanol, water/2-propanol) is favourable, while for nonpolar compounds, structure-forming hydrotropes (n-propanol, *tert*-butanol) are recommended for solubilisation. In case of very hydrophobic substances like limonene, solute-hydrotrope interactions are less pronounced due to missing functional groups. Thus, to solubilise such non-polar compounds, pre-structuring in the binary water/hydrotrope (e.g. water/*tert*-butanol) system becomes increasingly important as a nonpolar microenvironment (pseudo-phase) is provided for the solute. For DR-13 similar trends as for limonene were found, but the solubilisation mechanism is different. DR-13 bears polar functional groups and is assumed to be dissolved in the interfacial film of two pseudo-phases. Solubility depends on the chemical nature of both, the solute and the hydrotrope.

That study highlighted the pre-structuring in water/alcohol mixtures being important for microscopic phenomena in SFME besides the addition of a third hydrophobic compound to a water/hydrotrope mixture.

II.4 Characterisation and Analytical Methods

II.4.1 Vapour Pressure Osmometry (VPO)

VPO is an indirect method for the measurement of the vapour pressure of a solution. The signal originates from the voltage change between two thermistors being part of a Wheatstone bridge. The thermistors are located in the measuring cell (Figure II.8), which contains the solvent and a solvent saturated gas phase. The cell temperature is electronically controlled with an accuracy of ± 0.001 °C. If droplets of pure solvent are placed on each thermistor, the system is in equilibrium and the temperature difference is zero. If one droplet of pure solvent is replaced by a droplet of the solution, condensation of solvent from the vapour onto the solution droplet occurs due to the lower vapour pressure of a solution compared to the pure solvent. The vapour pressure of the solution is increasing due to the heat of condensation until the vapour pressure of both droplets is equal. This leads to a temperature difference ΔT between the thermistors, which is proportional to the number of osmotically active molecules or particles in the solution.

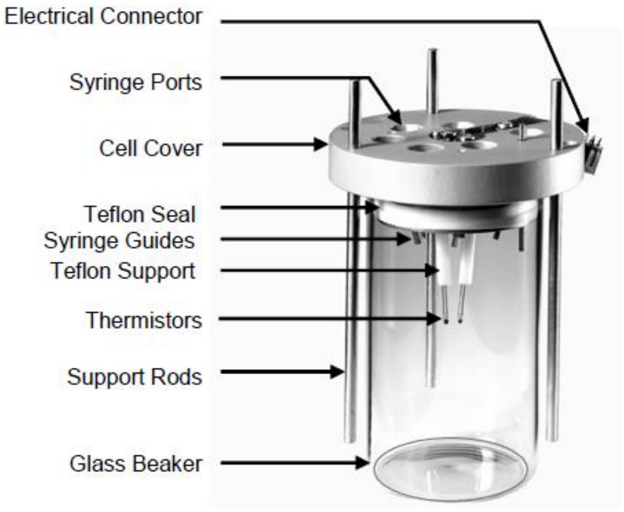

Figure II.8. Measuring Cell of the Vapour Pressure Osmometer.

The chemical potential of the solvent in a solution $\mu_s(p,T)$ is connected to the solvent activity by the following equation:

$$\mu_{\mathrm{s}}(\mathrm{p},\mathrm{T}) = \mu_{\mathrm{s}}^{0}(\mathrm{p},\mathrm{T}) + \mathrm{RT}\ln a_{\mathrm{s}} \qquad \text{(II-21)}$$

where $\mu_s^0(p,T)$ is the chemical potential of the pure solvent, R is the gas constant, T is the absolute temperature, and a_s is the activity of the solvent in solution. If the solvent is the only volatile component, the gas phase over the liquid consists of pure solvent vapour ($\mu_s^g = \mu_s^{0,g}$) and the liquid-gas equilibrium ($\mu_s^l = \mu_s^g$) is given by:

$$\mu_{\mathrm{s}}^{0,\mathrm{g}} = \mu_{\mathrm{s}}^{0,\mathrm{l}} + \mathrm{RT}\ln a_{\mathrm{s}} \qquad \text{(II-22)}$$

with the chemical potential of the pure solvent in the gas phase $\mu_s^{0,g}$ and the chemical potential of the pure solvent $\mu_s^{0,l}$ in the liquid phase. The relation between the solvent activity a_s and the practical osmotic coefficient ϕ and is given by the equation introduced by Bjerrum[343]:

$$\phi = -\frac{1000}{M_{\mathrm{s}}\sum_{\mathrm{i}}\nu_{\mathrm{i}}m_{\mathrm{i}}}\ln a_{\mathrm{s}} \qquad \text{(II-23)}$$

with M_s being the molecular weight of the solvent, v_i and m_i as the stoichiometric coefficient (numbers of species in solution) and the molality of the solute, respectively. From the calibration with NaCl solutions, a correlation is obtained between salt molalities m_{Ref} and the measured values (MW) from the osmometer according to the polynomial equation:

$$m_{\mathrm{Ref}} = \mathrm{a}_0\mathrm{MW} + \mathrm{a}_1\mathrm{MW}^2 \qquad \text{(II-24)}$$

Measured values from the sample solutions (binary: water/HMF; ternary: water/HMF/salt) are associated to NaCl molalities, for which osmotic coefficients are known. In other words, the sample solutions are assigned to NaCl solutions with the same vapour pressure (isopiestic) or water activity a_s:

$$a_{\mathrm{s}}(\mathrm{HMF}) = a_{\mathrm{s}}(\mathrm{NaCl}) \qquad \text{(II-25)}$$

$$a_{\mathrm{s}}(\mathrm{HMF/Salt}) = a_{\mathrm{s}}(\mathrm{NaCl}) \qquad \text{(II-26)}$$

Using Eq. (II-24) and (II-25) or (II-26) for two solutions with equal water activities, the following expression results:

$$\phi \sum_{\mathrm{solute\ i}} \nu_{\mathrm{i}} m_{\mathrm{i}} = \nu_{\mathrm{Ref}}\, m_{\mathrm{Ref}}\, \phi_{\mathrm{Ref}} \qquad \text{(II-27)}$$

where m_{Ref} is the molality of a NaCl solution having the same instrument readings as the solution under investigation (binary water/HMF or ternary water/HMF/salt). For binary water/HMF solutions, osmotic coefficients can be obtained from Eq. (II-28) and for ternary water/HMF/salt solutions, osmotic coefficients are obtained from Eq.(II-29).

$$\phi_1^0 = \frac{\nu_{\mathrm{Ref}}\, m_{\mathrm{Ref}}\, \phi_{\mathrm{Ref}}}{\nu_1\, m_1^0} \qquad \text{(II-28)}$$

$$\phi_{1,2} = \frac{\nu_{\mathrm{Ref}}\, m_{\mathrm{Ref}}\, \phi_{\mathrm{Ref}}}{\nu_1\, m_1 + \nu_2\, m_2} \qquad \text{(II-29)}$$

Osmotic coefficients of NaCl (ϕ_{Ref}) are calculated from associated NaCl molalities m_{Ref}, according to the equation set developed by Gibbard and Scatchard[344], see Apendix C.

A simple mixing rule for ternary mixtures of electrolytes 1 and 2 from the relation of the total molality, $m = m_1 + m_2$, in a ternary mixture to the molalities of the solutes in corresponding isopiestic binary solutions, m_1^0 and m_2^0, was derived by Zdanovskii[345].

$$\frac{1}{m} = \frac{x_1}{m_1^0} + \frac{x_2}{m_2^0} \qquad \text{(II-30)}$$

where $x_1 = m_1/(m_1+m_2)$ and $x_2 = m_2/(m_1+m_2)$ are the molality fractions of 1 and 2 in the ternary mixture. Independently, Stokes and Robinson derived Eq. (II-30) from solvation equilibria, if the average hydration number of a non-electrolyte depends only on the water activity[346]. This treatment is based on the concept of semi-ideal behaviour in solution, i.e., the solute 1-solute 2 interactions in a multicomponent mixture are mutually self-cancelling or negligible compared to solute-solvent interactions. Many mixed electrolyte solutions were measured by Kirgintsev and Luk`yanov [347], who proposed the following extension of Eq. (II-30) to account for deviations from the Zdanovskii-Stokes-Robinson (ZSR) linear approximation:

$$\frac{1}{m} = \frac{x_1}{m_1^0} + \frac{x_2}{m_2^0} + \mathrm{b} x_1 x_2 \qquad \text{(II-31)}$$

with b as an empirical parameter. Chen et al.[348] examined literature data and tabulated many ternary aqueous systems, including mixed electrolyte, electrolyte/non-electrolyte and non-electrolyte/non-electrolyte solutions, concerning their validity to the ZSR rule by applying Eq. (II-31). To give a general thermodynamic expression for the deviations (Δ) from the ZSR rule, Eq. (II-31) is written as:

$$\frac{1}{m} = \frac{x_1}{m_1^0} + \frac{x_2}{m_2^0} + \Delta \tag{II-32}$$

and Δ is related to the osmotic coefficients of the ternary ($\phi_{1,2}$) and the corresponding binary (ϕ_1^0, ϕ_2^0) solutions[349]:

$$\Delta = \frac{\nu_{1,2}\phi_{1,2} - \nu_1 x_1 \phi_1^0 - \nu_2 x_2 \phi_2^0}{\nu_{1,2}\phi_{1,2}} \tag{II-33}$$

where ν_i is the total number of moles of particles produced by complete dissociation (even in reality it is incomplete) of molecule i and $\nu_{1,2} = \nu_1 x_1 + \nu_2 x_2$. Similar relations and improvements have been derived by Clegg et al.[350]. If Δ is zero, the ZSR-rule is obeyed and Eq. (II-33) reduces to[349,351]:

$$\phi_{1,2} = \frac{\nu_1 x_1 \phi_1^0 + \nu_2 x_2 \phi_2^0}{\nu_{1,2}} \tag{II-34}$$

II.4.2 Dynamic Light Scattering

Dynamic light scattering (DLS) is a standard routine technique for the characterization of colloidal particles or microemulsion droplets in a liquid. The mesoscopic entities scatter light due to their different refractive index (RI) compared to the liquid medium. Due to Brownian motion, the distance between the scattering objects varies continuously. This results in fluctuating scattered light, which in turn leads to constructive and destructive interferences[352,353]. The time depend recording of the fluctuating intensity gives information about the motion of the mesoscopic entities. Thus, DLS is often used to determine diffusion coefficients and the size of colloidal particles or droplets. A DLS apparatus is schematically presented in Figure II.9. A liquid sample is illuminated by monochromatic coherent laser light with wavelength λ. Rayleigh scattering occurs if the diameter D of the scattering entities is smaller than the wavelength of the incident beam

($D < \lambda/10$). The scattered light is detected at a certain angle Θ and the scattering vector q is identical to:

$$q \equiv k_S - k_I = \frac{4\pi n}{\lambda} \sin\frac{\theta}{2} \tag{II-35}$$

with k_S and k_I as propagation vector of the scattered and incident light, respectively, n being the RI, λ the wavelength of the irradiated light in nm and θ the detection angle.

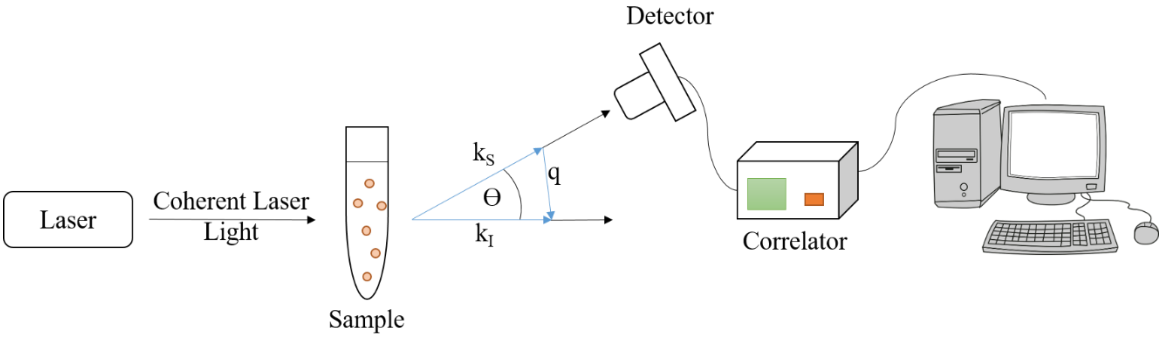

Figure II.9. Schematic presentation of a DLS apparatus. Coherent laser light from the radiation source is scattered from the sample at the angle Θ. Scattered light is collected by the detector and light intensity data is send to the correlator. Correlation function are displayed and analysed on the computer.

Smaller and faster particles lead to higher intensity fluctuations compared to bigger particles. A digital autocorrelator compares the intensities at different time intervals. The degree of similarity between two signals is measured. If an identical signal at t_0 is compared, a correlation value equal to 1.0 results. In contrast, a value of 0.0 indicates zero correlation. If the intensity of a signal at t_0 is compared to the intensity of signal at $t_0 + \tau$ (τ is the delay time of the correlator in ns or μs), there will be a strong correlation between these signals, if τ is small. With increasing sample time the correlation will be reduced. The decrease of the correlation depends on the particle size, which is visualised in auto-correlation functions. Evidently, for large and slow particles, the signal will change less rapidly compared to small and fast particles. As a consequence, the correlation detected for large particles will remain for a longer time period compared to small particles. The correlation function can be written as:

$$G(\tau) = \langle I(\mathrm{t}) \cdot I(\mathrm{t} + \tau) \rangle \tag{II-36}$$

where *I(t)* is the intensity signal and *I(t+τ)* is the function of the delay time.

The correlation function declines exponentially depending on the diffusion coefficient. A steep decay is typical for monodisperse particles, whereas for polydispers particles the decay is extended.

$$G(\tau) = a_0 + (a_1 \cdot e^{-a_2 \tau})^2 \qquad \text{(II-37)}$$

here, τ is the delay time, a_0 is a constant baseline value (usually equal to 1), a_1 refers to the dynamic part of the amplitude and a_2 is the decay rate linked to the diffusion coefficient D, which is connected to hydrodynamic radius R_H of a spherical particle *via* the Stokes-Einstein equation, see Eq. (III-4) in the experimental part of Chapter III.

II.4.3 Solubilisation of a Hydrophobic Compound

Solubilisation experiments are based on aqueous mixtures with excess solubilisate (very hydrophobic compound) and different amounts of a solubiliser. With increasing concentration of solubiliser, the amount of solubilised hydrophobic compound usually increses, which can be detected, e.g. by UV/VIS-spectrophotometry. The hydrophobic dye DR-13 was chosen as solubilisate, because of its negligible water solubility and its high molar attenuation coefficient that aids the spectrophotometric analysis. The absorption maximum is at a wavelength of $\lambda_{max} = 525$ nm. The azo-group within the chemical structure of DR-13 (Figure II.10) links two aryl functions leading to an extended conjugated π-system. DR-13 is very soluble in acetone, which is used as solvent for calibration and sample dilution steps.

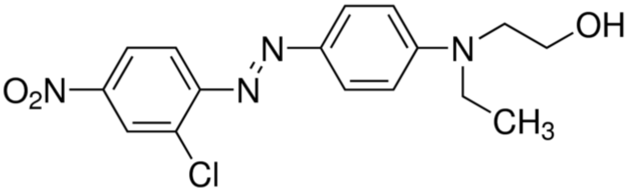

Figure II.10. Chemical structure of the hydrophobic dye Disperse Red 13 (DR-13).

II.4.4 Pendant Drop Tensiometry

The surface tensions of aqueous HMF solutions were captured by pendant drop tensiometry in a temperature-controlled room at 296 ± 1 K using a Profile Analysis Tensiometer (PAT-1M, Sinterface Technologies). One advantage of this method is the low quantity of chemicals required for sample preparation. Respecting the high price of pure HMF (99.1%, ~1000€/200g), the pendant drop method was preferred to the classical ring method of Du Noüy[354], for which a relatively large reservoir of sample would have been required.

The surface tension of the liquid strives for a minimization of the surface area aiming a spherical shaped droplet. But, due to gravitational force, the drop is stretched and the shape of the droplet becomes pear-like. Thus, two opposing forces define the shape of the droplet. Pendant drop tensiometry requires then the acquisition of a silhouette of an axisymmetric fluid droplet applying a charge-coupled device camera and automated iterative fitting of the Young-Laplace equation (Eq. (II-38)). This process is illustrated in Figure II.11. At equilibrium, a pendant drop follows the Young-Laplace equation, which links the curvature of the pendant drop and the pressure difference across the curved water/air interface by the surface tension:

$$\sigma\left(\frac{1}{R_1}+\frac{1}{R_2}\right)=\Delta\mathrm{P} \qquad \text{(II-38)}$$

where σ is the surface tension, R_1 and R_2 are the two principal radii for the description of the non-spherical drop shape and ΔP is the pressure difference across the interface. In the absence of external forces, other than gravity, the pressure difference is a linear function of the elevation (hydrostatic pressure):

$$\Delta\mathrm{P} = \Delta P_0 + (\Delta\rho)gz \qquad \text{(II-39)}$$

where ΔP_0 is the pressure difference at a reference plane (apex of the droplet; $z = 0$), $\Delta\rho$ is the density difference between the inner and the outer phase, g is the gravitational acceleration and z is the vertical height measured from the reference plane. The Young-Laplace equation can only be solved analytically for a sphere-shaped droplet. For other geometries, the equation has to be solved numerically, usually by axisymmetric droplet shape analysis. Starting from an initial guess, a form parameter (Bond number) is varied during this analysis, until the calculated shape best matches the actual shape of the droplet. The Bond number *Bo* describes the balance between surface tension and gravitational force and is defined by the following expression:

$$\mathrm{Bo} \equiv \frac{\Delta\rho g R_0^2}{\sigma} \tag{II-40}$$

with R_0 being the drop radius at the apex. If *Bo* and R_0 are determined simultaneously and $\Delta\rho$ is known, the surface tension σ is easily obtained from Eq. (II-40)[355–357].

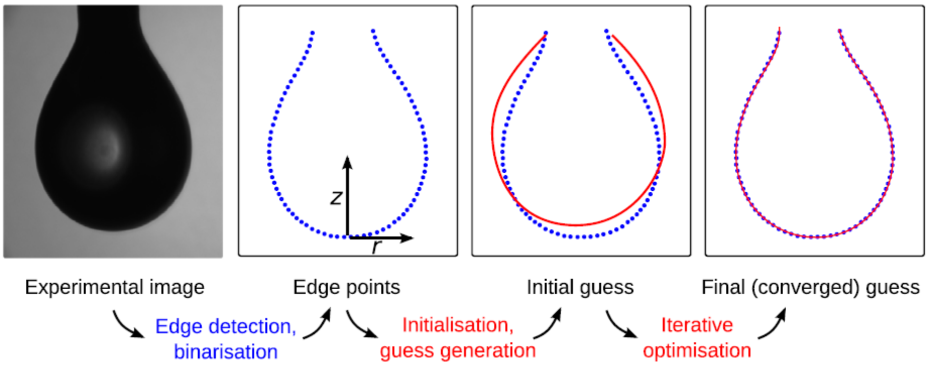

Figure II.11. Process of pendant drop tensiometry, starting from the experimental image to an initial guess and the final converged fit, from which the surface tension can be obtained. The picture was taken from literature[355].

II.4.5 Determination of LLE

There are three different categories of experimental approaches for the determination of liquid-liquid solubilities: synthetic, analytical and miscellaneous. In each category specific methods are offered depending on the nature of investigated chemicals or mixtures and the present conditions. Several factors like physical properties and especially stability of the components, accuracy of the desired data, the extent of mutual solubility and instrumental accessibility/availability affect the eventual decision of experimental strategy. Most investigations of liquid-liquid solubilities focus on temperature and composition as variables and are usually presented in corresponding phase diagrams. The system pressure is negligible up to 100 atm (10^7 Pa) for the most liquids, except near the critical solution temperature(s)[358].

An established method to determine LLE data is the analytic approach, which includes the preparation of a global heterogenous mixture by weighing, equilibrating and the quantitative analysis of all the components in each phase. Basically, it is sufficient to measure only n-1 components of one phase in an n-component system and only one component of the other phase. With these data it is then possible to accurately determine a tie-line provided that the quantitative analysis is accurate. The residual concentrations can be calculated from the total material balance (Eq.(II-41)) and that of each compound with Eq. (II-42).

$$m_1 + m_2 = m_G \tag{II-41}$$

$$m_1 w_{11} + m_2 w_{12} = m_G w_{1G} \tag{II-42}$$

$$m_1 w_{21} + m_2 w_{22} = m_G w_{2G}$$

$$\dots$$

$$m_1 w_{n1} + m_2 w_{n2} = m_G w_{nG}$$

where m_G is the mass of the global mixture, which is known from weighing. The masses m_1 of phase 1 and m_2 of phase 2 are unknown. The known weight fraction of a component i in the global mixture is denoted by w_{iG} and weight fractions of component i in the phases 1 and 2 are represented by w_{i1} and w_{i2}, respectively, of which n-1 are known for phase 1 and one is known for phase 2 from analysis. The above mentioned equations can also be written in mole fraction instead of weight fractions and mole numbers instead of masses. The resulting equations read:

$$\sum_{i=1}^{n} x_{i1} = 1 = \sum_{i=1}^{n} x_{i2} \tag{II-43}$$

$$\frac{x_{i1} - x_{iG}}{x_{iG} - x_{i2}} = constant\ (i\ =\ 1, 2, 3, \dots \mathrm{n}) \tag{II-44}$$

With Eq. (II-43) and Eq. (II-44) the unknown concentrations can be determined. This method is however error prone, because a small error in experimental determination of concentrations can in turn lead to large errors in calculated concentrations. Generally, the relative errors from measurements have only a small effect to the concentration value of main consituents of a phase, but a large effect to those, which are present in very small concentrations. This is the reason why it is more accurate to determine all components in each phase or at least all the minority components[359].

In this work, all components of each phases of equilibrated hetergenous mixtures are determined unless otherwise specified. These components are water, n-butanol, HMF, salts and glycerol and appear in the mixtures listed in Table II-3.

Table II-3. Different types of investigated LLE systems (ternary and quaternary).

Ternary	Quaternary
water/n-butanol/salt	water/ n-butanol /salt/HMF
water/ n-butanol /HMF	water/ n-butanol /salt/glycerol
water/n-butanol/glycerol	

II.4.5.1 Water

Water determination is performed by volumetric Karl Fischer-titration (KF-titration)[360], because this method allows direct measurements of the water content in both separated phases. The method is suitable for water contents from 1 up to 100% and is therefore advantageous compared to coulometric KF-titration, for which additional dilution steps with water-free methanol would be required. The latter method is favourable to detect low water contents (0.001 to 1%). The basis of KF-titration is the oxidation reaction between sulphur dioxide (SO_2) and iodine (I_2), for which the presence of water is mandatory (*Bunsen reaction*).

$$I_2 + SO_2 + 2H_2O \rightleftharpoons SO_4^{2-} + 2I^- + 4H^+ \tag{II-45}$$

The water stems from the sample to be investigated. Typically water free methanol is used as solvent. For the quantitative reaction, the reaction equilibrium should be shifted to the right side by an appropriate base. In addition, the solubility of sulphur dioxide in the KF-reagent solution should be high enough to keep a low vapour pressure of sulphur dioxide. Pyridine served the purpose of an appropriate base and solvent, which is why it was used in former KF-reagent solutions. Nowadays, pyridine is replaced by other substances because of its toxicity and odour nuisance. The volumetric method is technically easier whereby the water containing sample is titrated with a methanolic iodine solution. Endpoint determination occurs potentiometrically with a two-pin platinum electrode.

Water determination by GC coupled with a thermal conductivity detector is conceivable, but rejected because this method lacks in accuracy.

II.4.5.2 n-Butanol

Determination of n-butanol is perfomed by gas chromatography (GC) equipped with a flame ionisation detector (FID), which is a frequently applied method for alcohol analysis. Detection of n-butanol is also possible *via* the RI, but due to the presence of salts and other organic compounds in different concentrations, the proper construction of a calibration curve seems to be cumbersome and complicated.

High-Performance-Liquid-Chromatography (HPLC) coupled with RI-detection is conceivable, but HPLC was not that accessible than GC. Anyway, the GC method is very stable and reliable.

II.4.5.3 HMF

HMF has a maximum light absorbance in water at a wavelength of λ_{max} = 284 nm, see Figure II.12. Thus, UV-spectrophotometry can be applied for quantitative determination of HMF in water. The standard method for HMF detection is *via* HPLC and

UV-detection, which was established particularly for HMF analysis in foods and toxicological studies[30,35].

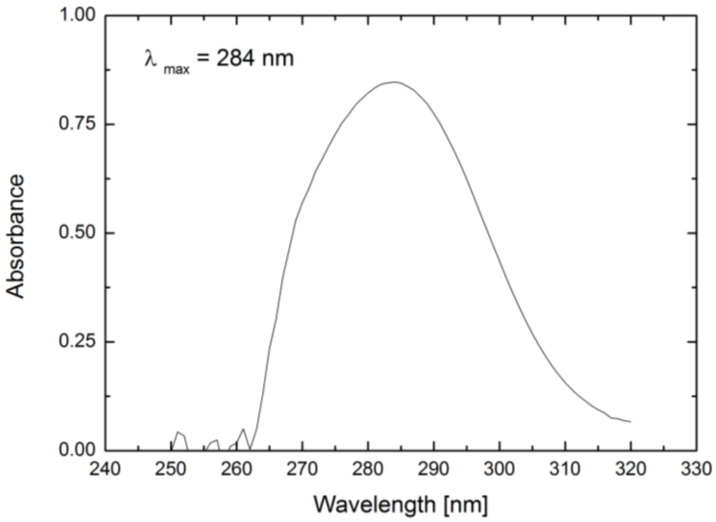

Figure II.12. Absorption spectrum of HMF in water with maximum absorbance at a wavelength of λ_{max} = 284 nm.

A comparison of HMF quantification between both methods, HPLC-UV and UV-spectrophotometry (without applying a chromatographic system), delivers similar results. The more direct and especially the more accessible method, UV-spectrophotometry, at the time of experimental investigations was chosen for further HMF quantifications. Generally, the quantification of HMF is also possible *via* GC[361] and could be performed simultaneously to n-butanol quantification. However, the relatively long retention times and high temperatures required (higher baseline shift) for accurate HMF detection, applying a polyethylene glycol packed column (INNOWax or DB-WAXetr), led to the decision of determining the n-butanol solely *via* GC. This allowed a more rapid and stable GC-analysis workflow.

II.4.5.4 Salts

In each case of analysis, only one salt was present in a sample. Electrolyte concentrations in both phases, aqueous and organic, are determined by anion-exchange chromatography (IC). In Figure II.13, a typical anion-exchange chromatography system is pictured. The processes occuring in the analysis column and the suppressor are highlighted. For elution of anions, electrolyte solutions (e.g. KOH-solution) are applied and the column material consists of a surface-functionalised (quaternary ammonium groups) polymer. The anion-exchange equilibrium between the mobile and stationary phase is determined by the affinity of the anions to the stationary phase, which determines the retention times of individual anions. For the quantification of ionic species, an electrical conductivity detector is applied. A continuously regenerated suppressor is installed between the analytical column and the detector, which reduces the background conductivity of the eluent and enhances the conductivity of the analyte. The reaction product of the eluent in the suppressor is water, which is not conductive, while the anion of the analyte reacts to the corresponding acid, which is highly dissociated. Therefore, the detection gets more sensitive and specific. Regeneration of the suppressor is maintained by water electrolysis.

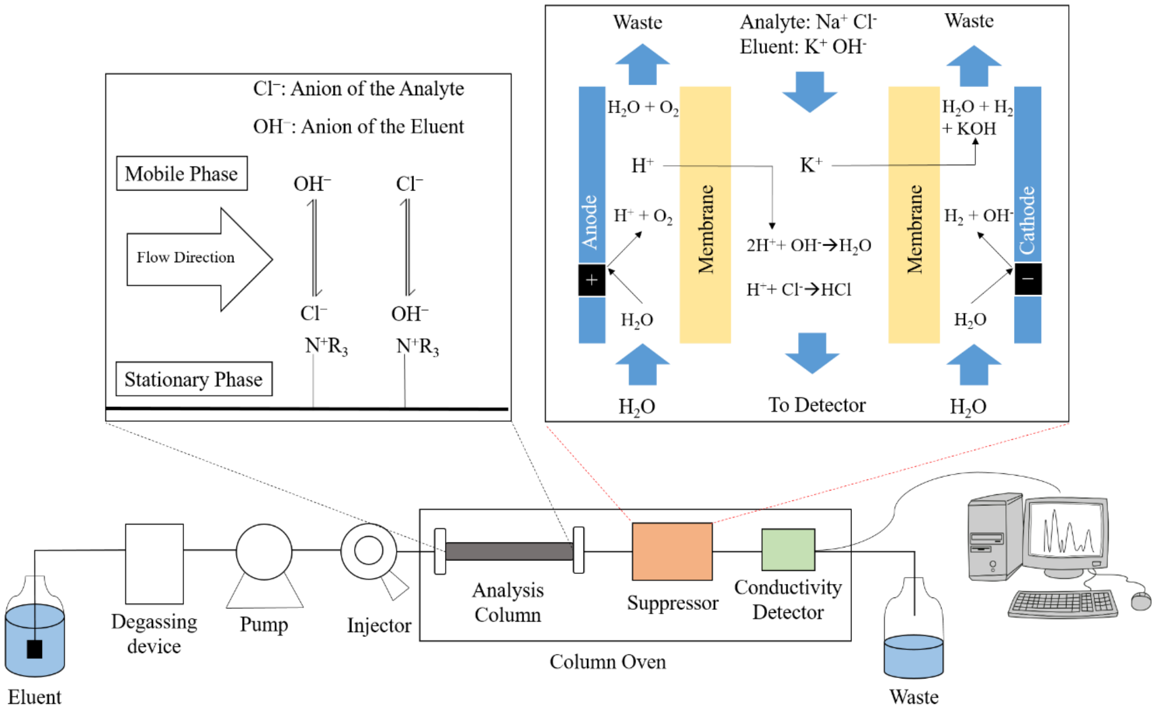

Figure II.13. Schematic presentation of an anion-exchange chromatography system with highlighted processes in the analysis column and the suppressor.

IC is more conventient compared to atomic emission spectroscopy (AES), because in the latter method, even small amounts of organic compounds lead to decreased accuracy. In some individual cases, the weight fractions of solid components (salts) were determined by the gravimetrical method or by mass balance. The gravimetrical method is not suitable for quaternary systems due to the presence of HMF or glycerol.

II.4.5.5 Glycerol

Many methods for glycerol determination are summerised in a publication of Hájek et al.[362]. Among them, photometric determination based on enzymatic reaction or periodate oxidation of glycerol, several GC and HPLC methods and iodometric determination. In this work, glycerol quantification in biphasic water/n-butanol/glycerol as well as water/n-butanol/glycerol/salt mixtures is performed by a modified colorimetric assay from Bondioli et al.[363] based on periodate oxidation of glycerol. No derivatisation of glycerol (e.g. for GC methods) is required and detection can be applied by simple UV/VIS-spectrophotometry. Glycerol gets split into three molecules of formaldehyde by use of $NaIO_4$ (glycol cleavage, *Malaprade* reaction). In a next step, formaldehyde reacts with two molecules of acetylacetone leading to the formation of 3,5-diacetyl-1,4-dihydrolutidine (*Hantzschs´* reaction). Chemical reations are shown in Figure II.14. The pyridine derivative has an absorption maximum (λ_{max}) at 410 nm allowing the indirect detection of very small amounts of glycerol.

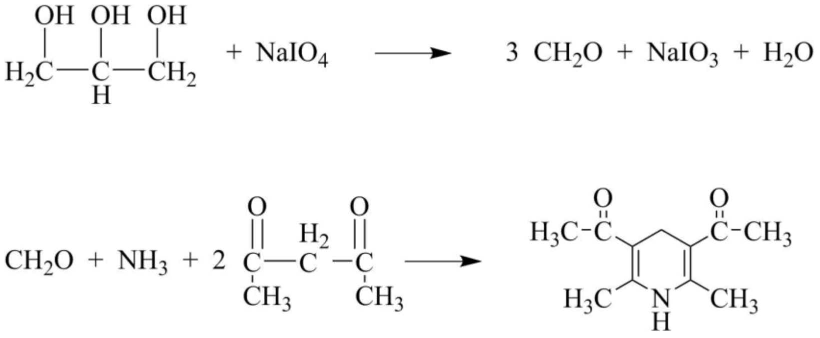

Figure II.14. Chemical reactions of the colorimetric assay for the quantification of glycerol in biphasic systems water/n-butanol/glycerol as well as water/n-butanol/glycerol/salt.

The highest standard deviations are obtained for water weight fractions in the aqueous phase (KF-titration) as well as for the n-butanol weight fractions in the n-butanol phase (GC). If the sum of the fractions of all components in one phase did not result in 100 wt%, the LLE data was adjusted by correction of the water weight fractions in the aqueous phase or n-butanol weight fractions in the organic phase using the mass balance. This correction is made with respect to the experimental error of the corresponding experimental technique (KF-titration or GC). This procedure of checking equilibrium data was described by Gomis et al.[359], besides a method to fit the experimental data, which was not applied.

II.5 Thermodynamic Modelling

The application of electrolytes in industrial processes gained increasing attention especially in the fields of biochemical engineering and separation operations. Information about aqueous electrolyte systems is crucial for the process design. Besides the great value of experimental thermophysical data of electrolyte systems, thermodynamic modelling of these systems is inevitable for the realisation of e.g. separation processes. Many models were developed to describe or predict industrial relevant mixtures.

Basically, there are two different approaches in thermodynamic modelling: Gibbs-excess energy (G^E) models, which are directly linked to activity coefficients and equations of state (EoS), which are based on the Helmhlotz energy A. By differentiation of A with respect to component (concentration) or system (pressure) properties, thermodynamic properties (e.g. densities, pressure and activity coefficients) can be determined.

The modelling of electrolyte solutions is based on the Debye-Hückel (DH) Theory[364] or on the Mean Spherical Approximation (MSA)[365] for both G^E-models and EoS. Theories for electrolyte solution describe the long-range (LR) interaction between ions (Coulomb forces) within a dielectric medium. Developed models also account for the short-range (SR) interactions, which are getting more pronounced beyond electrolyte concentration of 0.01 mol/kg[194,366]. In G^E-models and EoS, SR and LR are additive contributions, which are treated independently to the excess-Gibbs and Helmholtz energy, respectively:

$$G^E(p,T) = G^{SR} + G^{LR} \tag{II-46}$$

$$A(V,T) = A^{id} + A^{SR} + A^{LR} \tag{II-47}$$

where the sum: A^{SR}+A^{LR} is the residual Helmholtz energy (A^{res}), which is of interest for calculating thermodynamic properties. G^E-models and EoS differ in their reference states. The *excess* Gibbs energy (G^E) refers to the difference between the Gibbs energy of the *ideal* solution and of the *real* solution, whereas *residual* refers to the difference between a property of a *real* fluid to that of an *ideal* gas. Variables for the Gibbs energy (G) are temperature (T) and pressure (p), and for the Helmholtz energy (A) the variables are temperature (T) and volume (V). Thus, volume effects are captured by EoS, but not by G^E-models. Leading literature for this section were the PhD thesis of Christoph Held[366] as well as the textbooks from Lüdecke[367] and Prausnitz et al.[161].

II.5.1 Gibbs-Excess Energy G^E-Models

Empirical G^E-models for liquids were introduced by Margules[368] and van Laar[369]. Both models are based on the Wohl`s expansion and are often used for interpolating and extrapolating experimental data. The van Laar model is appropriate for simple non-polar systems and the Margules model is suitable for system with species of similar size. An advantage of both is that only parameter for the binary systems are needed to describe multi-component systems. Due to their simplicity and flexibility, these models are widely used to calculate activity coefficients.

Models, which also capture the behaviour of more complex mixtures require the treatment of statistical thermodynamics. Wilson[370] introduced a mathematically relative simple equation for G^E for strongly non-ideal mixtures in 1964. He assumed that in mixtures of polar compounds like alcohols, the molecules are not statistically distributed, but electrostatic interactions of the dipoles lead to local compositions, which differ strongly from the overall composition of the mixture. The Wilson equation is applicable to describe vapour-liquid equilibria (VLE) of strongly non-ideal mixtures, especially for polar or associating components in nonpolar solvents. Disadvantages of the Wilson model are that it is not suitable for the description of LLE. Renon and Prausnitz[371] further developed the local composition approach to overcome limitations of the Wilson model in 1968. They derived the Non-Random-Two-Liquid (NRTL) equation, which is applicable to completely miscible systems as well as to LLE. To reduce the number of adjustable parameters, Abrams and Prausnitz[372] derived an equation for G^E, which requires only two binary parameters. It is based on the quasi-chemical theory of Guggenheim and extended to molecules of different size and is called: the UNIversal QUAsi-Chemical model (UNIQUAC). A further model with the advantage of being predictive is the UNIversal Functional group Activity Coefficient (UNIFAC) method[373,374]. It is a group contribution method, in which the molecules are segmented into structural groups (e.g. $-CH_3$, -OH, saturated or unsaturated $-CH_2$, etc.). Interactions between these structural groups are then considered. The original UNIFAC model was further developed to the modified UNIFAC (Dortmund) by Weidlich and Gmehling[375], which provides more reliable results. The COSMO-RS[80] is also a G^E-model that performs predictions for mixtures based on a combination of quantum chemical calculations (COSMO)[376] with statistical thermodynamics of interacting surface pieces. It was refined by Klamt et al. in 1998[377] and turned out to be very useful for solvent screening[378].

Prominent extensions of G^E models to electrolyte system are the electrolyte NRTL model of Chen et al.[379,380] and the Pitzer-DH (PDH) model[381]. The electrolyte NRTL-model was applied by Nass[382] to describe the solubility of amino-acids in water. Liu et al.[383] also used the electrolyte NRTL-model to correlate the LLE water/n-butanol/NaCl. Their modelling results were in good agreement with experimental data but the salt content was overestimated in the organic phase. A drawback of this modelling approach is the large number of required interaction parameters. A semiempirical method, alternate to electrolyte-NRTL, was presented by Zerres and Prausnitz[384]. They considered solvated ions (chemical model) to respect the SR ion-solvent forces, which allowed for representation of mixtures containing salts up to their solubility limits. They rejected the Born-equation for changes of the reference state. For LR interactions they used an extended DH theory. Besides activity coefficients and vapour pressures of binary solvent salt systems, ternary VLE and LLE of water/alcohol/salt systems were well represented, among them the ternary LLE water/n-butanol/NaCl. Further approaches are the MSA-NRTL[385] and extended Pitzer model of Archer[386], which were both successfully applied to describe osmotic coefficients of lithium hydroxide solutions[387]. The quaternary LLE water/n-butanol/glycerol/NaCl was successfully modelled using the original NRTL and binary parameters from the ternary water/n-butanol/NaCl system. The residual binary parameters were fitted to that quaternary LLE[388]. That means, the ionic contributions have not been explicitly taken into account. A modified version of the extended UNIQUAC model was used by Pirahmadi and co-workers to correlate the LLE data of water/n-butanol/$NaNO_3$[389], water/n-pentanol/$NaNO_3$[390] and water/n-butanol/NH_4Cl[391]. In their model, the excess Gibbs energy consist of three terms: the PDH equation for LR interactions, the UNIQUAC model for SR interactions, and a Born term to account for the energy for changes in the reference state. Activity coefficients of amino-acids in aqueous solutions were determined by Kuramochi et al. [392] using the UNIQUAC equation and supporting data from vapour pressure measurements. The same work group further applied the UNIFAC model combined with a PDH-theory for activity coefficient calculations of biochemicals in aqueous solutions containing sugars, amino acids, urea, amino acid salts, inorganic salts, and sugar salts[393]. In the work-group of Irinia Smirnova, electrolyte extensions for COSMO-RS were developed by Ingram et al.[295] and Gerlach et al.[394]. In the fomer model, COSMO-RS was combined with the PDH term to account for LR ion-ion interactions. COSMO-radii of the alkali cations, which influence the screening charge densities and the surface areas of the ions, were parameterized. Interaction free energies of the alkali cations, the ammonium cation and the halide anions were adjusted as well. Element specific scaling factors were introduced to the hydrogen-bonding term of COSMO-RS. The model was based on mean ionic activity coefficients (MIACs) in aqueous solutions and was successfully applied to predict the influence of electrolytes on the LLE of the ternary systems water/n-butanol/NaCl and water/ACN/NH_4Cl (monophasic in absence of salts). The ternary LLE water/MIBK/salt[395] was also modelled by this COSMO-RS extension. More recently, distribution ratios of 1,3-PDO in the quaternary systems composed of water, 1,3-PDO, a salt (K_2HPO_4, K_2CO_3 or Na_2CO_3) and a short chain alcohol were predicted[294]. However, limitations of this model exist concerning the modification to the description of polyatomic ions like oxyanions. The more recent electrolyte extensions is called COSMO-RS-ES[394] (Conductor like Screening Model for Realistic Solvation in Electrolyte Solutions). Complete dissociation was assumed for all salts. Similar to the previous model, the SR activity coefficient from COSMO-RS is combined with the PDH-term for the LR ion-ion interactions. Both models differ in their description of the SR ionic interactions. In COSMO-RS-ES, the interaction energies terms of the ions are replaced with empirical interaction energy equations. The parameterisation is based on a large training set of MIACs and LLE data. It was shown that a significantly wider data set of salts can be described using interaction energy expressions instead of ion specific parameters like in their previous model. LLE predictions are possible with higher accuracy especially concerning the distribution behaviour of the salts. A further improvement is the ability to predict MIACs of salts containing oxyanions and LLE containing dipoatassium oxalate. These anions were not part of the training set. Therefore, COSMO-RS-ES can serve as a valuable tool especially when experimental data are not available or are insufficient.

The disadvantage of excess Gibbs enthalpy models is that they are not able to predict densities. The knowledge of mixture densities is, however, important for chemical engineering to plan container volumes of industrial plants and to respect the fluid mechanics e.g. for piping. To fill this gap, EoS are indispensable. Densities are also often used for model-parameter estimations.

II.5.2 Equations of State (EoS)

The first semi-empirical EoS was the Van-der-Waals equation. The cubic equation allowed for a better description of fluids compared to the ideal-gas law. The Redlich-Kwong EoS was developed in 1949, but only marginally improved the perfomance of the Van-der-Waals equation. However, it is still used due to its simplicity. Further cubic EoS are the Soave-Redlich-Kwong (SRK) and Peng-Robinson (PR) approaches.

Dahl et al.[396] used SRK-EoS and modified UNIFAC (MHV2-model) to describe the VLE and LLE of water/alcohol/NaCl systems. The ternary LLE water/n-butanol/NaCl was modelled in well agreement to experimental data. An EoS extension to electrolyte solutions was provided by Myers et al.[397], which was based on the PR-EoS in combination with a Born-energy term for charging up the system and a MSA for the ionic interactions. Osmotic and activity coefficients were described accurately but determining the density was not possible. Fürst and Renon combined a modified SRK-EoS with the MSA to account for ionic interactions. A further SR-contribution for ion-solvent intercations was added to predict osmotic coefficients of multinary aqueous solutions. An extension of the EoS of Fürst and Renon was presented by Zuo et al.[398], which allowed also for mixed-solvent electrolyte systems. A drawback of this approach was that the ion-parameters changes for different salts. Pertubation theory for the correlation of activity coefficients and solubilities of amino acids in water was applied by Khoshbarchi and Vera[399]. Spherical shape of molecules was assumed, which is strictly speaking not correct even for the smallest amino acid. In this context, segment-based models are favoured e.g. the Statistical-Association-Fluid Theory (SAFT), which was introduced by Chapman et al.[400]. It is based on Wertheims[401,402] contribution of associating fluids. Repulsive forces between hard-spheres and non-spherical hard-chains, dispersive and associative (hydrogen bonds) interactions are considered within the model. Schreckenberg et al.[403] used the SAFT-VRE approach to predict osmotic coefficients, freezing-point depression and calculate LLE of water/n-butanol/NaCl. Many more examples for SAFT extensions to electrolyte systems can be found in the literature. All of them use the hard-sphere as reference system, which is perturbed by dispersion, association and chain-formation. Further improvement was achieved by using directly the hard-chain as reference system, which led to the development of the PC-SAFT by Gross and Sadowski[186]. This model is presented in the next section together with its electrolyte extension ePC-SAFT[404].

II.5.3 PC-SAFT and ePC-SAFT Equations of State

The PC-SAFT EoS provides an expression for the residual Helmholtz-energy contribution (a^{res}). A residual quantity is the difference between a thermodynamic property of a real fluid and an ideal gas at equal temperature and volume.

$$a^{res}(T,V) = a(T,V) - a^{id}(T,V) \tag{II-48}$$

Residual properties can also be used for multicomponent mixtures. The PC-SAFT EoS is based on perturbation theory, in which the hard-chain fluid (a chain consisiting of hard spheres) is used as the reference system. This reference system is characterised by the Helmholtz-energy contribution (a^{hc}), which is perturbed by SR interactions like attractive van der Waals dispersion (a^{disp}) and associative hydrogen-bonding (a^{assoc}) forces[405]. These individual interaction contributions are additive and can be considered independently. Thus, the residual Helmholtz-energy in PC-SAFT can be written by the following:

$$a^{res} = a^{hc} + a^{disp} + a^{assoc} \tag{II-49}$$

The hard chain (*hc*) comprises a certain number of connected equal hard spheres (*hs*), which are movable round each other. Repulsive forces are acting between the *hc*s depending on the size and shape of the *hc*, which are captured by two adjustable parameters, the segment diameter σ_i and the segment number (m_{seg}). Dispersion forces are attractive, but not specific in direction. The dispersion energy term (a^{disp}) is described by the dispersion-energy parameter (u_i/k_B). The latter three parameter are illustrated in Figure II.15. The exact expressions for the uncharged energy contributions are listed in Appendix D.

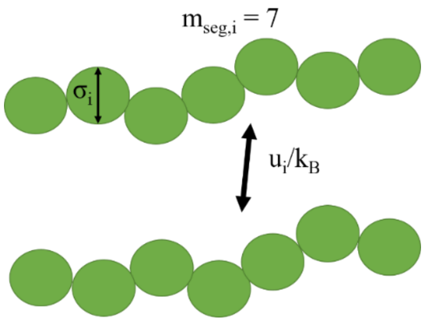

Figure II.15. Visualisation of PC-SAFT pure-component parameters of the hard chain and dispersion contribution for non-associating compounds.

Association interactions apart from dispersion can be found in systems with compounds bearing hydrogen-donor and hydrogen-acceptor sites, i.e. in case of hydrogen bond formation. Hydrogen bond interactions are strong and specific in direction but only short-ranged. The association term (a^{assoc}) is described by the association-energy parameter (ε^{AiBi}/k_B) and association-volume parameter (k^{AiBi}). Both are adjustable parameter and are assigned to each association site of compound i. Modelling with PC-SAFT requires three pure-component parameters for a non-associating component i.

- the segment number $\boldsymbol{m_i^{seg}}$
- the segment diameter $\boldsymbol{\sigma_i}$
- the dispersion-energy parameter $\boldsymbol{u_i/k_B}$

For associating components, two additional pure-component parameters are needed

- association-energy parameter $\boldsymbol{\varepsilon^{AiBi}/k_B}$
- association-volume parameter $\boldsymbol{\kappa^{AiBi}}$

Mixtures are described using the Lorentz-Bertelot combining rules for the segment diameters (σ) and the dispersion-energy parameters (u):

$$\sigma_{ij} = \frac{1}{2}\left(\sigma_i + \sigma_j\right)\left(l - l_{ij}\right) \qquad \text{(II-50)}$$

$$u_{ij} = \sqrt{u_i u_j}\,\left(l - k_{ij}\right) \qquad \text{(II-51)}$$

where l_{ij} and k_{ij} are binary parameters that correct for the deviations of σ_{ij} and u_{ij} from the arithmetic or geometric means of the pure-component parameters. For compounds, which may form hydrogen bonds, the combining rules of Wolbach and Sandler[406] are used for the association paramters.

$$\varepsilon^{A_i B_j} = \frac{1}{2}\left(\varepsilon^{A_i B_i} + \varepsilon^{A_j B_j}\right)\left(1 - k_{ij}^{hb}\right) \qquad \text{(II-52)}$$

$$k^{A_i B_j} = \sqrt{k^{A_i B_i} + k^{A_j B_j}}\left(\frac{\sqrt{\sigma_i \sigma_j}}{\frac{1}{2}\left(\sigma_i + \sigma_j\right)}\right)^3 \qquad \text{(II-53)}$$

The PC-SAFT EoS, which accounts for SR interactions between uncharged molecules, was extended with the DH-contribution to account also for the LR coulomb interactions a^{ion} arising from electrolytes. The resulting ePC-SAFT model was developed by Cameretti et al.[404] in 2005. Similarly to PC-SAFT, the ePC-SAFT EoS expresses the residual Helmholtz energy (a^{res}) with the hard-chain fluid as reference system. All energy contributions to a^{res} in ePC-SAFT are illustrated in Figure II.16 and the expression for a^{res} is given in (II-54).

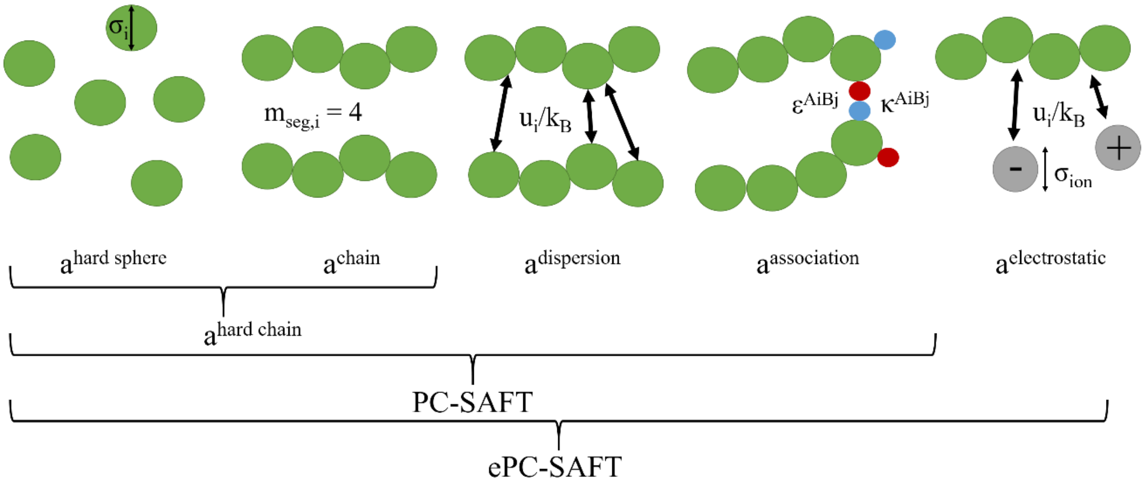

Figure II.16. Visualisation of the ePC-SAFT pure-component parameters corresponding to the hard chain, dispersion, association and the electrostatic contribution to the residual Helmholtz energy (a^{res}). The DH-term is implied in the electrostatic contribution.

$$a^{res} = a^{hc} + a^{disp} + a^{assoc} + a^{ion} \tag{II-54}$$

Applying ePC-SAFT, all ions are treated as charged hard spheres ($m_i^{seg} = 1$) in a dielectric continuum defined by the dielectric constant ε of the solvent. Two parameters are used to characterise each ion:

- the solvated-ion diameter ($\boldsymbol{\sigma_{ion}}$), which is the closest approach between two ions
- the dispersion-energy parameter ($\boldsymbol{u_{ion}/k_B}$), which reflects the strength of ionic hydration if the dispersion between an ion and water is considered

Dispersion between all components is allowed except between ions of equal charge sign. Respecting the dispersion interaction between ions of different charge was a successfull strategy for LLE modelling, which is explained in section II.5.3.3. The repulsive and attractive interactions of ions and the solvent are implied to a^{hc} and a^{disp}, respectively. The contribution (a^{ion}) accounting for the coulomb interactions is depending on ε, which is considered to be independent of the electrolyte and determined by the solvent, solely. No additional adjustable parameters are required for a^{ion}, which is given by the following equation:

$$a^{ion} = -\frac{\kappa}{12\pi\varepsilon}\sum_j x_j q_j^2 X_j \tag{II-55}$$

with x_j and q_j as the mole fraction and charge of ion *j*, respectively. The quantitiy X_j is defined as:

$$X_j = \frac{3}{(\kappa a_j)^3}\left[\frac{3}{2} + \ln\left(1+\kappa a_j\right) - 2\left(1+\kappa a_j\right) + \frac{1}{2}\left(1+\kappa a_j\right)^2\right] \tag{II-56}$$

with a_j as the minimum distance between ions (equivalent to the ion diameter σ_j) and κ as the inverse Debye screening length given by:

$$\kappa = \sqrt{-\frac{N_A}{k_B T\epsilon}\sum_j q_j^2 c_j} = \sqrt{-\frac{\rho_N e^2}{k_B T\epsilon}\sum_j z_j^2 x} \tag{II-57}$$

c_j, N_A and ρ_N are the molarity, the *Avogadro* constant and the numder density, respectively.

II.5.3.1 Intermolecular Potential

The radial distribution function ($g_{ij}(r)$) gives the relative probability of finding other molecules *j* surrounding a center molecule *i* in the distance of *r*. By integrating the product of each intermolecular potential with the corresponding radial distribution function over the surface of the molecules, expressions for the Helmholtz energy are obtained. In PC-SAFT a modified square-well potential is used, see Figure II.17. Negative values of the potential leads to attraction and positive potential to repulsion. At the distance $r = \sigma$, a strong repulsive force between the segments occurs due to the hard-cores of the spheres. In contrast to pure hard-cores, for which the repulsive force becomes infinite at smaller distances than σ, the modified square-well potential respects also the repulsion of soft-cores in real fluids. In PC-SAFT, a temperature dependent hard-sphere diameter $d_i(T)$ with the constant value for $D = 0.12$ is used to account for soft cores.

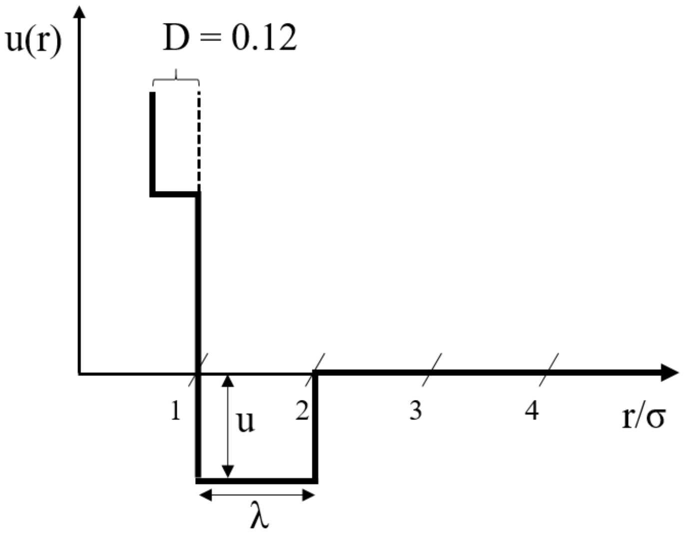

Figure II.17. Pair-interaction potential (modified square-well) depending on the distance between segments with diameter σ. With u as the depth of the attractive potential, λ as the width of the potential. *D* is a factor to account for the soft-core repulsive behaviour.

Temperature-dependent diameters d_i of pure components are required for PC-SAFT caclulations and can be derived from the modified square-well, according to Chen´s correlation[407]:

$$d_i = \sigma_i \left[1 - 0.12 exp\left(-3\frac{u_i}{k_B T}\right)\right] \tag{II-58}$$

with σ_i as the adjustable temperature-independent segment diameter, k_B as the *Boltzmann* constant and u_i as the pure component dispersion-energy parameter. As for two equal ions the dispersion-interaction paremeter (u_i) in ePC-SAFT is set to zero, the expression for the ion diameter for all ions results in:

$$d_{ion} = \sigma_{ion}(1 - 0.12)\,, \tag{II-59}$$

which is then temperature independent.

II.5.3.2 Calculation of Thermodynamic Properties with ePC-SAFT

Pressure

The total pressure p and the total compressibility factor Z of a system are the sum of their ideal and residual parts.

$$p = p^{id} + p^{res} = \frac{nRT}{V} - \left(\frac{A^{res}}{\partial V}\right)_{T,n_i} \tag{II-60}$$

$$Z = Z^{id} + Z^{res} = 1 + \rho_N \left(\frac{\partial A^{res}/nRT}{\partial \rho_N}\right)_{T,n_i} \tag{II-61}$$

The residual pressure p^{res} is obtained by a partial derivation of A^{res} with respect to V at constant T and n_i.

$$p^{res} = -\left(\frac{A^{res}}{\partial V}\right)_{T,n_i} \tag{II-62}$$

The residual compressibility factor is related to the pressure by the following.

$$Z^{res} = \frac{p^{res}V}{nRT} = \rho_N \left(\frac{\partial A^{res}/nRT}{\partial \rho_N}\right)_{T,n_i} \tag{II-63}$$

where R is the ideal gas constant and ρ_N is the total number density of the considered system.

Chemical potential and Fugacity Coefficient

If the chemical potentials of all components in all phases are known, the fugacities and the activity coefficients can be calculated, which is substantial for modelling purposes. The chemical potential of a pure ideal gas (*0i*) is defined by the following:

$$\mu_{oi}^{id}(T,p) = \mu_{0i}^{id,*}(T,p^*) + RTln\left(\frac{p}{p^*}\right) \tag{II-64}$$

with μ^* as the standard chemical potential of the ideal gas at the reference pressure p^*. To describe real behaviour, the fugacity f_{0i} of a pure compound is used:

$$f_{0i} = \varphi_{0i}p \tag{II-65}$$

with φ_{oi} as the fugacity coefficient, which accounts for the deviation from ideality. The chemical potential of a real fluid can then be written as:

$$\mu_{0i}(T,p) = \mu_{0i}^{id,*}(T,p^*) + RTln\left(\frac{p}{p^*}\right) + RTln\varphi_{0i} \tag{II-66}$$

If a mixture is considered, the chemical potential of the ideal gas of a pure component (Eq. (II-64)) has to be extended to the chemical potential of the ideal-gas mixture by introducing the partial pressure $p_i = x_i p$.

$$\mu_i^{id}(T,p,x_i) = \mu_{0i}^{id,*}(T,p^*) + RTln\left(\frac{p}{p^*}\right) + RTlnx_i \tag{II-67}$$

To account for real systems, the fugacity coefficient is again applied:

$$\mu_i(T,p,x_i) = \mu_{0i}^{id,*}(T,p^*) + RTln\left(\frac{p}{p^*}\right) + RTln(\varphi_i x_i) \tag{II-68}$$

By substitution of the standard chemical potential of the ideal gas $\mu*$ with Eq. (II-66), the expression for non-ideal fluid mixture becomes:

$$\mu_i(T,p,x_i) = \mu_{0i}(T,p) + RTlnx_i + RTln\left(\frac{\varphi_i}{\varphi_{0i}}\right) \tag{II-69}$$

The fact that the variables of the residual Helmholtz energy are T and V and not T and p, requires reformulation using the equilibrium condition:

$$\mu_i(T,p,x_i) = \mu_i(T,V,x_i) \tag{II-70}$$

Substraction of $\mu_i^{id}(T,V,x_i)$ from Eq. (II-69) leads to:

$$\mu_i(T,V,x_i) - \mu_i^{id}(T,V,x_i) = \mu_{0i}(T,p) - \mu_i^{id}(T,V,x_i) + RTln\left(\frac{x_i\varphi_i}{\varphi_{0i}}\right) \tag{II-71}$$

with $\mu_{0i}(T, p) = \mu_{0i}^{id}(T, p)$ + RTlnφ_{0i} and $\mu_i^{id}(T, V, x_i) = \mu_{0i}^{id}(T, V)$ + RTlnx_i, Eq. (II-71) becomes to:

$$\mu_i^{res}(T,V,x_i) = \mu_{0i}^{id}(T,p) - \mu_{0i}^{id}(T,V) + RTln\varphi_i \tag{II-72}$$

The difference between $\mu_{0i}^{id}(T, p)$ and $\mu_{0i}^{id}(T, V)$ is just equal to RTln$Z$. An expression for the fugacity coefficient is then obtained by a simple conversion:

$$ln\varphi_i = \frac{\mu_i^{res}(T, V, x_i)}{RT} + lnZ \tag{II-73}$$

Eq. (II-73) is used for all fugacity coefficient calculations required for modelling of osmotic coefficients or LLE. The residual Helmholtz energy (A^{res}), its derivation with respect to the mole fraction and the compressibility factor Z are required to calculate the fugacity. The residual chemical potential can be be derived from the residual Helmholtz energy (A^{res}):

$$\mu_i^{res} = \frac{A^{res}}{nRT} + Z - 1 + \left(\frac{\partial\left(\frac{A^{res}}{nRT}\right)}{\partial x_i}\right) - \sum_{j=1}^{N} x_j \left(\frac{\partial\left(\frac{A^{res}}{nRT}\right)}{\partial x_j}\right) \tag{II-74}$$

Activity and Osmotic Coefficient

For binary or multinary phase equilibria calculations, the activity coefficients have to be known, which can be calculated based on fugacity coefficients. The chemical potential (μ_i) in a mixture (Eq. (II-69)) is usually related to the chemical potential of the real pure component (μ_{0i}) as the reference state and the activity (a_i) of component i.

$$\mu_i(T, p, x_i) = \mu_{0i}(T, p) + RTlna_i \tag{II-75}$$

The activity (a_i) is equal to the product of the concentration (x_i) with the corresponding activity coefficient (γ_i). Comparing Eq. (II-75) and Eq. (II-69) reveals that γ_i also equals the ratio of the fugacity coeffcient at the actual conditions to the one at the reference state:

$$\gamma_i = \frac{\varphi_i(T, p, x_i)}{\varphi_{0i}(T, p, x_i = 1)} \tag{II-76}$$

The quantity (γ_i) is related to the pure component state of component i (0i) and is typically called: “symmetric activity coefficient”. The activity coefficient is a measure of intermolecular interactions and gives therefore information about the deviation from the ideal behaviour. Activity coefficients of the solvent only slightly deviate from unity, which is why the osmotic coefficient (ϕ) was introduced to accentuate the deviation from ideal behaviour. This characterisation method *via* the solvents` activity or osmotic coefficient is only possible for single-solvent solutions. The relation between the practical osmotic coefficient (ϕ) and the activity of the solvent ($a_s = \gamma_s x_s$) was already given in Eq. (II-23) and is presented here again for convenience.

$$\phi = -\frac{1000}{M_\mathrm{s} \sum_\mathrm{i} \nu_\mathrm{i} m_\mathrm{i}} \ln(\gamma_s x_s) \tag{II-77}$$

with M_s being the molecular weight of the solvent, ν_i and m_i as the stoichiometric coefficient (numbers of species in solution) and the molality of the solute, respectively.

Asymmetric and Mean Ionic Activity Coefficient (MIAC)

Whereas the activity coefficient of liquids can be related to the pure-component state, this reference state is not possible for solid solutes, as their pure form is not liquid. Therefore, another reference state is chosen for the solutes to allow for the liquid state: the "infinite dilution" reference state. At this state, an infinitesimal amount of solute is dissolved in the solvent indicated by the infinity symbol (∞). The resulting activity coefficient is called the asymmetrically normalised activity coefficient and reads:

$$\gamma_i^* = \frac{\varphi_j(T, p, x_j)}{\lim\limits_{x_j \to 0} \varphi_j^\infty(T, p)} = \frac{\gamma_j}{\gamma_j^\infty} \tag{II-78}$$

Asymmetric activity coefficients (γ*) can be obtained indirectly *via* vapour pressure data or osmotic coefficents applying the Gibbs-Duhem equation:

$$\ln \gamma^* = (\phi - 1) - \int_0^\mathrm{m} \frac{1 - \phi}{m} \mathrm{d}m \tag{II-79}$$

The definition of the activity coefficient depends on the considered concentration scale. The most common ones are:

a) the molarity *c* [mol·L^{-1}], which is the number of moles of species *i* per unit of volume of the solution. The molarity scale is usually used in thermodynamic models based on the MacMillan Mayer level, since in this framework, the solvent is not explicitly taken into account.

b) the mole fraction *x* [-], which is the ratio of the mole number *n* of component *i* to the sum of the mole numbers of all components in solution. The mole fraction scale is most often used in thermodynamics and engineering.

c) the molality m [mol·kg^{-1}], which is the number of moles n of species i per kilogram of solvent. The molality scale is usually used for experimental data determination. One advantage of this scale is that it is independent of volume changes due to temperature variations.

In this work, most of the concentrations are given in molality scale m [mol/kg]. It is easy to transform molality into weight w or mole x fractions, which are the typical quantities for chemical engineers. All given molalities are referred to the mass of water, unless otherwise specified. This specification of concentration is also named as aqua molality and indicated by [mol/kg (H_2O)]. For the sake of simplicity, the aqua molality is shortened by the general notation: 'molality [mol/kg]'.

The relation of the different activity coefficients in different concentration scales gets obvious in the following equation for the chemical potentials of solute i at equilibrium:

$$\mu_j = \mu_j^{*,x} + RT \ln a_j^{*,x} = \mu_j^{*,m} + RT \ln a_j^{*,m} = \mu_j^{*,c} + RT \ln a_j^{*,c} \,, \tag{II-80}$$

which allows for the conversion of asymmetric activity coefficients between different concentration scales[249]:

$$\gamma_j^{*,m} = \frac{\gamma_j^{*,x}}{\left(1 + 0.001 \nu_j M_s m_j\right)} \approx \gamma_j^{*,x} x_s \tag{II-81}$$

$$\gamma_j^{*,c} = \frac{m_j \rho_{Solution}}{1000 c_j} \gamma_j^{*,m} \tag{II-82}$$

with ν_j as the stoichiometric factor of the solute and $\rho_{solution}$ as the mixture density. If ν_j is equal to unity, the mole fraction can be used for conversion.

The situation becomes even more complicated in case of electrolytes, because free ions can only be present in solution. A pure component state for individual ions does not exist. Instead, the mean chemical potential ($\mu_\pm$) was introduced:

$$\mu_\pm = \nu_+ \mu_+ + \nu_- \mu_- \tag{II-83}$$

with ν_+ and ν_- as the stoichiometric factors of the ions in a given salt. The mean ionic chemical potential ($\mu_\pm$) can be written analogously to Eq. (II-75):

$$\mu_{\pm} = \mu_{\pm}^{ref} + RTln\left(m_{\pm}\gamma_{\pm}^{m}\right) \tag{II-84}$$

The MIAC ($\gamma_{\pm}$) of an electrolyte obeys electrical equivalence and is defined as the geometrical mean of the activity coefficients of the individual ions in solution:

$$\gamma_{\pm} = \left(\gamma_{+}^{\nu_{+}}\gamma_{-}^{\nu_{-}}\right)^{\frac{1}{(\nu_{+}+\nu_{-})}} \tag{II-85}$$

A similar definition holds for the mean molality ($m_{\pm}$). As there is no pure-component state for ions, the asymmetric activity coeffcient with the infinitely dilute reference state is again needed. Although MIACs are most often presented in molality, for ePC-SAFT, the mole-fraction based MIACs are required.

$$\gamma_{\pm}^{*,x} = \frac{\varphi_{\pm}^{x}(T,p,x_j)}{\lim\limits_{x_{\pm}\to 0}\varphi_{\pm}^{\infty,x}(T,p)} = \frac{\gamma_{\pm}^{x}}{\gamma_{\pm}^{\infty,x}} \tag{II-86}$$

The conversion from mole-fraction to molality based MIACs ($\gamma_{\pm}^{*,m}$) can be applied:

$$\gamma_{\pm}^{*,m} = \frac{\gamma_{\pm}^{*,x}}{\left(1+\sum_j 0.001\nu_j M_{solv} m_j\right)} = \frac{1}{\left(1+\sum_j 0.001\nu_j M_{solv} m_j\right)}\left[\frac{\varphi_{\pm}^{x}}{\lim\limits_{x_{\pm}\to 0}\varphi_{\pm}^{\infty,x}}\right] \tag{II-87}$$

where j denotes a nonsolvent species and M_{solv} is the mean molar mass of the solvent mixture:

$$M_{solv} = \sum_{i} x_{solv,i}M_{solv,i} \tag{II-88}$$

and i denotes solvents only[408].

All measured systems considered in this work were in thermodynamic equilibrium. That means, there was no difference in Gibbs energy (G) between both liquid phases, I and II. This state is characterised by equal temperature (T), pressure (p) and electrochemical potential (η) of each component in the equilibrated phases.

$$T^{I} = T^{II} \tag{II-89}$$

$$p^{I} = p^{II} \tag{II-90}$$

$$\eta_i^I = \eta_i^{II} \tag{II-91}$$

with $\eta_i = \mu_i + z_iF\Phi$. If the component is uncharged or the charge can be neglected, the electrochemical potential is equal the chemical potential:

$$\mu_i^I = \mu_i^{II} \tag{II-92}$$

Because of Eq. (II-68), the equality of the chemical potentials can be transferred to the fugacities, which is also called the *isofugacity* criterion:

$$f_i^I = f_i^{II} \tag{II-93}$$

The fugacity can be expressed in terms of the fugacity coefficient and the activity coefficient.

$$f_i^I = \varphi_i^I x_i^I p \tag{II-94}$$

$$f_i^I = \gamma_i x_i^I f_{0i}^I \tag{II-95}$$

For two liquid phases in equilibrium the φ-φ-concept can be applied, which reads:

$$\varphi_i^I(T,p,x_i^I)x_i^I = \varphi_i^{II}(T,p,x_i^{II})x_i^{II} \tag{II-96}$$

The expression containing the activity coefficient could also be used, but standard fugacities in the liquid phases would then be required. Thus, the φ-φ-concept is more convenient for LLE calculations. For salts, which were assumed to be fully dissociated into ν_{an} anions and ν_{cat} cations, the *isofugacity* criterion reads[409]:

$$(f_{an}^I)^{\nu_{an}} \cdot (f_{an}^I)^{\nu_{cat}} = (f_{an}^{II})^{\nu_{an}} \cdot (f_{an}^{II})^{\nu_{cat}} \tag{II-97}$$

The equations for the *isofugacity* criterion are usually solved iteratively, e.g. the pressure is iterated until the fugacities are equal.

II.5.3.3 Applications of ePC-SAFT for LLE Modelling

Many strong electrolyte/water systems were described by Held et al.[410] and in a following paper also weak electrolytes like acetates in the aqueous phase were described by introducing an association/dissociation equilibrium[411]. Thermodynamic properties (densities, osmotic coefficients and MIACs) of alcohol/salt systems were measured and successfully modelled using ePC-SAFT. Based on the binary solvent/salt systems, thermodynamic properties (densities and MIACs) of ternary water/alcohol/salt systems could be accurately modelled without additional parameters, which is a quantitative prediction. Even MIACs of NaCl in a quaternary system composed of water, methanol, ethanol and NaCl were predicted using the corresponding binary ion/solvent parameter and the dielectric constant of the salt-free solvent mixture[408].

In 2014, the ePC-SAFT model was revised[412] to improve accuracy especially for high salt concentrations and solutions containing weak electrolytes like phosphates, sulphates or acetates, which form ion pairs. High deviations between modelled and experimental osmotic coefficients at high electrolyte concentrations or for weak electrolyte solutions arise from the fact that for these systems the DH-Theory is no longer physically meaningful. SR interactions become increasingly important with increasing electrolyte concentration because ions are no longer completely hydrated and are approaching each other. Weak electrolytes, by nature, do not completely dissociate but may form ion pairs. Thus, to account for dispersion interactions between anions and cations seems to be necessary, while dispersion was not considered between ions of equal charge sign. The dispersion between anion and cation can be adjusted by the k_{ij} parameter. This new modelling strategy (including SR dispersion forces between anions and cations) led to a pronounced improvement of osmotic coefficient description of strong univalent-cation electrolyte solutions as well as of solutions containing bivalent anions (SO_4^{2-} and HPO_4^{2-}). In addition, the new modelling strategy allowed the description of osmotic coefficients of aqueous solutions containing the weak electrolytes (Li^+-, Na^+-, K^+-acetate) without applying association/dissociation equilibrium[411] (chemical model). Even though this chemical model is successful, it complicates the situation due to additional species (ion pairs), which have to be handled. To reduce the number of species is especially important and helpful if multicomponent systems are considered. A reasonable representation of the salt series reversal, observed for osmotic coefficients (or MIACs) of alkali halides and alkali acetates (as already mentioned in section II.2.3) was realised by accounting for dispersion between anions and cations. The reversal is represented by the k_{ij} parameter between alkali cations and the anions (halides and acetates). In case of halide anions (Cl^-, Br^-, I^-) the k_{ij} values increase in the following order: $K^+ < Na^+ < Li^+$ and for acetates this series is reversed. This means that the strength of cation-halide interactions increase in the order $Li^+ < Na^+ < K^+$ while cation-acetate interactions decrease in this order. Besides the description of the salt effects water/benzene and water/toluene systems, the new modelling strategy allowed to model the LLE of the ternary system water/n-butanol/NH_4Cl with good agreement to the experimentally determined data from Pirahmadi et al.[391]. For successful modelling of the ternary system, accurate modelling of the binary LLE water/n-butanol is a prerequisite. The pure-component parameter and binary interaction parameter were taken from Nann et al.[413]. In addition, binary interaction parameters between ions and the organic solvent are required, which were adjusted to experimental LLE data of the above-mentioned ternary system. These imply also the l_{ij} parameter, which correct the diameter of the solvated ion (σ_{ion}) in presence of an alcohol. Such corrections for σ_{ion} were already shown for mixtures with methanol and ethanol[408]. Modelling results of the ternary system water/n-butanol/NH_4Cl without respecting dispersion forces between cations and anions led to unsatisfactorily LLE data in terms of wrong tie-line lengths and slopes[412].

The LLE data of ternary systems water/MIBK/salt were experimentally determined with several salts (NaCl, LiCl, KCl, $NaNO_3$, Na_2SO_4, CH_3COONa and CH_3COOLi) and modelled with ePC-SAFT as well as with an extended version of COSMO-RS[395]. Modelling with ePC-SAFT provided very good agreement with experimental LLE data for all salts under investigation. The dielectric constant of pure water was used for the a^{ion} energy contribution. This was justified by ion pure-component parameters, which were fitted to osmotic coefficients and liquid-densities of water/salt solutions. Pure component parameter of water, MIBK and the ions were taken from the literature[412,414,415]. Water was modelled with the two-site 2B association approach[416] with parameters from literature[414,417] and MIBK was modelled as non-polar component accounting for induced association in aqueous mixtures according to Kleiner et al[418]. For MIBK two association sites were assumed. All salts are treated as completely dissociated. The pure-component parameters for the ions are specific, i.e. they do not change by combination to different salts. Binary parameters k_{ij} and k_{ij}^{hb} between water and MIBK were fitted to experimental LLE data of the binary system water/MIBK. Between ions and MIBK, the binary parameters k_{ij} and l_{ij}

were adjusted to LLE data of the ternary system water/MIBK/salt. Binary parameters between water and ions as well as between anions and cations were taken from revised version of ePC-SAFT[412]. With the electrolyte extension of COSMO-RS[295], predictions of the salting-out effect on MIBK were possible, but were less accurate than those of ePC-SAFT. This may be due to the fact that no system specific parameter are used for COSMO-RS predictions. However, it was suggested that COSMO-RS can serve as a very powerful tool for screening purposes. It could be used to reduce the number of experimental investigations by a pre-selection of potential electrolytes as candidates for salt-effect studies in hetereogenous mixed solvents systems. Short-listed systems can then be determined experimentally and accurately modelled using ePC-SAFT.

Studies were conducted to describe also quaternary systems water/MIBK/HMF/salt[419]. Ternary (without salt) and quaternary systems with LiCl, NaCl, KCl, $LiNO_3$, $NaNO_3$, CH_3COOLi, CH_3COONa, Na_2SO_4 or Li_2SO_4 as salt were determined experimentally at 298.15 K and 1 bar. It turned out that the influence of the anions on the strength of the salting-out effect is more pronounced compared to that of the cations. Modelling and prediction of the salt influence on $D^w(HMF)$ values as well as on ternary and quaternary LLE were performed using ePC-SAFT. Therefore, HMF parameters were needed, while the binary and ternary subsystems without HMF were already modelled in the previous publication[395]. Pure component parameters of HMF were obtained by fitting to density and osmotic coefficients of aqueous HMF solutions, which were determined experimentally in that publication. The two-site 2B association approach was also used to model association of HMF. Binary parameters (k_{ij} and l_{ij}) between HMF and MIBK were adjusted to the ternary LLE water/MIBK/HMF. The values of both parameters are very small. One binary parameter (k_{ij}) between HMF and water was fitted to the osmotic coefficients of aqueous HMF solutions at 273.15 K and ternary LLE water/MIBK/HMF at 298.15 K. With the gained parameterisation, the modelling results from ePC-SAFT were in well accordance to the experimental LLE data of the ternary system water/MIBK/HMF. To proceed with quaternary systems, binary parameters (k_{ij} and l_{ij}) between HMF and ions were determined by fitting to LLE data of quaternary water/MIBK/HMF/salt systems at constant salt molality of 3 mol/kg and HMF weight fractions up to 0.3 in the feed. Binary k_{ij} parameters between opposite charged ions were taken from the revised version of ePC-SAFT[412], similar to the previous publication[395]. Experimental and modelled LLE data were in quantitative agreement. Furthermore, the salt influence on $D^w(HMF)$ was accurately predicted using binary HMF/ion parameter adjusted at only one single salt concentration (m(salt) =3 mol/kg).

In the quaternary system water/MIBK/HMF/LiCl, experimental LLE data revealed an increasing salting-out effect of LiCl up to m(LiCl) = 3 mol/kg, rated by $D^w(HMF)$, and a less pronounced salting-out effect at higher LiCl (5 mol/kg) and even a salting-in effect at very high LiCl molalities (7.5 mol/kg). A cation or anion effect was excluded due to increasing $D^w(HMF)$ values for NaCl and CH_3COOLi. Thus, this special observation was further investigated by case studies using ePC-SAFT.

Association effects between water and HMF in the aqueous phase of the quaternary systems water/MIBK/HMF/LiCl and water/MIBK/HMF/CH_3COOLi were investigated by setting the cross-association parameter ε^{AiBj} from its original value to zero. Recalculation delivered very high $D^w(HMF)$ values at zero LiCl concentration, but also a maximum in $D^w(HMF)$ at m(LiCl) = 4 mol/kg. Thus, it could be concluded that the influence of LiCl on the association between water and HMF is not the reason for the salt concentration dependent change of the salt effects.

To account for dispersion interactions between the ions and between water and ions in the aqueous phase of the quaternary system, MIACs of LiCl and CH_3COOLi were calculated in these systems and compared to those present in binary salt/water mixtures. It turned out that the modelling results match very well with experimental MIACs in binary salt/water mixtures. MIACs of CH_3COOLi are lower than unity, which indicates weak ion hydration and strong attraction between the anions and cations. In contrast, MIACs of LiCl are lower than unity up to 3 mol/kg and get increasingly higher beyond this molality. High MIACs indicate strong ion-hydration and weak interactions between both ions. If MIACs and $D^w(HMF)$ were correlated, it appeared that low MIACs favour the salting-out of HMF, i.e. electrolytes, which have a certain tendency to form ion pairs, due to strong attraction between the oppositely charged ions, show a strong salting-out effect on HMF from the aqueous phase, as it is the case for e.g. CH_3COOLi. Strong ion-hydration reduces the strength of the salting-out effect on HMF and even turns salting-out to salting-in of HMF into the aqueous phase at very high salt concentrations. Thus, the strength of the interaction between cations and anions (accounted for in ePC-SAFT by the dispersion energy parameter $u_{\pm}/k_B$) corresponds to the strength and nature of the salt effect. Although the anions are dominating the salt effects, the decisive parameters for successful modelling are the dispersion energy parameters $u_{\pm}/k_B$ between the ions and not only parameters for the anions. If the $u_{\pm}/k_B$ parameter for the ion combination Li^+/Cl^- was increased to a much higher value, salting-out behaviour on HMF was predicted by ePC-SAFT over the whole LiCl concentration range. This gives evidence for the necessity of a small dispersion energy parameter $u_{\pm}/k_B$ for LiCl to capture the special salt-effect of LiCl by ePC-SAFT.

II.5.3.4 LLE Modelling Strategy of this Work

For modelling LLE with ePC-SAFT, pure-component parameters for water, n-butanol, HMF and the ions are required, which were determined in previous publications and are listed in Table II-4. The 2B association scheme was used for the associating components (water, n-butanol and HMF) under investigation. The binary parameters for the pairs n-butanol/water[413], ion/water and ion/ion[412], water/HMF and HMF/ions[419] were taken from the respective literature. Binary parameters for HMF/n-butanol and ion/n-butanol were additionally required for this work, whereas binary parameters of the pairs n-butanol/NH_4^+ and n-butanol/Cl^- already exist[412]. Thus, further parameters k_{ij} and l_{ij} between ion and n-butanol were fitted to the LLE data of ternary water/n-butanol/salt systems, which were experimentally determined in this work at 298.15 K and 1 bar. Similarly, the binary parameters between n-butanol/HMF were fitted to the LLE data of the ternary system water/n-butanol/HMF, which were also experimentally determined in this work at 298.15 K and 1 bar. The determined binary parameters in this work as well as the binary parameters determined in former publications are listed in Table II-5. Basically, the same methodology as described in the latter publictaion[419] was used for the modelling of the systems, considered in this work, with one essential difference; that is, no parameter fitting was done for the quaternary water/n-butanol/HMF/salt systems. Instead, the properties of the quaternary systems considered in this work were predicted, using parameters from the binary and ternary subsystems, while binary HMF/ion parameters are based on the quaternary water/MIBK/HMF/salt systems.

Table II-4. ePC-SAFT pure-component parameters used for modelling of LLE data in this work. Parameters are valid for a dielectric constant of pure water (78.385 at 298.15 K).

Component	Reference	σ_i(Å)	m_i^{seg}	u_i/k_B	$\varepsilon^{AiBi}/k_B(K)$	k^{AiBi}
n-butanol[b]	[413]	3.6139	2.7515	259.59	2544.7	0.0067
water[b]	[414]	[a]	1.2047	353.95	2425.67	0.0451
HMF[b]	[419]	4.038	2.310	320.38	3167.61	0.0010
Na^+	[412]	2.8232	1.000	230.00	-	-
Li^+	[412]	2.8449	1.000	360.00	-	-
K^+	[412]	2.9698	1.000	200.00	-	-
Cl^-	[412]	2.7560	1.000	170.00	-	-
NO_3^-	[412]	3.2988	1.000	130.00	-	-
SO_4^{2-}	[412]	2.6491	1.000	80.00	-	-
CH_3COO^-	[412]	3.9328	1.000	150.00	-	-

[a] $\sigma_{water} = 2.7927 + 10.11 \exp(-0.01775\ T) - 1.417 \exp(-0.01146\ T)$.

[b] 2B association scheme.

Table II-5. ePC-SAFT binary parameter used for LLE modelling in this work[a].

Pair	Reference	k_{ij}	l_{ij}
n-butanol/water [a]	[413]	$2.94\ 10^{-4}$ (T − 293.15 K) − 0.01436	−0.0044
n-butanol/HMF	this work	0.006	0.003
n-butanol/Na^+	this work	0.22	0.245
n-butanol/Li^+	this work	-	−0.08
n-butanol/K^+	this work	-	0.23
n-butanol/NH_4^+	[412]	0.29	0.14
n-butanol/Cl^-	[412]	0.22	0.245
n-butanol/NO_3^-	this work	0.25	0.30
n-butanol/SO_4^{2-}	this work	-	0.20
n-butanol/CH_3COO^-	this work	0.45	-
HMF/Na^+	[395]	0.92	−0.075
HMF/Li^+	[395]	0.38	−0.13
HMF/Cl^+	[395]	−0.40	-0.08
HMF/SO_4^{2-}	[395]	0.40	-
HMF/CH_3COO^-	[395]	−0.19	−0.060
HMF/water	[395]	$-3.832\ 10^{-3}$ (T − 298.15 K) − 0.042	-
MIBK/HMF	[395]	−0.002	0.001

[a] The k_{ij} parameter between water/ion and between anion/cation were taken from the literaure[395,412].

Chapter III

Properties and Characterisation of Aqueous HMF Mixtures

III.1 Introduction

Physico-chemical properties, such as osmotic or activity coefficients, of biochemicals and salts in aqueous solutions are of great interest to realise separation and purification processes in biotechnology and biorefinery. Osmotic coefficients are often used as starting point for any thermodynamic modelling. A well-established method for the determination of such properties is VPO. For instance, osmotic and activity coefficients of aqueous solutions of amino acids like glycine, glutamic acid, histidine and their salts have been determined using this method[420]. In the same manner, derivatives of histidine with protective groups[421], sodium glutamate and sodium aspartate[422] were investigated. The examination of ternary water/amino-acid/salt systems was conducted with glycine (Gly), sodium glutamate (NaGlu) and sodium aspartate (NaAsp) with salts composed of the cations Na^+ or K^+ and the anions Cl^-, Ac^-, NO_3^- or SCN^- [423,424]. Thermodynamic properties like osmotic, fugacity and activity coefficients of the systems water/NaGlu/NaCl, water/NaGlu/KCl, water/ NaAsp/NaCl, water/NaAsp/KCl, water/Gly/$NaNO_3$ and water/Gly/NaSCN were modelled with ePC-SAFT[425]. Solubility of amino-acids in aqueous electrolyte systems and osmotic coefficients of ternary water/amino-acid/salt systems with glycine, L-D/L-alanine, L-/DL-valine and L-proline as amino acids were determined experimentally and could be predicted quantitatively with ePC-SAFT[426]. Here, the influence of salt is more pronounced on osmotic coefficients than on the solubility of amino-acids. Osmotic coefficients and densities of aqueous HMF solutions at molalities from 0.2 to 1.0 mol/kg were already determined. The osmotic coefficients were obtained from cryoscopic osmometry measurements and also calculated using ePC-SAFT[419]. As osmotic and activity coefficients give information about the interactions between solute and solvent molecules, they can be used for molecular association considerations. E.g. osmometric studies of pyrimidines in aqueous solutions revealed involvement of hydrophobic interactions on solute self-association. Different association scenarios, including the isodesmic model[427], were analysed. For the non-electrolytes nicotinamide (NA) and caffeine (CAF), association behaviour in aqueous solution was also found. A decreased osmotic coefficient of $\phi_1^0 = 0.6334$ at m(CAF) = 0.0963 mol/kg (solubility limit) was reported. The CAF system was further examined in terms of Kirkwood Buff Integrals (KBI) and density fluctuations in aqueous solution. High positive values for the KBI (G_{cc}), describing the affinity between two CAF molecules, were found, reflecting a strong association tendency[428]. A decreased osmotic coefficient of ϕ_1^0 ~ 0.52 at m(NA) = 2.0 mol/kg was reported[317], which indicates much weaker association tendency compared to CAF. Association constants for dimerisation (K_2 = 0.203 L/mol) and trimerisation (K_3 = 14.1 L/mol) of NA were calculated from osmotic data. The association constant of NA for the isodesmic model (K = 1.44 L/mol) was already determined in a previous study[287].

For SCS in water, the osmotic coefficient decreases down to 0.35 at molalities smaller than 1 mol/kg[325]. A rapid decrease in ϕ_1^0 was also found for several sodium salts of short-chain alkyl benzene sulfonates[429]. Plots of ϕ_1^0 versus hydrotrope molality or the inverse molality showed kinks characterictic for the MHC of these ionic hydrotropes. Sodium salts of alkyl glycol sulphates and alkyl carbitol sulphates show milder asscociation behaviour compared to the latter mentioned hydrotropes. The kinks here, are less sharp and appear at higher hydrotope concentrations[430]. These hydrotropes bear an ionic hydrophilic function and a short hydrophobic tail resembling the surfactant structure and asscociation behaviour.

In this Chapter, investigations of aqueous HMF mixtures are presented. Osmotic coefficients (or water activities) of binary water/HMF solutions and ternary water/HMF/salt solutions were inferred from VPO measurements. Activity coefficients of HMF in water were calculated applying a Pitzer-type fit-function, while for ternary systems with added salt, a two-parameter fit was used for the calculation of HMF and salt activity coefficients according to Bower and Robinson[431]. From the determined activity coefficients of HMF in water and HMF in electrolyte solutions, conclusions were drawn concerning the aggregation or association behaviour of HMF in aqueous solutions.

Density measurements of water/HMF mixtures were performed at high HMF molalities (2-5 mol/kg) to complete literature data[419]. Dynamic light scattering (DLS) experiments with binary water/HMF and ternary water/HMF/LiCl mixtures were performed to get information about the size of possibly formed colloidal structures. The ability of HMF to solubilise a very hydrophobic compound was tested using the hydrophobic dye DR-13. Finally, the surface tensions of aqueous HMF solutions were determined experimentally and fitted by the Szyszkowski[432–434] equation with the assumption of ideal solution. Obtained fitting parameters were used to calculate the excess surface concentration of HMF and this was compared to those of n-pentanol and tert-butanol[434].

III.2 Experimental

III.2.1 Materials

Water from a Millipore purification system with a specific conductivity of $8*10^{-8}$ S.cm^{-1} at 298.15 K was used for the preparation of all solutions. 5-(Hydroxymethyl)furfural (5-(hydroxymethyl)furan-2-carbaldehyde, HMF), *Molekula* GmbH Munich, ≥ 99.1%) was used without further purification. Due to its low melting point (300.15-303.15 K), HMF was stored at 277 K. Just before use, the HMF container was placed into an ice-box. In addition, HMF is quite hygroscopic, which is why particular care was taken to ensure only temporary air contact. Volumetric KF-titration was applied to determine the water content (0.8 wt%) in HMF. The water content of HMF was accounted for the corresponding HMF and salt molalities in binary and ternary systems. Sodium chloride (*Merck*, ≥ 99.5%) and lithium chloride (*Merck*, ≥ 99%) were dried in an oven at 403.15 K until the mass remained constant. The remaining impurities of the salts after drying are traces of ions and metals with a maximum content of 0.04 wt% for NaCl and 0.06 wt% for LiCl. Thus, after purification (drying) of the salts, a mass-based purity of at least 0.9996 and 0.9994 can be stated for NaCl and LiCl, respectively. The dried salts were stored in a desiccator for further use. Disperse Red 13 (2-[4-(2-Chloro-4-nitrophenylazo)-N-ethylphenylamino]ethanol, DR-13, 95%) and acetone (ACS reagent grade, 99.5%) were obtained from *Sigma-Aldrich*. All solutions were prepared by weight with an accuracy of 0.0001g. If not otherwise specified, all concentrations are given in molality scale [mol/kg of water].

III.2.2 Methods

III.2.2.1 Vapour Pressure Osmometry

Osmotic coefficients of binary water/HMF and ternary water/HMF/salt systems (salt: LiCl, NaCl) were determined *via* VPO. All measurements (calibrations and sample investigations) were carried out at 298.15 K ± $1*10^{-3}$ K and 975 ± 7 hPa using the vapour pressure osmometer K-7000 from *Knauer*. A comparison between results obtained with this equipment and those from direct vapour pressure depression on classical equipment[435] has been done elsewhere[436] and showed good agreement of both techniques. The head of the osmometer was thermostated 2 K higher than the measuring cell to preheat the syringes and to reduce the influence of outside temperature variations. For the investigation of binary water/HMF systems, the gain stage of the osmometer was set to 4, while for ternary water/HMF/salt systems, it was set to 1. Wetted paper wicks were placed into the glass beaker of the measuring cell and 20 ml of water were filled in. The paper wicks are used to guarantee equal vapour distribution in the beaker and to provide an optimum solvent saturated vapour phase. Two droplets of pure water were placed onto the tip of each thermistor using syringes, and after three minutes of equilibration time the panel readings were set to zero. Then, a sample droplet was positioned on one thermistor and after the equilibration time, the panel readings were noted. Special care was taken to keep equal size and shape of the droplets on both thermistors. Each solution was measured nine times (with zero-point adjustment after three measurements) and the mean measured values were considered. For binary water/HMF solutions, measured values (the panel readings of the apparatus) ranged from 130 to 580 (Gain 4, relative error (RE) = 0.84%) and for ternary water/HMF/salt solutions from 210 to 755 (Gain 1, RE = 0.62%). The calibration of the apparatus was performed by measuring aqueous NaCl solutions with salt molalities from 0.2 to 1.6 mol/kg for the investigation of binary water/HMF solutions. Measured values ranged from 123 to 997 (Gain 4, RE = 0.51%). For ternary water/HMF/salt solutions, the NaCl concentrations for calibration were extended to 4.4 mol/kg and measured values ranged from 29 to 798 (Gain 1, RE = 0.33%).

III.2.2.2 Dynamic Light Scattering (DLS)

DLS measurements were carried out with a goniometer CGS-3 from ALV (Langen, Germany) equipped with an ALV-7004/Fast Multiple Tau digital correlator and a vertical-polarised 22mW He-Ne laser, which operates at a wavelength of 632.8 nm. The sample tubes for DLS were cleaned in a custom-designed reflux apparatus. Sample solutions were transferred into the cleaned glass tubes using syringes equipped with a PTFE filter (*VWR* syringe filter, PTFE membrane, 200nm) to remove potential contaminations like dust particles. Each solution was measured at least three times at 25°C and a scattering angle of 90°. Acquisition time of one single measurement was 300 seconds. The obtained correlation functions $G(\tau)$ were fitted with a mono-modal equation (Eq.(III-1) using the ALV-7004 Correlator Software.

$$G(\tau) = a_0 + (a_1 \cdot e^{-a_2\tau})^2 \tag{III-1}$$

here, τ is the delay time, a_0 is a constant baseline value (usually equal to 1), a_1 refers to the dynamic part of the amplitude and a_2 is the decay rate linked to the diffusion coefficient D:

$$a_2 = D \cdot q^2 \tag{III-2}$$

and q is the scattering vector, which is defined as:

$$q = \frac{4\pi n}{\lambda} \sin\frac{\theta}{2} \tag{III-3}$$

with n being the RI, λ the wavelength of the irradiated light in nm and θ the detection angle. In the case of spherical structures or objects, the hydrodynamic radius R_h can be calculated from the Stokes-Einstein equation:

$$R_h = \frac{k_b T}{6\pi \cdot \eta \cdot D} \tag{III-4}$$

with η being the dynamic viscosity, k_b the Boltzmann constant and T the temperature in K.

III.2.2.3 Density

The densities of binary water/HMF mixtures (m(HMF) = 2-5 mol/kg) were measured at 25 °C using an oscillating tube densimeter DMA 5000 M (*Anton Paar*, Austria) with a temperature precision of 0.01 °C. The uncertainty in densities is ± 0.005 kg/m^3. Calibration was perfomed by measuring the density of pure water and that of air (air check).

III.2.2.4 Solubilisation of Hydrophobic Dye DR-13

An excess of DR-13 (λ_{max} = 525 nm) was added to aqueous HMF solutions with different hydrotrope concentrations (m(HMF) = 0.1-5 mol/kg). The resulting water/hydrotrope/dye mixtures were extensively stirred for 48h and left to equilibrate for two days at room temperature 25 °C, filtered (PTFE, pore size: 200 nm) and appropriately diluted with acetone. The filtration step is very important to get truly homogeneous solutions for UV-VIS measurements. Otherwise, excess DR-13 may get in solution during the following dilution steps with acetone and erroneous samples would result. Samples with low HMF content were diluted 1:1 (w/w), in contrast to the deeply red coloured samples, which were diluted 1:100 (w/w) up to 1:300 (w/w). Absorbance measurements were carried out at a wavelength of λ = 525 nm using a spectrophotometer (Lambda 18 spectrophotometer, *Perkin Elmer*). It was expected that the absorbance increases due to increased solubilisation of the hydrophobic dye with increasing HMF concentration. All steps were performed at constant room temperature of 25°C. A corresponding calibration curve of DR-13 in acetone was recorded to assign the collected optical densities of the solubilisation experiments to actual amounts of dissolved DR-13 in the different water/HMF mixtures, see Figure III.1.

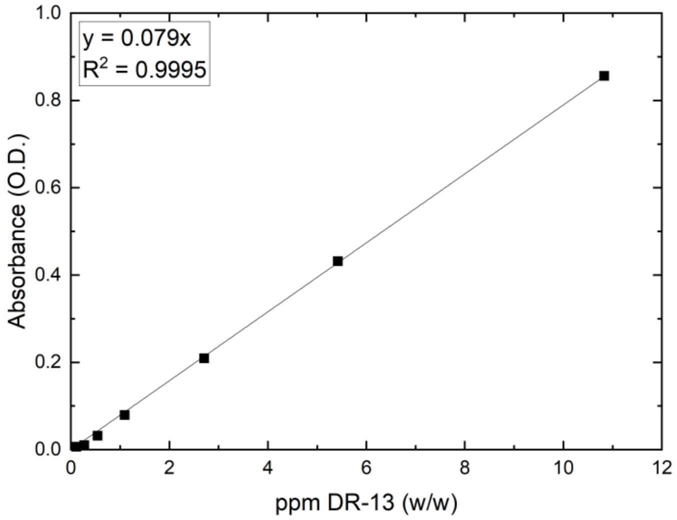

Figure III.1. Calibration curve of the hydrophobic dye Disperse Red (DR-13) dissolved in acetone by means of absorbance (optical density) recorded at a wavelength of 525 nm.

III.2.2.5 Pendant Drop Tensiometry

Two independant dilution series of HMF in water were prepared starting from two stock solutions (3.75 and 5 mol/kg). For each series, seven dilution steps with water (1:1, V/V) were performed while masses were detected. A polynomial relation between molality and density ($y = 0.997 + 0.0266x - 0.0017x^2$) was used to transform molality into molarity. The concentrations of the resulting 16 samples ranged from 0.026 to 4.911 mol/kg or from 0.021 to 3.296 mol/L. The capillary was rinsed with water (50 steps) followed by the sample solutions (10 steps) before the samples were measured. An automatic dispensing system places a droplet of defined volume (20 µL) onto the end of a capillary (3 mm in diameter). For highly diluted samples, the acquisition time was set to 300 seconds and for samples with high HMF concentration, prolonged acquisition times of 600 up to 1000 seconds were required to reach equilibrium and thus stable values for the surface tension. At higher HMF concentrations than 5 mol/kg, surface tension measurements by the pendant drop method were difficult to realise, because of unstable droplets. For each sample solution, the surface tension values of the last 50 seconds were considered to form averaged values.

The resulting function of the surface tension depending on the molarity of solute was fitted by the Szyszkowski[432,433] equation, which has already been applied to various aqueous mixtures, e.g. binary water/n-pentanol, water/tert-butanol and ternary water/n-pentanol/tert-butanol solutions[434]. This equation is based on the assumptions of low solute concentration so that the molarity c is proportional to mole fraction x and of ideal solution with the activity coefficient being equal to unity[437]. The Szyszkowski equation reads:

$$\sigma = \sigma_0 - \frac{RT}{\omega} \ln(1 + kc_1)\,, \qquad \text{(III-5)}$$

where σ_0 and σ are the surface tension of the pure solvent (water) and the solution, respectively, ω [m^2/mol] is the limiting partial molar area of the solute at the surface, k [L/mol] is the solute adsorption coefficient and c_1 is the solute molarity. For concentrated aqueous organic solutions, the Connors[438] equation is more suitable[437]. However, to apply the latter equation, the surface tension of the pure solute (HMF in liquid state) would be required. For very small solute concentrations (the solute activity coefficient approaches unity or is approximately constant), the Gibbs adsorption isotherm provides a relation between the surface tension and the molarity:

$$\Gamma_1 = -\frac{c_1 d\sigma}{RT dc_1} = -\frac{1}{RT}\frac{d\sigma}{d\ln c_1} = -\frac{1}{2.303\,RT}\frac{d\sigma}{d\log c_1}, \tag{III-6}$$

where Γ_1 is the surface excess concentration of the solute at the interface. In Eq. (III-6), the concentration scale must be normalised to avoid units in the logarithm. The derivative of Eq. (III-5) with respect to the solute concentration c_1 reads:

$$-\frac{d\sigma}{dc_1} = \frac{RT}{\omega} * \frac{k}{1+kc_1}, \tag{III-7}$$

which can be inserted into the first term of Eq. (III-6) to calculate Γ_1 with the expression:

$$\Gamma_1 = -\frac{1}{\omega} * \frac{kc_1}{1+kc_1} \tag{III-8}$$

III.3 Results and Discussion

III.3.1 Osmotic Coefficients and Water Activities in Binary Water/HMF and Ternary Water/HMF/Salt Systems

Experimentally determined osmotic coefficients of binary water/HMF(1) (ϕ_1^0) and ternary water/HMF/salt(2) ($\phi_{1,2}$) solutions are presented in Figure III.2 and listed in Table A-1 and Table A-3 of Appendix A, respectively. HMF molalities m_1^0 of binary water/HMF solutions ranged from 0.5 to 5 mol/kg and for ternary water/HMF/salt solutions, m_1 ranged from 1 to 5 mol/kg with salt molalities m_2 = 1 or 3 mol/kg (salt = NaCl, LiCl). Relative standard deviations of calibration and sample measurements were considered to account for the confidence intervals of the reference NaCl molalities, the water activities and the osmotic coefficients, which are also given in Table A-1 and Table A-3. Already published osmotic coefficients of binary water/HMF (ϕ_1^0) solutions determined by cryoscopic osmometry measurements[419] are also presented in Figure III.2 for comparison. The values obtained from cryoscopic osmometry (Gonotec Osmomat 030) are slightly lower than those obtained from VPO measurements (mean absolute deviation = 0.06). It can be noted that aqueous HMF solutions show a negative deviation from ideal behaviour ($\phi_1 < 1$), as osmotic coefficients ϕ_1^0 decrease with increasing HMF molality. This observation indicates molecular association of HMF in water, maybe due to hydrophobic clustering as it is known from classical hydrotropes, leading to the formation of associates e.g. dimers or trimers[317]. On the other hand, molecular dynamics (MD) simulations of HMF at ambient and hydrothermal conditions have revealed that hydrogen-bonding between HMF molecules are more stable compared to those between HMF and water. Further results of that study showed that oxygen atoms of the hydroxyl and the carbonyl group are involved in hydrogen-bonding to a higher degree compared to the oxygen atom within the furan ring. It was found that furfural molecules self-aggregate at ambient (298 K) but not at hydrothermal conditons (502 K)[439]. These findings provide quantitative microscopic insight to the behaviour of HMF molecules in solution, which supports the results obtained from VPO measurements of water/HMF mixtures in this work.

Similar to the binary water/HMF system, osmotic coefficients of ternary water/HMF/salt systems decrease with increasing HMF concentrations. Higher osmotic coefficients are observed in ternary systems compared to those of the binary system. Osmotic coefficients increase with increasing salt concentration, which is more pronounced for LiCl than for NaCl at both salt molalities (m = 1 or 3).

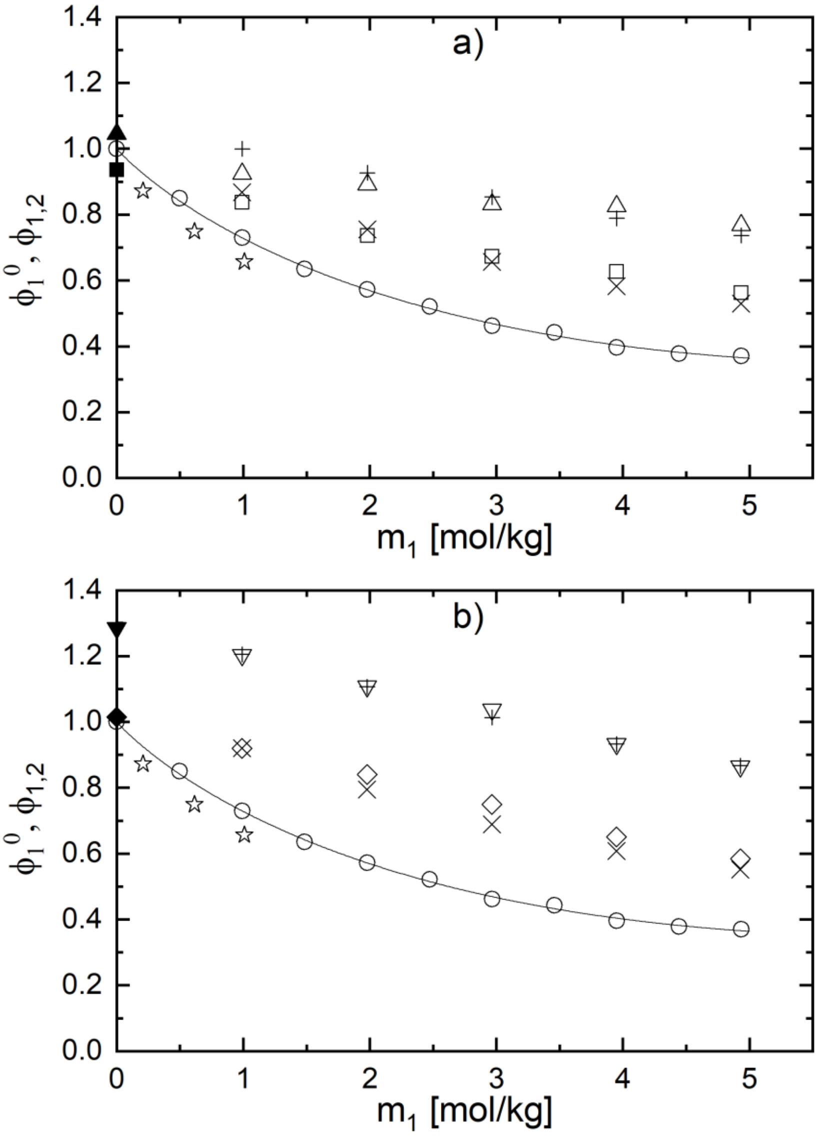

Figure III.2. Osmotic coefficients of binary water/HMF solutions (ϕ_1^0) and of ternary water/HMF/salt solutions ($\phi_{1,2}$). (○) Binary water/HMF, (☆) binary water/HMF from reference[419]. –a) (□) ternary, m(NaCl) = 1 mol/kg; (△) ternary m(NaCl) = 3 mol/kg; (■) binary water/NaCl, m(NaCl) = 1 mol/kg; (▲) binary water/NaCl, m(NaCl) = 3 mol/kg and –b) (◇) ternary m(LiCl) = 1 mol/kg; (▽) ternary m(LiCl) = 3 mol/kg; (◆) binary water/LiCl, m(LiCl) = 1 mol/kg; (▼) binary water/LiCl, m(LiCl) = 3 mol/kg. The solid symbols represent osmotic coefficients corresponding to binary salt solutions and were taken from literature[344,440]. The line (—) represents the approximated course of ϕ_1^0 using the Pitzer type function. (×) and (+) indicate osmotic coefficients of ternary solutions, calculated according to ZSR-rule, for salt molalities of 1 or 3, respectively.

With the assumption of semi-ideal behaviour and the validity of the ZSR-mixing rule, osmotic coefficients of the ternary water/HMF/salt systems are calculated using Eq. (II-34) and presented in Figure III.2. Here, x_1 and ϕ_1^0 as well as x_2 and ϕ_2^0 refer to the binary solutions at the same concentrations as the solutes are present in the ternary solution instead of using data from binary solutions with the same water activity as the ternary solutions. In this manner, it was checked if the osmolalities ($v_i*m_i*\phi_i^0$) of the binary solutions are additive. Water activities of ternary solutions were calculated from experimental data and compared to the sum of the water activities of the binary water/HMF and the binary water/salt solutions at the same concentrations as the solutes are present in the ternary solution. Within the experimental errors, the compared water activities were equal.

Due to the high concentrations, at which the decrease of the osmotic coefficients gets significant, the HMF molecular association is not that pronounced compared to classical hydrotropes. A decreased osmotic coefficient of $\phi_1^0 \sim 0.57$ at m(HMF) = 2.0 mol/kg was found in this work, see Table A-1, which seems to be comparable to that of NA. Association constants of HMF are approximated in section III.3.3.

III.3.2 Activity Coefficients of HMF in Water

The relation between the osmotic coefficient (ϕ) and the activity coefficient (γ) of the solute is accessible through the Gibbs-Duhem equation (Eq. (II-79)). To calculate the HMF activity coefficient in water (γ_1^0) from Eq. (II-79), the osmotic coefficient must be integrated from zero molality to the desired solute molality m_1. Therefore, the dependence of (ϕ_1^0) (for the aqueous non-electrolyte solution) down to zero concentration was approximated with a Pitzer-type function with missing DH- and m^2-term, see Eq. (III-9). Adjusted parameters and the standard deviation σ of the fit are given in Table III-1. The α_1 parameter was varied in the range of 0.3 to 1.6 and the best fit was obtained by setting α_1 equal to 0.4.

$$\phi = 1 + m\left[\beta^{(0)} + \beta^{(1)}\exp\left(-\alpha_1 m^{1/2}\right)\right] \tag{III-9}$$

Table III-1. Pitzer parameter of Eq. (III-9) for aqueous HMF solutions ($\alpha_1 = 0.4$ [kg$^{1/2}$/mol$^{1/2}$]).

$\beta^{(0)}$	$\beta^{(1)}$	σ
0.0992	-0.5540	0.0066

Inserting Eq. (III-9) into Eq. (II-79), the following expression results for the HMF activity coefficient in aqueous solution:

$$\ln\gamma = m\left\{2\beta^{(0)} + \frac{2\beta^{(1)}}{\alpha_1{}^2 m}\left[1 - \left(1 + \alpha_1 m^{1/2} - \frac{1}{2}\alpha_1{}^2 m\right)\exp\left(-\alpha_1 m^{1/2}\right)\right]\right\} \quad \text{(III-10)}$$

Activity coefficients of HMF are calculated using the parameters from Table III-1 and are listed in Table A-2 and presented as the natural logarithm depending on molality in Figure III.3. Similar to the osmotic coefficients, the $\ln(\gamma_1{}^0)$ decreases monotonically with increasing HMF concentration.

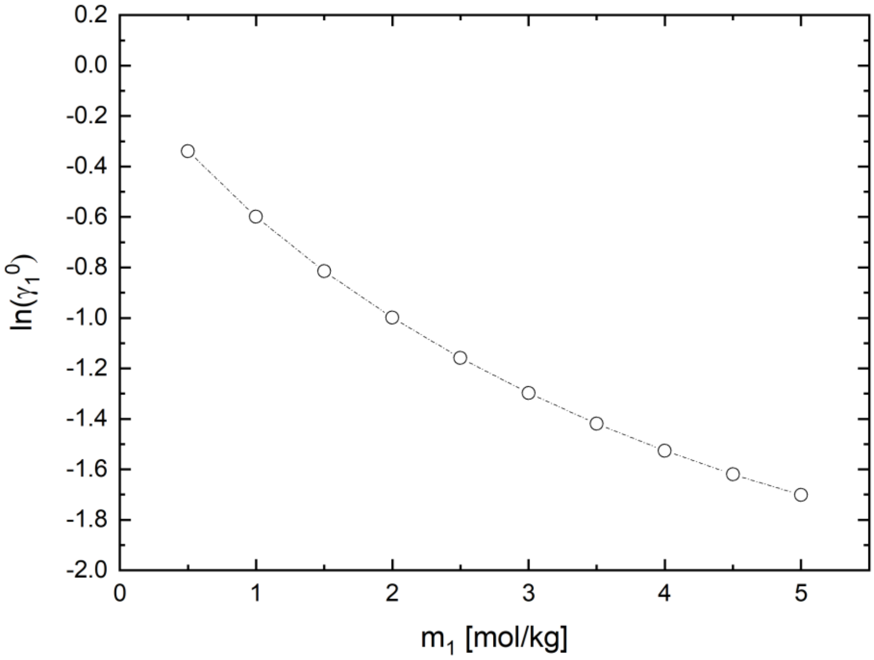

Figure III.3. Activity Coefficients of HMF in water depending on the HMF molality at 298.15 K and 975 hPa.

III.3.3 Association Constants of HMF in Water

Once the solute activity coefficients were calculated, the stepwise association model was used to determine association constants[316,317,441–443]. In this model, consecutive self-association of hydrotrope/co-solvent molecules is assumed. The formation of dimers, trimers, tertramers etc. are equilibrium processes with association constants for each association step, which is mathematically presented in the following:

$$\begin{aligned} M_1 + M_1 &\rightleftharpoons M_2 & K_2 &= m_2/m_1^2 \\ M_2 + M_1 &\rightleftharpoons M_3 & K_3 &= m_3/(m_2 m_1) \\ &\cdots \\ M_{n-1} + M_1 &\rightleftharpoons M_n & K_n &= m_n/(m_{n-1} m_1) \end{aligned} \tag{III-11}$$

Here, the concentrations of monomer (M_1), dimer (M_2) and trimer (M_3) species in solution are denoted by m_1, m_2 and m_3, etc. According to the association model described above, the actual molality of the solution or osmotic molality m_{osm} is then:

$$m_{osm} = m_1 + K_2 m_1^2 + K_2 K_3 m_1^3 + \cdots + K_2 K_3 \ldots K_n m_1^n \tag{III-12}$$

and the stoichiometric molality is expressed as:

$$m = m_1 + 2K_2 m_1^2 + 3K_2 K_3 m_1^3 + \cdots + nK_2 K_3 \ldots K_n m_1^n \tag{III-13}$$

Differentiation of Eq. (III-12) with respect to m_1 leads to Eq. (III-13) divided by m_1, thus

$$\frac{\mathrm{d}m_{osm}}{\mathrm{d}m_1} = \frac{m}{m_1} \tag{III-14}$$

For non-electrolytes in dilute solutions the osmotic molality m_{osm} is defined by

$$m_{osm} = \phi_1^0 m \tag{III-15}$$

Differentiation of Eq. (III-15) and inserting the obtained expression for $\mathrm{d}m_{osm}$ into Eq. (III-14) yields:

$$\mathrm{d}\ln\frac{m_1}{m} = (\phi_1^0 - 1)\mathrm{d}\ln m + \mathrm{d}\phi_1^0 \qquad \text{(III-16)}$$

Integration of Eq. (III-16) and respecting the condition that both m_1/m and ϕ approach unity at infinite dilution, gives

$$\ln\frac{m_1}{m} = (\phi_1^0 - 1) - \int_0^{\mathrm{m}} \frac{1 - \phi_1^0}{m}\mathrm{d}m \qquad \text{(III-17)}$$

The comparison of Eq. (II-79) and Eq. (III-17) results in the following equality:

$$\gamma = \frac{m_1}{m} = x_1\,, \qquad \text{(III-18)}$$

which means that the molal solute activity coefficient γ is equal to the mole fraction x_1 of monomers in solution. With activity coefficients obtained from osmometric data, Eq. (III-18) allows the calculation of the monomer molality m_1 depending on the stoichiometric molality m. The expression for the stoichiometric molality (Eq. (III-13)) divided by the monomer molality m_1 is identical to the inversion of Eq. (III-18) and leads directly to the following series of expansion, in which the unknowns are the consecutive equilibrium constants:

$$\frac{1}{\gamma} = 1 + 2K_2m_1 + 3K_2K_3m_1^2 + \cdots + nK_2K_3\ldots K_nm_1^{n-1} \qquad \text{(III-19)}$$

Values for the association constants can be obtained from a polynomial function fitted to the plot of the inverse of the solute activity coefficient $1/\gamma$ versus the monomer molality m_1. The problem here is to identify the degree of association n. There are some mathematical operations described in reference[442] to obtain n and K, which failed for the presented data set. To simplify the situation, isodesmic association is assumed, where all equilibrium constants are equal ($K_2 = K_3 = \ldots = K_n = K$) and the degree of association is not limited and arbitrarily set to n. Based on these assumptions, Schellman[444] derived the following equation for urea solutions:

$$K = \frac{1 - \phi_1^0}{m(\phi_1^0)^2} \qquad \text{(III-20)}$$

If only dimers are formed, that is only M_1 and M_2 species are present in solution, $K = K_2$ and K_3, $K_4 \ldots K_n$ are equal to zero, Schellmans approach leads to Eq. (III-21).

$$K = \frac{1 - \phi_1^0}{m(2\phi_1^0 - 1)^2} \tag{III-21}$$

According to the dimer model in Eq. (III-21), a plot of $(1 - \phi_1{}^0)/(2\phi_1{}^0 - 1)^2$ versus the molality would result in a linear relationship and the slope would deliver the association constant $K_2 = K$. Similarly, the slope of $(1 - \phi_1{}^0)/\ (\phi_1{}^0)^2$ versus the molality would represent K of the isodesmic model Eq. (III-20). The plots of both association models described above are illustrated and compared in Figure III.4 a) and b), respectively. The relationship presented in Figure III.4 a) resembles rather an exponential growth than a straight-line dependence over the studied concentration range. Thus, it can be concluded that association of HMF molecules takes place beyond the dimer stage and the potential involvement of higher order associates is suggested. The plot of the isodesmic model in Figure III.4 b) can be fitted by linear regression ($R^2 = 0.983$), which indicates that the isodesmic model is appropriate to describe the association behaviour of HMF in aqueous solution. The value for the association constant K is obtained from the slope of linear regression ($K = 0.89$ kg/mol), which is lower compared to that of NA ($K = 1.44$ L/mol).

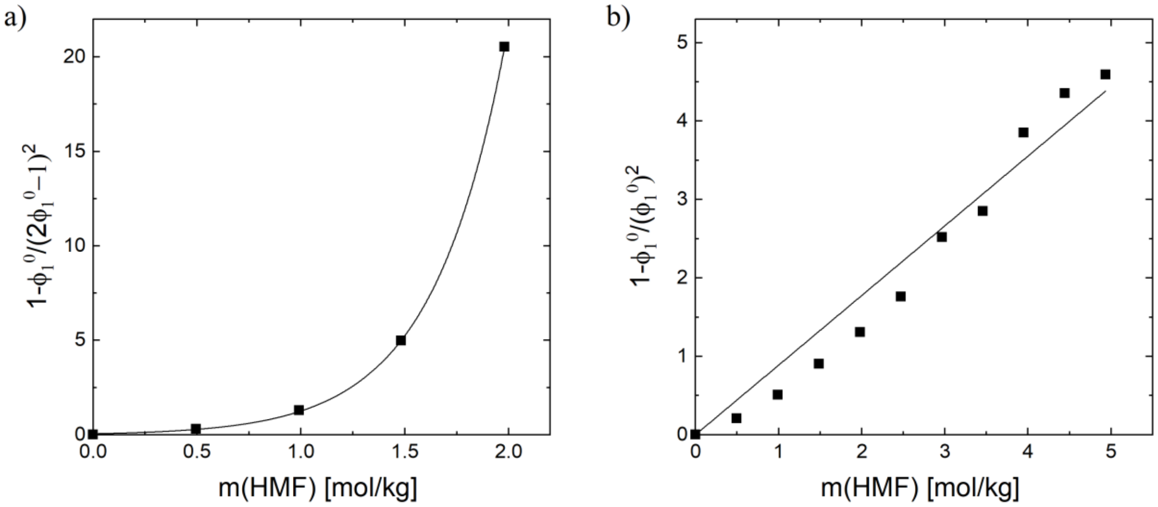

Figure III.4. -a) Plot of the dimer model: $(1 - \phi)/(2\phi - 1)^2$ vs. m(HMF); non-linear relationship and -b) plot of the isodesmic model: $(1 - \phi)/\phi^2$ vs. m(HMF); linear relationship.

III.3.4 Solute Activity Coefficients in Ternary Water/HMF/Salt Solutions

The molal activity coefficient of HMF (γ_1) in aqueous electrolyte solution may be expressed in a power series depending on the molality of HMF m_1 and the molality of salt (NaCl or LiCl) m_2.

$$\ln\gamma_1 = \sum_{\mathrm{i}=0}^{\infty}\sum_{\mathrm{j}=0}^{\infty} A_{\mathrm{ij}} m_1^{\mathrm{i}} m_2^{\mathrm{j}} (A_{00} = 0) \tag{III-22}$$

Neglecting all terms higher than third order in the power series, the expression for the non-electrolyte activity coefficient in ternary solutions can be written as:

$$\begin{gathered}\ln\gamma_1 = \ln\gamma_1^0 + A_{01}m_2 + A_{11}m_1m_2 + A_{02}{m_2}^2 + A_{21}{m_1}^2m_2 \\ +A_{12}m_1{m_2}^2 + A_{03}{m_2}^3\end{gathered} \tag{III-23}$$

The values for γ_1^0 (activity coefficients of HMF in water) were calculated in the previous section and are given in Table A-2. Using the cross-differentiation relation (Eq. (III-24)), which is derived on the basis of the Gibbs-Duhem equation, an expression for activity coefficients (γ_2) of solute 2 (NaCl or LiCl) in the ternary solution can be obtained, see Eq. (III-25). Salt activity coefficients are considered as MIACs. The factor 2 on the right hand side in Eq. (III-24) originates from the solute 2 being a 1:1 electrolyte[445].

$$\left[\frac{\partial \ln\gamma_1}{\partial m_2}\right]_{m_1} = 2\left[\frac{\partial \ln\gamma_2}{\partial m_1}\right]_{m_2} \tag{III-24}$$

$$\begin{gathered}\ln\gamma_2 = \ln\gamma_2^0 + \tfrac{1}{2}A_{01}m_1 + \tfrac{1}{4}A_{11}\,{m_1}^2 + A_{02}m_1m_2 \\ +\tfrac{1}{6}A_{21}{m_1}^3 + \tfrac{1}{2}A_{12}{m_1}^2m_2 + \tfrac{3}{2}A_{03}m_1{m_2}^2\end{gathered} \tag{III-25}$$

The values for γ_2^0 are taken from[344,440]. The coefficients in Eq. (III-23) and Eq. (III-25) for the calculation of the solute activity coefficients γ_1 and γ_2 in ternary solutions are related to the quantity Δ. It is introduced for each set of molalities as described by Robinson et al.[431,446,447] and can be directly determined from experimental data, see Eq.(III-26).

$$\Delta = 2m_{\mathrm{Ref}}\phi_{\mathrm{Ref}} - m_1\phi_1^0 - 2m_2\phi_2^0 = -55.51\ln a_{\mathrm{s}} - m_1\phi_1^0 - 2m_2\phi_2^0 \tag{III-26}$$

where m_{Ref} is the molality of the reference NaCl solution with the same water activity of the ternary solution, ϕ_{Ref} is the osmotic coefficient of the reference NaCl solution, a_{s} is the water activity in the ternary solution, $\phi_1{}^0$ is the osmotic coefficient of the binary system water/HMF at molality m_1 of the ternary solution and $\phi_2{}^0$ is the osmotic coefficient of the binary system water/salt at molality m_2 of the ternary solution. Values for $\phi_2{}^0$ are taken from the literature[344,440]. After integration and other transformations, it follows that the cross-differentials from Eq. (III-24) are identical to $\Delta/(m_1m_2)$[448]. The function $D = \Delta/(m_1m_2)$ was approximated by two-parameter fitting of the power series from Eq. (III-22) with neglected terms higher than third order.

$$D = A_{01} + A_{11}m_1 + 2A_{02}m_2 + A_{21}m_1^2 + 3A_{03}m_2^2 + (\frac{3}{2})A_{12}m_1m_2 \qquad \text{(III-27)}$$

Calculations were done by *E. Tsurko* with the use of the program *calc e2d* elaborated in the framework of the unified approach to the physico-chemical data treatment[449]. The coefficients of the two-parameter fit according to Eq. (III-28) were found to be: $a_0 = -12.04999$, $a_1 = 0.14215$, $a_2 = 15.80193$, $a_3 = -0.01415$, $a_4 = -3.95986$, $a_5 = -0.01143$ for the ternary system water/HMF/NaCl and for the ternary system water/HMF/LiCl, the coefficients were equal to: $a_0 = -17.30053$, $a_1 = 0.14396$, $a_2 = 22.98064$, $a_3 = -0.01520$, $a_4 = -5.74742$, $a_5 = -0.03342$.

$$D = a_0 + a_1m_1 + a_2m_2 + a_3m_1m_1 + a_4m_2m_2 + a_5m_1m_2 \qquad \text{(III-28)}$$

With $a_0 = A_{01}$, $a_1 = A_{11}$, $a_2 = 2A_{02}$, $a_3 = A_{21}$, $a_4 = 3A_{03}$, $a_5 = (3/2)A_{12}$, the coefficients from Eq. (III-27) are determined to be: $A_{01} = -12.04999$, $A_{11} = 0.14215$, $A_{02} = 7.90097$, $A_{21} = -0.01415$, $A_{03} = -1.31995$, $A_{12} = -0.00762$ for water/HMF/NaCl and for water/HMF/LiCl, the coefficients are: $A_{01} = -17.30053$, $A_{11} = 0.14396$, $A_{02} = 11.49032$, $A_{21} = -0.01520$, $A_{03} = -1.91581$, $A_{12} = -0.02228$. The route of calculating activity coefficients in ternary solutions was checked before with data from the reference system water/sucrose/NaCl[447]. The comparison of D^{obs} and D^{calc} shows the standard deviation of 0.013 or 0.015, which is less than the experimental error, see Table A-4.

With the use of the determined coefficients of Eq. (III-27) (A_{01}, A_{11}, A_{02}, A_{21}, A_{03}, A_{12}), activity coefficients of HMF (γ_1) and salt (γ_2) in ternary Water/HMF/Salt solutions are calculated according to Eq. (III-23) and Eq. (III-25) and listed in Table A-5 and Table A-6.

Very low values for HMF activity coefficients were obtained at salt background molality $m_2 = 1$ mol/kg ($\gamma_1 < 0.0001$). However, the absolute values are questionable. Therefore, the data are not shown (n.s.). The reason why the calculation failed for these systems is the relatively low quantity of data points (2 curves, 10 data points) for the surface representation, which complicates the determination of these sensible values. The coefficients that we can obtain by the data treatment in such case could not adequately describe all sectors of the surface in each composition, especially if the surface contains convexity and extremums.

In Figure III.5, HMF activity coefficients in binary water/HMF and ternary water/HMF/salt solutions are displayed depending on the HMF molality m_1. For each system, the activity coefficients are monotonically decreasing. In the binary system, $\ln(\gamma_1^0)$ decreases exponentially while for systems containing electrolytes a nearly linear decrease of $\ln(\gamma_1)$ is observed for both, NaCl and LiCl. The linear decrease is in accordance with the Long-McDevit[269] equation for activity coefficients of non-electrolytes. At about $m_1 = 3.4$, a crossover of the HMF activity coefficients in ternary systems occurs. At HMF molalities greater than 2 mol/kg, HMF activity coefficients are very similar (except at $m_1 = 5$ and m_2(LiCl) = 3) in binary and ternary systems, which indicates only a small influence of the added electrolytes on the HMF behaviour (chemical potential) in aqueous mixtures.

This latter finding was indirectly confirmed by ePC-SAFT modelling with and without the cross-association parameter ε^{AiBj} between water and HMF. The modelling results of Mohammad et al.[419] revealed that independently of the cross-association between water and HMF, a maximum in $D^w(HMF)$ depending on LiCl molality is obtained. Thus, LiCl does not influence the assocoiation behaviour between water and HMF, which was already discussed in section II.5.3.3.

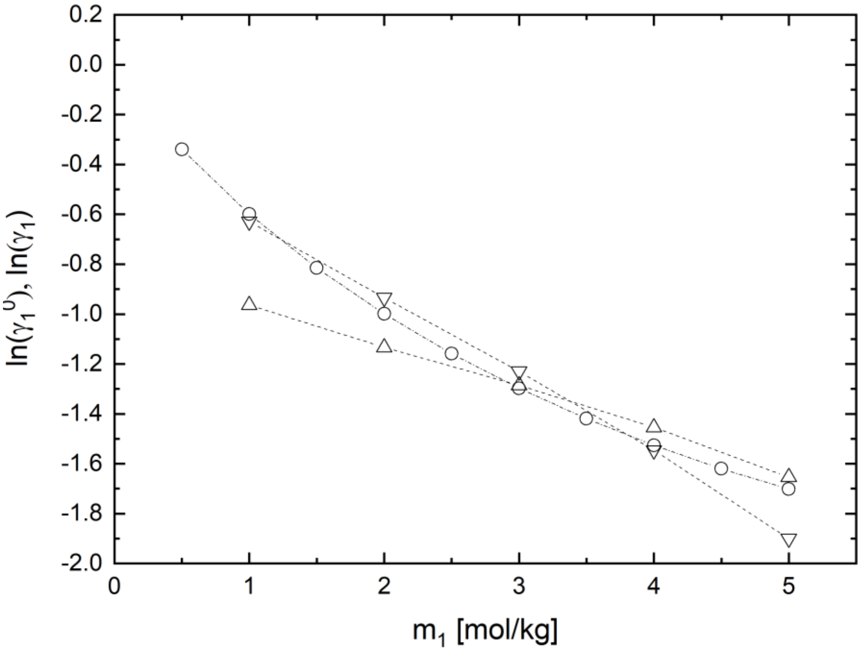

Figure III.5. HMF activity coefficients in binary Water/HMF solutions, $\ln(\gamma_1^0)$ and in ternary water/HMF/salt solutions at m_2 = 3 mol/kg, $\ln(\gamma_1)$. (○) Binary water/HMF, (△) ternary water/HMF/NaCl (3m NaCl), (▽) ternary water/HMF/LiCl (3m LiCl).

In Figure III.6, salt activity coefficients in ternary water/HMF/salt solutions depending on the HMF molality m_1 are shown. In case of NaCl at m_2 = 1, the salt activity coefficient decreases slightly until m_1 = 2 and increases again slightly until m_1 = 5. In case of LiCl at m_2 = 1, the salt activity coefficient increases above m_1 = 1. For both salts at m_2 = 3, the salt activity coefficients decrease monotonically with increasing HMF concentration. Higher salt activity coefficients are obtained for LiCl compared to NaCl at salt molalities of 1 and 3 mol/kg. In the ternary system containing LiCl, the obtained salt activity coefficients are higher at a higher salt concentration until m_1 = 4. In comparison, a higher activity coefficient at higher salt concentration is only found at m_1 = 1 for the ternary system containing NaCl. The crossovers of $\ln(\gamma_2)$ for the two salt molalities are at m_1 = 1.6 for NaCl and at m_1 = 4.0 for LiCl.

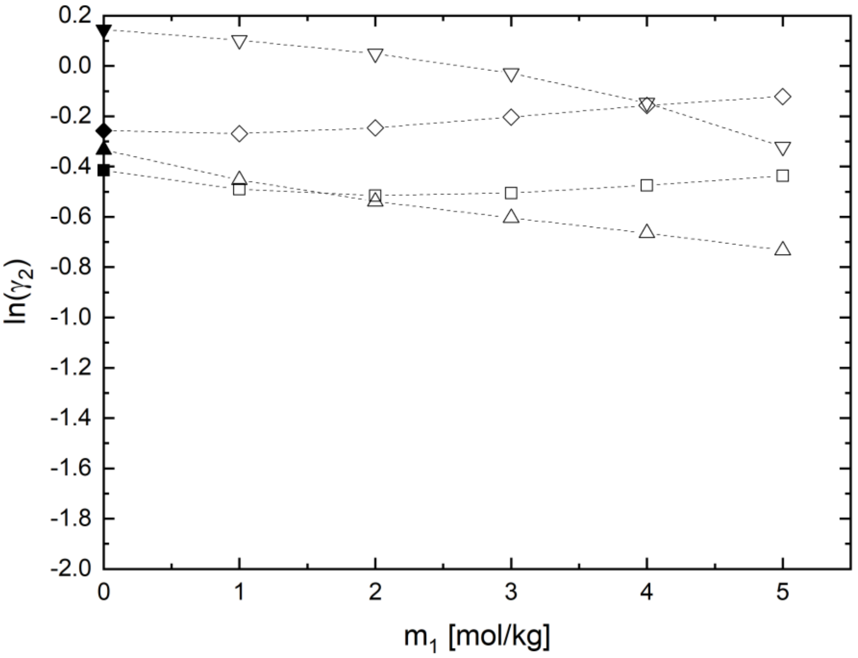

Figure III.6. Salt activity coefficients in ternary water/HMF/salt and in binary water/salt solutions, ln(γ_2). (□) Ternary water/HMF/NaCl (1m NaCl), (△) ternary water/HMF/NaCl (3m NaCl), (◇) ternary water/HMF/LiCl (1m LiCl), (▽) ternary water/HMF/LiCl (3m LiCl), (■) binary water/NaCl, m(NaCl) = 1 mol/kg, (▲) binary water/NaCl, m(NaCl) = 3 mol/kg, (◆) binary water/LiCl, m(LiCl) = 1 mol/kg, (▼) binary water/LiCl, m(LiCl) = 3 mol/kg. The solid symbols represent activity coefficients corresponding to binary salt solutions and were taken from[344] and[440].

III.3.5 Dynamic Light Scattering (DLS)

Binary water/HMF mixtures with HMF molalities ranging from 1.5 to 5.0 mol/kg and ternary water/HMF/LiCl mixtures with LiCl molalities of 3, 6 and 12 mol/kg and constant HMF molality of 4 mol/kg were investigated by means of DLS at 25°C. The corresponding correlation functions, obtained from DLS, are illustrated in Figure III.7 and Figure III.8. In case of the binary mixture, the correlations are increasing with increasing HMF concentration, a trend, which is usually observed for molecules with a certain propensity to self-aggregate in the present liquid medium. A single exponential decay can be observed for all correlation functions, which indicates mono-disperse spherical entities being present in the solutions. Nevertheless, the correlation functions of HMF molecules in water are less pronounced and point to only weak association or aggregation behaviour, because the decline of the functions is in too short time scales (~0.01 µs) and the maximum value of the correlation function (~0.5) is small as well. For comparison, well defined colloid structures like SDS-micelles in solution show maximum values of the correlation function near to 1.

“Particle” size evaluation of the HMF associates in water was done with simple mono-modal fitting using the ALV-7004 Correlator Software. Due to the weak signals from DLS, viscosity and RI measurements were not conducted, but reference values for pure water (RI = 1.332, $\eta(H_2O)$ = 0.8903 cp at 25°C)[450] were used to approximate the particle radii, which are presented in Figure III.7 b) depending on HMF molality.

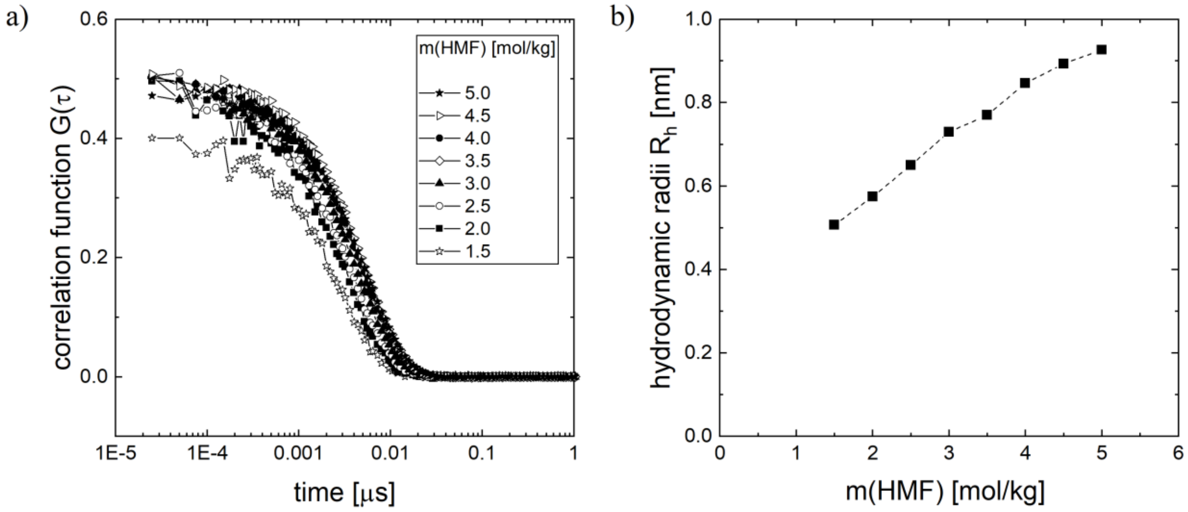

Figure III.7. –a) Time-dependent self-correlation functions obtained by DLS for the binary water/HMF mixtures at 25°C and –b) estimated hydrodynamic radii R_h of the HMF-associates in aqueous solutions depending on HMF molality.

In case of the ternary mixture water/HMF/LiCl at constant HMF molality of 4 mol/kg, the correlations are decreasing with increasing LiCl concentration from zero molality up to m(LiCl) = 12 mol/kg. This indicates a decreased HMF self-association with increasing LiCl concentration and implies a reduction of the HMF-HMF interactions. To be consistent with the additivity of the osmolalities of the respective binary subsystems, which was confirmed by the ZSR-mixing rule, the cost of HMF self-interactions must be balanced by interactions between LiCl and HMF. Thus, the solute 1-solute 2 interactions are not negligible compared to solute-solvent interactions, but compensate the reduced solute 1-solute 1 (HMF-HMF) interactions.

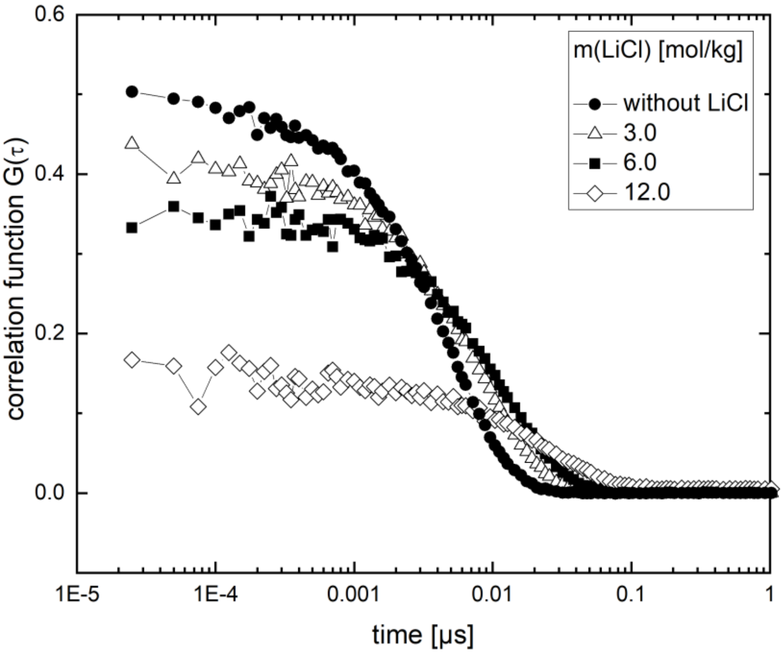

Figure III.8. Time-dependent self-correlation functions obtained by DLS for (●) binary water/HMF and ternary water/HMF/LiCl mixtures at m(HMF) = 4 mol/kg and 25°C. LiCl molalities in ternary mixtures are (△) 3m, (■) 6m and (◇) 12m.

III.3.6 Density of Binary Water/HMF Mixtures

Density measurements of binary water/HMF mixtures were performed at 298.15 K using an oscillating tube densimeter DMA 5000 M (*Anton Paar*, Austria) according to the experimental section III.2.2.3. By a polynomial relationship between density and HMF molality, it was possible to transform the concentration scale to molarity. The HMF molarity was required to compare the MHC of HMF to those of other solubilsers in solubilisation experiments and to fit the course of the surface tension by the Szyszkowski equation. The results of both mentioned experimental investigations are following in the next two sections III.3.7 and III.3.8.

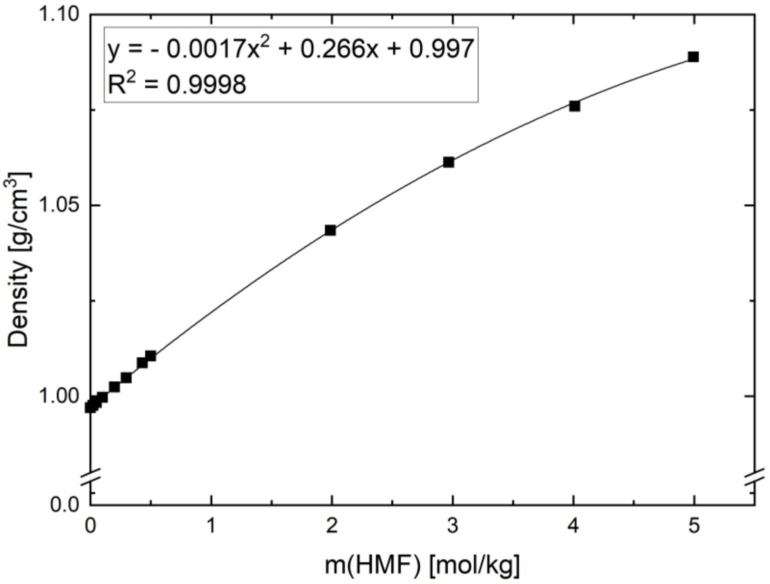

Figure III.9. Density data of binary water/HMF mixtures at 298.15 K. The data points at low concentration up to m(HMF) = 0.5 mol/kg were taken from Mohammad et al.[419].

III.3.7 Solubilisation of Hydrophobic Dye (DR-13)

To determine the hydrotopic efficiency of HMF, the solubilisation of the hydrophibic dye DR-13 in water was examined with the help of aqueous HMF solutions of different concentrations. The resulting ternary water/HMF/DR-13 mixtures with excess DR-13 and increasing amounts of HMF from left to right are illustrated in Figure III.10. The increasing solubilisation of the hydrophobic dye with increasing HMF concentration is obvious by the different intensities of the red coloration of the mixtures. At very low hydrotrope concentration, the hydrophobic dye DR-13 is sparingly in solution (extreme left). Whereas for high hydrotrope concentrations the mixtures get deeply red coloured (extreme right).

Figure III.10. Solubilisation of the hydrophobic dye DR-13 in aqueous HMF solutions with increasing HMF content from left to right.

The different amounts of solubilised DR-13 in aqueous HMF mixtures were examined by absorbance measurements *via* UV-VIS spectrophotometry after filtration and appropriate dilution with acetone. Relative optical densities (relative O.D.´s) were calculated from the collected absorbance values of diluted samples and the corresponding dilution factors. Results of the solubilisation experiments are listed in Table A-8 and presented in Figure III.11 by drawing relative O.D.´s against the HMF concentration in molality and molarity scale. For both concentration scales, a linear-linear and a log-linear plot was constructed. In the linear-linear presentation (Figure III.11 a) and Figure III.11 c)) the O.D.´s are increasing exponentially with increasing HMF concentration and are in the same magnitude as for solubilisation experiments with the co-solvents acetone and 1-propanol reported by Bauduin[299]. According to the PhD thesis of Bauduin[301], a possible MHC of a solubiliser can be approximated by the intersection of the abscissa with the tangent at the linear part of the solubility plot where solubilisation becomes significant. In this way, the graphically determined MHC of HMF is approximately 1.9 mol/kg in molality scale and in molarity scale the MHC is approximately 1.76 mol/L. The hydrotropic efficiency of HMF can thus be classified relative to the solubilisers tested by Bauduin in the following order: SXS (MHC = 0.8 mol/L) > C_3PO_1 (MHC = 1.2 mol/L) > C_3EO_1 (MHC = 1.45 mol/L) > HMF (MHC = 1.76 mol/L) > acetone (MHC = 1.8 mol/L) > 1-propanol (MHC = 2.1 mol/L) with the most effective hydrotrope on the left. Although the MHC values of HMF and acetone are similar, the amount of solubilised hydrophobic substance by HMF is much higher, because the relative O.D. values at a concentration of 2.3 mol/L are higher in the case of HMF (rel O.D. (2.3 mol/L) = 5.5) than in case of acetone (rel O.D. (2.3 mol/L) ≈ 0.5). The ordering of HMF between the classical co-solvents (acetone, 1-propanol), the solvosurfactants (C_3PO_1, C_3EO_1) and the classical hydrotrope SXS can be explained by their chemical structures. The existence of an aromatic function in the HMF molecule, which may favourably interact with the π-system of DR-13 is a plausible reason for the higher efficiency of HMF compared to those of the co-solvents. Enhanced hydrotropic efficiency due to interactions between aromatic rings was already proposed for SXS[299] and nicotinamide[321,329]. On the other hand, HMF may be less effective as a hydrotrope, compared to the solvo-surfactants and SXS, because of its smaller hydrophobic moiety. The extent of the hydrophobic part in a hydrotrope was postulated to be a determining factor for its hydrotropic efficiency[299,301].

In Figure III.11 b) and d), a log-linear plot of the relative O.D.´s against HMF concentration is presented in molality and in molarity, respectively. As proposed by Bauduin[299,301], the hydrotropic efficiency is preferredly characterized by the slope of the linear part in the log-linear plot. However, as no linear part can be detected in case of HMF as solubiliser, this method was not applied. The amounts (ppm) of solubilised DR-13 in the ternary solutions were calculated *via* the calibration curve (Figure III.1) obtained from standard solution of DR-13 dissolved in acetone and are given in Table A-8.

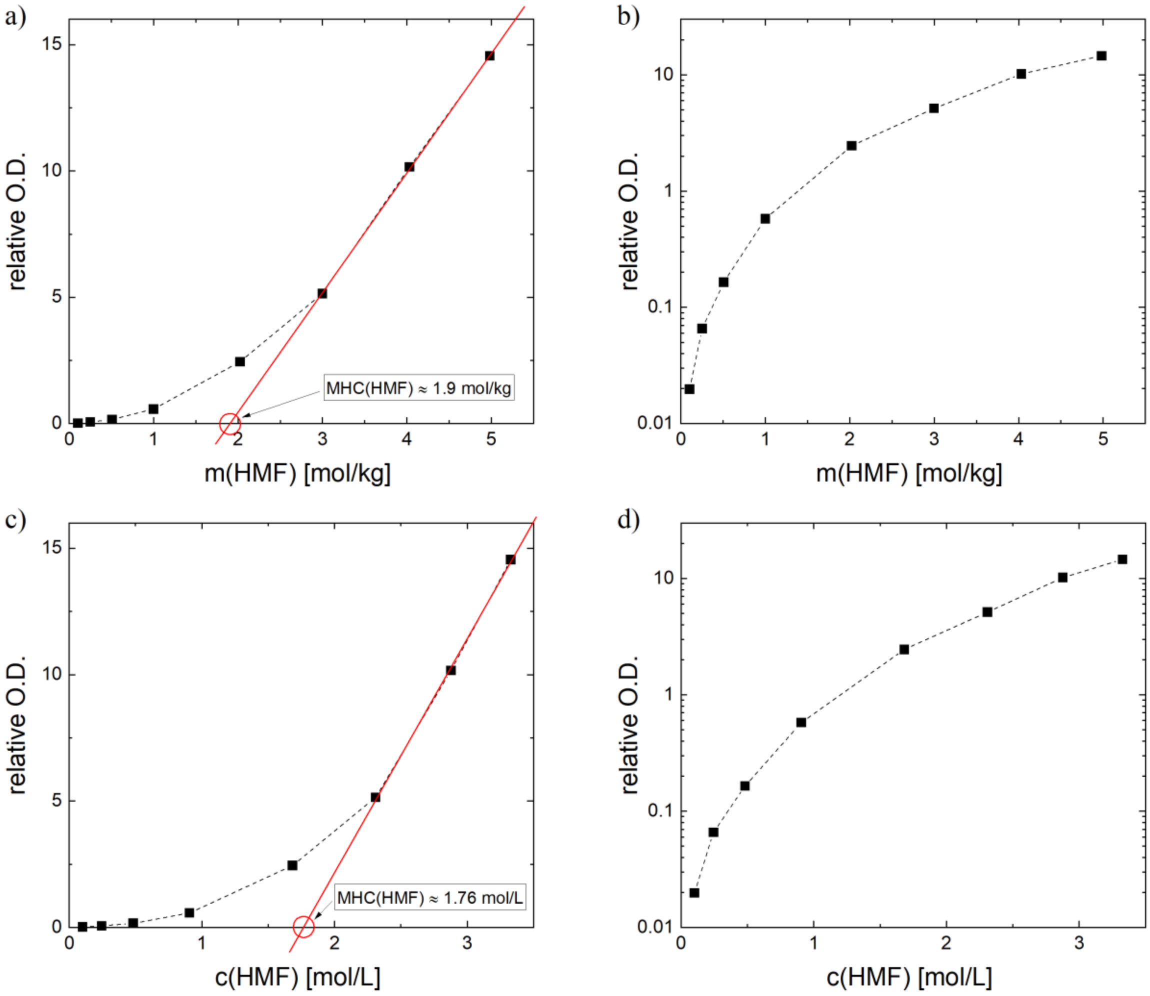

Figure III.11. Solubilisation curve of DR-13 with HMF as hydrotrope/solubiliser. Relative optical density (proportional to the amount of dissolved DR-13) against the hydrotrope concentration in water. –a) linear-linear plot in molality scale, –b) log-linear plot in molality scale, –c) linear-linear plot in molarity scale and –d) log-linear plot in in molarity scale.

III.3.8 Surface Tension of Binary Water/HMF Mixtures

The experimentally determined surface tensions (σ [mN/m]) of aqueous HMF solutions are presented in Figure III.12 depending on the HMF molality and molarity at 296 ± 1 K, and are listed in Table A-9. It can be observed that σ decreases monotonically with increasing HMF content from 72.40 (pure water, 23°C) to 37.68 mN/m within the measured concentration range (0-5 mol/kg; 0-3.3 mol/L). Propably, even lower values for the surface tensions would result at higher HMF concentrations. Like in the case of typical hydrotropes or co-solvents, such low values for σ are achieved at relatively high concentrations. Here, no CAC or MAC can be clearly identified for HMF in water within the measured concentration range. The course of the surface tension was approximated by the Szyszkowski equation (Eq.(III-5)) using *TableCurve2D v5.01*. Obtained fitting parameters are referred to the limiting partial molar area ω ($1.39\cdot10^5$ m^2/mol) and the solute adsorption coefficient k (1.68 L/mol), respectively. However, as they are gained form the course of σ against HMF concentration up to 3.296 mol/L, the values may not be valid for the entire possible concentration range ($x = 0\rightarrow1$).

In a publication, dealing with the surface tensions of mixed aqueouse alcohol solutions, data for the binary water/n-pentanol and water/tert-butanol system were compared in terms of the fitting parameters ω and k. They found higher ω values for *tert*-butanol ($2.25\text{x}10^5$ m^2/mol) than for n-pentanol ($1.48\text{x}10^5$ m^2/mol). Accordingly, the average molecular area for *tert*-butanol ($3.74\text{x}10^{-19}$ m^2) is also higher than that of n-pentanol ($2.46\text{x}10^{-19}$ m^2). This was explained by the larger cross-section of the *tert*-butyl chains compared to the unbranched n-pentyl chains. In contrast, a higher k value was found for n-pentanol (66 L/mol) than for *tert*-butanol (24 L/mol) due to the larger hydrophobic surface of n-pentanol exposed to water molecules than in the case of *tert*-butanol[434]. The calculated average molecular area for HMF ($2.30\text{x}10^{-19}$ m^2) in this work is even smaller than that of n-pentanol, which is unlikely, due to a probably larger space required for the furan ring compared to an alkyl chain. If the molecular structure of HMF is considered, anyway, the general question arises of how the surface tension in water/HMF mixtures is lowered; - by surface adsorption or simply by the effect of mixing water with an organic molecule. Due to its very polar nature, it may avoid the hydrophobic air-phase and rather stays in the bulk solution (and forms associates). This would justify the very small k (1.68 L/mol) value for

HMF compared to those of the other alcohols. But, as both parameters are dependent on each other and the fitted curve holds only for a limited HMF content, no physical meaning is designated to them. Probably, the HMF molecule behaves not like a typical surface-active compound, because such behaviour requires a certain hydrophobicity, which is not fulfilled in case of HMF. In addition, the lowering of surface tension becomes significant only at high concentration.

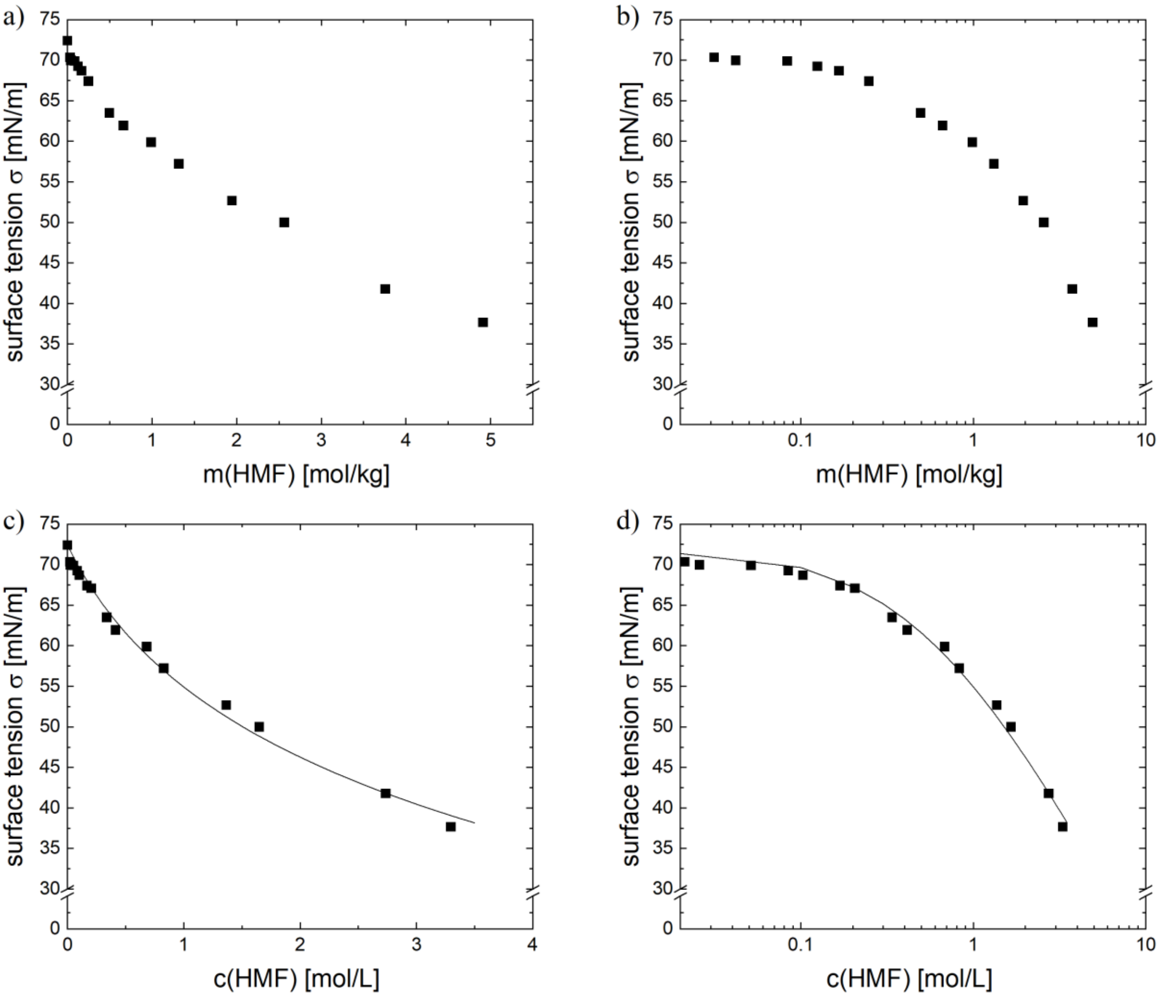

Figure III.12. The surface tension σ of aqueous HMF solutions depending on the HMF concentration at 296 K ± 1 K. –a) linear-linear plot in molality scale, –b) linear-log plot in molality scale, –c) linear-linear plot in molarity scale and –d) linear-log plot in in molarity scale.The data points are experimental values obtained from pendant drop tensiometry and the solid line represents the course of σ fitted by the Szyszkowski equation with $\omega = 1.38\text{x}10^5$ m^2/mol and $k = 1.68$ L/mol as constants.

With the assumption of ideal behaviour, the fitting parameters can be used to calculate the surface excess concentrations Γ_1 using Eq. (III-8), which are presented in Figure III.13 and compared to the other alcohols (n-pentanol and tert-butanol). It can be observed that Γ_1 increases more rapidly with increasing alcohol concentration in case of n-pentanol followed by *tert*-butanol and HMF. For n-pentanol, Γ_1 increases linearly up to its solubility limit in water (~0.07 mol/L). In case of *tert*-butanol (fully miscible with water), Γ_1 increases linearly up to ~0.14 mol/L. Further increases in concentration only slightly influences the excess of *tert*-butanol concentration at the surface, indicating the onset of saturation. The course of Γ_1 for *tert*-butanol was calculated only until 0.8 mol/L, because the corresponding surface tension data were only given up to this concentration in the related publication[434]. The fitting parameters from the Szyszkowski equation are thus only valid up to this concentration. For HMF, the increase of Γ_1 is linear up to ~0.1 mol/L similar to the other alcohols but with a lower slope. At high HMF concentrations (3.3 mol/L) one might expect HMF saturation at the liquid-air surface. The transition from linear behaviour to the onset of a propable saturation occurs very smooth compared to *tert*-butanol. However, to analyse surface behaviour properly, the solute activity has to be used instead of the solute concentration[313].

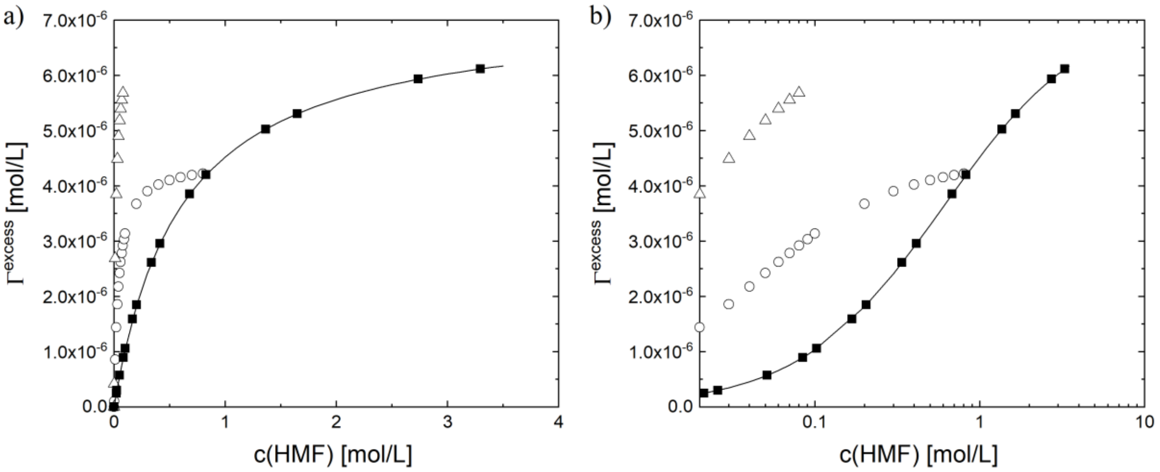

Figure III.13. Surface excess concentrations Γ of binary aqueous HMF (23°C), n-pentanol and *tert*-butanol (25°C) solutions. The Γ for n-pentanol and *tert*-butanol were calculated from values for ω and k taken from literature[434]. –a) linear-linear plot. –b) linear-log plot. (△), (○) and (—) refer to fitting results whereby (■) resemble experimental data points of water/HMF mixtures.

To compare the surface behaviour of HMF with water miscible alcohols, it is more convenient to use the mole fraction concentration scale. Surface tensions of binary aqueous alcohol mixtures (methanol[451], ethanol[313,452], n-propanol[313,453], *tert*-butanol[454] and the partially water miscible n-butanol[455]) are collected from literature and drawn in Figure

III.14 to compare the courses with that of aqueous HMF mixtures. A clear relationship between the surface tension and the chain length of the alcohols can be observed. It turns out that the surface tensions of binary water/ethanol and water/HMF mixtures are very similar up to a mole fraction of $x = 0.1$. Above $x = 0.1$, the surface tension in water/ethanol mixtures decreases less rapidly indicating a maximum occupation at the air-water interace. In the publication of Yano[456], a maximum of surface excess concentration was determined for ethanol at approximately this mole fraction. Unfortunately, surface tensions at higher HMF concentrations were not gained due to experimental limitation by the pendant drop method. Without knowing the course of σ at higher HMF concentrations, no information about the maximum surface excess concentration can be extracted.

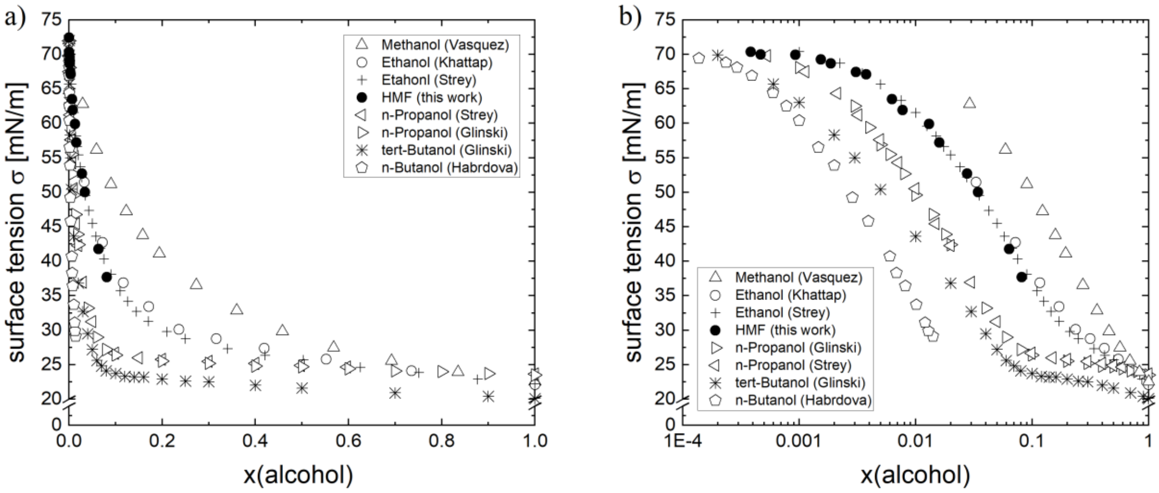

Figure III.14. Surface tensions of aqueous HMF mixtures (296 K) compared to aqueous alcohol mixtures (298 K). –a) linear-linear plot. –b) linear-log plot. (△) Methanol (Vasquez)[451], (○) Ethanol (Khattap)[381], (+) Ethanol (Strey)[313], (●) HMF (this work), (▷) n-propanol (Glinski)[382], (◁) n-propanol (Strey)[313], (✳) *tert*-butanol (Glinski)[454], (⬠) n-butanol (Habrdova)[455].

The Szyszkowski equation was not appropriate to fit the course of the surface tenions of all binary water/alcohol mixtures in the entire mole fraction range (except water/methanol). Only up to a mole fraction of $x \sim 0.1$, the Szyszkowski fit was also reasonable for the other alcohols (not shown).

However, according to Strey et al.[313], it is necessary to use the activity instead of the mole fraction of the solute for interpretation of surface tension data. If this is applied, the surface tension curves of ethanol and HMF do not match anymore, because the asymmetric activity coefficient of HMF in water is decreasing more rapidly with increasing concentration than that of ethanol in water, see Figure III.15. To calculate mole fraction-based activity coefficients (γ_x) from the molality-based activity coefficients (γ_m) (obtained from VPO measurements) Eq. (II-81) was applied. The course of the surface tension versus the HMF activity cannot be fitted very well by the Szyszkowski equation. Instead, the following polynomial approximation can be applied:

$$\sigma(HMF,aq) = \mathrm{A}a(HMF)^3 + Ba(HMF)^2 + Ca(HMF) + \sigma(water) \qquad \text{(III-29)}$$

The fitting paramters with units of surface tension [mN/m] are found to be: *A* = -10091000, *B* = 174971 and *C* = -2233. The derivation of Eq. (III-29) with respect to *a(HMF)* can be inserted to Eq. (III-6) to calculate the surface excess concentrations of HMF in water.

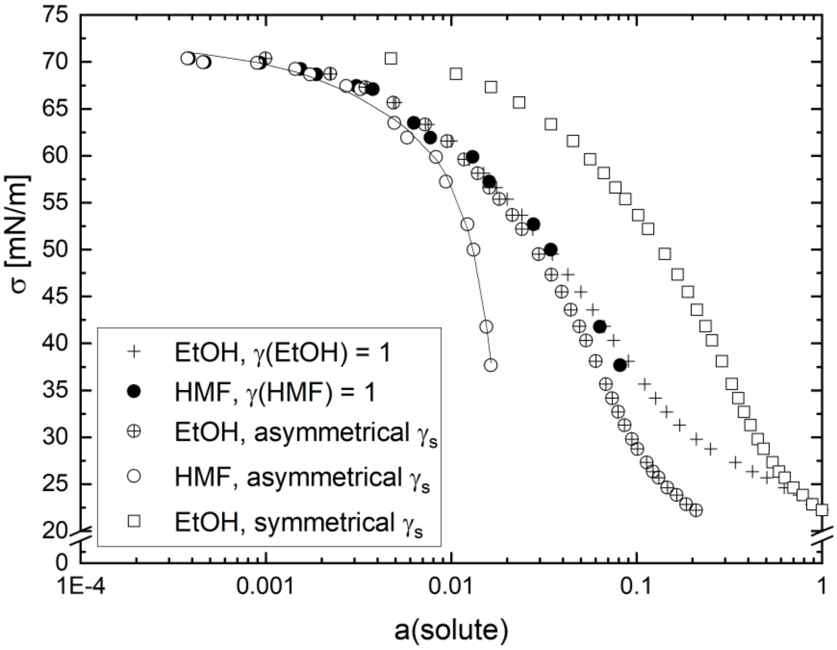

Figure III.15. Surface tension of aqueous HMF (296 K) and aqueous ethanol (298 K) mixtures depending on the solute activity. (●) HMF, assuming γ(HMF) = 1, (○) HMF, using experimental asymmetrical γ(HMF) derived from VPO. (+) Ethanol[313], assuming γ(ethanol) = 1, (⊕) ethanol, using experimental asymmetrical γ(ethanol) and (□) ethanol, using experimental symmetrical γ(ethanol) from literature[313]. The solid line represents the polynomial approximation.

III.4 Conclusion

Osmotic coefficients of the binary water/HMF system decrease with increasing HMF molality and represent negative deviation from ideal behaviour ($\phi < 1$). This observation indicates molecular association of HMF in water, may be due to hydrophobic clustering (as it is known from classical hydrotropes) and/or from hydrogen-bonding between HMF molecules[439]. However, the molecular association tendency of HMF is not very strong, because the decrease of the osmotic coefficients gets only significant at high concentrations. The association constant derived from the isodesmic asscociation model is also low. Further support for a low association behaviour is provided by the poorly pronounced correlation functions of binary water/HMF mixtures obtained from DLS.

Osmotic coefficients of binary water/HMF mixtures obtained in this work are in good agreement with already published data, obtained by cryoscopic osmometry (Gonotec Osmomat 030)[419]. Osmotic coefficients of ternary mixtures with added salt decrease also with increasing HMF content, but increase with increasing salt concentration for both salts. This increase is more pronounced in case of LiCl.

Small values for HMF activity coefficients in binary and ternary systems were found, which decrease monotonically with increasing HMF content. In case of $\ln(\gamma_1^0)$, an exponential decrease was detected. In the presence of electrolytes (NaCl, LiCl), $\ln(\gamma_1)$ decreased nearly linear, which is in accordance to the Long-McDevit equation[269]. Only a small influence of electrolytes on the HMF behaviour (chemical potential) in aqueous solution was observed, which was confirmed by a good approximation of osmotic coefficients in ternary systems using the ZSR-mixing rule. It was shown that the osmolalities ($v_i{*}m_i{*}\phi_i^0$) of the binary solutions are additive. Due to decreasing correlation functions (obtained from DLS) of ternary water/HMF/LiCl mixtures with increasing LiCl concentration, it is assumed that interactions between LiCl and HMF are occurring on the cost of HMF self-interactions.

With increasing HMF content, salt MIACs increase at a background salt molality of 1 mol/kg and decrease at a background salt molality of 3 mol/kg. The MIACs of LiCl are higher than those of NaCl, at both salt backgrounds. The values of NaCl and LiCl MIACs in corresponding binary systems (1 m and 3m) are in good agreement with obtained MIACs in the ternary systems of this work. The higher MIACs of LiCl and their increase with increasing salt concentration are probably a consequence of a more pronounced hydration of the Li^+ cation. The same feature is observed for binary water/NaCl and water/LiCl solutions.

From solubilisation experiments, the precise determination of the MHC of HMF is not possible, because the solubilisation of the hydrophobic dye DR-13 does not show a sigmoidal profile, but proceeds rather exponentially. This solubility behaviour is more characteristic for co-solvents like acetone, ethanol or 1-propanol[300]. However, the tangent method was applied to give an estimate of the MHC (1.9 mol/kg; 1.76 mol/L) for HMF. The hydrotropic efficiency of HMF was found to be higher than that of acetone and 1-propanol, but lower than that of C_3EO_1, C_3PO_1 and SXS[299].

Surface tension of the aqueous HMF solutions decreases monotonically with increasing HMF content. Similar to the solubilisation curve, no characteristic course for self-aggregating molecules can be deduced from surface tension measurements. Lowest detected value for σ (37.7 mN/m) was found at an HMF concentration of 5 mol/kg or 3.3 mol/L. The Szyszkowski equation was applied to fit the course of σ. A smaller average molecular area for HMF (2.30×10^{-19} m^2) compared to those of n-pentanol (2.46×10^{-19} m^2) and *tert*-butanol (3.74×10^{-19} m^2) and a very small adsorption coefficient (k = 1.68 L/mol) was obtained from the fitting parameters. Accordingly, the excess surface concentration Γ of HMF increases less rapidly than those of n-pentanol and *tert*-butanol. These findings lead to the conclusion that the HMF molecule does not have a pronounced affinity to the liquid-air surface, although the surface tension decreases to very low values. This decrease in surface tension is then rather attributed to mixing water with an organic compound. In this context, it would be interesting to know the surface tension of water/HMF mixtures in the entire mole fraction range (also from pure HMF in the liquid state). Further comparisons were made to short-chain alcohols in mole fraction scale. Here, a very similar course of the surface tension of water/HMF mixtures compared to that of water/ethanol mixtures up to approximately $x = 0.1$ was observed. If the solute activity coefficients are considered for interpretations, the surface tension curves of water/HMF and water/ethanol do not match anymore.

To classify the HMF molecule as a hydrotrope according to the definition of Kunz et al.[309], the investigation of the structuring in the ternary mixture (water/HMF/hydrophobic compound) would be required. However, some results indicate a co-solvent rather than a hydrotrope character.

Chapter IV

Salting-in and Salting-out Effects in Water/DPnP and Water/Ethanol Mixtures

IV.1 Introduction

Solvo-surfactants, a class of hydrotropes or solubilisers can have properties of both surfactants and solvents depending on their molecular composition and temperature[457]. They are non-ionic and constitute of monoethers of glycols and higher polyols like ethylene glycol monobutyl ether (2-butoxyethane-1-ol or butylglycol) and diethylene glycol monobutyl ether (2-(2-butoxyethoxy)ethane-1-ol or butyldiglycol). Generally, they are termed ethylene glycol alkyl ethers (EGAE, ethoxylated alcohols, C_iEO_j). They have been studied extensively[458] and are produced on a large scale e.g. for paint formulations or cleaning agents. Toxicological studies revealed that they have a certain reprotoxic activity[312]. Therefore, the less harmful propylene glycol alkyl ethers (PGAE, propoxylated alcohols, C_iPO_j) were used as substitutes. They meet the requirements for applications although they are less hydrophilic[304,315]. C_iPO_j are more hydrophobic than C_iEO_j due to one additional methyl-group per glycol repeating unit. Thus, an increased oil solubility can be realised by introducing propylene glycol groups (PGG) as spacer between the hydrophilic head and the lipophilic tail in order to design a surfactant for a certain solibilisation problem[459].

Physico-chemical properties like the temperature-dependent miscibility of 10 different C_iPO_j with water[315] and the influence of salts on the lower critical solution temperatures (LCST) of aqueous propylene glycol n-propyl ether (PnP, LCST = 31.9°C) and dipropylene glycol n-propyl ether (DPnP, LCST = 13.8°C) mixtures[460] were investigated by the cloud-point method using an automated apparatus[461] for the determination of liquid-liquid phase transitions. Salt effects on the cloud point of aqueous mixtures of non-ionic true surfactants were already studied by Holtzscherer and Candau[462] and Schott[463]. The LCST is related to a certain mixture compositon in water (w(PnP) = 0.45 and w(DPnP) = 0.55)[315]. The binary liquid system water/DPnP is completely miscible below the LCST and above it appears biphasic. In systems, for which the mutual solubility decreases with increasing temperature, the phase-transition temperature is named cloud-point, in analogy to non-ionic surfactants. This reversed solubility behaviour with temperature is found for hydrogen-bonding compounds, which are highly solvated by water[464]. For C_iPO_j as well as for classical C_iEO_j, the strong interactions with water arise from the hydrogen-bond donor and acceptor properties of the hydroxyl group (-OH) and from the hydrogen acceptor ability of the ether group (-O-). With increasing temperature, the interactions with water are reduced (dehydration of oxygenated groups[312]), which promotes phase separation. While C_iEO_j forms dimers in water, no associates were found for C_iPO_j in the water-rich regimes. This is probably due to the more bulky structure of PGG, which hinders self-association[315]. One advantage of the DPnP system over non-ionic surfactants is that the influence of additives can be compared in large composition range of water/DPnP, because no well-defined structures are appearing below the cloud point. The fact that the demixing temperature of aqueous DPnP mixtures is near room temperature provides a model system, which is relatively easy to study experimentally. In addition, such a system offers opportunities for LLEx by temperature variation and the transition temperature can be adjusted by additives like salts. Such an extraction process based on the cloud-point of solvo-surfactants (dialkyl glycerol ethers) have recently been demonstrated and was termed hydrotropic cloud-point extraction (HCPE)[465]. The chemical structures for PnP and DPnP are shown in Figure IV.1. There are two chemical isomers for PnP[315] and eight chemical isomers for DPnP[457].

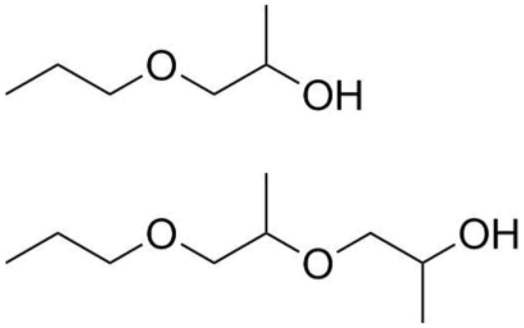

Figure IV.1. Chemical structure of propylene glycol n-propyl ether (PnP) and dipropylene glycol n-propyl ether (DPnP).

Another alternative to C_iEO_j and C_iPO_j are short chain glycerol 1-monoethers (C_iGly_j). They are considered as green solvo-surfactants due to the natural polar moity (glycerol). In contrast, C_iEO_j and C_iPO_j are derived from petrochemsitry. As glycerol is a side product, which arises in large scales, the use of glycerol for the production of solvo-surfactants comprises advantages concerning the use of an abundantly available substance and the reduction of toxic products. Physcio-chemical properties of aqueous C_5Gly_1, C_6Gly_1 solutions as well as of aqueous C_4EO_1, C_3PO_1 and C_3PO_2 solutions were studied. These comprise the surface tension, the temperature-dependent phase diagram and the effect of salt addition on the LCST (although in some cases the composition was different from that of the LCST to allow the investigation in a convenient temperature range)[312].

The discovered salt effects on the LCST of DPnP in water as well as on C_6Gly_1, C_4EO_1, C_3PO_1 and C_3PO_2 in water follow nicely the Hofmeister series. The investigated salts included Na_3PO_4, Na_2SO_4, Na_2CO_3, NaOH, CH_3COONa, NaCl, NaBr, NaI, $NaClO_4$ and NaSCN for the water/DPnP system and for the the other solvo-surfactants, Na_2SO_4, NaCl, NaBr, NaI, $NaClO_4$ and NaSCN were used. In both systems, NaI, $NaClO_4$ and NaSCN caused a salting-in effect by an increase of the cloud points and the other salts were salting-out by decreasing the cloud points, which is perfectly in accordance with the Hofmeister series. Additionally, the cloud-point dependence on the salt concentration appeared to be linear[312,460], hence a linear equation (Eq. (IV-1)) was proposed to evaluate the strength of the salting-in and salting-out effects.

$$LST(c) = LST(c = 0) + \alpha c \qquad \text{(IV-1)}$$

where *LST(c)* is the minimum demixing temperature (in °C) for a mixture at a certain additive concentration c (in mmol of additive per 1 mole of water/DPnP mixture), *LST(c = 0)* is the minimum demixing temperature (in °C) of the binary water/DPnP mixture and α represents the salt effect coefficient. Positive values indicate a salting-in behaviour, whereas negative values indicate a salting-out behaviour.

In this work, the influence of different additives like inorganic salts, charged and uncharged organic compounds on the LST of a binary water/DPnP mixture was investigated. Depending on the additives' nature, a salting-in or salting-out behaviour was observed. For the binary mixture, a salting-out effect is associated with a decrease of the LST (increase of the biphasic region) with increasing additive concentration. Inversely, a salting-in effect is related to an increase of the LST (decrease of the biphasic region) with increasing additive concentration.

A liquid-liquid, ethanol-water separation was considered using pentasodium phytate ($(Phy^{5-}, 5Na^+)$) as salting-out agent and the results were compared to those obtained using $(NH_4)_2SO_4$ and $K_4P_2O_7$.

IV.2 Experimental

IV.2.1 Materials

Dipropylene glycol propyl ether (≥ 98.5%) and ethanol (≥ 99.8%) were purchased from *Sigma-Aldrich*. n-Butanol was obtained from *VWR* (≥ 99.8%). Choline chloride (≥ 99%), L-arginine, malic acid disodium salt (≥ 95%), nicotinic acid sodium salt (≥ 98%), oxalic acid (≥ 99%), phytic acid sodium salt (≥ 99%), saccharin sodium salt (≥ 98%), sodium acetate (≥ 99%), sodium chloride (≥ 99%), potassium pyrophosphate (≥ 97%), aluminium sulphate octadecahydrate (≥ 98%) and sodium N-cyclohexylsulfamate (≥ 99%) were received from *Sigma-Aldrich*. Citric acid trisodium salt (≥ 99%), citric acid monohydrate (≥ 99%), fructose (≥ 99%), glucose (≥ 99%), glycolic acid (≥ 99%), glycine (≥ 99%), L-proline (≥ 99%), L-cysteine (≥ 99%), L-alanine (≥ 99%), malonic acid (≥ 99%), ammonium sulphate (≥ 99%) sodium triphosphate (≥ 98 %), tetrasodium pyrophosphate decahydrate (≥ 99%) and sorbitol (≥ 99%) were purchased from *Merck*. Acesulfame K (≥ 99%), betaine hydrochloride (≥ 99%), L-serine (≥ 99%), sodium thiocyanate (≥ 98%), sodium sulphate (≥ 99%) tartaric acid (≥ 99%) and trimethylamine N-oxide dihydrate (≥ 99%) were received from *Fluka*. DL-Carnitine hydrochloride (≥ 98%), lithium sulphate (≥ 99.99%) and xylitol (≥ 99%) were obtained from *Alfa Aesar*. Isomalt was received from *Beneo-Palatinit*. Triethylphenylammonium chloride (≥ 99%) was purchased from *TCI*. Ectoine (≥ 96%) was obtained from *bitop*. Aspartame (≥ 99%) was received from *Ajinomoto*. Water was taken from a Millipore purification system. The content of sodium in the phytic acid sodium salt was checked using AES and was found to be equal to 5 moles/mole of phytic acid sodium salt. The water content of phytic acid sodium salt was determined by KF-titration and was found to be less than 1%.

IV.2.2 Methods

IV.2.2.1 Determination of the LST

All samples were prepared by weight using a balance with an accuracy of 0.0001g. The phase transition from clear to turbid was determined as a function of temperature. The samples were cooled to approximately 0°C using an ice-water bath while continuously stirring of the bath and of the samples was provided by magnetic stirring. A digital thermometer ($\Delta T = 0.1°C$) was used to measure the temperature of the bath. During slowly heating, the phase behaviour was determined by visual observation and the temperature, at which samples turned turbid, was referred to as the LST. In the binary system water/DPnP, the LST was found to be at weight fraction of $w(DPnP) = 0.55$[315]. All determined cloud-points were reproducible on cooling and heating.

IV.2.2.2 Relative Volume of the Ethanol-rich Phase

Samples were prepared by first weighing the desired salt masses into graduated test tubes of 20 mL, followed by the addition of equal amounts of water and ethanol (w/w). Complete dissolution of the salt in the mixture was carried out by mechanical stirring. The volume of the upper phase (V_{UP}) is determined after a complete phase separation detected by visual observation. The relative volume of the upper phase ($V_{rel,\,UP}$) is calculated by dividing V_{UP} by the volume of the corresponding binary system water/ethanol without salt (V_i), see Eq.(III-9). $V_{rel,\,UP}$ is equal to 1, if no phase separation occurs and cannot be lower than 0.5 due to the lower density of ethanol compared to water. All the measurements were performed at room temperature (25°C ± 1).

$$V_{rel,UP} = \frac{V_{\mathrm{UP}}}{V_i} \tag{IV-2}$$

IV.2.2.3 Determination of the Ethanol Purification Coefficient

The ethanol mass fraction ($w_{UP}(EtOH)$) of the upper phases was determined by gas chromatography; HP 6890 Series (*Hewlett-Packard*). Samples from the ethanol-rich phases were carefully taken using syringes and were diluted with water by factor 1:100. An aqueous n-propanol (1 wt%) solution was used as internal standard. The diluted samples were combined gravimetrically 1:1 with the internal standard solution. Peak separation of ethanol (3.7 min) and n-propanol (4.1 min) was realized *via* a column temperature gradient of 10°C/min ranging from 60-120°C using a polyethylene glycol packed column (DB-WAXetr, 30m*320µm*0.5µm, *Agilent*). Three replicate measurements of each sample were carried out and average values were considered. The ethanol mass in the upper phase $m_{UP}(EtOH)$ was determined by the following equation:

$$m_{UP}(EtOH) = \frac{V_{\mathrm{UP}}}{d_{UP}} * w_{UP}(EtOH) \qquad \text{(IV-3)}$$

Densities of the upper phase d_{UP} were measured according to the procedure described in section III.2.2.3. The ethanol ratio in the upper phase $R_{UP}(EtOH)$ is calculated by dividing $m_{UP}(EtOH)$ by the value of the total mass of ethanol in the original prepared samples $m_i(EtOH)$.

$$R_{UP}(EtOH) = \frac{m_{\mathrm{UP}}(EtOH)}{m_i(EtOH)} \qquad \text{(IV-4)}$$

Finally, the purification coefficient $P(EtOH)$ is calculated using the following equation:

$$P(EtOH) = \frac{R_{UP}(EtOH)}{V_{UP}} * V_i \qquad \text{(IV-5)}$$

IV.3 Results and Discussion

IV.3.1 Evolution of the LST in DPnP/water upon Additive Concentration

The temperature-dependent phase diagram of water/DPnP is presented in Figure IV.2 a). The mixtures are clear and monophasic below the LST and become biphasic with increasing temperature above the LST. At high water and at high DPnP contents (extreme left and extreme right side of the phase diagram), the binary mixture remains monophasic even at high temperatures. The evolution of the LST in the water/DPnP system with increasing concentration (mol of additive per kg of liquid) of the NaSCN and NaCl are presented in Figure IV.2 b). NaCl shows a salting-out and NaSCN shows a salting-in effect. The phase diagram of water/DPnP and the salting-effects were reproduced from former publications of Bauduin[315,460]. The star (★) in the monophasic region, near to the phase boundary, corresponds to the binary mixture used for the present investigation. Its location is the composition of the LST (*w(DPnP)* = 0.55) at a temperature of 14.2°C, which is slightly above the LST.

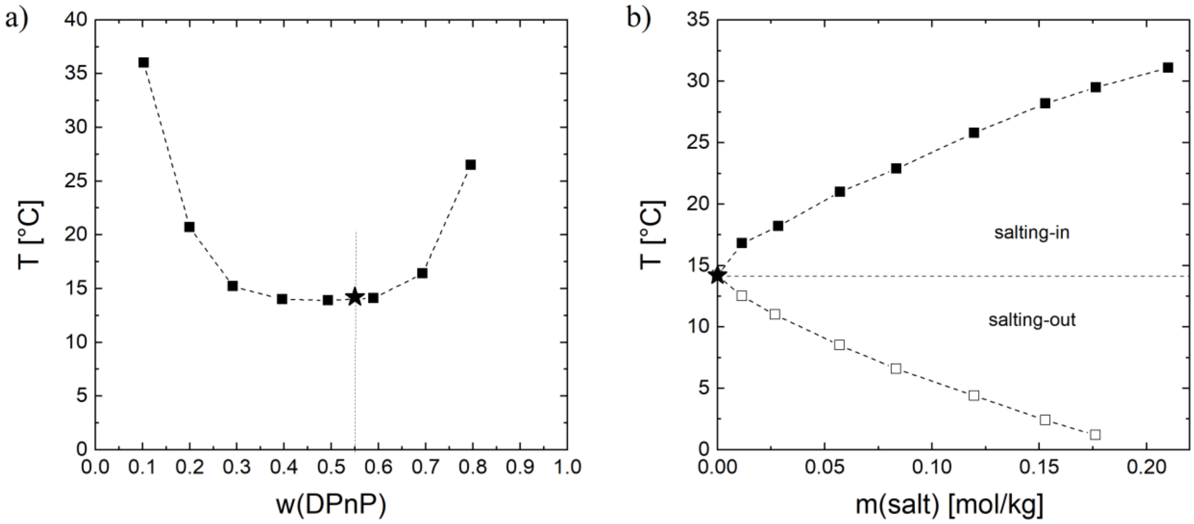

Figure IV.2. –a) Phase diagram of the binary mixture water/DPnP as a function of temperature. The star (★) in the monophasic area corresponds to the binary mixture used for the present investigation. –b) Effect of (□) NaCl and (■) NaSCN on the binary mixture DPnP/water (★). Above the dashed lines (--) mixtures turned turbid and are biphasic.

According to Bauduin, the salting-out effect arises from the water withdrawing effect of the ions and thus from the competition for water between the salt, the OH and the ether groups of DPnP. The salting-in effect must be related with a lowering of the chemical potential of DPnP. The origin might be an association of the DPnP with the SCN^- anion or at least a weak interaction or simply the presence of different/some preferred conformations of the DPnP molecules. Results for the evolution of the LST of the DPnP/water mixture upon the addition of further inorganic salts, short organic acids, short organic sodium carboxylate salts, natural sugars, sweeteners, amino acids and ammonium salts are presented in Figure IV.3 to Figure IV.7. In all investigations, the additive concentration is given in mol of additive per kilogram of liquid (water + DPnP).

IV.3.1.1 Inorganic salts

The influence of sulphate and phosphate salts on the LST of the binary water/DPnP system have been tested and depicted in Figure IV.3. All salts cause a decrease of the LST resembling a salting-out effect. The strength of the salt effect decreases in the following order: $Na_4P_2O_7 \geq Al_2(SO_4)_3 > Na_5P_3O_{10} > K_4P_2O_7 > Na_2SO_4 > Li_2SO_4 > (NH_4)_2SO_4$. Aluminium sulphate shows the highest salting-out effect of the investigated sulphate salts. This feature is propably due to the higher ionic strength of aluminium sulphate compared to those of the others ($I(Al_2(SO_4)_3) = 15c(\text{salt}) > I(Na_2(SO_4), Li_2(SO_4), (NH_4)_2SO_4) = 3c(\text{salt})$). For sulphate salts, the influence of the cation on the salting-out effect was found to follow the order: $Al^{3+} > Na^+ > Li^+ > NH_4^+$. This cation series correlates with the charge density and polarisability if a large hydration shell around Li^+ is assumed. It is also in accordance with the *Setchenov* constants found for these sulphate salts and for the individual cations with $CHCl_3$, benzene and chlorobenzene as solutes to be salted-out[277]. $(NH_4)_2SO_4$ is the least effective investigated sulphate salt, which may be due to the more chaotropic cation.

$Na_4P_2O_7$ has a similar effect like $Al_2(SO_4)_3$, which is slightly more pronounced compared to that of $Na_5P_3O_{10}$. For the phosphate salts, $Na_4P_2O_7$ lead to the most pronounced decrease of the LST followed by $Na_5P_3O_{10}$ and $K_4P_2O_7$. *Setchenov* constants[277] found for Na^+ are greater than that of K^+, which confirms the trend for the pyrophosphates found in this work. $K_4P_2O_7$ is the least effective investigated phosphate salt, which may be due to the more chaotropic cation.

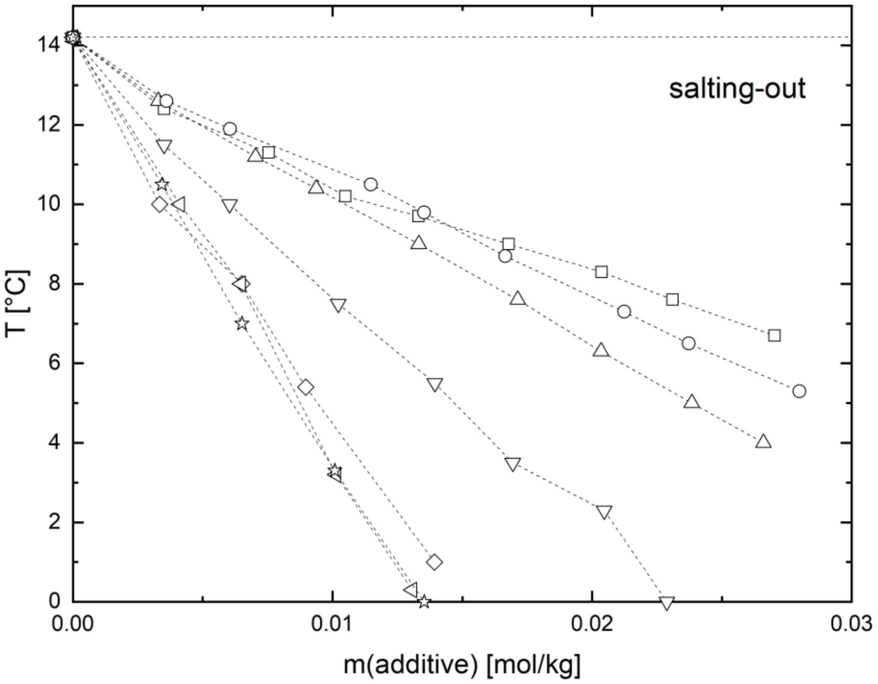

Figure IV.3. Shift in the LST of the DPnP/water mixture upon the addition of sulphate or phosphate salts. Symbols represent experimental data: (□) $(NH_4)_2SO_4$, (○) Li_2SO_4, (△) Na_2SO_4, (▽) $K_4P_2O_7$, (◇) $Na_5P_3O_{10}$, (☆) $Al_2(SO_4)_3$, (◁) $Na_4P_2O_7$.

IV.3.1.2 Short Organic Acids and Sodium Carboxylate Salts

The effects of the addition of short organic acids and short sodium carboxylate salts are shown in Figure IV.4 depending on additive concentration. It can be observed that the short organic acids are salting-in and the short organic sodium carboxylate salts are salting-out; with the salting-out effect being more pronounced.

The short organic acids are very soluble in water and can form molecular associations with the DPnP molecule in favour of its hydration, similarly to NaSCN (or to the solute-hydrotrope interaction described in the fundamentals part II.3). The energy cost for DPnP dehydration is then higher and the LST increases (decrease of the biphasic region in water/DPnP) with increasing concentration of the short organic acids. The nearly linear LST increases are strongly specific to the short organic acids and follow the order: citric acid > tartaric acid > malonic acid > glycolic acid > oxalic acid. Citric acid shows the highest salting-in effect, which may be explained by the formation of pronounced intermolecular hydrogen bonds promoting the tendency of self-association and thus the solubilisation of DPnP in water and vice versa.

The strength of the salting-in effect can be related to the occurrence of the functional groups within the molecular structures. E.g. a correlation of the number of carboxylic groups occurring in organic acids with the α-parameter (obtained from water activity) has been reported for lactic acid, malic acid, tartaric acid and citric acid[466]. The detected order of the strength of the salting-in effect can also be deduced to the number of carboxyl and hydroxyl groups: citric acid (3 carboxyl groups, 1 hydroxyl group) > tartaric acid (2 carboxyl groups, 2 hydroxyl group) > malonic acid (2 carboxyl groups) > glycolic acid (1 carboxyl group, 1 hydroxyl group) > oxalic acid (2 carboxyl gropus). Here, the only exception is presented by oxalic acid and glycolic acid. For the first three organic acids, solubilistaion properties for sparingly water-soluble compounds have already been reported[467]. In that study, the same trend for the solubility enhancement of terfenadine and RBF in aqueous organic acid mixtures was found as it is presented here for water/DPnP. Generally, the organic acids have a strong propensity for hydrogen-bonding to hydrogen acceptor solutes, which helps to increase their solubilty in water. Furthermore, the hydrophilic-lipophilic balance of organic acids leads to an amphilic nature, which is known to be favourable for solubilistaion properties. Citric acid has also been found to improve the solubility of other water-insoluble drugs[468,469].

The pronounced hydration of carboxylate salts leads to less water molecules being available as solvent for DPnP molecules. The nearly linear decreases of the LST are also specific. As for organic acids, the number of functional groups provides a reasonable argument for the observed salting-out trend: trisodium citrate (3 carboxyl groups, 1 hydroxyl group) > disodium malate (2 carboxyl groups, 1 hydroxyl group) > sodium acetate (1 carboxyl group) > sodium nicotinate (1 carboxyl group). Salting-out properties of carboxylate salts of lower molecular weight and multiple charge are well known, e.g. for the separation of 2-butanol, 1-propanol and 2-propanol from water with acetate salts[470]. Furthermore, the citrate^{3-} anion is the most salting-out anion within the classical Hofmeister series, see Figure II.3. The fact that sodium nicotinate has a lower salting-out effect compared to sodium acetate may be due to the heterocycle within its molecular structure. It is worth to note that the most salting-in acid corresponds to the most salting-out salt.

The salting-out effect of monosodium L-glutamate is also depicted in Figure IV.4 for comparison. It appears that its salting-out effect is comparable to that of disodium malate and is more pronounced than that of the other tested amino acids (see Figure IV.5).

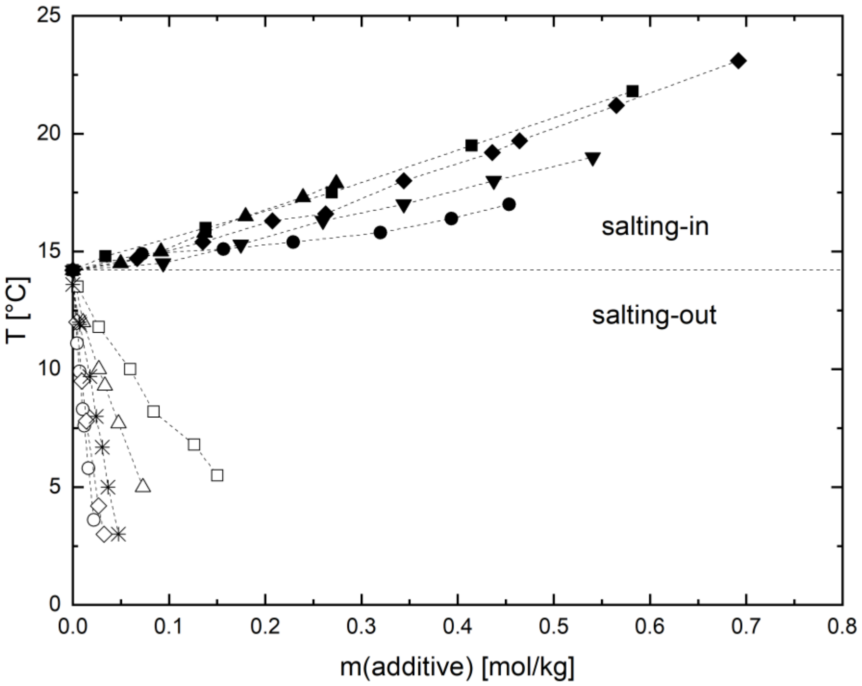

Figure IV.4. Shift in the LST of the DPnP/water mixture upon the addition of short organic acids or short organic sodium carboxylate salts. Symbols represent experimental data: (■) citric acid, (▲) tartaric acid, (◆) malonic acid, (▼) glycolic acid, (●) oxalic acid, (□) sodium nicotinate, (△) sodium acetate, (✳) monosodium L-glutamate, (◇) disodium malate, (○) trisodium citrate.

IV.3.1.3 Amino Acids

The evolutions of the LST values depending on the amino-acids concentrations are depicted in Figure IV.5. All the tested amino-acids show a salting-out behaviour, weakly specific of the added molecule. The strength of the salting-out effect was found in the following order: monosodium L-glutamate > ectoine > L-serine > L-alanine > L-arginine > L-glycine > L-proline > L-cysteine. The well-known food additive monosodium L-glutamate shows the highest salting-out power due to two carboxylate functions in the molecular structure and shows a behaviour comparable to the one of disodium malate, see Figure IV.4. Monosodium L-glutamate is responsible of the Umami taste[471]. The fact that it shows a salting-out effect in comparison to the salting-in effect observed for the sweeteners (see Figure IV.7), may reflect a different mode of action on the G proteins, which are present at the surface of the tongue. At high concentrations of L-cysteine, the decrease of the LST values is significantly lower compared to the other investigated amino-acids. This feature may be attributed to the occurrence of sulfur (thiol group) in the molecular structure of L-cysteine. The strongest salting-out effect among the tested amino-acids, except the glutamate, was observed for ectoine. It is considered as a zwitterionic osmolyte, which was found to be strongly hydrated in aqueous solutions even in the presence of NaCl[472]. Thus, the water withdrawing effect of ectoine may be the reason for the stronger LST decrease in the water/DPnP mixture (salting-out effect).

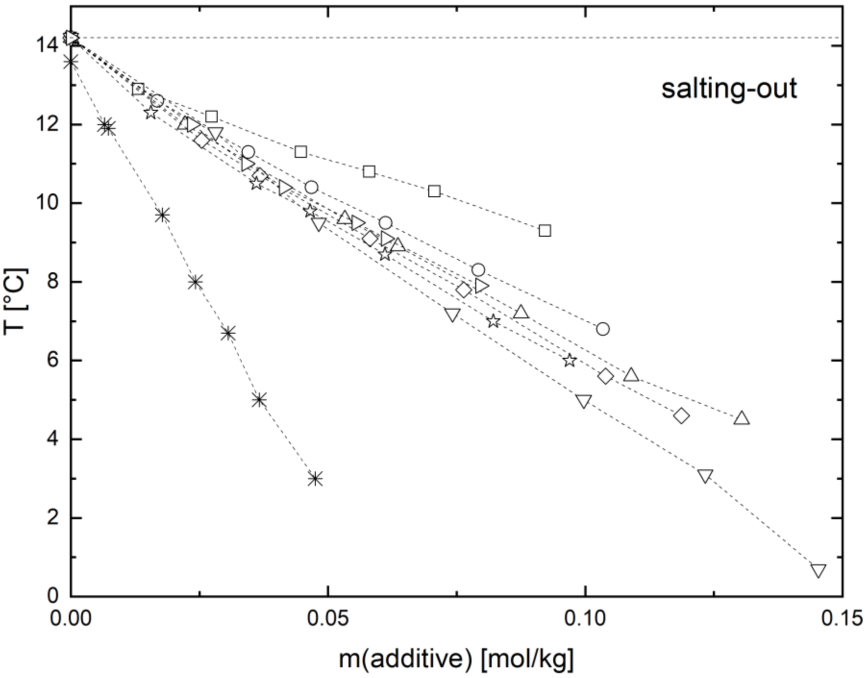

Figure IV.5. Shift in the LST upon the addition of amino acids. Symbols represent experimental data: (□) L-cysteine, (○) L-proline, (△) glycine, (▷) L-arginine, (◇) L-alanine, (☆) L-serine, (▽) ectoine, (✳) monosodium L-glutamate.

IV.3.1.4 Quaternary Ammonium Salts

The change of the LST upon addition of quaternary ammonium salts is presented in Figure IV.6, depending on the additive concentration. A nearly linear decrease of the LST can be observed with increasing additive concentration and thus, a salting-out effect in the water/DPnP system was detected for all quaternary ammonium salts. The strength of the salting-out effect is only slightly specific and decreases in the following order: trimethylamine N-oxide (TMAO) > choline chloride > DL-carnitine hydrochloride > betaine hydrochloride > triethylphenylammonium chloride. Trimethylamine N-oxide is a zwitterionic salt in contrast to the cationic character of the other quaternary ammonium salts. In case of the betaine and carnitine hydrochlorides, the carboxylic functions in the molecular structures propably contribute to their salting-out effect. For choline chloride, water is bound to the hydroxyl group *via* hydrogen bonds with an effective hydration number of ~2 upon choline chloride molarities higher than 0.5[473]. Similarly to ectoine, TMAO belongs to the group of osmolytes and is particularly present in sea organisms to counteract external osmotic or hydrostatic pressure. It has been shown that stable complexes of $TMAO \cdot 2H_2O$ and/or $TMAO \cdot 3H_2O$ are formed in aqueous solutions and that these complexes have an extraordinary long life-time[474]. This indicates strong interactions between water and TMAO and thus, the competition between TMAO and DPnP for water molecules may results in the observed salting-out effect. The weak salting-out effect of triethylphenylammonium chloride is propably due to the absence of polar carboxyl or hydroxyl-groups. Even a salting-in effect on benzene in water induced by quaternary ammonium bromides was already reported. In that study, the alkyl chain length and the number of alkyl groups on the nitrogen atom were correlated with the salting-in effect, which increased with increasing hydrophobicity of the quaternary ammonium bromide salt[475].

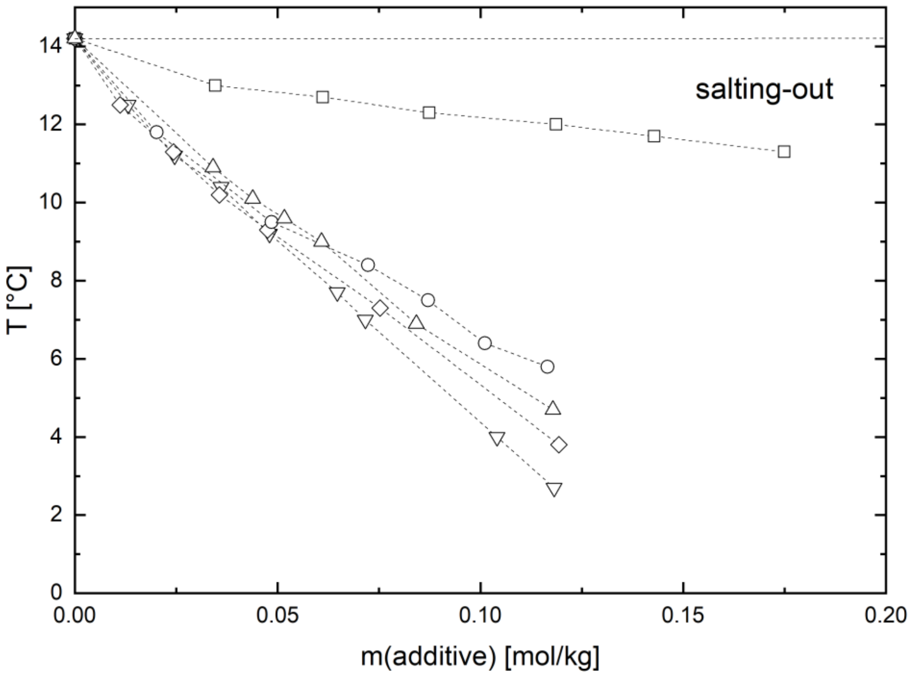

Figure IV.6. Shift in the LST upon the addition of quaternary ammonium salts. Symbols represent experimental data: (□) triethylphenylammonium chloride, (○) betaine hydrochloride, (△) DL-carnitine hydrochloride, (◇) choline chloride, (▽) trimethylamine-N-oxide.

IV.3.1.5 Sugars and Sweeteners

In Figure IV.7, the evolution of the LST is illustrated depending on the sugar and sweetener concentrations. All sweeteners show a salting-in behaviour, which may result from direct weak interactions (association of the sweeteners with the DPnP molecules) or a higher degree of hydration of DPnP. Both cases would lead to a lowering of the chemical potential of DPnP molecules in solution. The curves are all increasing nearly linearly and no pronounced specific effect can be observed. This salting-in behaviour agrees with the fact that these sweeteners have to salt-in the G-proteins of the tongue to be active and to give a strong sugar taste.

In contrast, a salting-out effect was observed for all sugar molecules. The ability of sugars to induce phase separation was already reported for the system ACN/water system[125] and termed "sugaring out". Compared to the four tested sugar molecules (glucose, fructuose, xylitol and sorbitol), a significantly stronger salting-out effect is observed in the presence of isomalt and (Phy5^-, $5Na^+$). The strong salting-out power of isomalt can be explained by the presence of nine alcoholic functions in the molecular structure, compared to five or six in the case of glucose, fructose, xylitol and sorbitol. Phytic acid contains six phosphate functions, which are even more water-binding than the nine alcoholic functions of isomalt. The organic phosphate salt is a cheap and a food-agreed ingredient, e.g., as preservative. Further fields of application are medicine, dental care and corrosion inhibition[476].

The number of water molecules in the hydration sphere of the sugars is proportional to the number of OH-groups in the sugar molecule. It has been found that the average number of the equatorial hydroxyl groups *n*(*e-OH*) existing in the various conformers of sugars in aqueous solution correlate well with their partial molar heat capacities at infinite dilution[477], the relative increments in the ultrasonic velocity[478], their limiting diffusion coefficient[479], and the dynamic hydration numbers inferred from water oxygen-17 magnetic relaxtion measurements[480]. From viscosity B-coefficients of aqueous sugar solutions, a hydration parameter *h* was derived[481], which also correlates well with the *alpha*-parameter determined from water activity coefficients and both parameters *h* and *alpha* were related to the *n*(*e-OH*)[481,482]. As the *e-OH* groups on pyranose sugars are able to interact with water resulting in a long-lived hydration structure, the hydration of sugar molecules is essentially determined by the *n*(*e-OH*)[479,480]. The mentioned findings strongly support the proposal that sugar molecules, which have a large number of *e-OH* groups, have a stabilising effect on the water structure. In other words, to the ambiguous term “water structure”, one can designate a high salting-out effect to sugar molecules bearing many *e-OH* groups by a water withdrawing effect. If this criterion is used for interpretation, glucose (*n*(*e-OH*) = 4.6) should have a stronger salting-out effect than fructose (*n*(*e-OH*) = 3.0). However, the effects of the added sugars (glucose and fructose) on the LST in water/DPnP are comparable and no clear trend could be observed in this investigation, which is probably due to the accuracy of the experimental examination, which is not high enough to detect different effects originating from *n*(*e-OH*). Common hydration chatacteristics of the tested sugars and sugar alcohols are their similar hydration numbers (n_h(glucose) = 8-8.6), n_h(xylitol) = 7.39, n_h(fructose) = 8.8-9.01) and n_h(sorbitol) = 8.4-8.68) determined by acoustic methods, as summerised in the review of Burakowski and Glinski[483]. Now one may conclude that the salting-out properties do not depend strictly on the *n*(*e-OH*), but on the hydration numbers. This would justify the stronger salting-out effect of isomalt bearing nine alcoholic functions within its chemical structure.

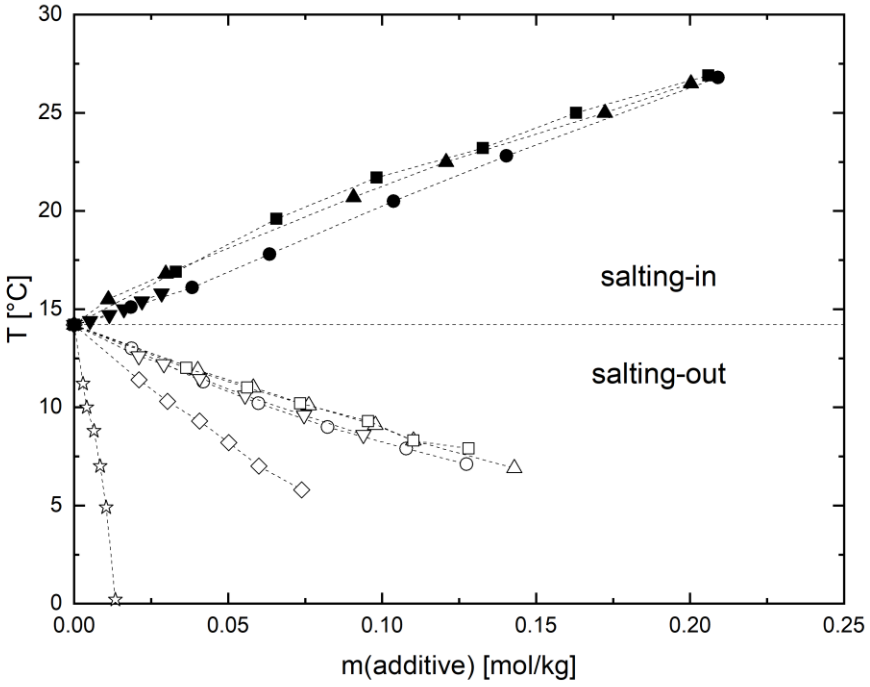

Figure IV.7. Shift in the LST upon the addition of sugar or sweetener. Symbols represent experimental data: (■) potassium acesulfamate, (▲) sodium saccharinate, (●) sodium N-cyclohexylsulfamate, (▼) aspartame, (□) glucose, (△) fructose, (▽) sorbitol, (○) xylitol, (◇) isomalt, (☆) (Phy^{5-}, $5Na^+$).

For all kinds of additives, independently whether there is a salting-out or salting-in effect, a linear shift in the LST was found over a wide concentration range. With Eq.(IV-1), the slopes of the linear shifts are calculated and the obtained α values are given in Table IV-1 for comparison. The tetraphenylphosphonium chloride (PPh_4Cl) is a representative of antagonistic salts and was found to increase the solubility of hydrophobic compounds in water[484]. Its salting-in effect in water/DPnP has not been depicted in a figure due to the high concentrations (up to $m(PPh_4Cl) = 8.5$ mol/kg) used for the investigation. Nevertheless, the determined α value is listed in Table IV-1 and reveals the highest salting-in effect in water/DPnP upon the investigated additives.

Table IV-1. α coefficients for different additives (in °C/mmol of additive in 1 mole of DPnP/water mixture).

Chemical compound	α
sodium thiocyanate	2.20
sodium chloride	-2.01
lithium sulphate	-8.65
sodium sulphate	-10.48
aluminium sulphate	-29.06
ammonium sulphate	-7.19
potassium pyrophosphate	-16.53
sodium triphosphate	-25.65
tetrasodium pyrophosphate	-30.03
citric acid	0.66
tartaric acid	0.40
malonic acid	0.37
glycolic acid	0.26
oxalic acid	0.16
sodium nicotinate	-1.58
sodium acetate	-3.34
disodium malate	-9.46
trisodium citrate	-13.33
L-cysteine	-1.41
L-proline	-1.98
glycine	-2.08
L-arginine	-2.21
L-alanine	-2.22
L-serine	-2.32
ectoine	-2.58
monosodium L-glutamate	-6.36
triethylphenylammonium chloride	-0.42
betaine hydrochloride	-1.96
DL-carnitine hydrochloride	-2.25
choline chloride	-2.35
trimethylamine N-oxide	-2.73
potassium acesulfamate	1.72
sodium saccharinate	1.69
sodium N-cyclohexylsulfamate	1.73
aspartame	1.61
glucose	-1.39
fructose	-1.43
xylitol	-1.58
sorbitol	-1.65
isomalt	-3.19
pentasodium phytate (Phy^{5-}, 5Na^{+})	***-27.41***
tertraphenylphosphonium chloride	3.10

IV.3.2 Relative Volume of the Ethanol-rich Phase and Ethanol Purification Coefficient

In Figure IV.8 a), the relative volumes of the upper phase $V_{rel,\,UP}$ after ethanol separation from water at 25 °C and 1 bar are presented depending on the weight percentages (wt%) of different added salts, (Phy^{5-}, $5Na^{+}$), $K_4P_2O_7$ and $(NH_4)_2SO_4$. At a total amount of 9 wt% of salt, $(NH_4)_2SO_4$ is the most efficient additive for ethanol separation from water ($V_{rel,\,UP} = 0.89$) and in addition, the phase separation occurs very fast compared to the other salts. At a salt content of 33 wt%, the ammonium salt is precipitated and shows a less effective ethanol separation from water compared to the other salts. $K_4P_2O_7$ is the best salting-out agent followed by (Phy^{5-}, $5Na^{+}$).

In Figure IV.8 b), the purification coefficients of ethanol $P(EtOH)$ at 25 °C and 1 bar are presented depending on the used salt and its total concentration in the samples. It appears that the purification coefficients at 9 wt% of salt are equal for $(NH_4)_2SO_4$ and $K_4P_2O_7$ ($P(EtOH) = 1.09$) and higher than that induced by (Phy^{5-}, $5Na^{+}$) ($P(EtOH) = 1.04$). In presence of 33 wt% of salt, the purification coefficients induced by (Phy^{5-}, $5Na^{+}$) ($P(EtOH) = 1.25$) and $K_4P_2O_7$ ($P(EtOH) = 1.45$) are superior to the one of $(NH_4)_2SO_4$ ($P(EtOH) = 1.07$), for which at this concentration, $P(EtOH)$ is limited by its solubility in water. In presence of 40 wt% of salt, a higher purification coefficient is observed in case of $K_4P_2O_7$ ($P(EtOH) = 1.53$) compared to the one obtained using (Phy^{5-}, $5Na^{+}$) ($P(EtOH) = 1.31$). The purification coefficient in the presence of 50 wt% of added $K_4P_2O_7$ is the best one of all tested mixtures ($P(EtOH) = 1.60$). All values of $V_{rel,\,UP}$ and $P(EtOH)$ are summarized for the investigated salts in Table IV-2.

Table IV-2. Relative volumes of the upper phase $V_{rel,\,UP}$ and ethanol purification coefficients $P(EtOH)$ after phase separation induced by (Phy^{5-}, $5Na^{+}$), $K_4P_2O_7$ and $(NH_4)_2SO_4$.

Salt	$V_{rel,\,UP}$	$P(EtOH)$
(Phy^{5-}, $5Na^{+}$) at 9, 33, 40 wt%	0.95, 0.79, 0.76	1.04, 1.25, 1.31
$K_4P_2O_7$ at 9, 33, 40, 50 wt%	0.90, 0.70, 0.64, 0.61	1.09, 1.45, 1.53, 1.60
$(NH_4)_2SO_4$ at 9, 33 wt%	0.89, 0.85	1.09, 1.07

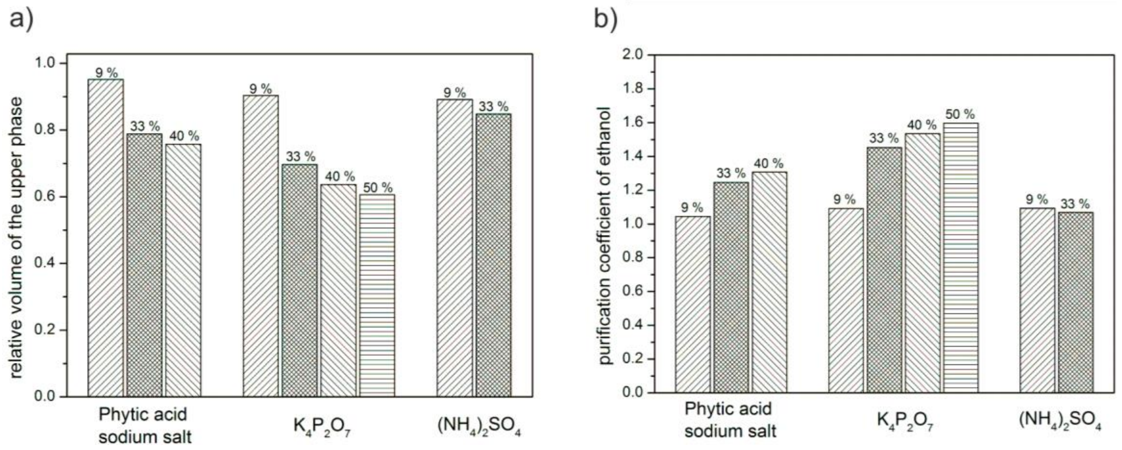

Figure IV.8. –a) Relative volume of the upper phase $V_{rel,\ UP}$ and to a comparable monophasic binary solution of ethanol and water (1:1, w/w) without salt, obtained at 25°C and 1 bar after the addition of (▨) 9; (▩) 33; (▧) 40; (▤) 50% of (Phy^{5-}, $5Na^+$), $K_4P_2O_7$ and $(NH_4)_2SO_4$. –b) Corresponding ethanol purification coefficients *P(EtOH)*.

IV.4 Conclusion

Salting-in and salting-out properties of different inorganic and organic compounds on the LST in water/DPnP have been reported. The salting-in and -out properties (in this Chapter these expressions were kept also for the uncharged molecules and for molecules, to which hydrotropy is associated) were related to the molecular structure and therefore to the molecular family. In the scope of the tested compounds, a salting-out effect was observed for inorganic sulphate and phosphate salts, short carboxylate sodium salts, amino-acids, quaternary ammonium salts and typical sugars. In contrast, a salting-in effect appeared using short organic acids, sweeteners or an antagonistic salt (Ph_4PCl). Obviously, similar effects are typical of a certain class of molecules with common biological functions. Ph_4PCl showed the most pronounced salting-in effect and among the tested organic molecules and the sodium salt of phytic acid (Phy^{5-}, $5Na^+$) was found to be the most efficient organic salting-out compound. For all additives a linear relationship between the LST and the concentration of additive was detected.

In case of the examined sulphates salts, $Al_2(SO_4)_3$ showed the strongest salting-out effect followed by Na_2SO_4, Li_2SO_4 and $(NH_4)_2SO_4$. For the phosphate salts, $Na_4P_2O_7$ leads to the most pronounced decrease of the LST followed by $Na_5P_3O_{10}$ and $K_4P_2O_7$. $Al_2(SO_4)_3$ and $Na_4P_2O_7$ show similar salt-effects.

The strength of the salting-in effect of short organic acids was found to be related to the number of carboxylic and hydroxylic groups and thus the following series was detected: citric acid > tartaric acid > malonic acid > glycolic acid > oxalic acid. Similary, the number of functional groups in short organic carboxylate salts was found to be related to the strength of the salting-out in the water/DPnP system. The strength of the salting-out power follows the order: trisodium citrate > disodium malate > sodium acetate > sodium nicotinate. It can be noted that the most salting-in acid corresponds to the most salting-out carboxylate salt.

Amino acids were found to have a salting-out effect in the water/DPnP system, which is weakly specific. The most pronounced salting-out was observed for monosodium L-glutamate, which is due to its two carboxylic functions and thus a similar effect was found for disodium malate. A significantly lower salting-out effect was observed for L-cysteine at high concentrations, which was deduced from the occurrence of the thiol group within its chemical structure.

The salting-out effects of quaternary ammonium salts were found to be of similar magnitude compared to those of the amino-acids and they were also only slightly specific. The most pronounced salting-out effect was observed for the zwitterionic osmolyte TMAO whereas the least pronounced effect was detected for triethylphenylammonium chloride.

For all sweetners a salting-in effect was observed, which was not specific. The decrease of the LST by the addition of sugars was related to the “sugaring-out” effect. The strength of the sugaring-out effect was deduced to the number of OH-groups being present in the sugar molecules. A more detailed correlation considering $n(e\text{-}OH)$ was not possible propably due to insufficient accuracy of the experimental examination. Thus, the effects of glucose, fructuose, xylitol and sorbitol addition are similar whereas a pronounced sugaring-out effect was observed for isomalt. The six phosphate functions within (Phy^{5-}, $5Na^+$) were assumed to induce the most pronounced salting-out effect of all tested organic additives in the water/DPnP mixtures.

Concerning the ethanol separation from water using salting-out salts, $(NH_4)_2SO_4$ showed the best performance at low concentrations (9 wt%). Due to a higher water solubility, (Phy^{5-}, $5Na^+$) allowed a more pronounced separation of ethanol from water than $(NH_4)_2SO_4$. At higher salt concentrations (33, 40, 50 wt%), $K_4P_2O_7$ is the most effective additive for ethanol separation. The use of $(NH_4)_2SO_4$ and (Phy^{5-}, $5Na^+$) are limited at 33 wt% and 40 wt% respectively. Among the investgated salts, the most water-soluble agent $K_4P_2O_7$ turned out to be also the most efficient salt to separate ethanol and water.

Chapter V

Liquid-Liquid Equilibrium

V.1 Introduction

The isolation of biotechnology-derived chemical products from the reaction medium (e.g., fermentation broth) remains a challenging issue. Several studies considered integrating an *in-situ* LLEx step into the total production processes[26,55,60,97]. *In-situ* extraction uses an extractive solvent, which is immiscible with the reaction solvent (mostly water) in order to separate the desired product from the reaction medium. Energy and purification costs of LLEx processes are usually much lower compared to distillation, which has its limitations in separation of heat sensitive compounds or compounds of very close volatility[150,485].

In many biotechnological processes, salts are already present in the reaction system or are even added intentionally to the reaction medium in order to modify reaction conditions. Electrolytes are known to have a strong influence on the mutual solubility of water and organic solvents as well as on the partitioning of a product between water and the organic solvent. Fully water miscible organic compounds (e.g. THF[486,487], propanols[488–490]) separate from the aqueous medium by the addition of salt and the solubility gap between water and a partial miscible organic solvent can even be increased in presence of electrolytes. Thus, the systematic study of the salt effects on LLE of involved liquid mixtures is a prerequisite for the design of extraction processes[181,491].

To systematically understand the salt effects in quaternary systems water/n-butanol/solute (HMF or glycerol)/salt, the knowledge of ternary water/n-butanol/salt LLE data is required in a first step. Comprehensive studies on phase equilibria of water/n-butanol/NaCl mixtures at temperatures ranging from 293.15 to 313.15 K were carried out by De Santis et al.[492,493]. They found that n-butanol was beneficial for the desalination of sea water by solvent-induced precipitation. LLE of the ternary water/n-butanol/NaCl system at 298.15 K was also investigated by Marcilla et al.[168], Li et al.[494] and Oudshoorn et al.[150]. Li et al.[494] also investigated the effect of KCl and KBr on the water/n-butanol system and that of KCl was further examined by Gomis et al.[495]. Al-Sahhaf and Kapetanovic[496] found that the n-butanol solubility in water decreases upon salt addition in the order: KI < KBr < NaBr < LiCl. Interestingly, the solubilities of LiCl and KI were found to be remarkably high in the n-butanol-rich phase, which is explained by mixed solvation effects affected by water and n-butanol. The salting-out efficiency of $CaCl_2$ in the water/n-butanol mixture was shown to be of similar magnitude to that observed for LiCl[150]. Pirahmadi et al.[389,391] investigated the salting-out effect of NH_4Cl (298.15, 308.15 and 318.15 K) as well as of $NaNO_3$ (298.15 and

308.15 K) on n-butanol from the aqueous phase. The influence of temperature was shown to be of minor impact on the LLE of water/n-butanol. Some related examples for salt effects in quaternary systems, in which butanols were used as extractive solvent are water/2-butanol/citric acid/NaCl[497], water/n-butanol/ethanol/NaCl[168] or KCl[498], water/n-butanol/acetone/NaCl[499], water/acetic acid/n-butanol/NaCl or KCl[500], water/propionic acid/n-butanol/NaCl[491] and water/n-butanol/glycerol/NaCl[388]. The latter quaternary systems containing n-butanol were correlated using a modified Eisen-Joffe[181] equation or by the Othmer-Tobias[179] method. Salt effects in quaternary systems, in which n-butanol, acetone and ethanol were the solutes to be extracted, were presented by Malinowski and Daugulis[501]. Many more ternary and quaternary systems can be found in the literature.

More recently, LLE data of ternary and quaternary systems including HMF were determined applying different organic solvents and salts in case of quaternary systems.

Dalmolin et al.[502] presented LLE data of ternary water/organic solvent /HMF mixtures with n-butanol, 2-butanol and 2-pentanol as organic solvent at 298.2 K and 1 bar. Experimental methods were density and RI measurements besides the binodal curve determination *via* the cloud point method. In their studies, n-butanol and 2-butanol showed similar capacity for HMF and 2-pentanol showed the best selectivity for HMF.

Altway et al.[503] measured LLE data of ternary water/organic solvent/HMF and quaternary water/organic solvent/HMF/salt systems with MIBK and 2-pentanol as solvent and NaCl, KCl, Na_2SO_4 and K_2SO_4 as salt at 313.15 K and 1 bar. They applied the analytical method with GC-FID (HMF, organic solvent), ICP-OES (salts) and KF-titration (water). Correlation using NRTL and UNIQUAC were applied for the ternary systems and NRTL was applied for the quaternary system with salt. Although higher HMF distribution ratios ($D^w(HMF)$) were achieved in the ternary system using 2-pentanol, MIBK as extractive solvent showed a better selectivity in terms of higher $\alpha^w(HMF, water)$ values. They compared $D^w(HMF)$ and $\alpha^w(HMF, water)$ values of ternary water/MIBK/HMF and water/2-pentanol/HMF systems at 313.15 K to those measured by Mohammad et al.[419] and Dalmolin et al.[502] at 298.2 K, respectively. A slight increase of both extraction parameters was observed at the higher temperature. Concerning the salt-effects on extraction performance, they stated an increased salting-out effect in the order: NaCl > Na_2SO_4 > KCl > K_2SO_4 with NaCl being the most effective salting-out agent. They also stated that this corresponds to the reversed Hofmeister series as Cl^- has a stronger salting-out effect than SO_4^{2-} with the same cation. They used binary aqueous HMF mixtures (5 to 40 wt%) and added salt to a constant weight fraction in the ternary systems. For NaCl and KCl, 10 wt%, while for Na_2SO_4 and K_2SO_4 3 and 2.5 wt% of salt were used, respectively. This results in different salt molalities relative to water at a fixed HMF concentrations for all salts. E.g. at 40 wt% of HMF in water, the salt molalities are 3.16 (NaCl), 2.48 (KCl), 0.36 (Na_2SO_4) and 0.25 (K_2SO_4) according to the given constant salt weight fractions. And the ionic strength of the chlorides is approximately 3 times higher than that of the corresponding sulphate salt. Based on these different numbers of ions and ionic strengths in their investigated mixtures, the statement about a reversed Hofmeister series in these sytems is not understood and doubtful. For the MIBK system, Mohammad et al.[419] found a stronger salting-out effect for SO_4^{2-} than for Cl^- based on salt molality, which supports this doubt.

Zhang et al. [504] experimentally determined LLE data of ternary water/organic solvent/HMF mixtures at different temperatures (313.15, 323.15 and 333.15 K). The organic solvents were n-butanol, isobutanol and MIBK. Analytical methods were LC-UV (HMF), GC-FID (organic solvent) and the water fraction was obtained by mass balance. Higher $D^w(HMF)$ values were obtained for the butanols compared to those obtained with MIBK as organic solvent. The influence of temperature on the $D^w(HMF)$ values was insignificant. The NRTL model was used to correlate the LLE data.

LLE data of ternary water/THF/salt and quaternary water/THF/HMF/salt systems were determined experimentally by Xie et al.[487] at 303.15 K, applying the analytical method for all compounds. LiCl, NaCl and KCl were used as salts, which induced a salting-out effect on THF from the aquous phase upon salt addition. This effect was more promounced in case of NaCl and KCl in comparison to that of LiCl, which was rather weak. Salt effects in quaternary systems were detected in terms of increased $D^w(HMF)$ values with increasing salt content. At a salt concentration of 0.1 g/ml relative to water, the strength of the salting-out effect was NaCl > KCl > LiCl while at 0.25 g/ml the series changed to NaCl > LiCl > KCl. In contrast, the $\alpha^w(HMF, water)$ decreased with increasing salt concentration for NaCl and KCl. In case of LiCl, $\alpha^w(HMF, water)$ was rather independent on the salt concentration. Quaternary LLE data were correlated using the NRTL model.

Cavalcanti et al.[505] used a series of primary alcohols (n-pentanol, n-hexanol, n-heptanol) for HMF recovery from the aqueous phase. LLE data of ternary water/organic solvent/HMF mixtures were measured at 298.15 K and 1 bar and correlated with the NRTL and UNIQUAC models. Their results revealed that n-pentanol is superior to n-hexanol and n-heptanol as well as to the alcohols studied by Dalmolin et al.[502] (n-butanol, 2-butanol and 2-pentanol) in terms of better solvent capacity and selectivity.

Mohammad et al.[395,419] measured ternary water/MIBK/salt, water/MIBK/HMF and quaternary water/MIBK/HMF/salt system with many different salts at different salt and different HMF concentration at 298.15 K. They applied ePC-SAFT to model the influence of 8 salts on the distribution behaviour of HMF. Pure-ion parameter, which are valid independent of the salt, were obtained by adjusting to experimental data of the corresponding subsystems.

In the present work, the influence of salts on the binary LLE of water/n-butanol was measured at 298.15 K and 1 bar for lithium, sodium, potassium and ammonium salts of chlorides, sulphates, acetates and nitrates in a broad range of salt concentration. In addition, sodium propionate (C_2H_5COONa) and sodium butyrate (C_3H_7COONa) were tested. A modified *Setchenov* equation and the evolution of the tie-line length (TLL) depending on the salt concentration were used to correlate the salt effects in ternary water/n-butanol/salt sytems. The influence of $LiNO_3$, Li_2SO_4, Na_2SO_4, CH_3COOLi and CH_3COOLi on the LLE of water/n-butanol was modelled using ePC-SAFT.

Furthermore, LLE data of the ternary systems water/n-butanol/HMF and water/n-butanol/glycerol were determined at 298.15 K and 1 bar. Solute (HMF, glycerol) distribution ratios and separations factors were calculated based on the LLE data. LLE data of the ternary system containing HMF were modelled with PC-SAFT and predicted by COSMO-RS.

The target systems of the AiF-project were quaternary mixtures composed of water, organic solvent, product molecule (HMF or glycerol) and salt. The focus of investigations was set to the quaternary systems with HMF as product molecule. Few further investigations were made with glycerol as product molecule. n-Butanol was used as extractant and the influence of salts on the LLE of water/n-butanol/HMF was investigated for the same salts as used for ternary water/n-butanol/salt systems, except $LiNO_3$ and CH_3COOLi but additionally with LiCl and $Al_2(SO_4)_3$. For C_3H_7COONa and (Phy^{5-}, $5Na^+$) as salting-out agents, only $D^w(HMF)$ values were determined. Quaternary systems were investigated at constant salt concentration with varying HMF concentration and vice versa. $D^w(HMF)$ and $\alpha^w(HMF, water)$ values were parameters to evaluate the salting-out effects on HMF. The same concept of investiagtions was applied for quaternary water/n-butanol/glycerol/salt systems, whereby LLE data were only determined for NaCl and Li_2SO_4 as salt. For (Phy^{5-}, $5Na^+$), $Na_5P_3O_{10}$ and $K_4P_2O_7$ as salting-out agent, only glycerol distribution ratios were determined. Quaternary LLE of water/n-butanol/HMF/salt with NaCl, LiCl, CH_3COONa and Li_2SO_4 as salt were predicted with ePC-SAFT using binary parameters fitted to experimental data of the corresponding binary and ternary subsytems.

V.2 Experimental

V.2.1 Materials

HMF (Molekula GmbH, Munich, ≥ 99.1%, GC) was stored at 277 K concerning its low melting point (300.15-303.15 K). Just before use, the HMF container was placed into an ice-box. In addition, HMF is quite hygroscopic, which is why particular care was taken to ensure only temporary air contact. Glycerol (≥ 99.5%), n-butanol (≥ 99.8%), lithium chloride (≥ 99%) and sodium chloride (≥ 99%) were purchased from *VWR* and used without further purification. Acetylacetone (≥ 99%), sodium periodate (≥ 99%), potassium chloride (≥ 99.5%), sodium acetate (≥ 99%), sodium butyrate (≥ 98%), lithium nitrate (≥ 98%), ammonium nitrate (≥ 99%), sodium triphosphate (≥ 98%) and tetrasodium pyrophosphate decahydrate (≥ 99%) were obtained from *Merck*. Lithium acetate (≥ 99.95%), sodium propionate (≥ 99%), sodium sulphate (≥ 99%), aluminium sulphate octadecahydrate (≥ 98%), potassium pyrophosphate (≥ 97%) and phytic acid sodium salt (≥ 99%) were received from *Sigma-Aldrich*. Lithium sulphate (≥ 99.99%) was obtained from *Alfa Aesar*. All salts were used without further drying or other treatments. For all experiments, water was taken from a Millipore purification system. Hydranal Methanol dry (*Sigma-Aldrich*, ≥ 99.98%) and the Combititrant 5 (*Merck*, efficiency ≥ 5 mg/ml) were used for KF-titration. The content of sodium in the phytate salt was checked using AES and was found to be equal to 5 moles/mole of phytate. The water content of pentasodium phytate was determined by KF-titration and was found to be less than 1%.

V.2.2 Methods

V.2.2.1 General Experimental Procedure

Determination of LLE data in this work was carried out by the analytical method. That is, biphasic mixtures of known weight fractions were prepared in double-walled glass vessels with four individual sample chambers (see Figure V.1) and equilibrated. Components of each liquid phase were quantified with appropriate analytical methods. For the preparation of the biphasic mixtures, at first the solid substances (salt and/or HMF) were weighed and dissolved in water before n-butanol was added. All components were weighed using a precision balance (± 0.2 mg). The mixtures were brought into thermal equilibrium at 298.15 ± 0.15 K and 1 bar by intensively stirring (1200 rpm) for at least 1 hour. Phase separation was allowed for at least 12 hours to assure thermodynamic equilibrium. Longer stirring and settling periods than those mentioned above had no measurable effects on the resulting phase compositions. Samples of the n-butanol and aqueous phase were taken carefully using syringes with long cannula passing through the septum of the caps, beginning with the upper phase, naturally. The upper organic phase was withdrawn keeping the needle tip distant from the liquid-liquid interface while the lower aqueous phase was withdrawn keeping the needle tip close to the bottom of the glass vessel. A second needle was used to make an additional tiny perforation in the septum caps to avoid unintentional mixing of the separated phases due to a pressure drop induced by the withdrawal of liquid.

Figure V.1. Double-walled glass vessels with four individual sample chambers for the determination of LLE data. In this case, a quaternary system with HMF is pictured.

All samples and dilutions for the determination of LLE data were prepared gravimetrically allowing to draw corresponding phase diagrams in weight fraction scale. The opportunity to transform weight fractions to mole fractions and molality scale bears additional advantages. The analysis of the phase compositions was performed utilising KF-titration, UV-spectrophotometry, gas chromatography, anion-exchange chromatography and the gravimetrical method. Different apparatuses of the same kind were used due to partially different stays for the experimental work. All measurements were carried out with appropriate calibrations and the basic procedures for the instrumental analysis were kept constant independently of the individual device. The different devices are mentioned in the following part of the experimental methods.

V.2.2.2 Karl Fischer-Titration (KF-Titration)

For the determination of the water content in both, the n-butanol-rich and the water-rich phases, volumetric KF-titration was applied. In Dortmund, the 915 KF Ti-Touch (*Metrohm*) and in Regensburg, the 870 KF Titrion plus *(Methrom*) were used. The Combititrant 5 (one-component reagent, titer efficiency ≥5 mg/ml, *Merck*) and dried Methanol (Hydranal, *Sigma-Aldrich*, > 99.98 %) were used as titrant and solvent, respectively, independently of the applied titrator. Titer determination for KF-titrants is indispensable, because the titer is subjected to changes by the humidity in the air. Basically, the procedures of titer determination and water content determination are similar. The water or sample containing syringes were weighed (± 0.2 mg) before a few droplets (~3 to 5) were added to the conditioned (water-free) solvent in the titration cell. The mass of added liquid is entered to the titrator and volumetric titration occurs automatically. With the known mass of water or sample and the consumed volume of the titrant solution, the titrator performed the titer (mg/ml) or water content (in wt%) calculation. Titer determination was repeated until sufficient convergence was observed (< 1% relative standard deviation). At least, three repetitions of water quantifications were carried out for each sample and the results were averaged.

V.2.2.3 UV/VIS Spectrophotometry

The UV/VIS-spectrometers (BioSpectrometer, *Eppendorf*) and (Lambda 18 spectrophotometer, *Perkin Elmer*) were used in Dortmund and in Regensburg, respectively. Calibration was carried out with aqueous HMF solutions in a concentration range of 4 to 20 ppm (w/w). Samples with higher HMF weight fractions were diluted with water using mass-based dilution factors of up to 1:50,000. Due to the highly diluted samples, matrix effects were assumed to be negligible. Absorbance measurements were carried out at a wavelength of λ = 284 nm. Diluted samples from one single mixture preparation were measured three times and the results were averaged.

V.2.2.4 Gas Chromatography (GC)

The n-butanol weight fractions in the aqueous and n-butanol-rich phases were determined by gas chromatography (GC) equipped with a polyethylene glycol packed column and a flame ionisation detector (FID). In Dortmund, the GC 7890A Series (*Agilent*) equipped with the column HP-INNOWax (30m*320µm*0.5µm, *Agilent*) was applied using hydrogen as carrier gas. In Regensburg, the GC HP 6890 Series (*Hewlett-Packard*) equipped with the column DB-WAXetr (30m*320µm*0.5µm, Agilent) was applied using helium as carrier gas. For both GC systems, the flow rate of the carrier gas was set to 1 ml/min and the injector volume was 1µl of the sample in split mode using the split ratio 1:10. The samples of the aqueous or organic layers were diluted with water gravimetrically by factors 1:10 and 1:100, respectively. For quantitative analysis, the diluted samples were combined gravimetrically 1:1 with an aqueous n-pentanol (1 wt%) solution as internal standard. The reason for using water as solvent for the GC-samples lies in the risk of precipitating salt, while diluting samples with an organic solvent like ethanol, propanol or acetone. This would lead to incorrect n-butanol weight fraction determinations. A similar problem was also described by Marcilla et al.[168].

Calibration was performed by measuring 1:1 (w/w) mixtures of aqueous n-butanol standard solutions (0.1 up to 0.8 wt%) combined with the internal standard solution. Peak separation of n-butanol (4.1 min) from the internal standard (5.2 min) was realized by a column temperature gradient of 10 K/min ranging from 373.15 to 423.15 K. The temperature of the detector (FID) was set to 523.15 K. All samples were analysed at least three times and the results were averaged. To protect the GC column from electrolytes, glass wool (serving as a filter) was placed into the inlet liner. In case of samples including HMF, the column temperature was raised from 423.15 K to 513.15 K with a temperature gradient of 40 K/min upon 8 mintues (after the signals for n-butanol and n-pentanol were detected) and the temperature was hold further 3 minutes (total run time 13.25 min). This ‘purge’ step was required to remove residual HMF attached at the GC column. If this step would have been skipped, detection of the alcohols in the following measurements would have been error prone in terms of baseline-shifts and displaced retention times in the chromatograms.

V.2.2.5 Anion-Exchange Chromatography (IC)

The weight fractions of anions in the separated liquid phases were determined by IC. An ICS-2100 ion chromatograph (*Dionex*, *Thermo Scientific*) assembled with the column RFIC IonPac AS22, the autosampler AS-AP and the eluent generator ICS 2100 EGC was applied. The aqueous and organic samples were diluted with water gravimetrically by factors 1:1000 and 1:100, respectively. Organic phases from extraction systems containing sodium acetate were diluted 1:30 to remain within the concentration range of the corresponding calibration curve. Sulphate quantification in organic n-butanol phases was not possible due to high standard deviations in case of undiluted samples and sulphate concentrations below the detection limit in case of diluted samples. Gradient elution (50mM/3min) from 50 to 100 mM KOH-buffer solution was applied to realise short retention times (2-3 min) of the anions (Cl^-, SO_4^{2-} and NO_3^-). The elution with 100 mM KOH buffer was hold further 1.5 min and upon 4.5 min, the elution continued with 50 mM for further 1 min. In total the method duration for Cl^-, SO_4^{2-} and NO_3^- anions was 5.5 minutes. For the analysis of acetate anions, the gradient elution (8 mM/min) from 10 mM to 50 mM upon 3 min of retention time was applied and was hold further 2 min. Upon 10 min of retention time, the elution continued with 10 mM for further 5 min. For acetate anions, the total method duration was 15 minutes. In each case, the flow rate was set to 0.25 ml/min and the column temperature was 35°C. The anions were detected by electrical conductivity after their specific delay, due to interactions with the column material. The suppressor (current: 62 mA) was connected to an external water supply to protect the suppressor from any organic compounds, which might be harmful for the device.

For each anion, a calibration curve was constructed. Similar to GC-analysis, each sample was analysed at least three times and the results were averaged.

V.2.2.6 Gravimetrical Method

Salt determination in heterogenous ternary systems composed of water/n-butanol/salt (salt = NH_4NO_3, C_2H_5COONa, C_3H_7COONa) was performed by the gravimetrical method. Small tared glass vials containing ~1g of sample were put into a heated oven (130°C) over night. As the liquid evaporated, the warm glass vials, containing the residual solid, were put in a desiccator under vaccum, until the samples cooled down to room temperature. The cooled vials were weighed and with the detected mass of the residual solid, salt weight fractions of the samples were calculated. All masses were detected using a high resolution balance (± 0.01mg).

V.2.2.7 Colorimetric Assay for Glycerol Quantification

Quantification of the glycerol content in aqueous and organic phases was performed using a modified colorimetric assay described in section II.4.5.5. Aqueous and organic samples were diluted with water using dilution factors of 1/1000 up to 1/3000 (w/w) and subsequently 0.5 ml of each dilution were combined with 1.5 ml of working solvent (ethanol-water mixture 1/1 (v/v)). After the addition of 1.2 ml of ammonium acetate buffered $NaIO_4$ solution and 1.2 ml of an ammonium acetate buffered acetylacetone solution, all samples were thermostated at 70°C for 5 minutes to ensure the quantitative chemical reaction. The samples were cooled to room temperature with tab water and absorbance values were collected by applying UV/VIS spectrophotometry at a wavelength of $\lambda = 410$ nm. Weight fractions of glycerol were calculated using a corresponding calibration curve for each approach of investigation.

V.2.2.8 Determination of the Critical Point (cp)

The composition of the critical point was estimated by an experimental approach based on the titration method. Graduated test tubes (20 mL) were used to prepared different compositions of the ternary mixture water/n-butanol/HMF in the monophasic region near the binodal curve. Small amounts of water and n-butanol were added one by one until samples appeared turbid and turned to heterogenous mixtures. The biphasic samples were allowed to settle 12 h to reach thermodynamic equilibrium. The critical point is then identified by extrapolation to unity volume ratio of both phases.

V.2.2.9 COSMO-RS Calculations

The COSMO*therm* program is based on the COSMO-RS theory of interacting molecular surface charges, which are computed by quantum chemical methods (QCM). The LLE of the ternary system composed of water, n-butanol and HMF was calculated using the COSMO*therm*X 17 program with the COSMObase-1701. BP-TZVPD-FINE was chosen as parametrisation level. All conformers of n-butanol (7) and HMF (9) were considered for the calculations using the VLE/LLE property panel on the guide user interface (GUI). Pre-set conditions for the LLE calculation were '*isothermal*', 25°C for the temperature and '*ternary*' for the type of system. Weight or mole fraction can be chosen as concentration scale. The concentration grid was set so that 10 tie-lines were calculated. To account for thermodynamic fluctuations in the liquid mixture, which are usually most pronounced near the critical point, the '*COMPUTE RENORMALIZED LLE*' checkbox was activated. Without this renormalisation, a larger biphasic region would have been predicted for the ternary system.

V.3 Results and Discussion

V.3.1 Ternary LLE Water/n-Butanol/Salt

The LLE data of the ternary systems composed of water, n-butanol and salt were determined at 298.15 K and 1 bar, following the procedure described in section II.4.5. Investigated mixtures included one of the different salts: NaCl, KCl, Na_2SO_4, Li_2SO_4, $LiNO_3$, NH_4NO_3, CH_3OOLi, CH_3COONa, C_2H_5COONa and C_3H_7COONa. The used salt feed molalities of the investigated ternary water/n-butanol/salt systems and the applied method for the salt quantification in this work are presented in Table V-1. The LLE data of the mixed solvent systems including NaCl and KCl were reproduced from the literature to confirm the experimental procedure, see Figure V.2 and Figure V.3. One further reason for the investigation of these two systems was due to inconsistent LLE data found in the literature from Marcilla et al.[168] and Oudshoorn et al.[150] for NaCl and from Gomis et al.[495] and Li et al.[494] for KCl. Own measurements confirmed the results of Marcilla et al.[168] for NaCl and of Gomis et al.[495] for KCl. In the studies of Oudshoorn et al.[150], lower n-butanol concentrations were found in the organic phases and following the publication of Li et al.[494], KCl would have a stronger salting-out effect on n-butanol from water than NaCl, which was refuted in this work.

Table V-1. The used salt feed molalities and salt quantification method for the corresponding ternary water/n-butanol/salt systems, investigated in this work.

Salts	m_{Salt}^{Feed} [mol/kg]	Method for salt quantification
NaCl	0.3, 0.9, 2.2, 3.1, 4.4, 5.0	IC
KCl	0.5, 1.0, 2.0, 4.0	IC
Li_2SO_4	0.5, 1.0, 2.1	IC
Na_2SO_4	0.5, 0.7, 0.8, 1.1	IC
$LiNO_3$	1.3, 3.1, 5.2, 7.5	IC
NH_4NO_3	1.0, 4.9, 9.8, 14.9	gravimetric
CH_3COOLi	2.0, 3.0, 6.0	IC
CH_3COONa	1.0, 1.8, 2.7, 3.4	IC
C_2H_5COONa	1.0, 2.0, 4.0	gravimetric
C_3H_7COONa	0.2, 0.4, 0.6, 0.8	gravimetric

The experimentally determined LLE data in this work and the initial mixture compositions of the aforementioned ternary systems are presented in ternary phase diagrams for chlorides (Cl^-), sulphates (SO_4^{2-}), nitrates (NO_3^-), acetates (CH_3COO^-) and two further sodium carboxylates (C_2H_5COONa, C_3H_7COONa) in Figure V.2, Figure V.6, Figure V.8, Figure V.10 and Figure V.12, respectively, and are tabulated in Table B-1 and Table B-11.

In all cases, the salts are predominantly dissolved in the aqueous phases and tie-lines pass through the initial mixture compositions. As can be seen in the ternary diagrams, the addition of salts to the biphasic water/n-butanol system leads to an increase of the miscibility gap between water and n-butanol (indicated by the red diamonds). This salt induced increase of the miscibility gaps is represented in Figure V.19 by means of the increase of the tie-lines in ternary systems relative to the TLL in the binary system without salt. Absolute values for the TLL and TLS in these ternary systems are also given in Table B-1. The mutual solubility of both liquids decreases with increasing salt content, as the n-butanol content in the aqueous phases as well as the water content in the organic phases decrease. One exceptional case is presented by C_2H_5COONa, for which the miscibility gap decreases at high salt concentration.

Corresponding binary diagrams were constructed to visualise the salting-out effect by drawing the weight fractions of n-butanol in the aqueous phase depending on the salt weight fractions and salt molalities in the aqueous phase, see Figure V.3, Figure V.7, Figure V.9, Figure V.11 and Figure V.13. Here, the molality scale of salt concentration is more appropriate to compare the efficiency of the salts because mass effects do not appear. This is especially important, if the hydration theory is used for discussions, as the theory states that each ion binds a constant number of water molecules, which are then unavailable for solvation of the organic solvent to be salted-out. In many papers, salting-out effects of different salts (with different molar mass) are explained by this theory, but presenting salt weight fractions as abscissa. By doing so, an evaluation of the salting-out effects of different salts is not possible in a chemical sense. Alternatively to molality, the mole fractions could be used addressing this issue (accounting the number of particles). If available, LLE data from literature were integrated to the corresponding binary diagrams to extend the scope of salt-effect evaluation. The comparison of different salts with equal anions represents the cation effects on the n-butanol solubility in water. The salt molalities m_{salt} were calculated using the following conversion:

$$m_{salt} = \frac{w_{salt}}{M_{salt} * w_{water}} * 1000 \qquad \text{(V-1)}$$

with w_{salt} and w_{water} being the weight fractions of salt and water, respectively, in the corresponding aqueous phase. M_{salt} is the molar mass of the salt. To evaluate the anion effect on the water solubility of n-butanol, additional binary ‘salting-out’ diagrams were constructed for lithium, sodium, potassium and ammonium salts, see Figure V.15 to Figure V.18 in section V.3.1.6. A numerical way for the evaluation of the salting-out effects in the ternary systems composed of water, alcohol and salt, is the correlation of equilibrium data using a modified *Setchenov* equation. The procedure was adapted from a publication[506], in which the unusual S-shaped binodal curves of water/butanol systems with added LiCl were studied and *Setchenov* plots of those systems were shown for the aqueous and the organic phases. Calculated *Setchenov* coefficients of ternary water/organic solvent/salt systems with several pentanols, n-butanol and n-butanone as organic solvents and nitrates, chlorides and bromides as salts were tabulated by El-Dossoki[507]. The equations are on a salt free-basis and can be written on weight or mole fraction scale. The equation for the aqueous phase reads:

$$\ln\left(\frac{x_{buOH,0}}{x_{buOH}} * (1 - x_{salt})\right)_{aq\ phase} = K_s * x_{salt,aq\ phase} \tag{V-2}$$

and for the organic phase:

$$\ln\left(\frac{x_{water,0}}{x_{water}} * (1 - x_{salt})\right)_{org\ phase} = K'_s * x_{salt,aq\ phase} \tag{V-3}$$

where $x_{buOH,0}$ and $x_{water,0}$ are the mole fraction solubilities without salt of the organic solvent in water and of water in the organic solvent, respectively. x_{buOH} and x_{water} are the equilibrium mole fractions of n-butanol in the aqueous phase and of water in the organic phase, respectively, in the presence of salt. x_{salt} is the mole fraction of salt in the corresponding phases. K_s and K'_s are the *Setchenov* constants, which represent the magnitude of the salting-out effect in the water-rich and organic solvent-rich phases, respectively. Equilibrium data of systems with salt are well fitted by the *Setchenov* equations written on a free salt scale, see the following *Setchenov* plots in Figure V.4 and Figure V.5. A further advantage is that activity coefficient models (e.g. NRTL) for the extended *Setchenov* equation as proposed by Tang et al.[508] can be avoided.

V.3.1.1 Chlorides

In Figure V.2, LLE data of the ternary systems water/n-butanol/salt (salt = NaCl, KCl) are presented in ternary phase diagrams. LEE data of the water/n-butanol/NaCl system from this work agree well with those in the literature[168,493,494], but not with those from Oudshoorn et al.[150]. Tie-lines from the latter publication bear higher slopes, compared to those from the former mentioned publications and those determined in this work. Here, it is worthy to note that de Santis et al.[493] (in 1976) were able to determine LLE data quite accurately without determining the water content in both phases. Even in the organic phase, only the NaCl concentration was determined and n-butanol and water concentrations in the organic phases were determined by material balance based upon starting quantities and compositions. Such a procedure was already described in section II.4.5.

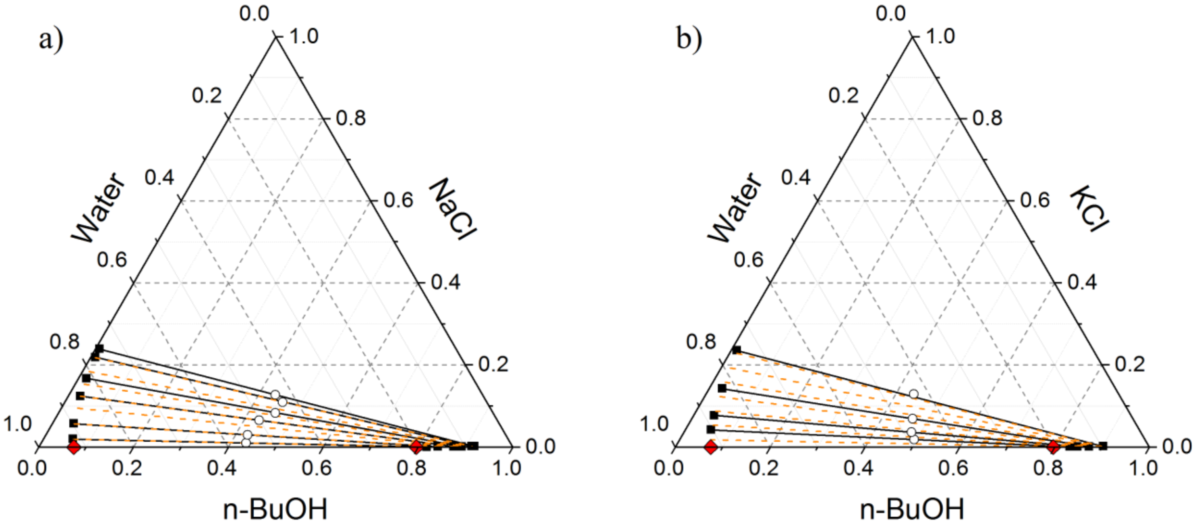

Figure V.2 LLE of ternary water/n-butanol/salt systems in weight fractions at 298.15 K and 1 bar: –a) salt = NaCl and –b) salt = KCl. (■) Experimental LLE data, (○) initial mixture compositions, (—) tie-lines of this work, (--) tie-lines taken from the literature for the systems water/n-butanol/NaCl[168] and water/n-butanol/KCl[495], (◆) mutual solubility compositions of water and n-butanol.

Although the LLE data determination *via* the mass balance and starting compositions bears potential errors for the overall equilibrium concentrations, the statements from Oudshoorn et al.[150] about high deviations of organic phase compositions of their studies compared to those of de Santis et al.[493], especially for n-butanol in the organic phase, are not justified. This doubt is supported by own measurements, those of Marcilla et al.[168] and Li et al.[494]. However, the salting-out effect of NaCl on n-butanol from water found from Oudshoorn et al.[150] is in accordance with that found in this work and in those[168,493,494] discussed above.

LLE data of the water/n-butanol/KCl system from this work are in line with those of Gomis et al.[495], but not with those of Li et al.[494], who measured a higher salting-effect for KCl than for NaCl in weight fractions. Although Li et al. presented consistent LLE data for the NaCl system, doubts exist for the ternary system including KCl. In this work, the effect of NaCl in weight fractions at 298.15 K and 1 bar is even more pronounced compared to that of KCl, but similar in molality scale. The salting-out efficiency on n-butanol from the aqueous phase mediated by chloride salts increases in weight fractions in the order: $NH_4^+ < K^+ < Li^+ \approx Na^+$ and in molality scale in the order: $NH_4^+ < Li^+ < K^+ \approx Na^+$, see Figure V.3.

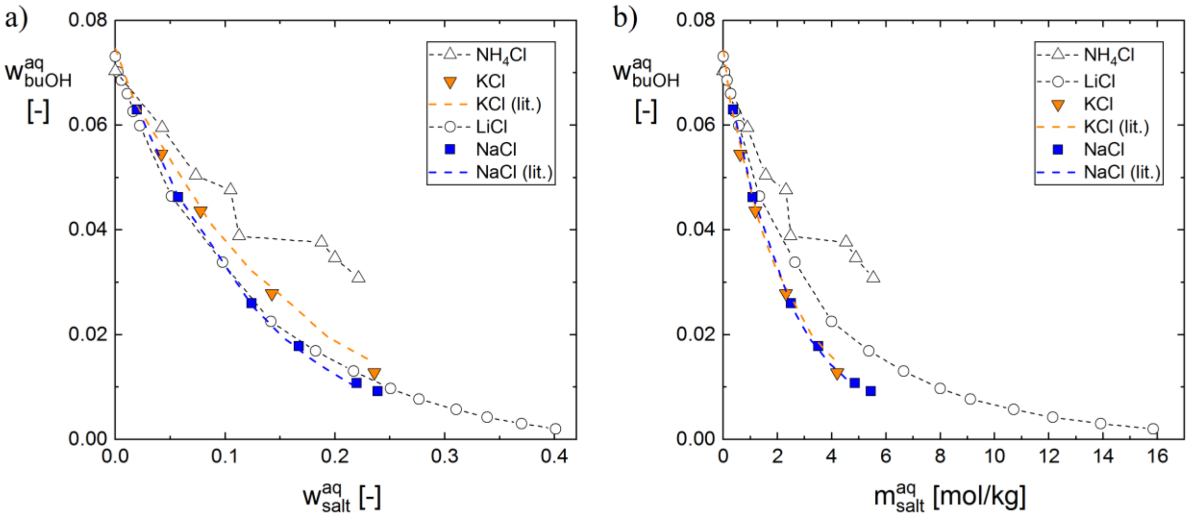

Figure V.3. Weight fractions of n-butanol in the aqueous phase of water/n-butanol/salt systems at 298.15 K and 1 bar vs. -a) salt weight fractions in the aqueous phase and -b) molality of salt in the aqueous phase close to the respective salt solubility limit. (■) NaCl and (▽) KCl are experimental data from this work. (--) NaCl and (--) KCl represent reproduced experimental data from literature[168,495]. (○) LiCl and (△) NH_4Cl are experimental data from literature[391,496].

A comparison with other alcohols can be made, using data from Gomis et al.[489], who investigated also the effect of NaCl and KCl on the miscible solvent systems water/n-propanol and water/2-propanol. They found that the two liquid phase regions are larger for NaCl than for KCl, i.e. the salting-out effect here is also higher with NaCl than with KCl in weight fractions and similar in molality scale. If 2-propanol is the organic solvent, the addition of KCl does not even lead to two liquid phases. Gomis et al.[488] conducted the investigation with LiCl and the same solvent systems. Here, the shape of the ternary phase diagram appeared different to those with NaCl and KCl due to the possible presence of two different solid phases. However, the addition of LiCl to the water/propanol systems leads to liquid phase separations and salting-out effects could be detected. The salting-out effect on n-propanol by chloride salts increases in the order: $Li^+ < K^+ < Na^+$ in weight fractions and in molality scale in the same order as for n-butanol: $Li^+ < K^+ \approx Na^+$. For n-pentanol, the series is: $Li^+ \approx K^+ < Na^+$ in weight fractions and in molality scale also in the same series as for n-butanol: $Li^+ < K^+ \approx Na^+$ is observed, following the data from literature[509–511]. Thus, Na^+ always leads to the most pronounced decrease in solubility of C3 to C5 primary alcohols induced by alkali chloride salts. However, the discussion above indicates that the nature of the organic solvent can also play an important role if salting-effects are considered.

In Figure V.4, the application of the *Setchenov* equation to both phases of the water/n-butanol/NaCl system is illustrated in weight fractions. LLE data taken from Marcilla et al.[168], Li et al.[494], Oudshoorn et al.[150], de Santis et al.[493] and from own measurements are correlated for comparison. In the aqueous phase, the salting-out effect on n-butanol is of similar magnitude for all presented studies. In contrast, the *Setchenov* plot for the organic phase reveals deviations for the data of Oudshoorn et al.[150], compared to the others. The reason for the deviations is probably the lower detected n-butanol content in the organic phases and thus a higher water content resulting from mass balance determination. So, the ‘salting-out’ of water in the organic phase is of lower magnitude and probably wrong, due to the low quality of regression ($R^2 = 0.7219$) and the strong deviation of the *Setchenov* coefficient ($K'_S = 1.754$) compared to those ($K'_S = 4.592$, $R^2 = 0.9895$; $K'_S = 4.532$, $R^2 = 0.9929$; $K'_S = 4.254$, $R^2 = 0.9554$; $K'_S = 3.933$ $R^2 = 0.9940$) of the other studies.

In Figure V.5, the application of the *Setchenov* equation to both phases of the water/n-butanol/KCl system is illustrated in weight fractions. LLE data taken from Gomis et al.[495], Li et al.[494] and from own measurements are correlated for comparison. As a result, and as already stated above, a higher salting-out effect of KCl was detected by Li et al.[494] ($K_S = 10.52$, $R^2 = 0.9676$) compared to that found by Gomis et al. ($K_S = 5.729$, $R^2 = 0.9964$) and by own measurements ($K_S = 6.196$, $R^2 = 0.9987$). In addition, the regression of the data from Li et al.[494] is of minor quality than those of the latter ones, which show comparable K_S and R^2 values. The correlations of the organic phases are comparable for all presented studies.

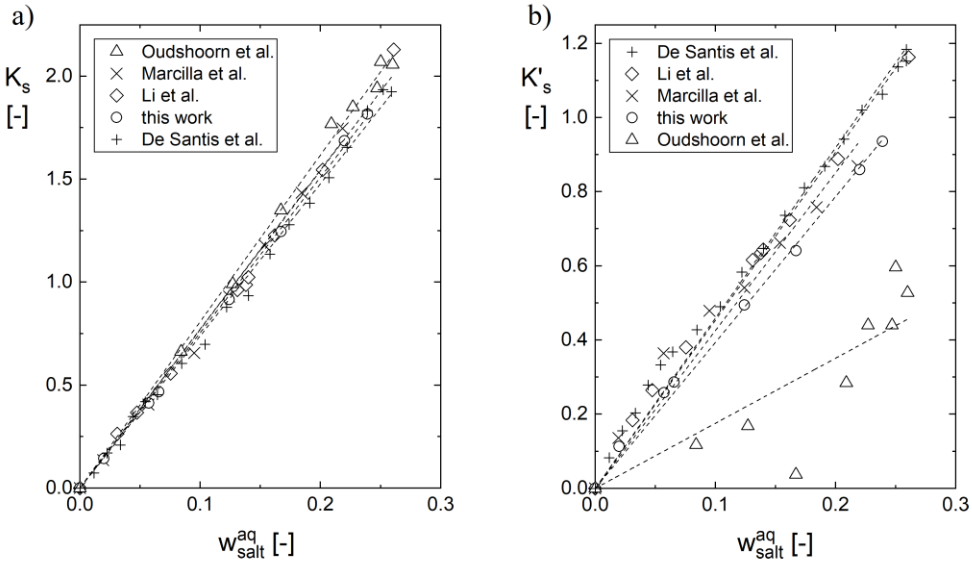

Figure V.4. *Setchenov* correlation of LLE data from the system water/n-butanol/NaCl. –a) the aqueous phase (K_s) and –b) the organic phase (K'_s). (△), (×), (◇) and (+) data from literature, (○) data from this work. The legend is arranged from highest to lowest *Setchenov* coefficients K_s and K'_s.

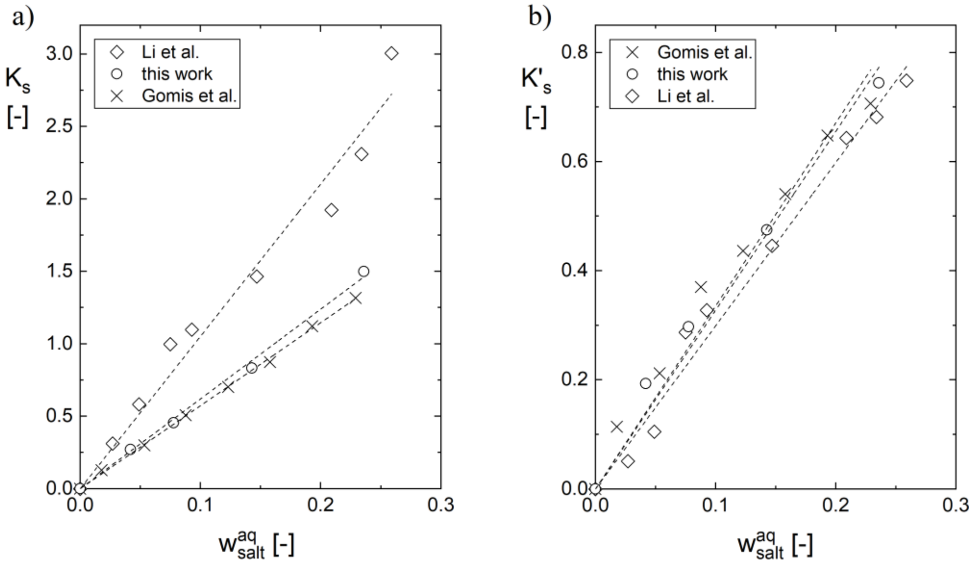

Figure V.5. *Setchenov* correlation of LLE data from the system water/n-butanol/KCl. –a) the aqueous phase (K_s) and –b) the organic phase (K'_s). (×) and (◇) data from literature, (○) data from this work. The legend is arranged from highest to lowest *Setchenov* coefficients K_s and K'_s.

V.3.1.2 Sulphates

In Figure V.6, LLE data of the ternary systems water/n-butanol/salt (salt = Li_2SO_4, Na_2SO_4) are presented in ternary phase diagrams. Due to the higher water solubility of Li_2SO_4 compared to that of Na_2SO_4, a higher reduction of the mutual solubility of the two liquids is possible with Li_2SO_4. The salting-out efficiency on n-butanol from the aqueous phase mediated by sulphate salts increases in weight fractions in the order: $NH_4^+ < Na^+ \approx Li^+$ and in molality scale in the order: $NH_4^+ < Li^+ < Na^+$, see Figure V.7.

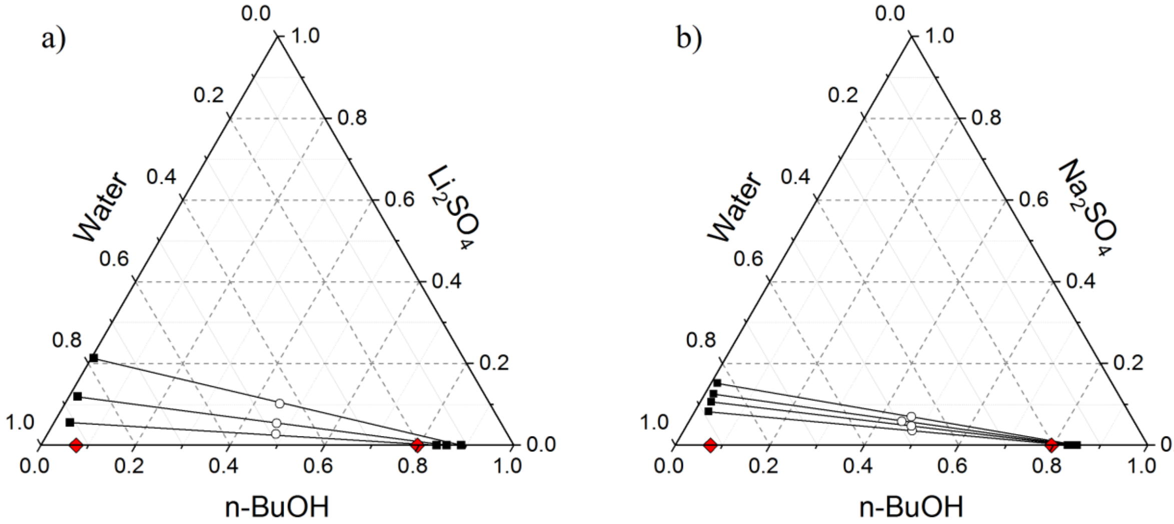

Figure V.6. LLE of ternary water/n-butanol/salt systems in weight fractions at 298.15 K and 1 bar: –a) salt = Li_2SO_4 and –b) salt = Na_2SO_4. (■) Experimental LLE data, (○) initial mixture compositions, (—) tie-lines and (◆) mutual solubility compositions of water and n-butanol.

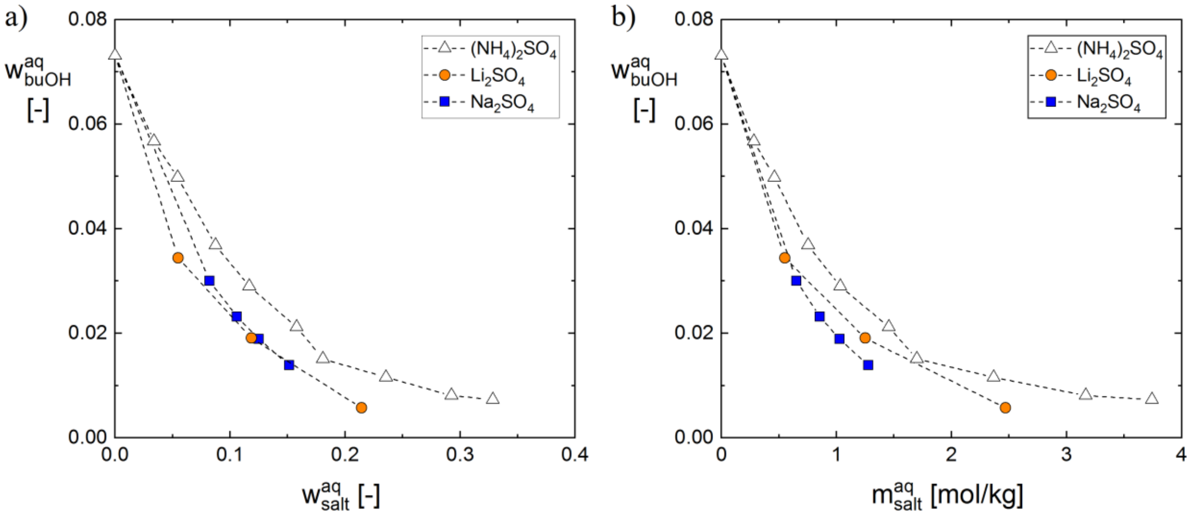

Figure V.7. Weight fractions of n-butanol in the aqueous phase of water/n-butanol/salt systems at 298.15 K and 1 bar vs. –a) salt weight fractions in the aqueous phase and –b) molality of salt in the aqueous phase close to the respective salt solubility limit. (△) $(NH_4)_2SO_4$ experimental data from literature[512]. (■) Na_2SO_4 and (●) Li_2SO_4 are experimental data from this work.

V.3.1.3 Nitrates

In Figure V.8, LLE data of the ternary systems water/n-butanol/salt (salt = $LiNO_3$, NH_4NO_3) are presented in ternary phase diagrams. In case of $LiNO_3$, the enlargement of the miscibility gap is less pronounced compared to chloride or sulphate salts. This feature is attributed to the relatively high solubility of $LiNO_3$ in the organic phase and the reduction of the n-butanol content in the organic phase, which is contrary to the other aqueous organic systems with added salt. This issue will be discussed in more details at the end of this section. Due to the higher water solubility of NH_4NO_3 compared to that of $LiNO_3$, a higher reduction of the mutual solubility of the two liquids is possible with NH_4NO_3. For NH_4NO_3, a slightly higher solubility of the salt in the organic phase could be detected compared to the chloride and sulphate salts. The salting-out efficiency on n-butanol from the aqueous phase mediated by nitrate salts increases in weight fractions and in molality scale in the order: $NH_4^+ < Li^+ < Na^+$, see Figure V.9. Although nitrate salts are often considered as to be salting-in, at such high salt concentrations even salting-in salts turn to salting-out behaviour[201].

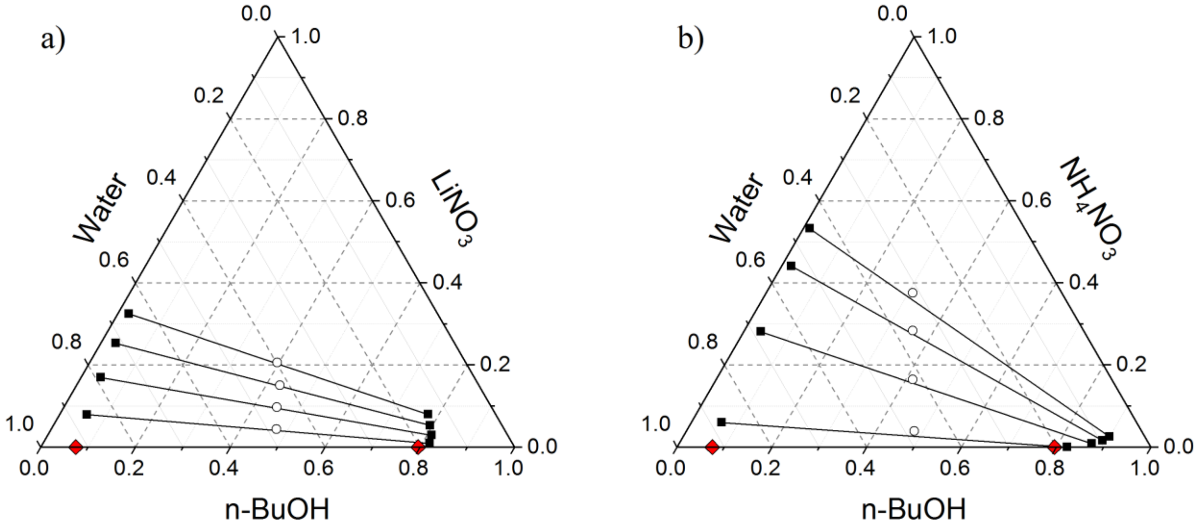

Figure V.8. LLE of ternary water/n-butanol/salt systems in weight fractions at 298.15 K and 1 bar: –a) salt = $LiNO_3$ and –b) salt = NH_4NO_3. (■) Experimental LLE data, (○) initial mixture compositions, (—) tie-lines and (◆) mutual solubility compositions of water and n-butanol.

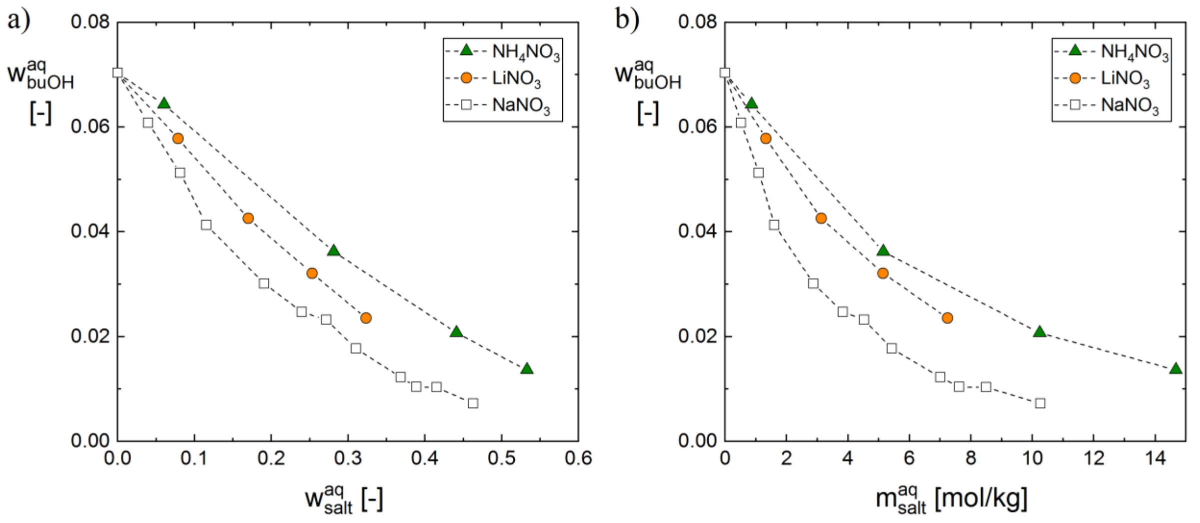

Figure V.9. Weight fractions of n-butanol in the aqueous phase of water/n-butanol/salt systems at 298.15 K and 1 bar vs. –a) salt weight fractions in the aqueous phase and –b) molality of salt in the aqueous phase close to the respective salt solubility limit. (□) $NaNO_3$ experimental data from literature[389], (●) $LiNO_3$ and (▲) NH_4NO_3 are experimental data from this work.

V.3.1.4 Acetates

In Figure V.10, LLE data of the ternary systems water/n-butanol/salt (salt = CH_3COOLi, CH_3COONa) are presented in ternary phase diagrams. For CH_3COOLi, a slightly higher solubility of the salt in the organic phase could be detected compared to CH_3COONa, chloride and sulphate salts. The salting-out efficiency on n-butanol from the aqueous phase mediated by acetate salts increases in weight fractions and in molality scale in the order: $Li^+ < Na^+$, see Figure V.11.

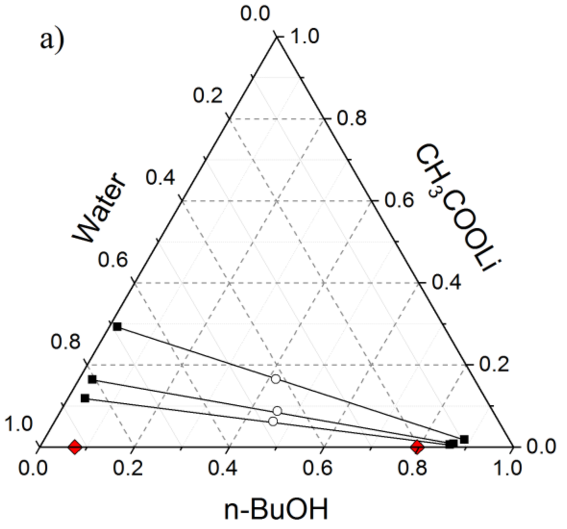

Figure V.10. LLE of ternary water/n-butanol/salt systems in weight fractions at 298.15 K and 1 bar: –a) salt = CH$_3$COOLi and –b) salt = CH$_3$COONa. (■) Experimental LLE data, (○) initial mixture compositions, (—) tie-lines and (◆) mutual solubility compositions of water and n-butanol.

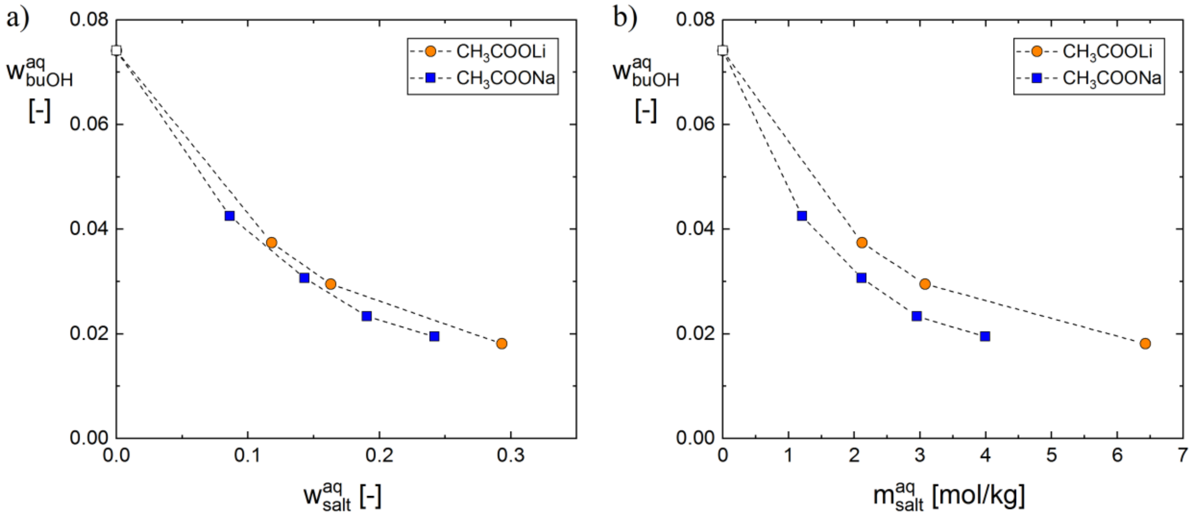

Figure V.11. Weight fractions of n-butanol in the aqueous phase of water/n-butanol/salt systems at 298.15 K and 1 bar vs. –a) salt weight fractions in the aqueous phase and –b) molality of salt in the aqueous phase close to the respective salt solubility limit. (■) CH$_3$COONa and (●) CH$_3$COOLi represent experimental data from this work.

V.3.1.5 Carboxylates

In Figure V.12, LLE data of the ternary systems water/n-butanol/salt (salt = C_2H_5COONa, C_3H_7COONa) are presented in ternary phase diagrams. For C_2H_5COONa, an increase of the miscibility gap between water and n-butanol can be detected up to a salt molality of 2 mol/kg in the feed. At m(salt) = 4 mol/kg, the mutual solubility of water and n-butanol is increased and the solubility of the carboxylate salt in the organic phase is increased as well. At higher C_2H_5COONa molality, the ternary mixture gets even monophasic. This feature is attributed to the ionic hydrotropic behaviour of C_2H_5COONa, which was already shown for the water/n-pentanol/C_2H_5COONa system[513]. Therefore, C_2H_5COONa is an example for a salting-out salt at low concentration, which turns to salting-in behaviour at higher concentration. The addition of C_3H_7COONa to the water/n-butanol system influences only marginally the miscibility gap. The striking difference of both systems is the different water solubility of the carboxylate salts. Whereas C_2H_5COONa is soluble in water up to 995 g/l[514] ≈ 10 mol/kg, the water solubility of C_3H_7COONa is limited to 100 g/l[515] ≈ 0.9 mol/kg and thus, the solubilising effect, which occurs usually at very high hydrotrope or co-solvent concentrations, is possible for C_2H_5COONa, but not for C_3H_7COONa. The salting-out efficiency on n-butanol from the aqueous phase mediated by sodium carboxylates (C_1 to C_3) increases in weight fractions and in molality scale in the order: C_3H_7COONa < C_2H_5COONa < CH_3COONa with the exception of C_2H_5COONa at m(salt) = 4 mol/kg. Here, C_2H_5COONa shows salting-in behaviour indicated by higher n-butanol weight fractions in the aqueous phase compared to the binary water/n-butanol system without salt, see Figure V.13. The same salting-out series for these carboxylate salts was reported for aromatic compounds[276].

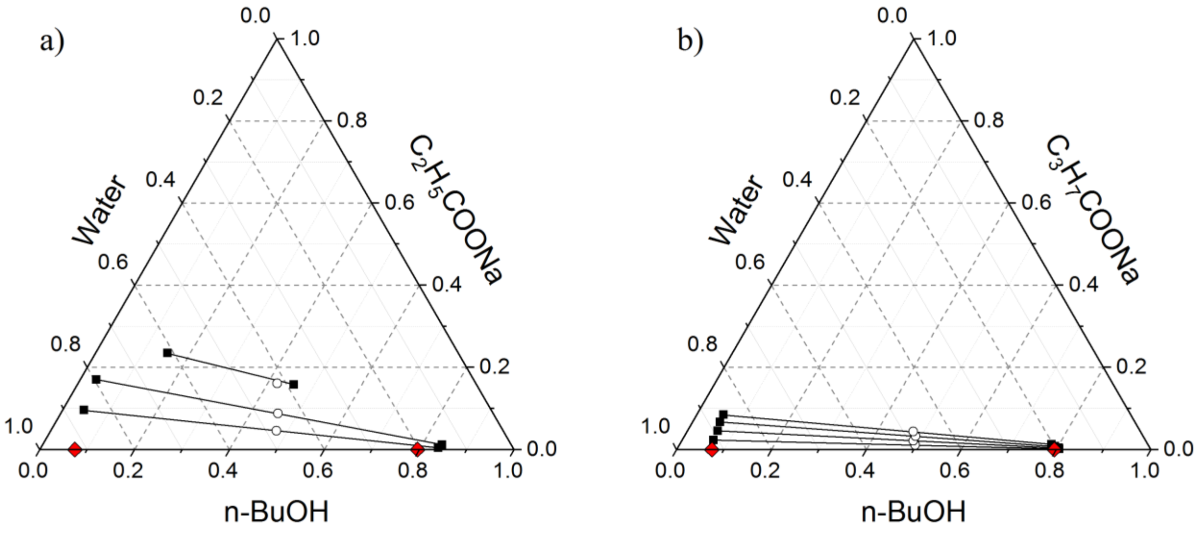

Figure V.12. LLE of ternary water/n-butanol/salt systems in weight fractions at 298.15 K and 1 bar: –a) salt = C_2H_5COOLi and –b) salt = C_3H_7COONa. (■) Experimental LLE data, (○) initial mixture compositions, (—) tie-lines and (◆) mutual solubility compositions of water and n-butanol.

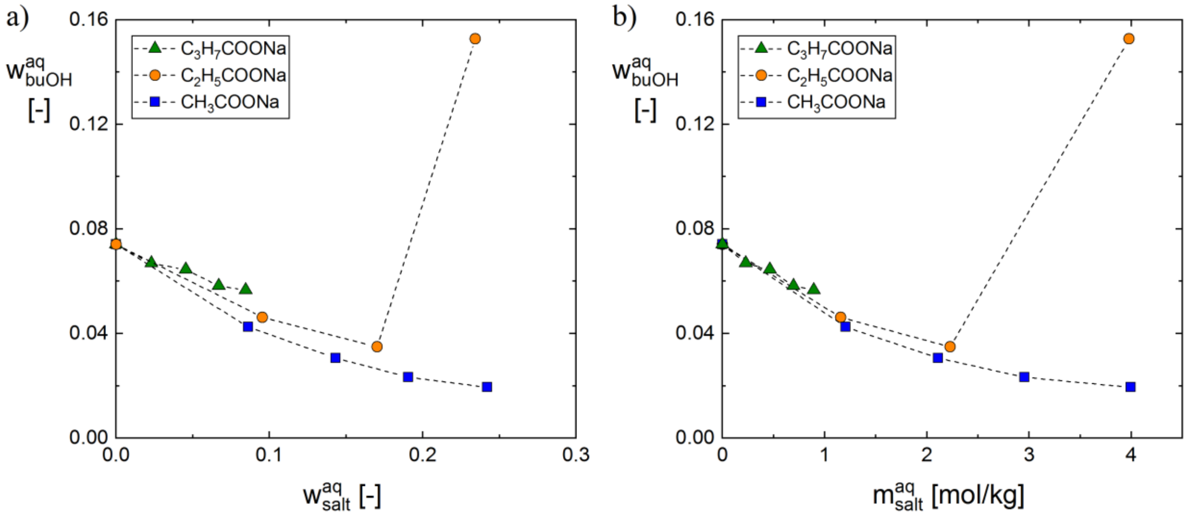

Figure V.13. Weight fractions of n-butanol in the aqueous phase of water/n-butanol/salt systems at 298.15 K and 1 bar vs. -a) salt weight fractions in the aqueous phase and -b) molality of salt in the aqueous phase close to the respective salt solubility limit. (■) CH_3COONa, (●) C_2H_5COONa and (▲) C_3H_7COONa represent experimental data from this work.

V.3.1.6 Discussion

Summarising the effect of cations on the water solubility of n-butanol, the strength of the salting-out effect for chloride, sulphate and nitrate salts in molality scale increases in the following order: $NH_4^+ < Li^+ < Na^+$. For chloride salts, K^+ has a similar effect to that of Na^+. For acetate salts, the sodium salt has a stronger salting-out effect on n-butanol than the lithium salt and data for ammonium and potassium acetate are missing or were not found. The salting-out effect of sodium carboxylates decreases with a higher number of carbon atoms. A change from salting-out to salting-in behaviour was detected for C_2H_5COONa at a feed salt molality of m(salt) = 4 mol/kg. If the effect of cations on the n-butanol solubility in water is compared to that of anions, it turns out that the influence of anions is more pronounced. For example, by comparison of the two lithium salts Li_2SO_4 and $LiNO_3$, the salting-out effect of the sulphate salt is very strong and that of the nitrate salt is rather weak. By comparison of the sulphate salts Na_2SO_4 and Li_2SO_4, similar effects are detected. Thus, anions are dominating the salt effects on the LLE of mixed aqueous organic solvent systems with added salt. The influence of the anions on the water solubility of n-butanol is focused on in the next section V.3.2.

For almost all investigated ternary water/n-butanol/salt systems in this work, the water and the n-butanol weight fractions in the aqueous phases decrease with increasing salt concentration. In the organic phases by contrast, the n-butanol weight fractions increase, while the water weight fractions decrease. This is the ‘usual’ effect of salt addition to a liquid-liquid water/organic solvent system. It can be explained qualitatively by the hydration theory[181]. That is, each salt ion binds a constant number of water molecules by the formation of hydration shells (orientated water dipoles around the ions). Consequently, less water molecules are available for the solvation of the non-electrolyte, resulting in a decrease of the organic solvent solubility in water (salting-out effect). Concerning the organic phase, the water solubility decreases, because water molecules preferably interact with the ions (formation of hydration shells) and the hydrated ions cannot be easily solvated by the organic solvent. In a water-free organic solvent, the salts like NaCl or KCl bear extremely low solubility (< 0.01 wt%).

In the exceptional case of $LiNO_3$, the n-butanol weight fractions decrease in the organic phases, which is probably due to a relatively high solubility of $LiNO_3$ in the n-butanol-rich phase (7.98 wt%). The solubility of $LiNO_3$ in pure n-butanol is 2.162 mol/kg (~ 12.97 wt%)[516].

Such high salt solubilities in n-butanol-rich phases were also found for LiCl by Al-Sahhaf et al.[496] in the water/n-butanol (11.76 wt%) system and by Gomis et al. in the water/2-butanol (10.7 wt%), the water/2-methyl-1-propanol (9.91 wt%)[506] and the water/*tert*-butanol (11.3 wt%)[517] systems. The solubility of LiCl in pure n-butanol is 3.023 mol/kg (~ 11.36 wt%)[496].

At low LiCl concentration in water/butanol systems, the usual salting-out effect retains, as water is in excess and the ions are completely solvated by water. Concurrently, the butanol concentration in the organic phase increases with increasing LiCl concentration. At a certain LiCl concentration in the aqueous phase (18.24 wt% for n-butanol; ~ 22 wt% for 2-butanol and 2-methyl-1-propanol; ~ 18.5 wt% for *tert*-butanol), a maximum of the butanol concentration is detected in the organic phase. Upon further salt addition, the butanol content decreases and the salt content sharply increases, while the water content remains rather constant in the organic layer. Thus, a threshold from 'usual' to 'unusual' behaviour can be observed upon a certain LiCl concentration, when both, butanol and water, start to be involved in the solvation process of the ions in the organic phase. For *tert*-butanol, this threshold is rather in a concentration range (18.5 – 21.7 wt%) than at a certain LiCl concentration, as the maximum of butanol and the minimum of the water content in the organic phase are not at the same LiCl concentration in the aqueous phase. Unusual S-shaped binodal curves were also observed for LiCl in water/pentanol systems[511].

The unusual behaviour is explained by the small size of the Li^+ (69 pm) cation compared to that of the Na^+ (102 pm) and K^+ (138 pm) cations. The higher charge density on Li^+ cations can even induce ion dipole forces between Li^+ and butanol molecules, which can lead to ion solvation in the organic phase. Consequently, the solubilities of LiCl in the organic layer of the water/butanol systems are higher (≥ 10 wt%) and the unusual S-shaped solubility curve in the organic branch results.

Probably, similar solvation effects hold true for $LiNO_3$ in the organic phase. Although, 'unusual' behaviour is also seen for the $LiNO_3$ system in terms of decreasing n-butanol content in the organic phase, the water content decreases as well, which is different to the LiCl system, where the water content remains rather constant in the salt concentration regimes of unusual behaviour. Thus, no threshold concentration for $LiNO_3$ can be detected within the measured concentration range in the organic phase.

In Figure V.14, the *Setchenov* plots for the aqueous and the organic phases for the water/n-butanol/LiCl and the water/n-butanol/$LiNO_3$ systems are displayed. Due to the comparison of different salts, the salt mole fractions were used as abscissa. The salting-out effect in the aqueous phases follow the usual linear trend for both salts. By contrast, the curve of LiCl for the organic phase initially increases sharply, until a maximum is reached at the threshold salt concentration x^{aq}(LiCl) = 0.0879 (5.373 mol/kg; 18.24 wt%). Upon higher salt concentration, the curve decreases and at very high salt concentrations, the curve slightly increases again, representing the salt concentration regime exhibiting unusual behaviour. In case of $LiNO_3$, the salting-out curve in the organic phase increases monotonically until the solubility limit of the salt in water. The increase is not linear, which is due to the high solubility of $LiNO_3$ in the organic phase. This course is different to the usual behaviour observed e.g. for the water/n-butanol systems with NaCl or KCl, see Figure V.4 and Figure V.5. The nitrate ions, which are larger, more polarisable and considered to be more salting-in, compared to chloride ions, see Figure II.3, may also be a reason for the high solubility of $LiNO_3$ in the organic phase.

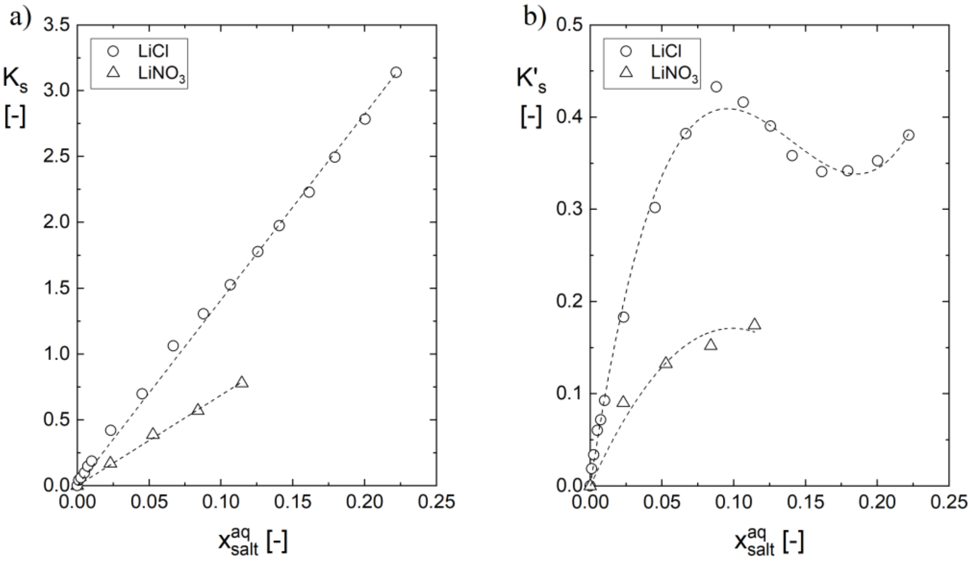

Figure V.14. *Setchenov* correlation of LLE data from the system water/n-butanol/salt. –a) the aqueous phase (K_s) and –b) the organic phase (K'_s). (○) data from literature for LiCl[496]. (△) data from this work for the water/n-butanol/$LiNO_3$ system of this work.

Considering the high solubility of LiCl in pure butanol (11.36 wt%), the presence of water is not necessary for the solvation of LiCl (to this extent) in the organic solvent. The solubility of LiCl in pure water is 44.89 wt% (19.21 mol/kg). Despite its high solubility in water, LiCl enters the organic phase increasingly upon the threshold concentration of 18.24 wt% (m = 5.373 mol/kg) in the aqueous phase[496]. Keeping in mind that 1 kg of water include 55.51 moles of water molecules, hydration numbers Z_{ib} = 8-12 are associated to the Li^+ cations by means of a second hydration shell[518,519] and assuming Z_{ib} (Cl^{-}) = 0 [520], the amount of free water molecules in aqueous LiCl (m = 5 mol/kg) solution tends to zero. Although, the above rough estimation indicates that no more free water molecules are present in aqueous LiCl solution at that high concentrations, even higher salt concentrations are possible in water. Thus, with increasing salt concentration, cations and anions are forced to closer proximity and a transition from water-electrolyte to electrolyte-water solvent may occur[521]. The resulting altered solvent structure resembles to molten salts and ionic liquids. The solvation of LiCl affected by both water and n-butanol must be energetically favoured compared to the solvation of LiCl by water alone at these high LiCl concentrations. In this context, the applicability of LLEx for the recovery of LiCl from aqueous electrolyte solutions with n-butanol as extracting solvent was already demonstrated[522].

V.3.2 Influence of Anions on the n-Butanol Solubility in Water

To evaluate the anion influence on the salting-out effect on n-butanol from the aqueous phase, binary diagrams were constructed, in which n-butanol weight fractions in the aqueous phase are drawn against the salt weight fractions and the salt molalities in the aqueous phase, see Figure V.15 to Figure V.18 a) and b). The comparison includes different lithium, sodium, potassium and ammonium salts. The molality scale of salt concentration is more appropriate to compare the efficiency of the individual anions, because mass effects do not appear. In contrast, for practical large-scale applications, the weight fraction-based salt efficiency becomes more important.

The evaluation of the salting-out effects on n-butanol from the aqueous phase is based on LLE data from this work and from those found in the literature. For the numerical comparison of the salting-out effects of the different salts, a modified *Setchenov* correlation was applied on mole fraction scale according to Eq. (V-2) and (V-3). The correlations are pictured in Figure V.15 to Figure V.18 c) and d). Calculated *Setchenov* constants K_s and K'_s for aqueous and organic phases, respectively, are listed in Table V-2.

Non-linear relationship was found for CH_3COOLi, CH_3COONa, C_2H_5COONa and $(NH_4)_2SO_4$ in the aqueous phases and for LiCl, $LiNO_3$, CH_3COOLi, C_2H_5COONa, C_3H_7COONa and $(NH_4)_2SO_4$ in the organic phases. For LiCl and $LiNO_3$, the given K'_s values correspond to salt concentration regimes, in which linearity is still provided ($R^2 > 0.9$). For C_2H_5COONa, only the tie-lines showing salting-out behaviour were considered for the aqueous and organic phase correlations. Linear correlation of C_3H_7COONa and $(NH_4)_2SO_4$ in the organic phases was not satisfactory. To all the other non-linear relationships, linear regression was applied with respect to all salt concentrations leading to correlation coefficients $R^2 > 0.9$. Resulting *Setchenov* constants are given in Table V-2 and can be compared to other systems showing linear relationship.

For lithium salts (Figure V.15), the strength of the salting-out effect of anions on n-butanol from the aqueous phase increases in the order: $NO_3^- < CH_3COO^- < Cl^- < SO_4^{2-}$ for both salt concentration scales.

For sodium salts (Figure V.16), the same strength of the salting-out effect of anions is detected as for the lithium salts. Here, the Br^- anion and the carboxylates $C_2H_5COO^-$ and $C_3H_7COO^-$ are additionally introduced, resulting in the following series:

$C_3H_7COO^- < C_2H_5COO^- < NO_3^- < Br^- < CH_3COO^- < Cl^- < SO_4^{2-}$ in weight fractions and in molality scale, the series is: $C_3H_7COO^- < NO_3^- < C_2H_5COO^- < CH_3COO^- < Cl^- \leq Br^- < SO_4^{2-}$ with the most salting-out anion on the right. The K_s value for C_3H_7COONa is higher than that of $NaNO_3$ on mole fraction basis. The trend of the obtained K_s values for sodium salts for the salting-out of n-butanol from water matches perfectly with that reported for the salting-out of benzene from water[276], with the only exception of NaBr.

For potassium salts (Figure V.17), the strength of the salting-out effect of anions increases in the order: $I^- < Br^- < Cl^-$ in weight fractions and in molality scale in the order: $I^- < Cl^- \leq Br^-$. The K_s value for KCl is slightly higher than that of KBr on mole fraction basis.

For ammonium salts (Figure V.18), the salting-out series for anions is in the same order as for lithium and sodium salts: $NO_3^- < Cl^- < SO_4^{2-}$ for both salt concentration scales.

Besides the correlation with the modified *Setchenov* equation, the anion effect was evaluated by means of the evolution of the tie-line length (TLL), depending on the salt mole fractions in the aqueous phases. The TLLs were calculated for each measured system as well as of the systems found in the literature according to Eq. (II-10). For a better comparison, the change of the TLLs in the ternary water/n-butanol/salt systems compared to the TLL in the binary water/n-butanol system (binary data from Marcilla et al.[168]) were plotted in Figure V.19. Only the tie-lines showing salting-out behaviour were considered (rejection of C_2H_5COONa at high concentration). In each case, salt addition leads to extended tie-lines, which was already stated and observed in the ternary diagrams. In general, the same trends of the salting-out effects noticed for the *Setchenov* correlation can be observed for the evolution of the TLLs.

V.3.2.1 Lithium Salts

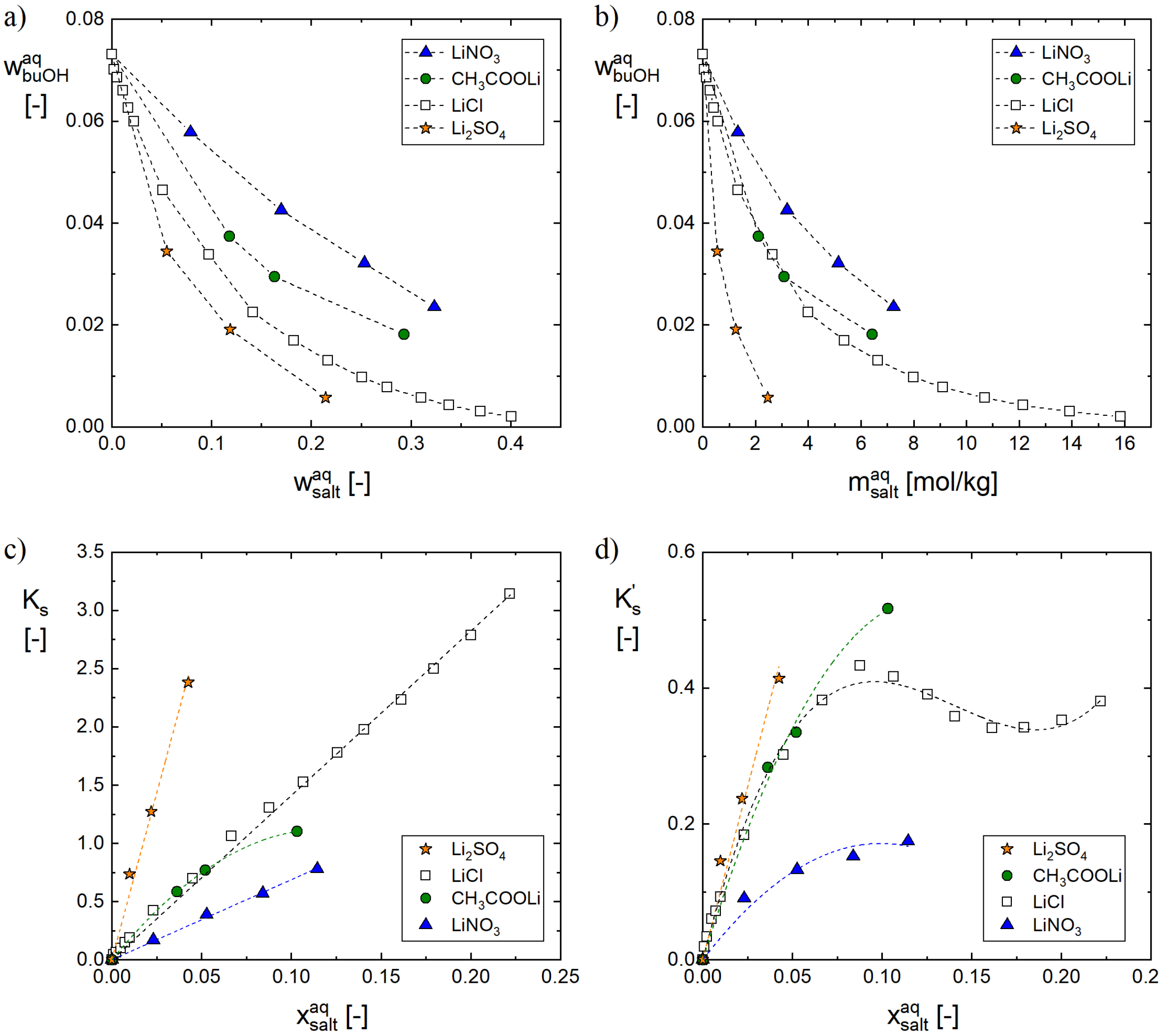

Figure V.15. Comparison of the salting-out effect of different lithium salts on n-butanol from the aqueous phase at 298.15 K and 1 bar. Weight fractions of n-butanol in the aqueous phase of water/n-butanol/salt systems vs. –a) salt weight fractions in the aqueous phase and –b) molality of salt in the aqueous phase close to the respective salt solubility limit. *Setchenov* correlation of LLE data from water/n-butanol/lithium salt systems of –c) the aqueous phase (K_s) and –d) the organic phase (K'_s). (□) LiCl experimental data from literature[496]. (★) Li_2SO_4, (●) CH_3COOLi, (▲) $LiNO_3$ experimental data from this work. The legend is arranged from highest to lowest *Setchenov* coefficients K_s and K'_s.

V.3.2.2 Sodium Salts

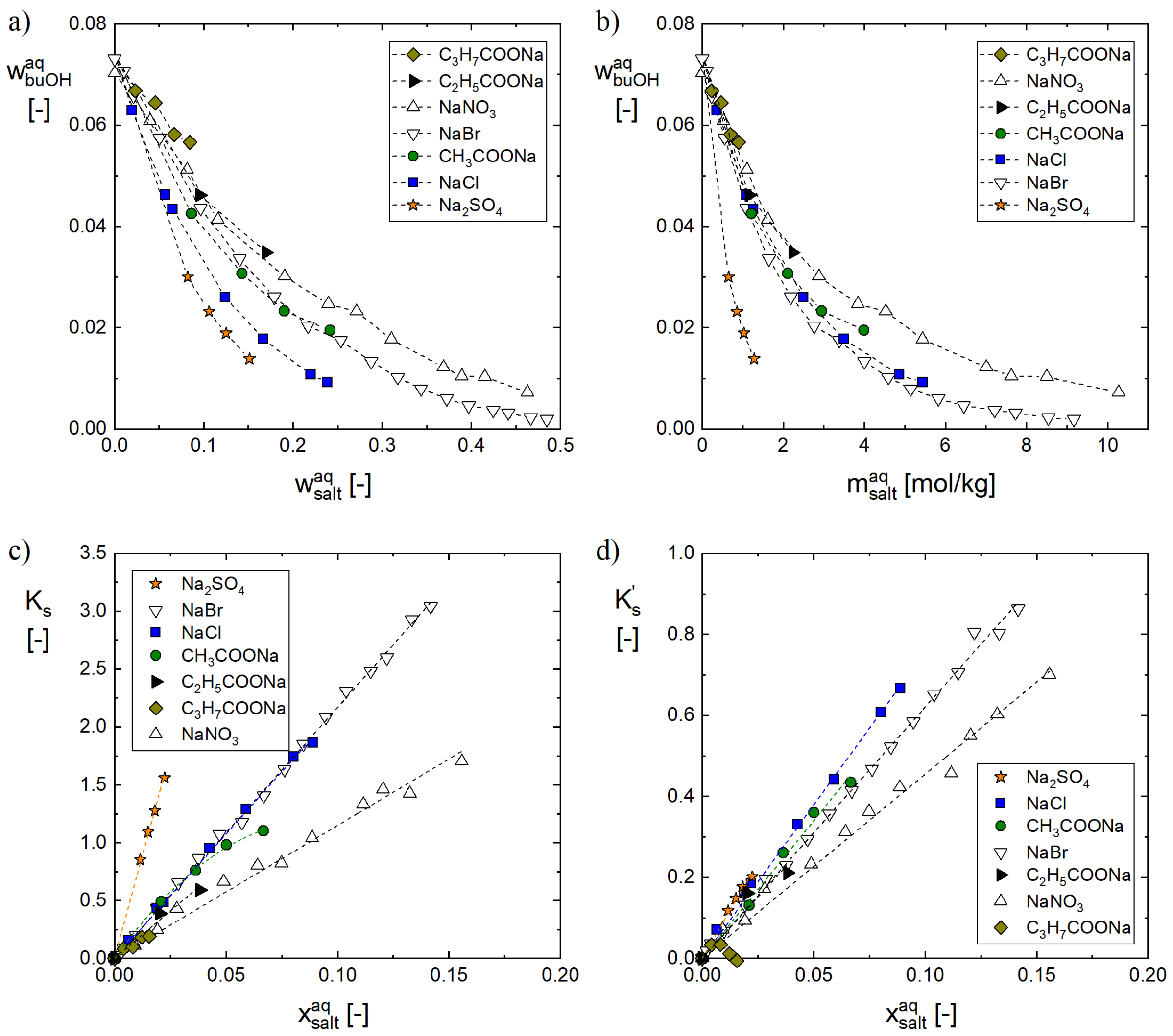

Figure V.16. Comparison of the salting-out effect of different sodium salts on n-butanol from the aqueous phase at 298.15 K and 1 bar. Weight fractions of n-butanol in the aqueous phase of water/n-butanol/salt systems vs. –a) salt weight fractions in the aqueous phase and –b) molality of salt in the aqueous phase close to the respective salt solubility limit. *Setchenov* correlation of LLE data from water/n-butanol/sodium salt systems of –c) the aqueous phase (K_s) and –d) the organic phase (K'_s). (▽) NaBr and (△) $NaNO_3$ represent experimental data from literature[389,496]. (☆) Na_2SO_4, (■) NaCl, (●) CH_3COONa, (▶) C_2H_5COONa) and (◆) C_3H_7COONa are experimental data from this work. The legend is arranged from highest to lowest *Setchenov* coefficients K_s and K'_s.

V.3.2.3 Potassium Salts

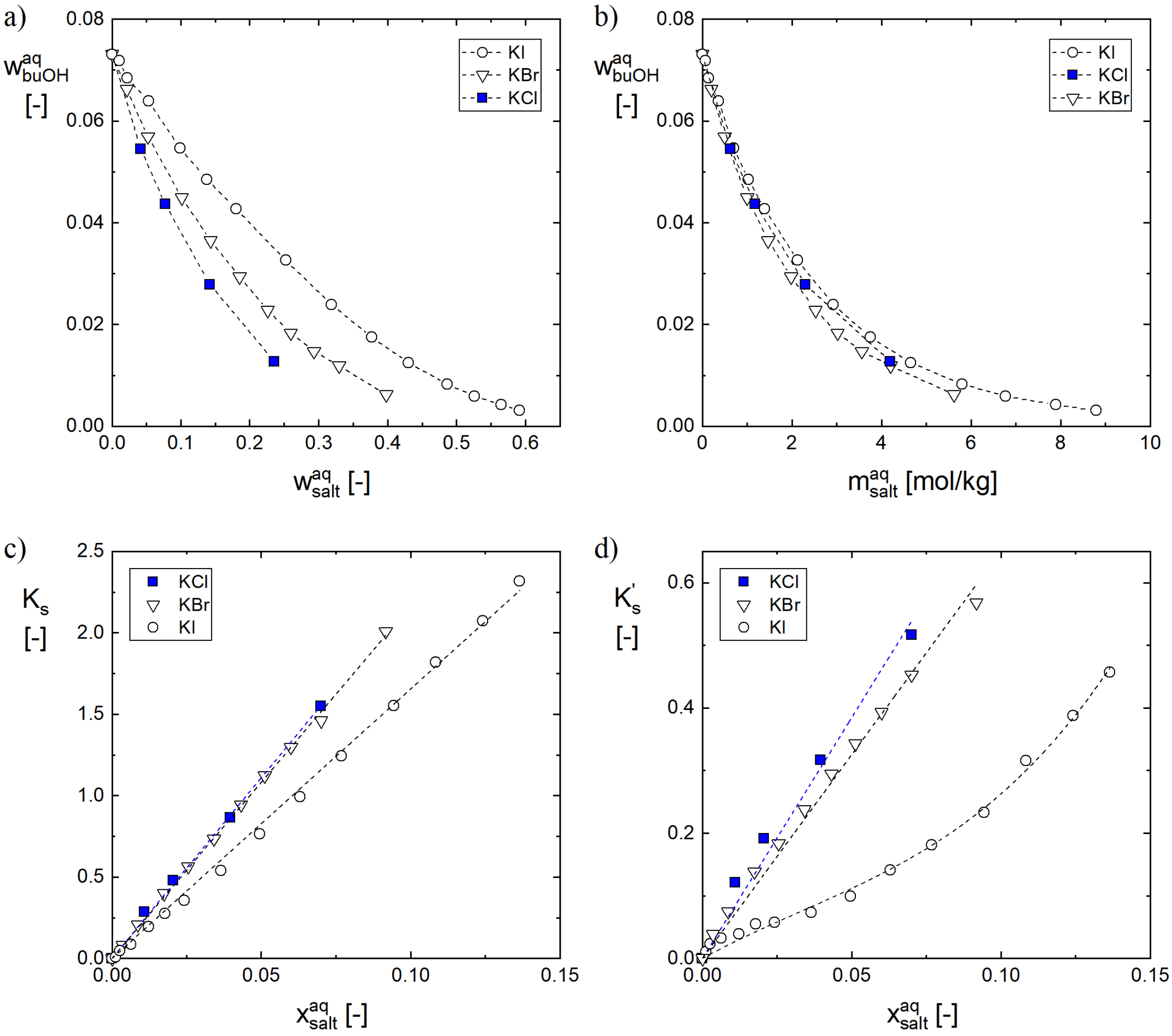

Figure V.17. Comparison of the salting-out effect of different potassium salts on n-butanol from the aqueous phase at 298.15 K and 1 bar. Weight fractions of n-butanol in the aqueous phase of water/n-butanol/salt systems vs. –a) salt weight fractions in the aqueous phase and –b) molality of salt in the aqueous phase close to the respective salt solubility limit. *Setchenov* correlation of LLE data from water/n-butanol/potassium salt systems. –c) the aqueous phase (K_s) and –d) the organic phase (K'_s). (▽) KBr and (○) KI represent experimental data from literature[496]. (■) KCl experimental data from this work. The legend is arranged from highest to lowest *Setchenov* coefficients K_s and K'_s.

V.3.2.4 Ammonium Salts

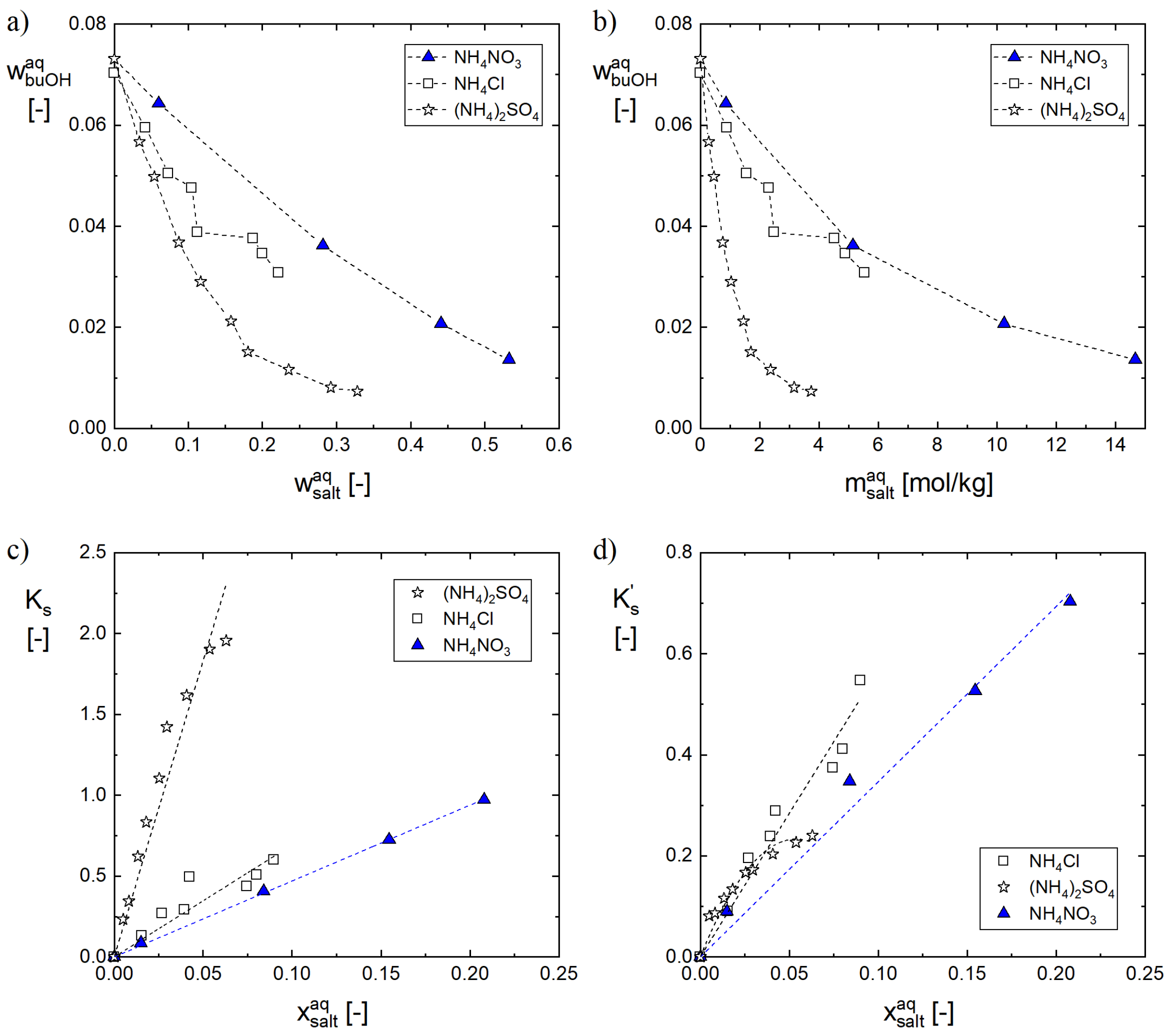

Figure V.18. Comparison of the salting-out effect of different ammonium salts on n-butanol from the aqueous phase at 298.15 K and 1 bar. Weight fractions of n-butanol in the aqueous phase of water/n-butanol/salt systems vs. –a) salt weight fractions in the aqueous phase and –b) molality of salt in the aqueous phase close to the respective salt solubility limit. *Setchenov* correlation of LLE data from water/n-butanol/ammonium salt systems. –c) the aqueous phase (K_s) and –d) the organic phase (K'_s). (☆) $(NH_4)_2SO_4$ and (□) NH_4Cl represent experimental data from literature[391,512]. (▲) NH_4NO_3 experimental data from this work. The legend is arranged from highest to lowest *Setchenov* coefficients K_s and K'_s.

Table V-2. Calculated *Setchenov* constants K_s, K'_s and correlation coefficients in brackets on mole fraction scale for ternary LLE data of water/n-butanol/salt systems. Tabulated systems were investigated in this work and selected from literature. Bold numbers are maximum values for K_s or K'_s. Italic numbers are correlation constants of doubted LLE data for NaCl and KCl from literature.

Salts	Reference	K_s	K'_s
LiCl	[496]	14.12 (0.9977)	7.137 (0.9645) non-linear
$LiNO_3$	this work	6.879 (0.9978)	2.737 (0.9050) non-linear
Li_2SO_4	this work	57.17 (0.9885)	**10.16** (0.9700)
CH_3COOLi	this work	11.92 (0.9053) non-linear	5.214 (0.9143) non-linear
NaCl	[150,168,493,494] and this work	22.39 (0.9994), 22.49 (0.9910), 22.01 (0.9983), 20.75 (0.9972), 21.48 (0.9987)	8.226 (0.9577), *3.181 (0.7432)*, 8.850 (0.9938), 8.934 (0.9912), 7.571 (0.9967)
NaBr	[496]	21.69 (0.9987)	6.205 (0.9973)
$NaNO_3$	[389]	11.49 (0.9850)	4.547 (0.9876)
Na_2SO_4	this work	**70.74** (0.9983)	9.489 (0.9900)
CH_3COONa	this work	18.36 (0.9507) non-linear	6.788 (0.9914)
C_2H_5COONa	this work	16.34 (0.9741) non-linear	6.0546 (0.9207) non-linear
C_3H_7COONa	this work	13.34 (0.9301)	non-linear
KCl	[494,495] and this work	20.69 (0.9954), *36.89 (0.9606)*, 22.18 (0.9984)	7.910 (0.9620), 7.032 (0.9798), 7.689 (0.9801)
KBr	[494,496]	21.63 (0.9987)	6.506 (0.9913)
KI	[496]	16.55 (0.9980)	2.883 (0.9552) non-linear
NH_4Cl	[391]	6.927 (0.8045)	5.675 (0.9547)
NH_4NO_3	this work	4.693 (0.9995)	3.467 (0.9855)
$(NH_4)_2SO_4$	[512]	36.54 (0.9243) non-linear	non-linear

Linearity of the *Setchenov* plots suggests additivity of salt effects up to high salt concentrations.

V.3.2.5 Tie-Line Length (TLL)

Similar to the *Setchenov* correlation, the salting-out effects in the ternary water/n-butanol/salt systems can be represented by the evolution of TLLs. In each case, salt addition leads to extended tie-lines. It appears that the curves for the lithium salts are very similar to those obtained by the *Setchenov* plots in the corresponding organic phases. For sodium, potassium and ammonium salts, the increase of the TLLs shows almost the same trends as for *Setchenov* plots in the corresponding aqueous phases.

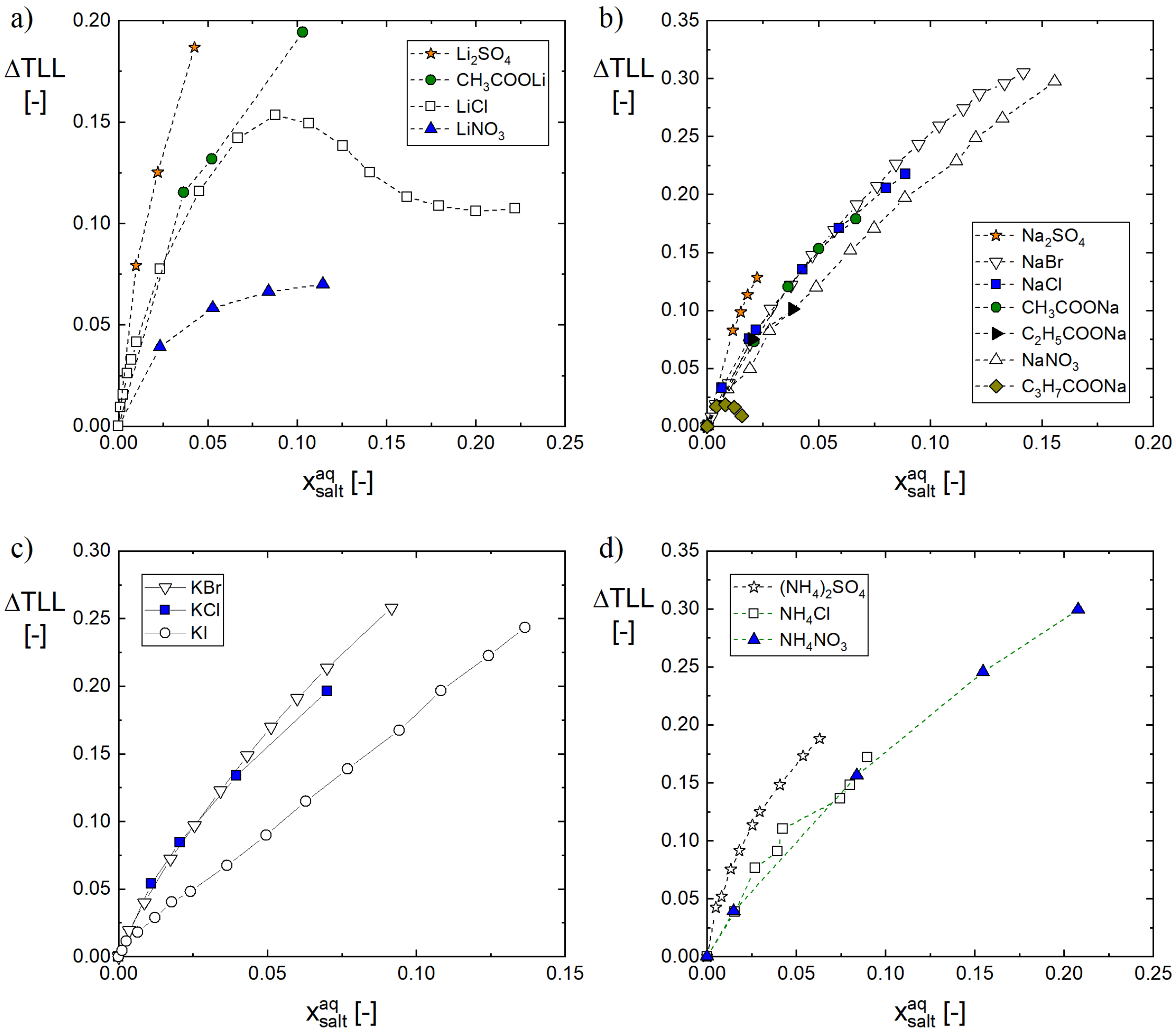

Figure V.19. The increase of the TLLs in ternary water/n-butanol/salt systems depending on the salt mole fractions in the aqueous phases: –a) Lithium salts. -b) Sodium salts. -c) Potassium salts. -d) Ammonium salts.

V.3.3 Ternary LLE without Salt

LLE data of the ternary system composed of water, n-butanol and solute (HMF or glycerol) were determined at 298.15 K and 1 bar. The ternary phase diagrams with the corresponding tie-lines are illustrated in Figure V.20 a) and Figure V.22 a) for HMF and glycerol as product molecule, respectively. Related D^{w}*(solute)* values depending on the solute molality are presented in Figure V.20 b) and Figure V.22 b), respectively. Mass balances were fulfilled, and the tie-lines pass through the initial mixture compositions. The experimentally determined LLE data, tie-line lengths (TLLs), tie-line slopes (TLSs) and initial mixture compositions are given in Table B-2 and Table B-12 for HMF systems and in Table B-3 and Table B-13 for glycerol systems, respectively. D^{w}*(solute)* values and α^{w}*(solute, water)* values are given in Table B-6 for both systems.

D^{w}*(HMF)* values calculated from experimental LLE data from literature[502] were also pictured in Figure V.20 b). Besides experimental data, modelling results from ePC-SAFT and predictions from COSMO-RS are included in Figure V.20. A graphical projection of the ternary LLE data to the distribution curve of HMF is shown in Figure V.21.

V.3.3.1 Water/n-Butanol/HMF

For a clear display of the ternary water/n-butanol/HMF system, the initial compositions were not depicted in Figure V.20 a). The critical point was found at the composition of w(n-butanol) = 0.26, w(HMF) = 0.19, w(water) = 0.55. By applying a non-linear curve fit, the binodal curve was reasonably approximated. It can be noted that the miscibility gap (between water and n-butanol) disappears at 298.15 K, 1 bar and an HMF concentration of approximately 20 wt%. (This feature of HMF is generally related to co-solvent or hydrotropic characteristics, as the mutual solubility of water and n-butanol increases by the addition of the HMF). Therefore, the extraction system water/n-butanol/HMF exhibits a relatively small biphasic region for the LLEx application. However, the slopes of the tie-lines are in favour of HMF-extraction into the organic n-butanol-rich phase. Although the tie-line slopes increase, D^{w}*(HMF)* values decrease with increasing HMF content, see Figure V.20 b). This decrease is attributed to the relatively small biphasic region and the course of the binodal curve, which results in reduced TTLs with increasing HMF content. The relatively large amount of water in the organic phase may increase the affinity of HMF towards the organic phase. $D^{w}(HMF)$ values obtained from Dalmolin et al.[502] are higher compared to those determined in this work. Reasons for differences may be the different experimental approaches. While in this work the LLE data was determined by the analytical method, Dalmolin et al. measured densities and refractive indices of mixtures in combination with the cloud point method for the binodal curve determination. Here, it should be mentioned that own data for n-butanol are preferred. Three independent experimental trials of ternary water/n-butanol/HMF LLE determination in this work lead all to comparable $D^{w}(HMF)$ values.

The LLE of the ternary system water/HMF/n-butanol of this work was reasonably reproduced by COSMO-RS calculations using the COSMO*therm*X 17 program and the COSMObase-1701. It is important to note that renormalisation of LLE (correction factor) was required to obtain good results. Otherwise, the predicted miscibility gap was too big due to the overestimation of the binodal curve. This was especially pronounced for the organic branch in the ternary phase diagram. The modelling result with ePC-SAFT shows a good agreement with the experimental results with an absolute average deviation (AAD) of only 0.0331. At HMF weight fractions higher than 0.15, the miscibility gap is slightly overestimated by ePC-SAFT. More details about the ePC-SAFT modelling including the used parameters are described in section II.5.3.4.

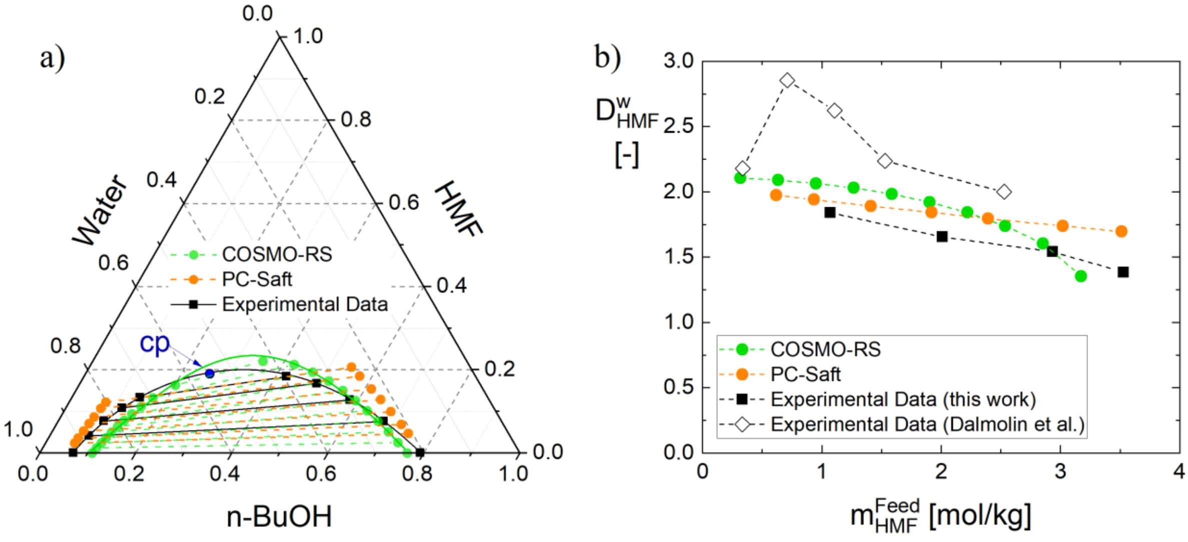

Figure V.20. LLE of water/n-butanol/HMF in weight fractions at 298.15 K and 1 bar: –a) (■) experimental LLE data from this work, (●) critical point (cp), (●) and (●) are LLE results from COSMO-RS and PC-SAFT, respectively. –b) Corresponding $D^{w}(HMF)$ values depending on the HMF feed molality and (◇) experimental $D^{w}(HMF)$ values from Dalmolin et al.[502].

The simplest distribution curve is the plot of the HMF weight fractions in the organic phase against the HMF weight fractions in the aqueous phase in equilibrium. The resulting curve in Figure V.21 lies above the 45° line, because HMF is favourably distributed in the organic phase, but the curve will necessarily terminate at the critical point. Such a distribution curve can be used to estimate further tie-lines for LLEx application and resembles to the McCabe-Thiele diagram for analysis of binary distillations.

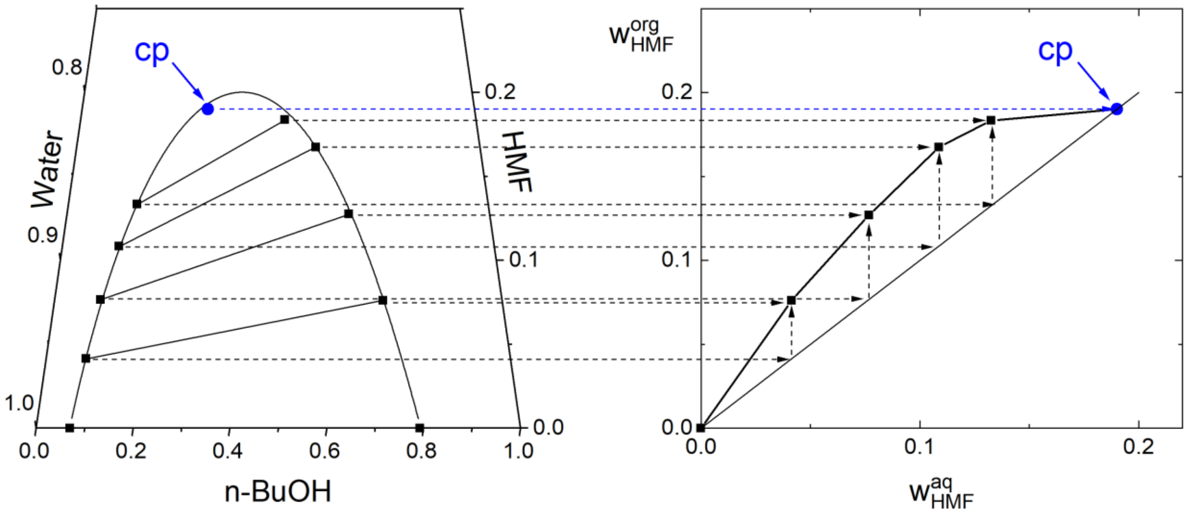

Figure V.21. Graphical projection of the ternary LLE data (■) to the distribution curve of HMF including the critical point (cp) (●).

V.3.3.2 Water/n-Butanol/Glycerol

The water/n-butanol/glycerol system is a ternary mixture of *Class I,* i.e. only one binary pair of components (water, n-butanol) exhibit a closed miscibility gap. Ternary phase diagrams of this system including the tie-lines and the binodal curve were already published by Patel[133] and Matsumoto and Sone[523]. Unfortunately, no data tables could be found to extract the LLE. In this work, the ternary mixtures remain biphasic within the investigated glycerol concentration range. Following the slopes of the tie-lines, glycerol is favourably dissolved in the aqueous phase and therefore, n-butanol is not an appropriate solvent for the separation of glycerol from the aqueous phase. With increasing glycerol feed concentration, the TLL, the absolute value of the TLS, $D^{w}(glycerol)$ and $\alpha^{w}(glycerol, water)$ values are increasing. Nevertheless, $D^{w}(glycerol)$ values remain far below unity and the increase of $\alpha^{w}(glycerol, water)$ from 0.7 to 0.75 is only very small. By contrast, in the studies of Patel[133], decreasing α^{w}*(glycerol, water)* values from 1.8 to 1.1 are reported with increasing glycerol concentration. However, in each case, glycerol is preferably distributed in the aqueous phase, which is probably due to the high polarity of glycerol and the more pronounced hydrogen-bonding interactions in water than in n-butanol.

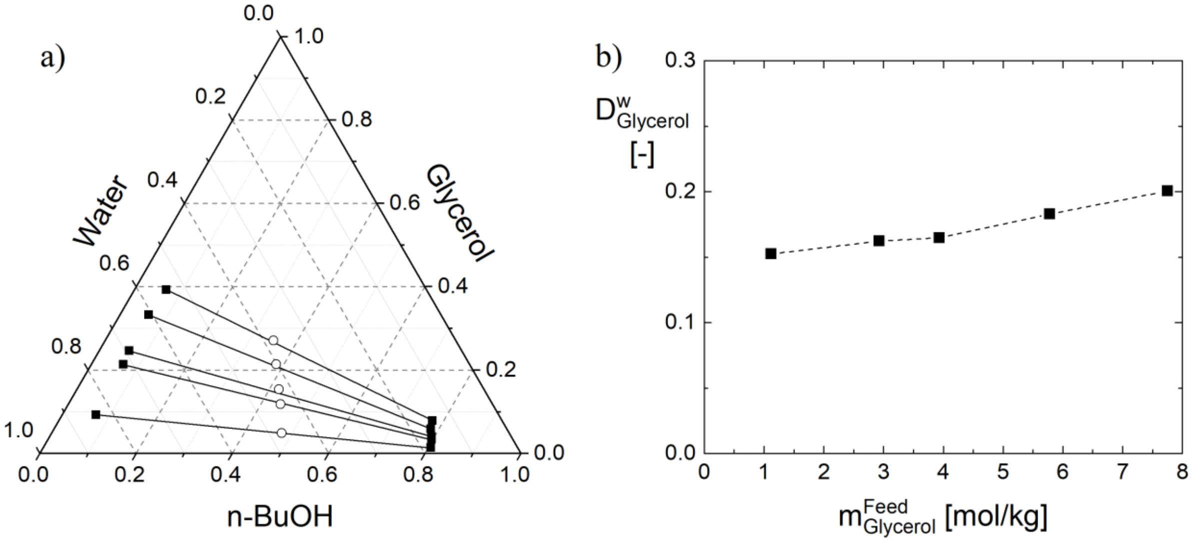

Figure V.22. LLE of the ternary system water/n-butanol/glycerol at 298.15 K and 1 bar. –a) Ternary phase diagram of the system water/n-butanol/glycerol presented in weight fractions. (■) Experimental LLE data, (○) initial mixture compositions and (—) tie-lines. –b) Corresponding D^{w}*(Glycerol)* values depending on the glycerol feed molality.

V.3.4 Quaternary LLE with HMF as Product

The LLE data of the quaternary systems composed of water, n-butanol, HMF and salt were determined at 298.15 K and 1 bar following the procedure described in section II.4.5. The investigated mixtures included one of the different salts: LiCl, NaCl, KCl, Na_2SO_4, Li_2SO_4, $Al_2(SO_4)_3$, NH_4NO_3, CH_3COONa and C_2H_5COONa. For the salts C_3H_7COONa and pentasodium phytate ($(Phy^{5-}, 5Na^+)$) only *D*^{w}*(HMF)* values were measured without determination of the complete LLE. (Phy^{5-}, $5Na^+$) showed the most pronounced salting-out effect within the water/DPnP system (Figure IV.7), which is why it was also tested for *D*^{w}*(HMF)*. In the same way, additional *D*^{w}*(HMF) values* were collected (for LiCl, NaCl, $Al_2(SO_4)_3$ and CH_3COONa) to extend the concentration range for the investigation of the salt influence on *D*^{w}*(HMF)*. Such data points are indicated by open symbols in the corresponding figures. The salt influence on quaternary LLEs was examined at constant salt molality with varying HMF molality and at constant HMF molality with varying salt molality. Overviews of the investigated systems in both concentration screens are presented in Table V-3 and Table V-4 for HMF as product.

The presentation of quaternary LLE data in pseudo-ternary diagrams by grouping salt and water in a single component is not recommended, because tie-lines, which go through initial mixtures with e.g. constant salt to water ratio, lie not in the plane of the ternary illustration nor parallel to it. In addition, and even more striking, LLE results of quaternary systems including salts with relatively high solubility in the organic phase would be wrongly interpreted, because distribution of the salt between the aqueous and organic phases is different for different salts[168]. In this context, tetrahedral diagrams are recommended, but drawbacks appear concerning the readability of the data points and the scaled axis in the diagram. Thus, results of all experimental determined LLE data of quaternary systems are presented in pseudo-ternary phase diagrams *via* normalisation of the LLE data with regard to the compound (salt or HMF), which was held constant. Pseudo-ternary phase diagrams for chlorides (Cl^-), sulphates (SO_4^{2-}), nitrates (NO_3^-) and carboxylates ($RCOO^-$) were constructed for both concentration screens. The salts are predominantly dissolved in the aqueous phases and tie-lines pass through the initial mixture compositions. The LLE data and initial mixture compositions are given in Table B-4 and Table B-14. *D*^{w}*(HMF)*, *α*^{w}*(HMF, water)* values, TLLs and TLSs for systems at constant HMF and constant salt concentration are given in Table B-7 and Table B-8, respectively. Here, it has to be mentioned that TLLs and TLSs in quaternary systems were calculated based on normalised LLE data to be consistent with the pictured ternary phase diagrams.

V.3.4.1 Water/n-Butanol/HMF/Salt at constant Salt Concentration

Experimentally determined tie-lines of quaternary water/n-butanol/HMF/salt systems at constant salt concentration and varying HMF content are displayed in pseudo-ternary phase diagrams for chloride, sulphate, carboxylate and nitrate salts in Figure V.23 to Figure V.26. The binary (water/n-butanol, red diamonds) and the ternary (water/n-butanol/HMF, orange diamonds) subsystems are also pictured in the phase diagrams for comparison. For all systems, the salt addition to the ternary system leads to an enlargement of the biphasic region (increased TLLs). This behaviour is attributed to the salting-out effect on n-butanol as already discussed in section V.3.1. Corresponding $D^w(HMF)$ values with and without salt are presented, depending on the HMF feed molality. $D^w(HMF)$ values obtained with (Phy^{5-}, $5Na^+$), $Al_2(SO_4)_3$ and Na_2SO_4 as salting-out agents are shown in Figure V.27, at m(salt) = 0.8 mol/kg. In addition to increased TLLs, in most cases, the TLSs and $D^w(HMF)$ values are increasing as well in the presence of salt, which is beneficial for the HMF extraction.

Table V-3. Investigated quaternary systems at constant salt and varying HMF concentration at 298.15 K and 1 bar.

Salts	m_{Salt}^{Feed} [mol/kg]	m_{HMF}^{Feed} [mol/kg]	Data
LiCl	3	1, 2, 4	LLE
NaCl	3	1, 3, 6	LLE
KCl	3	1, 2, 4, 6	LLE
Li_2SO_4	2	1, 2, 4	LLE
Na_2SO_4	0.5	1, 2, 3, 4	LLE
$Al_2(SO_4)_3$	0.5	1, 2, 3, 4	LLE
NH_4NO_3	5	1, 2, 3	LLE
CH_3COONa	1.75 3	0.9, 1.8, 2.9, 3.6 1, 2, 3, 4	LLE
C_2H_5COONa	1	1, 2, 3, 4	LLE
C_3H_7COONa	0.8	1, 2	$D^w(HMF)$ values
(Phy^{5-}, $5Na^+$)	0.8	1, 2, 4, 6	$D^w(HMF)$ values

V.3.4.1.1 **Chlorides**

The systems containing chlorides salts were measured at a constant salt molality of 3 mol/kg and thus the chloride salts can be directly compared regarding their salting-out effects on HMF, see Figure V.23. It can be noted that the $D^w(HMF)$ values in quaternary systems remain rather constant with increasing HMF concentration, which is contrary to the ternary system without salt. The strength of the salting-out effect of the chloride salts, rated by the enhanced of $D^w(HMF)$ values, increases in the following order: LiCl < KCl < NaCl.

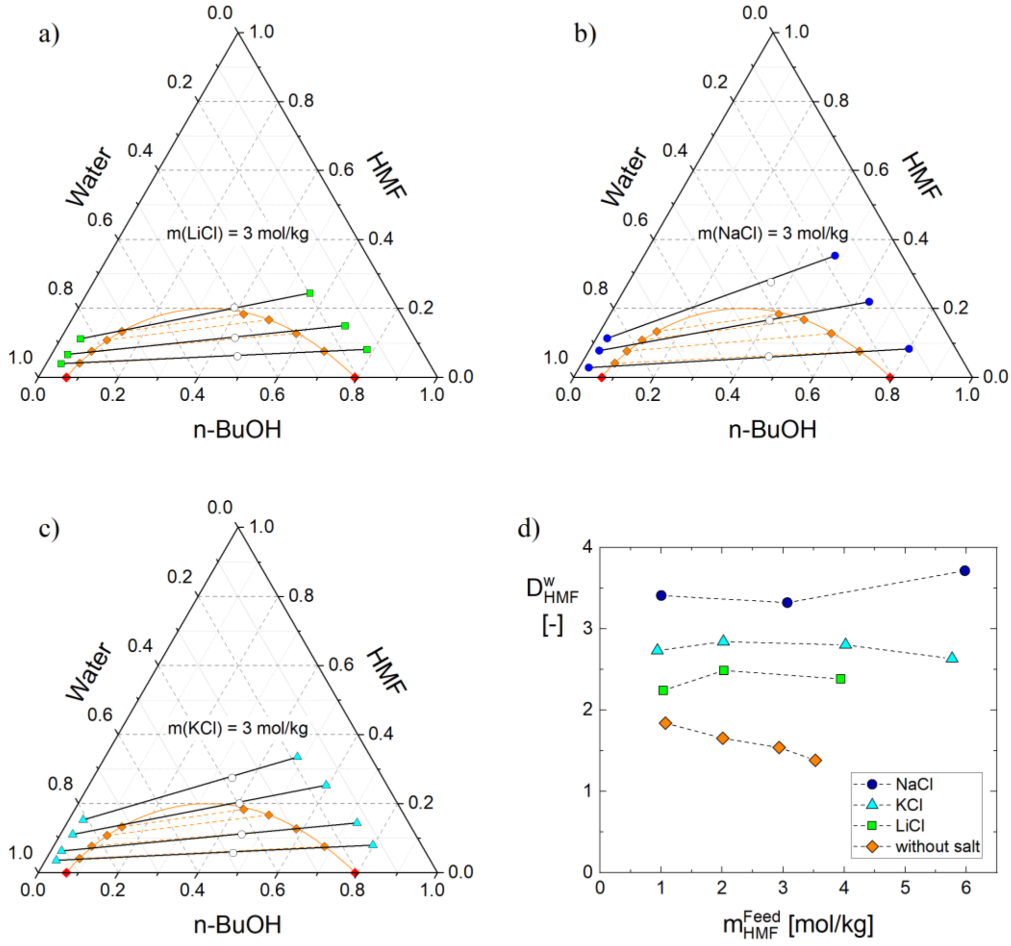

Figure V.23. LLE of quaternary water/n-butanol/HMF/salt systems in pseudo-ternary phase diagrams in weight fractions on salt free basis at constant salt molality (m(salt) = 3 mol/kg), 298.15 K and 1 bar: –a) (🟩) salt = LiCl, –b) (●) salt = NaCl and –c) (△) salt = KCl. (—) Tie-lines of the quaternary systems, (○) initial mixture compositions, (◇) LLE and (--) tie-lines of the ternary subsystem water/n-butanol/HMF and (◆) mutual solubility compositions of water and n-butanol. –d) Corresponding $D^w(HMF)$ values with and without salt depending on the HMF feed molality.

V.3.4.1.2 Sulphates

Higher $D^w(HMF)$ values (compared to the ternary subsystem) are also obtained for quaternary systems including sulphate salts. The effect of sulphate salt addition at constant concentrations is different to that of chloride salts with respect to increasing values for $D^w(HMF)$ with increasing HMF concentration. Thus, further addition of HMF to a quaternary system including a sulphate salt, leads to further accumulation of HMF in the organic phase, whereas the increase of the HMF concentration in the aqueous is very low. The strength of the salting-out effect increases in the order: $Na_2SO_4 < Al_2(SO_4)_3 < Li_2SO_4$, whereby the molality of Li_2SO_4 (m = 2 mol/kg) is 4 times higher than that of the other sulphate salts (m = 0.5 mol/kg). If the ionic strength (I) is considered, $Al_2(SO_4)_3$ (I = 7.5 mol/kg) is indeed less effective than Li_2SO_4 (I = 6 mol/kg) due to lower achieved $D^w(HMF)$ values at a higher ionic strength. If the increase of the $D^w(HMF)$ (relative to the ternary system), which was achieved by Na_2SO_4 (I = 1.5 mol/kg) addition, is multiplied by factor 4, lower values are resulting compared to the increase obtained by Li_2SO_4 addition. Doing the same with factor 5, similar values are resulting compared to the increase of $D^w(HMF)$ obtained by $Al_2(SO_4)_3$ addition. Thus, respecting the ionic strength as criteria for the evaluation, the following series appears for salting-out strength: $Na_2SO_4 \leq Al_2(SO_4)_3 < Li_2SO_4$. However, this is only a rough estimation. If statements about the properties of aqueous solution of the sulphate salts are made, ion association has to be considered.

In aqueous Li_2SO_4 and Na_2SO_4 solutions, the predominant types of ion pairs are double-solvent-shared ion pairs (2SIPs) and solvent-shared ion pairs (SIPs), whose fractions in solution vary with electrolyte concentration. Rather weak ion association occurs in both sulphate salt solution with similar standard (infinite dilution) association constants (K_A^0 ($LiSO_4^-$) ~ 6.4, K_A^0 ($NaSO_4^-$) ~ 6.7)[518,524]. By contrast, it is known that $Al_2(SO_4)_3$ in aqueous solution has a strong tendency to form ion pairs even in dilute solutions. Ion association occurs due to the large coulombic attraction between Al^{3+} and SO_4^{2-}. All three types of ion pairs (2SIPs, SIPs and contact-ion pairs (CIPs)) were found with a dominance of CIPs at high salt concentrations. The standard association constant for $AlSO_4^+$ (log K_A^0 ($AlSO_4^+$) ~ 3.56) is much higher than those for the previously discussed ion pairs. Both ions are strongly hydrated with high effective hydration numbers Z_{ib} extrapolated to zero electrolyte concentration ($Z_{ib}^0(Al^{3+}) = 30$, $Z_{ib}^0(SO_4^{2-}) = 10$). The very high value of Z_{ib} for Al^{3+} compared to other cations (mono- or bivalent) is in line with its high surface charge density and its large Gibbs energy of hydration. At higher $Al_2(SO_4)_3$ concentration (0.7 mol/L), a value of approximately 8.5 was found for $Z_{ib}(Al^{3+})$, i.e. hydration is still highly pronounced, which is in line with the unusual persistence of 2SIPs and SIPs at high $Al_2(SO_4)_3$ concentrations[525]. To explain the relative salting-out efficiency of the mentioned sulphate salts on a molecular level remains difficult. In this case thermodynamic modelling with ePC-SAFT might be helpful, taking interaction parameters between the present species into account. Another issue is the very small HMF concentrations in the aqueous phases. Even a small error in experimental determination leads to a large error for *D^w(HMF)*.

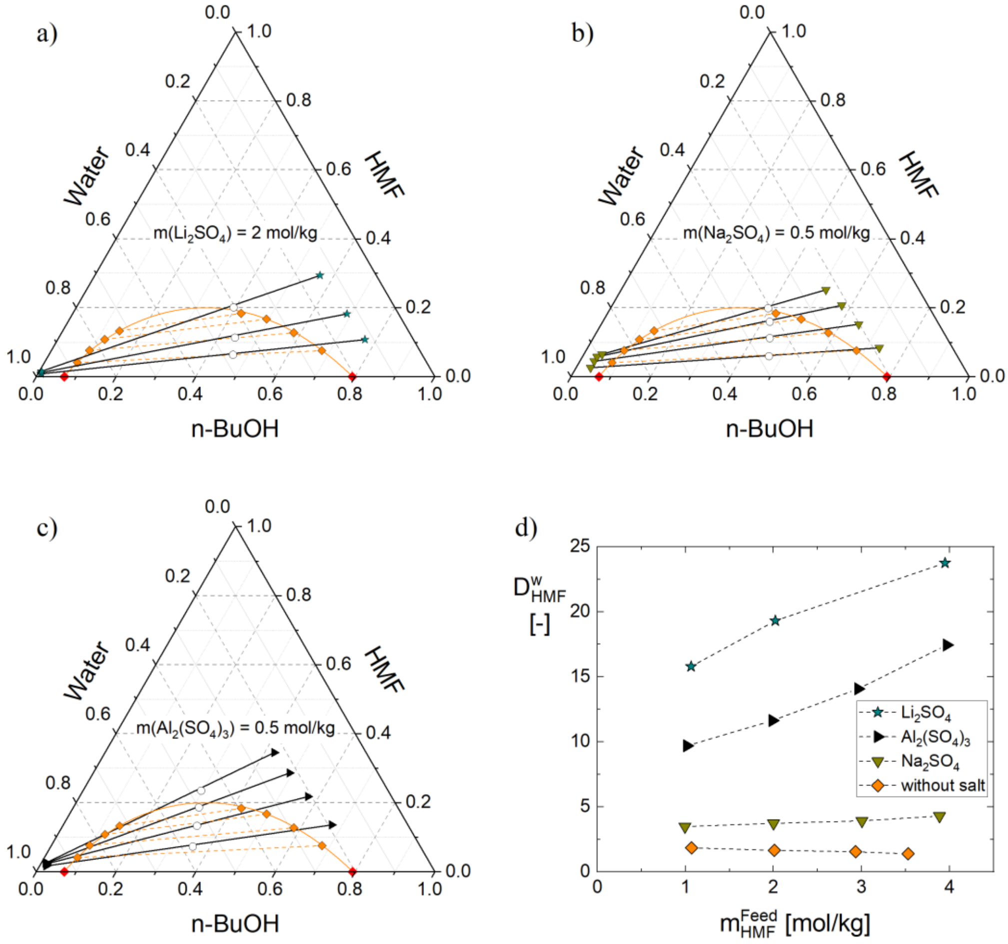

Figure V.24. LLE of quaternary water/n-butanol/HMF/salt systems in pseudo-ternary phase diagrams in weight fractions on salt free basis at constant salt molality, 298.15 K and 1 bar: –a) (★) m(Li_2SO_4) = 2 mol/kg, –b) (▼) m(Na_2SO_4) = 0.5 mol/kg and –c) (▶) m($Al_2(SO_4)_3$) = 0.5 mol/kg. (—) Tie-lines of the quaternary systems, (○) initial mixture compositions, (◇) LLE and (--) tie-lines of the ternary subsystem water/n-butanol/HMF and (◆) mutual solubility compositions of water and n-butanol. –d) Corresponding *D^w(HMF)* values with and without salt depending on the HMF feed molality.

V.3.4.1.3 Carboxylates

For carboxylate salts, it can be stated that increased *D^w(HMF)* values are obtained by addition of CH_3COONa at m(salt) = 1.75 and 3 mol/kg as well as by addition of C_2H_5COONa at m(salt) = 1 mol/kg. Addition of C_3H_7COONa at m(salt) = 0.8 mol/kg decreases the *D^w(HMF)* values, see Figure V.25. In the latter case, a monophasic liquid was obtained at m(HMF) = 2.9 mol/kg and m(C_3H_7COONa) = 0.8 mol/kg. The *D^w(HMF)* values obtained with CH_3COONa at m(salt) = 3 mol/kg remain constant with increasing HMF concentration whereas a slight decrease is observed for C_2H_5COONa and for CH_3COONa at m(salt) = 1.75 mol/kg.

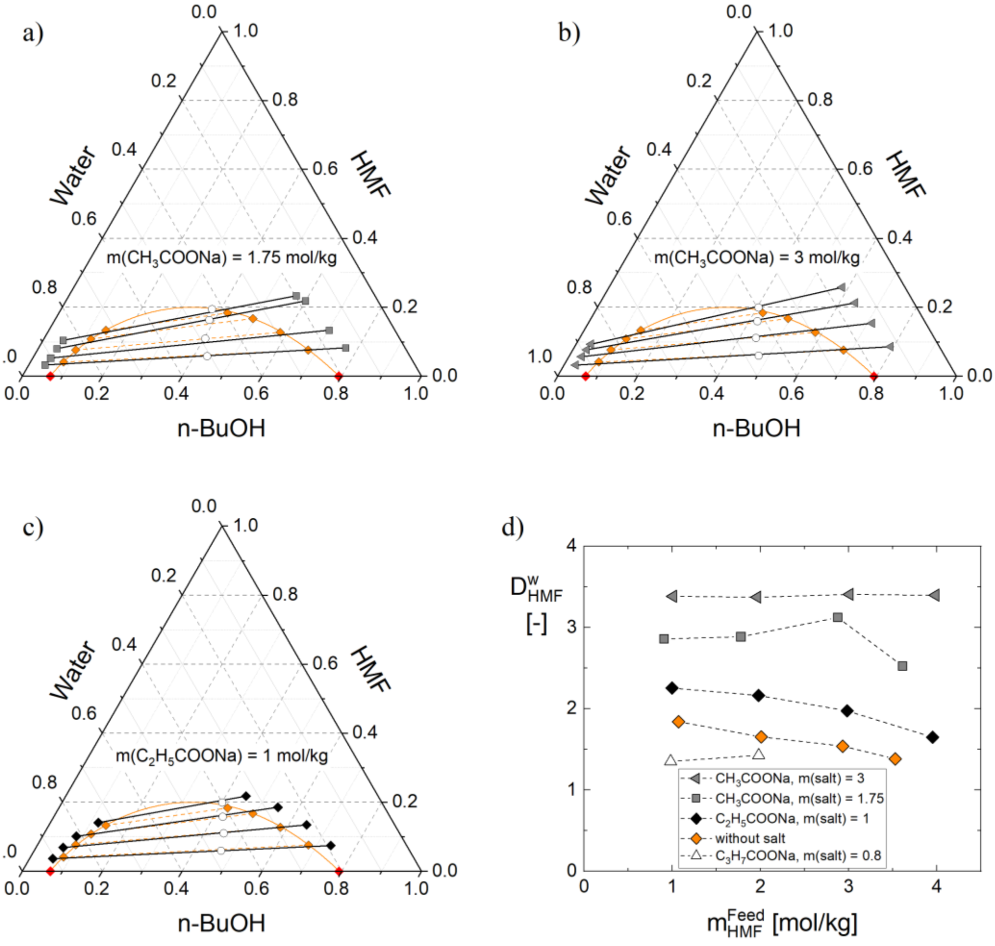

Figure V.25. LLE of quaternary water/n-butanol/HMF/salt systems in pseudo-ternary phase diagrams in weight fractions on salt free basis at constant salt molality, 298.15 K and 1 bar: –a) (■) m(CH_3COONa) = 1.75 mol/kg, –b) (◁) m(CH_3COONa) = 3 mol/kg and –c) (◆) m(C_2H_5COONa) = 1 mol/kg. (—) Tie-lines of the quaternary systems, (○) initial mixture compositions, (◇) LLE and (--) tie-lines of the ternary subsystem water/n-butanol/HMF and (◆) mutual solubility compositions of water and n-butanol. –d) Corresponding *D^w(HMF)* values with and without salt depending on the HMF feed molality. (△) m(C_3H_7COONa) = 0.8 mol/kg (*D^w(HMF)* values, without LLE determination).

In case of C_2H_5COONa, the decrease proceeds nearly in parallel to that of the ternary subsystem. If the effect of CH_3COONa addition at m(salt) = 3 mol/kg is compared to that of NaCl at the same concentration, it appears that both salts have a very similar effect on the HMF distribution.

V.3.4.1.4 **Ammonium nitrate**

NH_4NO_3 was the only nitrate salt, which was investigated in quaternary mixtures. $LiNO_3$ showed relatively high solubility in n-butanol (see Figure V.8) and $NaNO_3$ only marginally influenced the HMF distribution in quaternary systems with MIBK as extracting solvent[419]. The salting-out effect of NH_4NO_3 on n-butanol was least pronounced compared to the other nitrate salts, see Figure V.9. Here, it should represent a salting-in or at least a weak salting-out salt. As can be seen in Figure V.26, the tie-lines bear very low slopes and are almost horizontally aligned. Although the miscibility gap is increased by the salt addition, HMF distribution into the organic phase is not enhanced. The obtained values for $D^w(HMF)$ at HMF feed molalities of 2 and 3 mol/kg are even smaller compared to the ternary subsystem without salt, which resembles a salting-in effect of NH_4NO_3 on HMF.

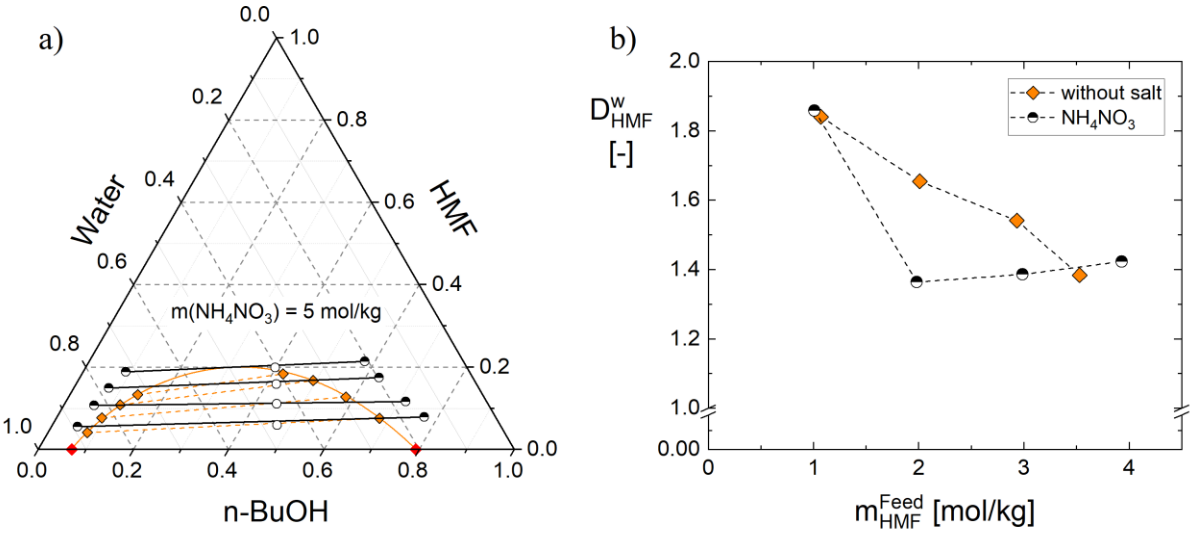

Figure V.26. –a) (◓) LLE of the quaternary water/n-butanol/HMF/NH_4NO_3 system in a pseudo-ternary phase diagram in weight fractions on salt free basis at constant salt molality ($m(NH_4NO_3)$ = 5 mol/kg), 298.15 K and 1 bar, (—) tie-lines of the quaternary system, (○) initial mixture compositions, (◇) LLE and (--) tie-lines of the ternary subsystem water/n-butanol/HMF and (◆) mutual solubility compositions of water and n-butanol. –b) Corresponding $D^w(HMF)$ values with and without salt depending on the HMF feed molality.

V.3.4.1.5 **Pentasodium phytate (Phy^{5-}, $5Na^+$)**

The addition of the organic salt (Phy^{5-}, $5Na^+$) to the ternary water/n-butanol/HMF system was investigated at a constant salt molality of m(salt) = 0.8 mol/kg and varying HMF concentration. No LLE data were determined but $D^w(HMF)$ values, which are pictured in Figure V.27, depending on the salt weight fraction relative to water and the molality. Similar to sulphate salts, $D^w(HMF)$ values are increasing with increasing HMF concentration, although the salt concentration is constant. This indicates a very strong salting-out effect of the organic salt (Phy^{5-}, $5Na^+$). For comparison, data points of $Al_2(SO_4)_3$ and Na_2SO_4 obtained at the same salt molality and m(HMF) = 4 mol/kg are also displayed and at these concentrations the salting-out effect of $Al_2(SO_4)_3$ is superior to that of (Phy^{5-}, $5Na^+$) followed by Na_2SO_4.

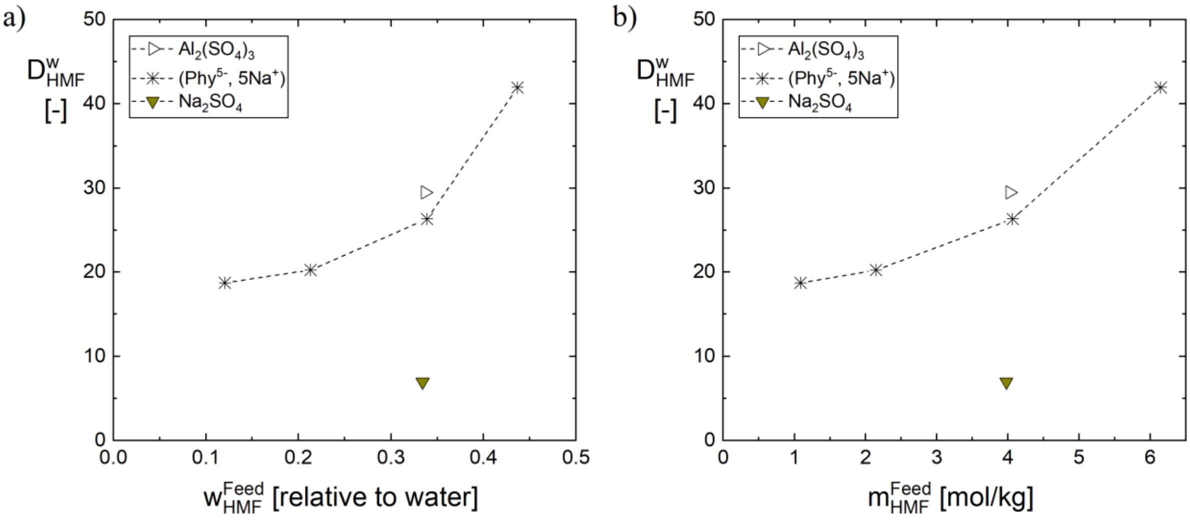

Figure V.27. $D^w(HMF)$ values at constant salt ((▼) Na_2SO_4, (▷) $Al_2(SO_4)_3$, (✳) (Phy^{5-}, $5Na^+$)) molality m(salt) = 0.8 mol/kg, depending on the HMF feed concentration relative to water at 298.15 K and 1 bar. $D^w(HMF)$ values depending on -a) the HMF feed weight fraction relative to water and -b) the HMF feed molality. (✳) (Phy^{5-}, $5Na^+$) and (▷) $Al_2(SO_4)_3$ refer to $D^w(HMF)$ values, without determination of the complete LLE.

V.3.4.2 Water/n-Butanol/HMF/Salt at constant HMF Concentration

Experimentally determined tie-lines of quaternary water/n-butanol/HMF/salt systems are presented in pseudo-ternary phase diagrams at constant HMF molality (m(HMF) = 4 mol/kg) and varying salt concentration up to the respective solubility limit at 298.15 K and 1 bar for chloride, sulphate, carboxylate and nitrate salts in Figure V.28 to Figure V.31, respectively. The binary (water/n-butanol, red diamonds) and the ternary (water/n-butanol/salt, orange squares) subsystems are also pictured in the phase diagrams for comparison. For all quaternary systems, the presence of HMF leads to a reduction of the biphasic region (decreased TLLs) compared to the ternary subsystems water/n-butanol/salt. In contrast, the presence of HMF, if at all, only marginally influences the TLSs.

Corresponding $D^w(HMF)$ values are presented, depending on the salt feed molality. $D^w(HMF)$ values at zero salt concentration could not be reported, due to a monophasic water/n-butanol/HMF mixture resulting at m(HMF) = 4 mol/kg. Extrapolation of $D^w(HMF)$ to this HMF molality leads to $D^w(HMF) \approx 1.3$. In almost all cases (except LiCl), $D^w(HMF)$ values are increasing monotonically with increasing salt feed molality.

Table V-4. Investigated quaternary systems at constant HMF and varying salt concentration at 298.15 K and 1 bar.

Salts	m_{Salt}^{Feed} [mol/kg]	m_{HMF}^{Feed} [mol/kg]	Data
LiCl	3, 6, 12	4	LLE + $D^w(HMF)$ values
NaCl	1, 2, 4	4	LLE + $D^w(HMF)$ values
KCl	1, 2, 4	4	LLE
Li_2SO_4	1, 2, 2.5	4	LLE
Na_2SO_4	0.2, 0.8	4	LLE
$Al_2(SO_4)_3$	0.2, 0.8	4	$D^w(HMF)$, α values
NH_4NO_3	5, 10, 15	4	LLE
CH_3COONa	1, 1.7, 2.7	4, 3.84, 3.65	LLE
(Phy^{5-}, $5Na^+$)	0.07, 0.15, 0.32, 1.25	4	$D^w(HMF)$ values

V.3.4.2.1 **Chlorides**

Results of the quaternary systems water/n-butanol/HMF/chlorides measured at a constant HMF feed molality (m(HMF) = 4 mol/kg) and different chloride salt (LiCl, NaCl and KCl) concentrations are depicted in pseudo-ternary phase diagrams in Figure V.28, together with the corresponding $D^w(HMF)$ values depending on the salt feed molality. As already stated above, the TLLs in quaternary systems are shorter than those in the ternary subsystem without HMF. At all LiCl concentrations, the TLLs are even shorter than that in the binary water/n-butanol system. For NaCl and KCl, this is only the case at low salt concentrations. According to the normalised equilibrium data, the TLLs shortening is significant in the organic branch, while in the aqueous branch the difference to the ternary subsystem without HMF is small. This is explained by electrolytes dominating the aqueous phase behaviour; i.e. the salting-out effect on n-butanol from the aqueous phase is only marginally influenced by the addition of HMF. A linear increase of $D^w(HMF)$ with increasing salt molality can be detected for all mixtures containing NaCl, for KCl up to m(salt) = 3 mol/kg and for LiCl up to 6 mol/kg. At m(KCl) = 4 mol/kg, salt precipitated and the $D^w(HMF)$ value is only slightly increased, compared to that at m(KCl) = 3 mol/kg. The strength of the salting-out effect on HMF increases in the following order: LiCl < KCl < NaCl.

The 'unusal' S-shaped binodal curve in the organic branch of the ternary subsystem water/n-butanol/LiCl (orange squares in Figure V.28 a)) appears also in the organic branch in the corresponding quaternary system with HMF (green squares in Figure V.28 a)). A similar behaviour is also reflected by the $D^w(HMF)$ values depending on the LiCl concentration. Up to m(LiCl) = 6 mol/kg, an increase in $D^w(HMF)$ can be detected while upon further increase in salt concentration the $D^w(HMF)$ values decrease again. Thus, a maximum in $D^w(HMF)$ is observed, at which the LiCl molality in the equilibrated aqueous phase is equal to 5.7651 mol/kg. At a similar LiCl molality (5.3734 mol/kg) in the aqueous phase of ternary water/n-butanol/LiCl systems, a maximum in n-butanol concentration in the organic phase was observed. Concurrently, upon higher LiCl concentration in the ternary system, the LiCl concentration in the organic phase increases sharply[496], see discussion in V.3.1.6. The behaviour of LiCl in the ternary systems seems to be related to that observed in the quaternary system, which is characterised by a linearly increasing salting-out effect on HMF up to m(LiCl) = 6 mol/kg and a less pronounced salting-out effect on HMF upon higher LiCl concentrations. A similar effect was found in the quaternary systems with MIBK as extractive solvent. Here, the maximum in D^w*(HMF)* was found at m(LiCl) = 3 mol/kg[419] and the reason for the weakening of the salting-out effect of LiCl at higher concentrations was proposed to be the strong ion-hydration and weak interaction between both oppositely charged ions.

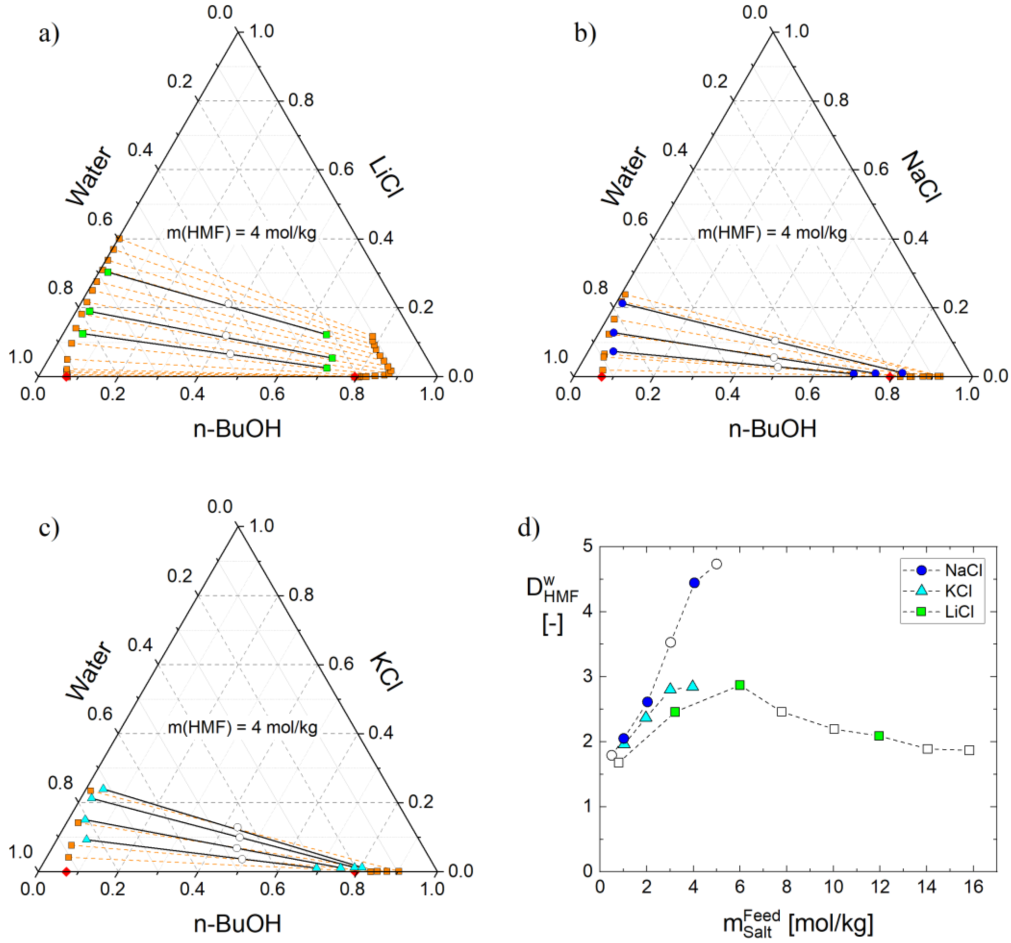

Figure V.28. LLE of quaternary water/n-butanol/HMF/salt systems in pseudo-ternary phase diagrams in weight fractions on HMF free basis at constant HMF molality (m(HMF) = 4 mol/kg), 298.15 K and 1 bar: –a) (🟩) salt = LiCl, –b) (●) salt = NaCl and –c) (▲) salt = KCl. (—) Tie-lines of the quaternary systems, (○) initial mixture compositions, (🟧) LLE and (--) tie-lines of the ternary subsystems water/n-butanol/salt and (◆) mutual solubility compositions of water and n-butanol. –d) Corresponding D^w*(HMF)* values depending on the salt feed molality. (○) and (□) refer to distribution coefficient measurements, without determination of the complete LLE.

V.3.4.2.2 **Sulphates**

The tie-lines of quaternary systems water/n-butanol/HMF/sulphates at a constant HMF feed molality (m(HMF) = 4 mol/kg) and different sulphate salt (Li_2SO_4 and Na_2SO_4) concentrations are pictured in pseudo-ternary phase diagrams in Figure V.29, together with the corresponding $D^w(HMF)$ values depending on the salt feed molality. Additional $D^w(HMF)$ values, measured for $Al_2(SO_4)_3$ as salting-out agent at different concentrations, were also presented. The data points at a salt molality equal to 0.5 mol/kg originate from investigations presented in the previous sectionV.3.4.1.2. The salt molalities for Na_2SO_4 and $Al_2(SO_4)_3$ were 0.2, 0.5 and 0.8 mol/kg, while those for Li_2SO_4 were equal to 1, 2 and 2.5 mol/kg. These higher salt molalities for Li_2SO_4 were chosen due to its higher water solubility. Similar to the chloride salts, the TLLs are reduced compared to the ternary subsystem without HMF. This is less pronounced in case of Li_2SO_4, propably due to the higher salt molalities. For all sulphate salts, a strong salting-out effect on HMF can be observed, which increases with increasing salt molality in the following order: $Na_2SO_4 < Li_2SO_4 < Al_2(SO_4)_3$. It is assumed that the course of $D^w(HMF)$ for Li_2SO_4 can be extrapolated to low salt concentrations similar to that of Na_2SO_4. Thus, the salting-out efficiency of Li_2SO_4 is perceived to be comparable to that of Na_2SO_4 at low salt concentrations. Nevertheless, the higher solubility of Li_2SO_4, of course, drives to an enhanced HMF distribution towards the organic phase. The high $D^w(HMF)$ values, obtained by $Al_2(SO_4)_3$ at lower molalities than those of Li_2SO_4, justify the above stated series, based on salt molality. If ionic strength is considered, $Al_2(SO_4)_3$ and Li_2SO_4 are comparable at their lowest concentration (I = 3 mol/kg for both salts), but at higher molalities again Li_2SO_4 is more effective than $Al_2(SO_4)_3$. Similar to the rough estimation in section V.3.4.1.2, the salting-out efficiency of Na_2SO_4 in this part of investigation is also comparable to that of $Al_2(SO_4)_3$, if the ionic strength is taken into account and the series is: $Na_2SO_4 \leq Al_2(SO_4)_3 < Li_2SO_4$.

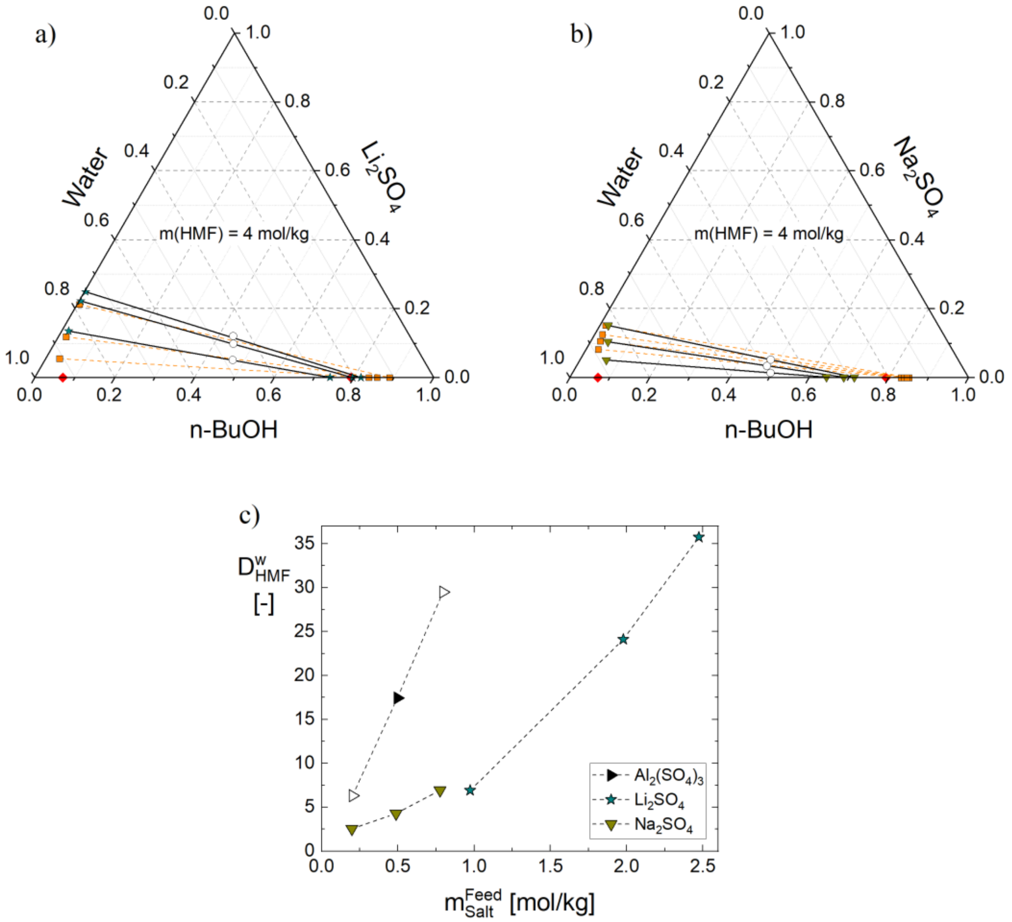

Figure V.29. LLE of quaternary water/n-butanol/HMF/salt systems in pseudo-ternary phase diagrams in weight fractions on HMF free basis at constant HMF molality (m(HMF) = 4 mol/kg), 298.15 K and 1 bar: –a) (★) salt = Li_2SO_4, –b) (▼) salt = Na_2SO_4. (—) Tie-lines of the quaternary systems, (○) initial mixture compositions, (■) LLE and (--) tie-lines of the ternary subsystems water/n-butanol/salt and (◆) mutual solubility compositions of water and n-butanol. –c) Corresponding *D^w(HMF)* values depending on the salt feed molality. (▶) $Al_2(SO_4)_3$ stems from LLE investigations at constant salt concentration of the previous section V.3.4.1.2. (▷) refer to *D^w(HMF)* values, without determination of the complete LLE.

V.3.4.2.3 Carboxylates

Results for the quaternary system water/n-butanol/HMF/CH_3COONa at a constant HMF feed molality (m(HMF) = 4 mol/kg) and different CH_3COONa concentrations are shown in a pseudo-ternary phase diagram Figure V.30, together with the corresponding $D^w(HMF)$ values, depending on the salt feed molality. The TLLs in quaternary systems are shorter than those in the ternary subsystem without HMF and even shorter than those in the binary water/n-butanol system at all CH_3COONa concentrations. Here, it must be mentioned that the HMF concentration is not strictly constant at 4 mol/kg, but varies slightly with increasing salt content. From lowest to highest salt content, the actual HMF concentrations are 4, 3.84 and 3.65 mol/kg. The $D^w(HMF)$ values obtained with CH_3COONa are increasing roughly linear with increasing salt concentration and are very similar to those obtained with NaCl, compared with Figure V.28. The $D^w(HMF)$ values for CH_3COONa at m(salt) = 3 mol/kg and C_2H_5COONa at m(salt) = 1 mol/kg were taken from the previous section V.3.4.1. The strength of the salting-out effect is higher for the acetate than for the propionate salt.

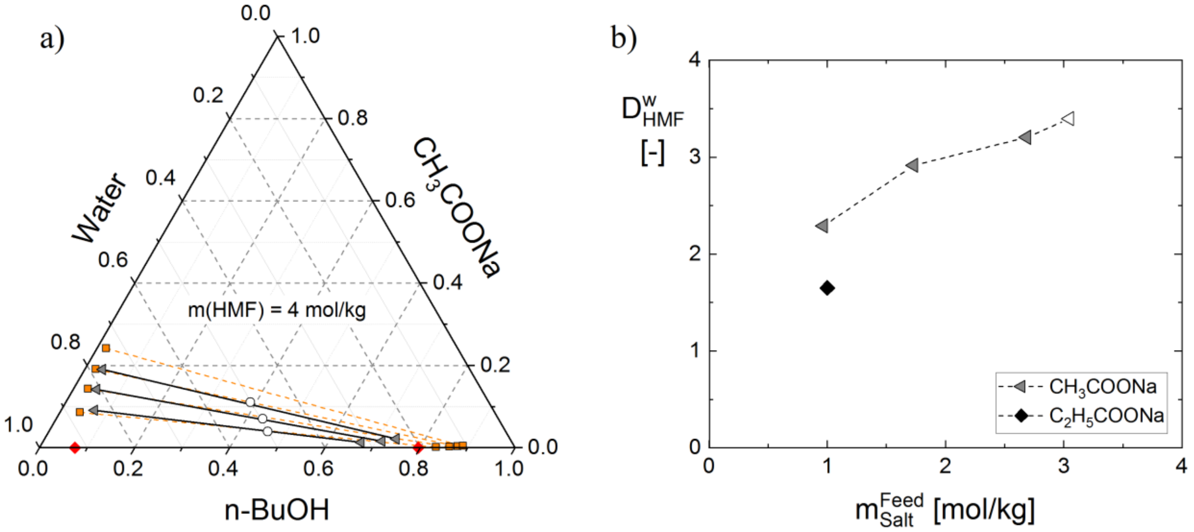

Figure V.30. –a) (◁) LLE of the quaternary water/n-butanol/HMF/CH_3COONa system in a pseudo-ternary phase diagram in weight fractions on HMF-free basis at constant HMF molality (m(HMF) = 4 mol/kg), 298.15 K and 1 bar. (—) Tie-lines of the quaternary system, (○) initial mixture compositions, (□) LLE and (--) tie-lines of the ternary subsystem water/n-butanol/CH_3COONa and (◆) mutual solubility compositions of water and n-butanol. –b) Corresponding $D^w(HMF)$ values depending on the salt feed molality. (◁) CH_3COONa and (◆) C_2H_5COONa stem from LLE investigations at constant salt concentration of the previous section V.3.4.1.3.

V.3.4.2.4 **Ammonium nitrate**

Tie-lines of the quaternary system water/n-butanol/HMF/NH_4NO_3 at a constant HMF feed molality (m(HMF) = 4 mol/kg) and different NH_4NO_3 concentrations are presented in a pseudo-ternary phase diagram Figure V.31, together with the corresponding $D^{w}(HMF)$ values, depending on the salt feed molality. The TLLs in quaternary systems are shorter than those in the ternary subsystem without HMF at all NH_4NO_3 concentrations and at m(NH_4NO_3) = 5 mol/kg the TLL is even shorter than that in the binary water/n-butanol system. The quaternary mixture appeared monophasic at m(NH_4NO_3) = 1 mol/kg and m(HMF) = 4 mol/kg. A large biphasic liquid region in the pseudo-ternary phase diagram is possible, due to the high water solubility of NH_4NO_3, which also leads to very high TLSs. However, the salt shows also a relatively high solubility in the organic phases and the $D^{w}(HMF)$ values are only marginally increasing with increasing salt concentration. NH_4NO_3 is the least effective salting-out agent for HMF within the scope of investigated salts.

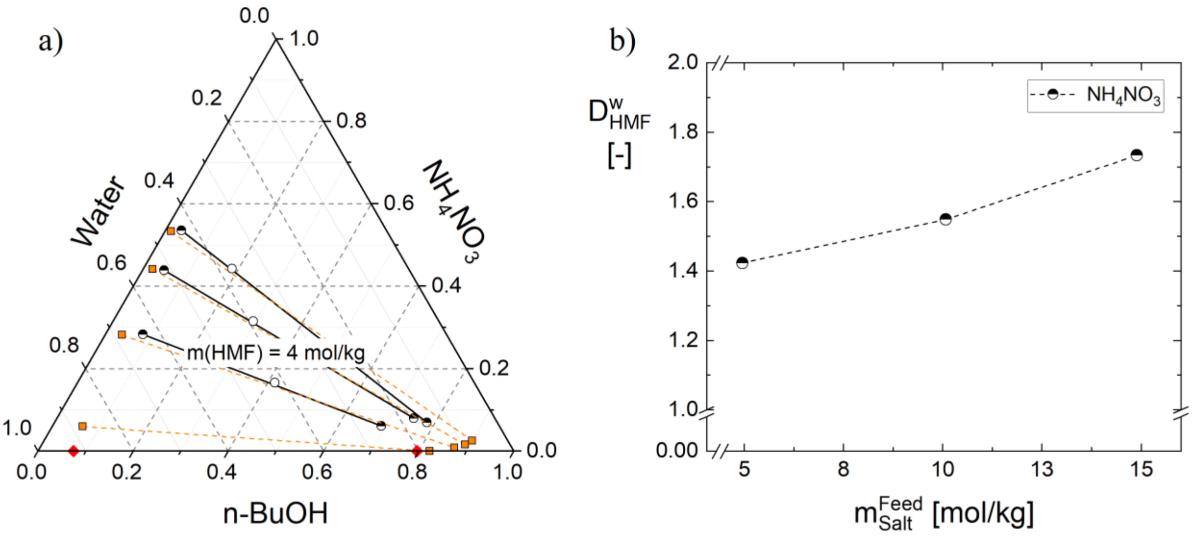

Figure V.31. –a) (◓) LLE of the quaternary water/n-butanol/HMF/NH_4NO_3 system in a pseudo-ternary phase diagram in weight fractions on HMF free basis at constant HMF molality (m(HMF) = 4 mol/kg), 298.15 K and 1 bar. (—) Tie-lines of the quaternary system, (○) initial mixture compositions, (■) LLE and (--) tie-lines of the ternary subsystem water/n-butanol/NH_4NO_3 and (◆) mutual solubility compositions of water and n-butanol. –b) Corresponding $D^{w}(HMF)$ values depending on the salt feed molality.

V.3.4.2.5 Pentasodium phytate (Phy^{5-}, $5Na^+$)

In Figure V.32, experimentally determined $D^w(HMF)$ values obtained with pentasodium phytate (Phy^{5-}, $5Na^+$) as salting-out agent at a constant HMF feed molality (m(HMF) = 4 mol/kg) are compared to those obtained with the most effective inorganic salting-out agents (Li_2SO_4, Na_2SO_4, $Al_2(SO_4)_3$), depending on the salt feed weight fractions relative to water (Figure V.32a)) and the molality (Figure V.32b)). It can be noted that (Phy^{5-}, $5Na^+$) has a lower efficiency at low salt concentrations compared to the inorganic salts (Li_2SO_4, Na_2SO_4, $Al_2(SO_4)_3$). $D^w(HMF)$ values obtained with Li_2SO_4 and $Al_2(SO_4)_3$ are comparable and superior to those obtained with Na_2SO_4. Due to the high water solubility of (Phy^{5-}, $5Na^+$) (≥ 50 mg/ml) a higher $D^w(HMF)$ value can be achieved at high salt concentration. In molality scale, the HMF extraction with the agent (Phy^{5-}, $5Na^+$) leads to results comparable with the most effective inorganic salt $Al_2(SO_4)_3$ in molality scale. But as the solubility of (Phy^{5-}, $5Na^+$) in water is higher than that of $Al_2(SO_4)_3$, a higher value for the HMF distribution can be achieved.

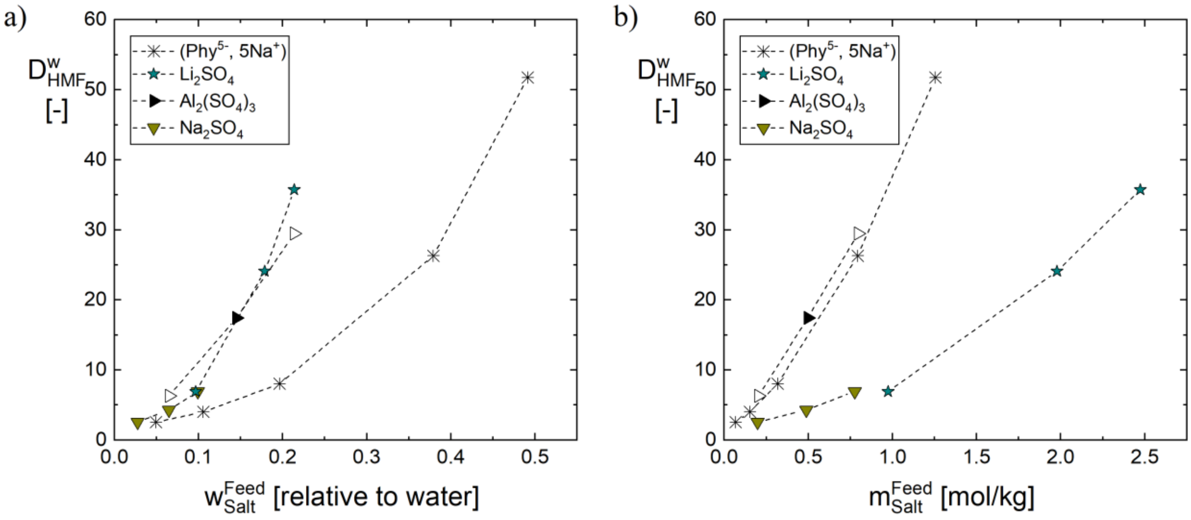

Figure V.32. $D^w(HMF)$ values depending on the salt ((★) Li_2SO_4, (▼) Na_2SO_4, (▶) $Al_2(SO_4)_3$, (✳) (Phy^{5-}, $5Na^+$)) feed concentration relative to water at constant HMF molality (m(HMF) = 4 mol/kg), 298.15 K and 1 bar. $D^w(HMF)$ values depending on -a) the salt feed weight fraction relative to water and -b) the salt feed molality. (✳) (Phy^{5-}, $5Na^+$) and (▷) $Al_2(SO_4)_3$ refer to $D^w(HMF)$ values, without determination of the complete LLE.

V.3.4.3 Water/n-Butanol/HMF/Na_2SO_4 at elevated Temperature

The solubility of sodium sulphate in water increases with rising temperature up to 32.38°C (305.53 K) and decreases then slightly at higher temperatures, see Figure V.33. The maximum solubility of Na_2SO_4 in water is 2.34 mol/kg at 32.38 °C. Below this transition temperature, sodium sulphate occurs as mirabilite ($Na_2SO_4 \cdot 10H_2O$; Glauber's salt) and above as thenardite (Na_2SO_4)[526]. This solubility behaviour is extraordinary among all of the other alkali metal sulphates. While the solubility of Li_2SO_4 decreases, that of K_2SO_4, Rb_2SO_4 and Cs_2SO_4 increases almost linearly with rising temperature[527].

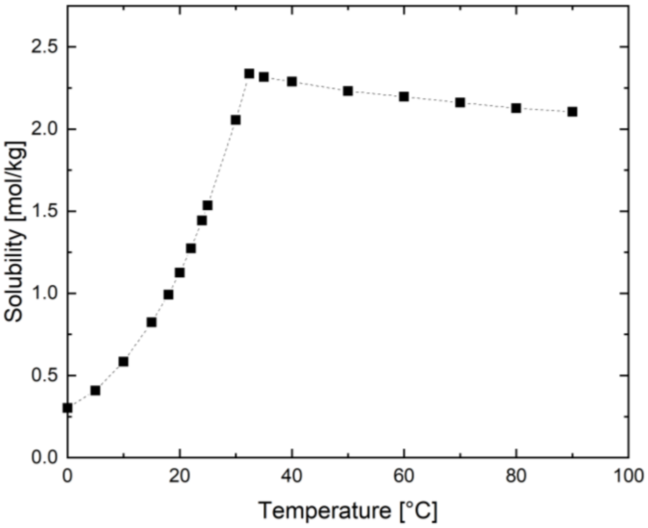

Figure V.33. Temperature-dependent water solubility of sodium sulphate Na_2SO_4. Data points were taken from literature[526].

To investigate the influence of temperature on the LLE of quaternary systems and to exploit the increased solubility of Na_2SO_4 (efficient salting-out agent) at higher temperatures, LLE measurements of the quaternary system water/n-butanol/HMF/Na_2SO_4 were conducted at 30°C (303.15 K) and at salt concentrations of $m(Na_2SO_4)$ = 0.5, 1, 2 mol/kg. In Figure V.34a), the LLE results of the quaternary system at 30°C are depicted in terms of a pseudo-ternary phase diagram on HMF-free basis. The corresponding $D^w(HMF)$ values and those gained at 25°C (298.15 K) are shown in Figure V.34b). At a salt concentration of 0.5 mol/kg, similar $D^w(HMF)$ values are obtained independently of temperature. Thus, no influence of temperature on the partitioning of HMF between the two liquid phases could be detected. But, the enhanced salt solubility induced by elevated temperature allows for higher $D^w(HMF)$

values, up to 35 at m(Na_2SO_4) = 2 mol/kg. Thus, the salting-out of Na_2SO_4 on HMF at 303.15 K is even more pronounced compared to that of Li_2SO_4 at 298.15 K (Figure V.29).

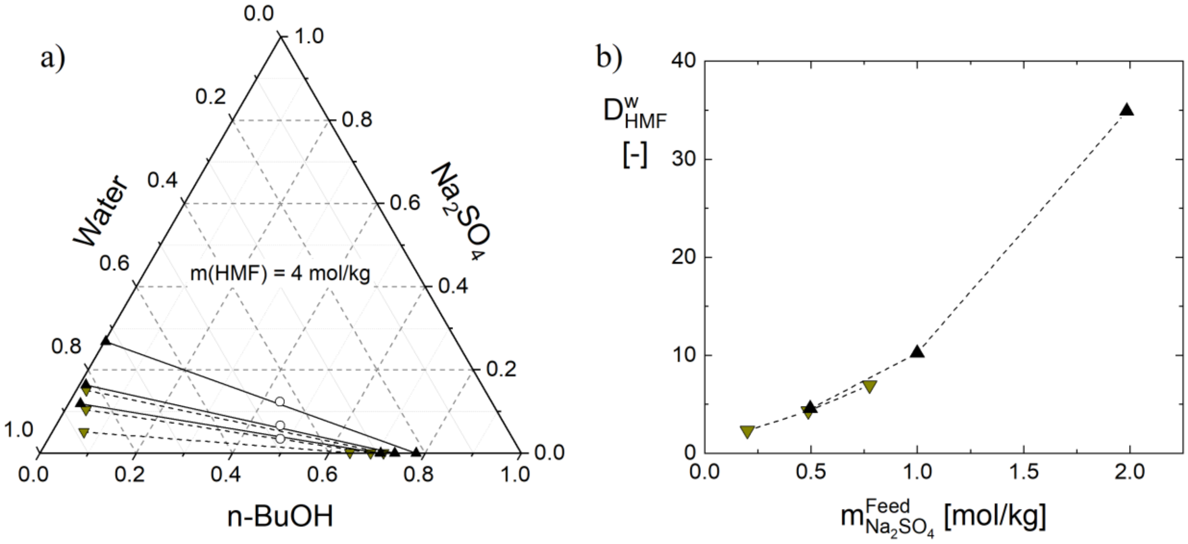

Figure V.34. –a) LLE of the quaternary water/n-butanol/HMF/Na_2SO_4 system in a pseudo-ternary phase diagram in weight fractions on HMF free basis at constant HMF molality (m(HMF) = 4 mol/kg), (▼) 298.15 K, (▲) 303.15 K and 1 bar. (--) 298.15 K and (—) 303.15 K are tie-lines of the quaternary systems and (○) initial mixture compositions. –b) Corresponding *D^w(HMF)* values depending on the salt feed molality.

V.3.5 Separation Factor and Selectivity

Besides the $D^{w}(HMF)$, $\alpha^{w}(HMF,water)$ according to Eq. (II-5) is a further measure of the LLEx quality. In Figure V.35, $\alpha^{w}(HMF,water)$ values of quaternary water/n-butanol/HMF/salt systems at a constant salt feed molality and of the ternary subsystem without salt are presented, depending on the HMF feed molality. Sulphates ($m(Li_2SO_4)$ = 2 mol/kg, $m(Na_2SO_4)$ = $m(Al_2(SO_4)_3)$ = 0.5 mol/kg) are presented in Figure V.35 a). Chloride (m(NaCl) = m(KCl) = m(LiCl) = 3 mol/kg), sulphate ($m(Na_2SO_4)$ = 0.5 mol/kg), carboxylate ($m(CH_3COONa)$ = 3 mol/kg; 1.75 mol/kg, $m(C_2H_5COONa)$ = 1 mol/kg) and nitrate ($m(NH_4NO_3)$ = 5 mol/kg) salts are presented in Figure V.35 b).

First, it can be noted that the $\alpha^{w}(HMF,water)$ values are decreasing with increasing HMF concentration, except for the systems including Li_2SO_4 and $Al_2(SO_4)_3$. This decrease of the $\alpha^{w}(HMF,water)$ values is related to the solubilising ability of HMF (closed miscibility gap between water and n-butanol, see Figure V.20), which leads to higher water contents in the organic layers with increasing HMF content in the feed compositions. Due to the very strong salting-out effect of Li_2SO_4 and $Al_2(SO_4)_3$, the increase of the water content in the organic layers with increasing HMF concentration is overcompensated by the strong increase of the $D^{w}(HMF)$ values, achieved by these salts, see Figure V.24 d). Thus, although the water content in the n-butanol-rich phases is increased also for Li_2SO_4 and $Al_2(SO_4)_3$, the $\alpha^{w}(HMF,water)$ values are increasing as well. For Na_2SO_4, the decrease of the $\alpha^{w}(HMF,water)$ is only weakly pronounced, which is also a consequence of a strong salting-out effect. Here, it has to be mentioned that the molality of Li_2SO_4 is four times higher than that of $Al_2(SO_4)_3$ and Na_2SO_4.

Secondly, the addition of each salt leads to higher $\alpha^{w}(HMF,water)$ values compared to those obtained from the ternary subsystem without salt. Even for NH_4NO_3, which leads to reduced $D^{w}(HMF)$ values (Figure V.26), slightly increased $\alpha^{w}(HMF,water)$ values are obtained at a salt molality of $m(NH_4NO_3)$ = 5 mol/kg. Only salts with equal molality can be compared directly and the following series at m(salt) = 3 mol/kg: LiCl < KCl < CH_3COONa < NaCl and at m(salt) = 0.5 mol/kg: Na_2SO_4 < $Al_2(SO_4)_3$ can be detected with increasing $\alpha^{w}(HMF,water)$ values from left to right. C_2H_5COONa induces slightly higher $\alpha^{w}(HMF,water)$ values compared to those of NH_4NO_3, but at a 5 times lower molality. The effect of CH_3COONa at m(salt) = 1.75 mol/kg is comparable to that of LiCl at m(salt) = 3 mol/kg. Generally, the same trend of salt effects are observed for $\alpha^{w}(HMF,water)$ and $D^{w}(HMF)$ values.

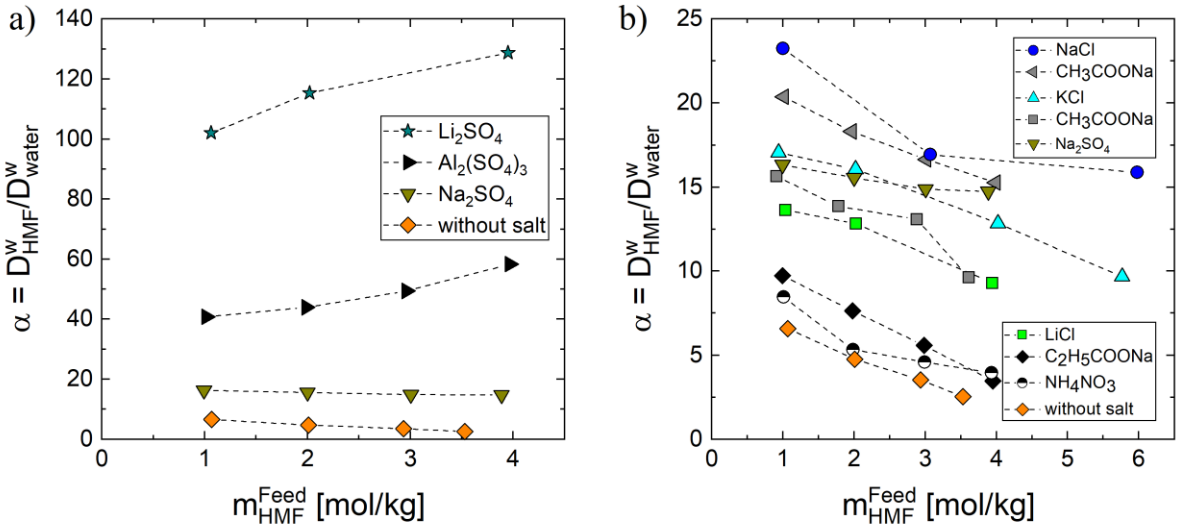

Figure V.35. Separation factors $\alpha^{w}(HMF,water)$ of quaternary water/n-butanol/HMF/salt systems depending on the HMF feed molality at a constant salt molality at 298.15 K and 1 bar. –a) sulphate ((★) m(Li_2SO_4) = 2 mol/kg, (▼) m(Na_2SO_4) = (▶) m($Al_2(SO_4)_3$ = 0.5 mol/kg) salts and –b) chloride ((●) m(NaCl) = (△) m(KCl) = (■) m(LiCl) = 3 mol/kg), sulphate ((▼) m(Na_2SO_4) = 0.5 mol/kg), carboxylate (m(CH_3COONa) = (■) 3 mol/kg; (◁) 1.75 mol/kg, (◆) m(C_2H_5COONa) = 1 mol/kg) and nitrate ((◓) m(NH_4NO_3) = 5 mol/kg) salts.

In Figure V.36, $\alpha^{w}(HMF,water)$ values of quaternary water/n-butanol/HMF/salt systems at a constant HMF feed molality (m(HMF) = 4 mol/kg) are presented, depending on the salt feed molality of several salts. Figure V.36 is separated in –a) for sulphate salts (Li_2SO_4, Na_2SO_4, $Al_2(SO_4)_3$) and –b) for chloride (NaCl, KCl, LiCl), carboxylate (CH_3COONa, C_2H_5COONa) and nitrate (NH_4NO_3) salts.

For all salts except LiCl, the $\alpha^{w}(HMF,water)$ values increase with increasing salt concentration. The addition of sulphate salts leads to clearly higher $\alpha^{w}(HMF,water)$ values, compared to chloride, acetate and nitrate salts with a maximum value of $\alpha^{w}(HMF,water)$ = 207 at m(Li_2SO_4) = 2.5 mol/kg. With $Al_2(SO_4)_3$ and Na_2SO_4, $\alpha^{w}(HMF,water)$ values of 142 and 26 at m(salt) = 0.8 mol/kg are achieved, respectively. The highest value for Na_2SO_4 (α = 26) was also found for NaCl, but at much higher salt molality (m(NaCl) = 4 mol/kg). KCl and sodium acetate show similar behaviour, in contrast to LiCl, for which a maximum of α values at m(LiCl) = 6 mol/kg was detected. The lowest $\alpha^{w}(HMF,water)$ value was found for C_2H_5COONa followed by those of NH_4NO_3. At a temperature of T = 303.15 K, higher amounts of Na_2SO_4 can be introduced to the quaternary system, which leads to increased $D^{w}(HMF)$ values (Figure V.34) in connection with increased $\alpha^{w}(HMF,water)$ values (Figure V.36 a). At elevated temperature T = 303.15 K, even higher $\alpha^{w}(HMF,water)$ values are achieved by the addition of Na_2SO_4, compared to Li_2SO_4 at 298.15 K. This result is analogue to the $D^{w}(HMF)$ values. The courses of the $\alpha^{w}(HMF,water)$ values generally resemble to those of the $D^{w}(HMF)$ values, depending on salt concentrations, but are different in magnitude. The slopes may also differ for some salts, but in general, the relations are similar and the same salt series for the strength of the salting-out effect on HMF, rated by the $D^{w}(HMF)$ values, is found for the influence of salt addition on the $\alpha^{w}(HMF,water)$ values in molality scale: $Al_2(SO_4)_3$ < Na_2SO_4 (T = 303.15 K) < Li_2SO_4 ≤ Na_2SO_4 < NaCl < CH_3COONa < KCl < LiCl < C_2H_5COONa < NH_4NO_3.

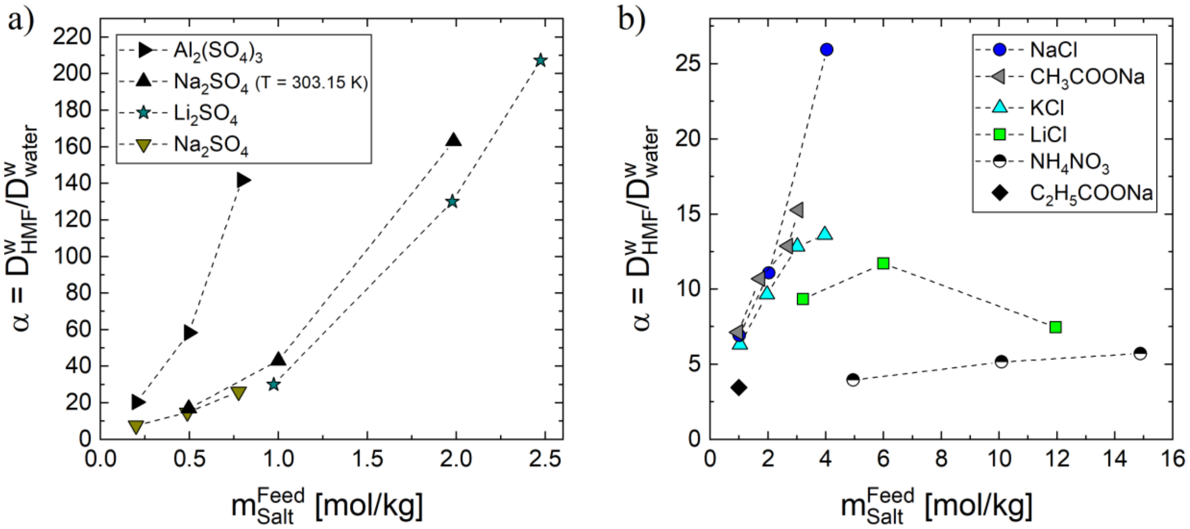

Figure V.36. Separation factors $\alpha^{w}(HMF, water)$ of quaternary water/n-butanol/HMF/salt systems depending on the salt feed molality at constant HMF molality (m(HMF) = 4 mol/kg) at 298.15 K and 1 bar. – a) sulphate salts ((▶) $Al_2(SO_4)_3$, (★) Li_2SO_4, (▼) Na_2SO_4) and ((▲) Na_2SO_4 at 303.15 K). – b) Chloride ((●) NaCl, (△) KCl, (■) LiCl), carboxylate ((◁) CH_3COONa, (◆) C_2H_5COONa) and nitrate ((◓) NH_4NO_3) salts.

V.3.6 Quaternary LLE with Glycerol as Product

LLE data of the quaternary systems composed of water, n-butanol, glycerol and salt were determined at 298.15 K and 1 bar following the procedure described in section II.4.5. The investigated mixtures included NaCl or Li_2SO_4 as salt. Analogue to the quaternary systems including HMF, the salt influence on quaternary LLEs was examined at constant glycerol molality with varying salt content and at constant salt molality with varying glycerol content. Overviews of the investigated systems in both concentration screens are presented in Table V-5 and Table V-6 for glycerol as product. Results of the quaternary systems are presented in pseudo-ternary phase diagrams for NaCl and Li_2SO_4 in both concentration screens *via* normalisation of the LLE data with regard to the compound (salt or glycerol), which was held constant. The salts as well as glycerol are predominantly dissolved in the aqueous phases and tie-lines pass through the initial mixture compositions. For (Phy^{5-}, $5Na^+$), $Na_5P_3O_{10}$ and $K_4P_2O_7$, additional $D^w(glycerol)$ were determined without determination of the complete LLE. The LLE data and initial mixture compositions are given in Table B-5 and Table B-15, respectively. $D^w(glycerol)$, $\alpha^w(glycerol, water)$ values, TLLs and TLSs for systems at constant glycerol and constant salt concentration are given in Table B-9 and Table B-10, respectively. Similar to the quaternary systems containing HMF, TLLs and TLSs in quaternary systems containing glycerol as product molecule were calculated, based on normalised LLE data to be consistent with the pictured ternary phase diagrams.

V.3.6.1 Water/n-Butanol/Glycerol/Salt at constant Salt Concentration

Experimentally determined tie-lines of quaternary water/n-butanol/glycerol/salt systems at constant salt concentration and varying glycerol content are displayed in pseudo-ternary phase diagrams for NaCl or Li_2SO_4 in Figure V.37. The binary (water/n-butanol, red diamonds) and the ternary (water/n-butanol/glycerol, orange diamonds) subsystems are also pictured in the phase diagrams for comparison. For systems including NaCl and Li_2SO_4, the salt addition to the ternary system leads to an enlargement of the biphasic region (increased TLLs), which is attributed to the salting-out effect on n-butanol, as already discussed in section V.3.1. In contrast, the presence of salt only marginally influences the TLSs of the ternary subsystem without salt. D^w*(glycerol)* values obtained with NaCl, Li_2SO_4, (Phy^{5-}, $5Na^+$) and without salt are presented, depending on the glycerol feed molality in Figure V.37 c). Decreased D^w*(glycerol)* values are observed in presence of NaCl or Li_2SO_4, compared to the ternary system without salt. D^w*(glycerol)* values remain rather constant in the quaternary systems with increasing glycerol concentration. Higher D^w*(glycerol)* values compared to the ternary system without salt are obtained with (Phy^{5-}, $5Na^+$) at m(salt) = 0.8 mol/kg and m(HMF) = 1 and 2 mol/kg.

Table V-5. Investigated quaternary systems at constant salt and varying glycerol concentration at 298.15 K and 1 bar.

Salts	$m_{\mathrm{Salt}}^{\mathrm{Feed}}$ [mol/kg]	$m_{\mathrm{Glycerol}}^{\mathrm{Feed}}$ [mol/kg]	Data
NaCl	3	1.2, 2.7, 3.7, 5.7	LLE
Li_2SO_4	2	1, 2, 4, 6	LLE
(Phy^{5-}, $5Na^+$)	0.8	1, 2	D^w*(Glycerol)* values

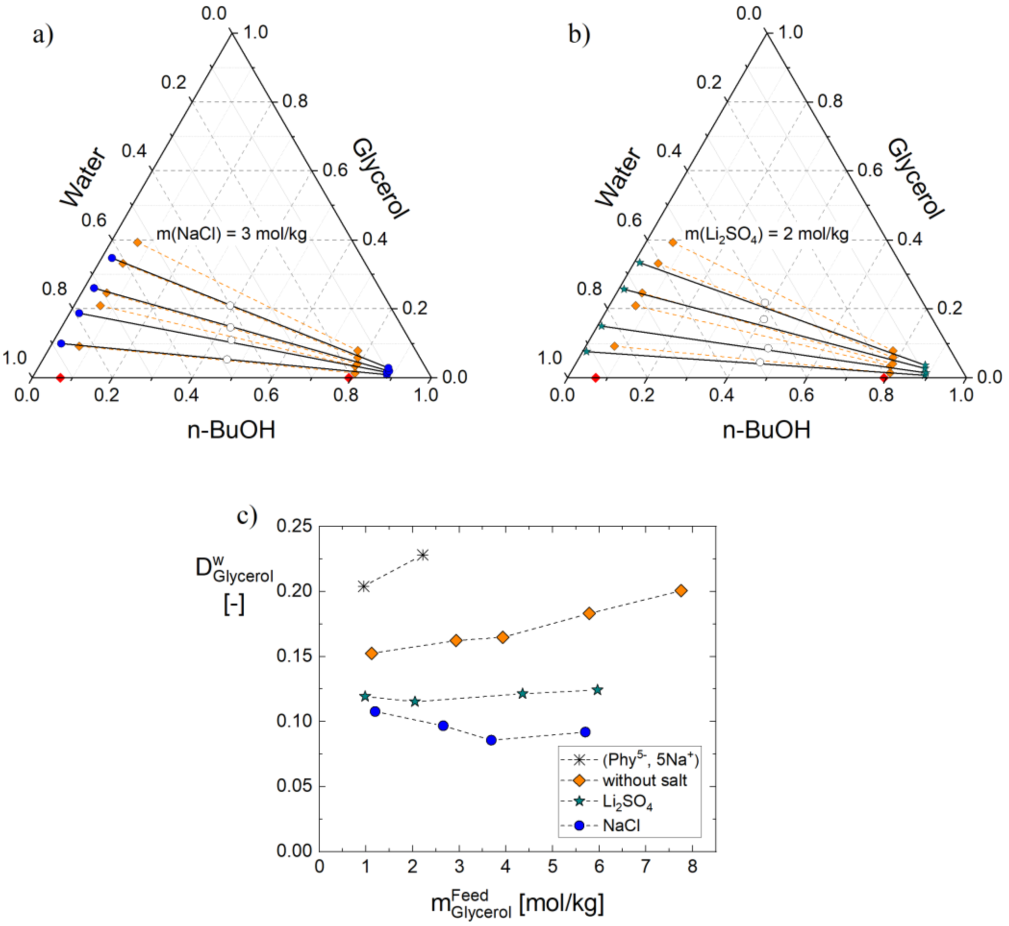

Figure V.37. LLE of quaternary water/n-butanol/glycerol/salt systems in pseudo-ternary phase diagrams in weight fractions on salt free basis at constant salt molality, 298.15 K and 1 bar: –a) (●) m(NaCl) = 3 mol/kg, –b) (★) m(Li$_2$SO$_4$) = 2 mol/kg. (—) Tie-lines of the quaternary systems, (○) initial mixture compositions, (◇) LLE and (--) tie-lines of the ternary subsystem water/n-butanol/glycerol and (◆) mutual solubility compositions of water and n-butanol. –c) Corresponding D^w*(glycerol)* values with and without salt depending on the glycerol feed molality. (✳) (Phy^{5-}, 5Na$^+$) refer to D^w*(glycerol)* values, without determination of the complete LLE.

V.3.6.2 Water/n-Butanol/Glycerol/Salt at constant Glycerol Concentration

Experimentally determined tie-lines of quaternary water/n-butanol/glycerol/salt systems at constant glycerol concentration and varying salt content are displayed in pseudo-ternary phase diagrams for NaCl or Li_2SO_4, in Figure V.38. The binary (water/n-butanol, red diamonds) and the ternary (water/n-butanol/salt, orange squares) subsystems are also pictured in the phase diagrams for comparison. In presence of glycerol, the TLLs as well as the TLSs are hardly changed, compared to the corresponding ternary subsystems water/n-butanol/salt. D^w*(glycerol)* values obtained with NaCl, Li_2SO_4, (Phy^{5-}, $5Na^+$), $Na_5P_3O_{10}$, $K_4P_2O_7$ and without salt are presented, depending on the salt feed weight fractions relative to water (Figure V.39 a)) and on the molality (Figure V.39 b)). In the ternary system water/1-butanol/glycerol without added salt, the D^w*(glycerol)* is equal to 0.16 at a glycerol molality of 4 mol/kg water. In case of NaCl and Li_2SO_4, D^w*(glycerol)* decreases with increasing salt concentration. That is, the salts have a salting-in effect on glycerol, which is more pronounced for NaCl. All used phosphate salts induce a salting-out effect on glycerol with (Phy^{5-}, $5Na^+$) being the most effective one. Due to a higher water solubility of $K_4P_2O_7$, higher D^w*(glycerol)* values can be achieved compared to (Phy^{5-}, $5Na^+$). The salt effect of $Na_5P_3O_{10}$ is limited due to its low solubility in water.

Table V-6. Investigated quaternary systems at constant glycerol and varying salt concentration at 298.15 K and 1 bar.

Salts	m_{Salt}^{Feed} [mol/kg]	$m_{Glycerol}^{Feed}$ [mol/kg]	Data
NaCl	1, 3, 5	4	LLE
Li_2SO_4	0.5, 1, 2	4	LLE
(Phy^{5-}, $5Na^+$)	0.1, 0.3, 0.6, 1.3	4	D^w*(glycerol)* values
$Na_5P_3O_{10}$	0.1, 0.2	4	D^w*(glycerol)* values
$K_4P_2O_7$	1, 3, 5	4	D^w*(glycerol)* values

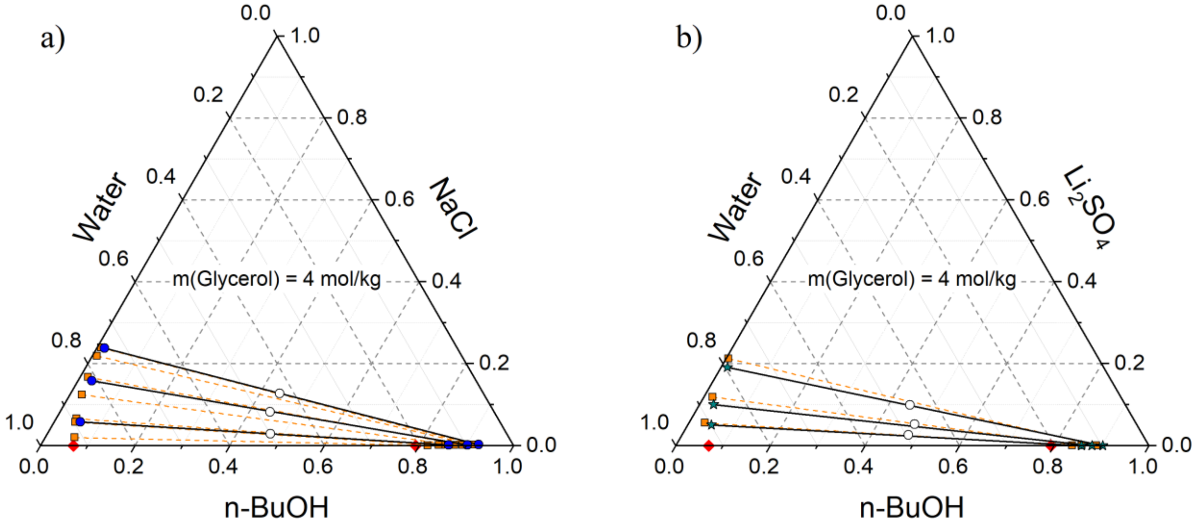

Figure V.38. LLE of quaternary water/n-butanol/glycerol/salt systems in pseudo-ternary phase diagrams in weight fractions on glycerol free basis at a constant glycerol molality (m(glycerol) = 4 mol/kg), 298.15 K and 1 bar: –a) (●) salt = NaCl, –b) (★) salt = Li_2SO_4. (—) Tie-lines of the quaternary systems, (○) initial mixture compositions, (■) LLE and (--) tie-lines of the ternary subsystem water/n-butanol/glycerol and (◆) mutual solubility compositions of water and n-butanol.

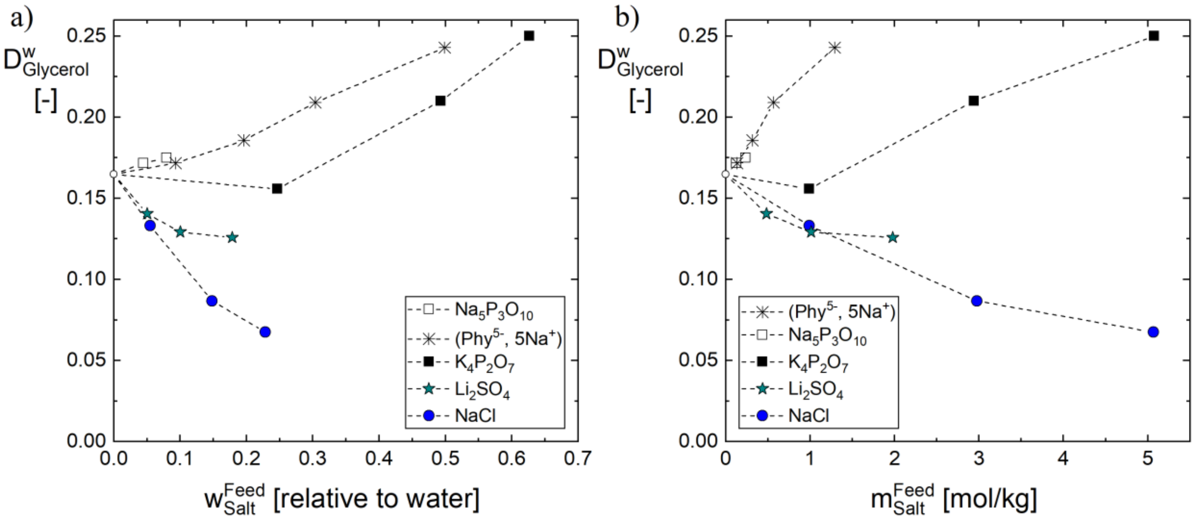

Figure V.39. D^w*(glycerol)* values at constant glycerol molality (m(glycerol) = 4 mol/kg) depending on the salt ((●) NaCl, (★) Li_2SO_4, (■) $K_4P_2O_7$, (✳) (Phy^{5-}, 5Na$^+$), (□) $Na_5P_3O_{10}$) feed concentration relative to water at 298.15 K and 1 bar. D^w*(glycerol)* values depending on –a) the salt feed weight fraction relative to water and –b) the salt feed molality. (✳) (Phy^{5-}, 5Na$^+$), (□) $Na_5P_3O_{10}$ and (■) $K_4P_2O_7$ refer to D^w*(glycerol)* values, without determination of the complete LLE.

V.3.7 Modelling results with ePC-SAFT

In this work, ePC-SAFT was used to model LLEs of the systems water/n-butanol/salt, water/n-butanol/HMF and water/n-butanol/HMF/salt. Besides the pure-component parameters for water, n-butanol, HMF and the ions (Table II-4), binary parameters for the pairs n-butanol/water, ion/water, HMF/water, HMF/ions, HMF/n-butanol, ion/ion and ion/n-butanol were applied, which are valid for all systems under consideration. The absolute average deviation (AAD) was applied for the deviation between the experimental and the modelled data points of the tie-lines:

$$AAD = \frac{1}{N_p}\sum_{k}^{TL}\sum_{m}^{2}\sum_{i}^{4}\left|w_{i,m}^{k.mod} - w_{i,m}^{k.exp}\right| \tag{V-4}$$

where $w_{i,m}^{k}$ is the mass fraction of the component *i* in the phase *m* of tie-line *k*. *TL* stands for the number of the measured tie-lines or data from literature and N_p denotes the number of data points. AAD values for the ternary water/n-butanol/salt and the water/n-butanol/HMF system are given in Table V-7 and Table V-8, respectively.

V.3.7.1 Water/n-Butanol/Salt

The salt influence on the LLE of ternary water/n-butanol/salt systems was modelled for the salts LiCl, KCl, $LiNO_3$, Li_2SO_4, Na_2SO_4 and CH_3COONa. Using ePC-SAFT, the pure-component parameters from Table II-4 and binary parameters from Table II-5 allows a satisfactory describtion of the salt effects on the LLE of water/n-butanol. ePC-SAFT accurately describes the tie-lines and the binodal curves in these systems. E.g., the high solubility of $LiNO_3$ in the n-butanol-rich phase as well as the broader miscibility gap of water/n-butanol/Na_2SO_4 compared to water/n-butanol/$LiNO_3$ were quantitatively described by ePC-SAFT.

The AAD values in Table V-7 show that the modelling results are in quantitative agreement with the experimental data. Please note that the results can be considered semi-predictive as the binary parameters between n-butanol and ions are ion-specific (Table II-5) and might be applied independently of the ions a salt is composed of.

Table V-7. AAD values between modelled and experimental equilibrium weight fractions in the system water/n-butanol/salt at 298.15 K and 1 bar.

Absolute average deviation (AAD)					
CH_3COONa	Li_2SO_4	Na_2SO_4	$LiNO_3$	KCl	LiCl
0.01793	0.0107	0.0138	0.03134	0.0132	0.0315

V.3.7.2 Water/n-Butanol/HMF

In Figure V.20, modelling results for the LLE of the ternary system water/n-butanol/HMF are compared with the experimental results at 298.15 K and 1 bar. For the modelling of the system with ePC-SAFT, binary parameters k_{ij} and l_{ij} (Table II-5) between n-butanol and HMF were fitted to LLE data of the ternary system water/n-butanol/HMF at 298.15 K and 1 bar. The binary parameters between water and HMF were fitted in a previous work to cryoscopic osmotic coefficient data at 273.15 K and LLE data of the ternary system water/MIBK/HMF at 298.15 K[419]. The modelling results with ePC-SAFT show a good agreement with experimental results with AAD of 0.0331 (LLE data used for modelling are given in Table B-2). The miscibility gap between water and n-butanol is described accurately for the system. At HMF weight fractions higher than 0.15, the miscibility gap is slightly overestimated by ePC-SAFT.

V.3.7.3 Water/n-Butanol/HMF/salt

The salt influence on the LLE of the quaternary system water/n-butanol/HMF/salt was predicted with ePC-SAFT by using the binary parameters fitted to experimental data of the binary systems water/n-butanol, water/salt, water/HMF, as well as to the ternary systems water/n-butanol/salt and water/n-butanol/HMF at 1 bar and 298.15 K. Parameters were not adjusted to LLE data (or any other data) of the quaternary water/n-butanol/HMF/salt systems considered in this work. The salts under investigation for the salt influence on the LLE of water/n-butanol were NaCl, LiCl, Li_2SO_4 and CH_3COONa. The AAD values for these LLEs are listed in Table V-8, which illustrate that the modelling results are in quantitative agreement with the experimental data. These are highly promising results, as these calculations are pure predictions without any fit of parameters to the quaternary systems water/n-butanol/HMF/salt. In Figure V.40 a), experimental and predicted $D^w(HMF)$ values of the quaternary systems water/n-butanol/HMF/salt at 298.15 K, 1 bar and constant HMF molality of 4 mol/kg are illustrated depending on the salt (LiCl, Li_2SO_4, NaCl and CH_3COONa) feed molality. The salt effects on $D^w(HMF)$ values, which were already discussed in section V.3.4, were predicted in good agreement with ePC-SAFT. The course of $D^w(HMF)$ depending on LiCl molality was also predicted qualitatively correctly with ePC-SAFT. Compared to the experimental data, the found maximum of $D^w(HMF)$ with ePC-SAFT was slightly overestimated and shifted to a lower LiCl molality, similar to that found for the quaternary system with MIBK as extractive solvent, see Figure V.40 b). The reason for this special behaviour was already investigated in a previous publication[419] for the quaternary system water/MIBK/HMF/LiCl. Strong cation/anion attractions (the formation of ion pairs) were found to strongly contribute to the salting-out on HMF from the aqueous phase. In contrast, the strongly hydrated Li^+ ions in aqueous LiCl solutions were found to cause a reduced salting-out effect on HMF, and at very high LiCl molalities even a salting-in effect was found, which is also described in section II.5.3.3. The data of this work (quaternary system water/n-butanol/HMF/LiCl) lead to the same conclusions. LiCl also causes a reduced salting-out effect on HMF from the aqueous phase at high LiCl molalities. LiCl dissociation and strong hydration prevent the formation of ion pairs. Due to the observation of this effect using two different extractive solvents (n-butanol, MIBK), it can be concluded that the qualitative influence of LiCl on the $D^w(HMF)$ values is independent of the kind of the organic solvent. However, differences in the magnitude of $D^w(HMF)$ values and the location of the $D^w(HMF)$ maximum may result from different organic solvents. Thus, besides the different HMF distribution behaviour in different extraction solvents, the salt effects are also differently pronounced with different extraction solvents. This is illustrated for the two organic solvents n-butanol and MIBK with LiCl and Li_2SO_4 as salts in Figure V.40 b). It can be seen that n-butanol leads to higher $D^w(HMF)$ values in quaternary systems with added salt, compared to those obtained with MIBK. This is probably also due to the fact that HMF preferably partitions to n-butanol than to MIBK in the ternary subsystems without salts. As the electrolytes are predominantly present in the aqueous phase and their salt-effects are qualitatively the same (with different organic solvents), it can be concluded that the different strength of the salting-out effect of one single salt depends then only on the different solubility of HMF in the organic extractive solvent.

The binary HMF/ion parameters can be considered to be valid independently of the salt, its concentration and the organic solvent used in quaternary water/organic solvent/HMF/salt systems. This is a highly promising result, because the determined parameters, by using ePC-SAFT, are transferrable to other systems (as in case of this work: HMF/ion parameters from water/MIBK/HMF/salt to water/n-butanol/HMF/salt).

Table V-8. AAD values between modelled and experimental equilibrium weight fractions in the system HMF/salt/n-butanol/water at 298.15 K and 1 bar.

Phase	Absolute average deviation (AAD)			
	CH_3COONa	Li_2SO_4	NaCl	LiCl
	m(salt) [mol/kg] = constant, m(HMF) [mol/kg] = variable			
aqueous	0.0227	0.0036	0.0184	0.0498
n-butanol	0.0102	0.0197	0.0094	0.0147
	m(HMF) [mol/kg] = constant, m(salt) [mol/kg] = variable			
aqueous	0.0252	0.0050	0.0305	0.02722
n-butanol	0.0168	0.0186	0.0094	0.06219

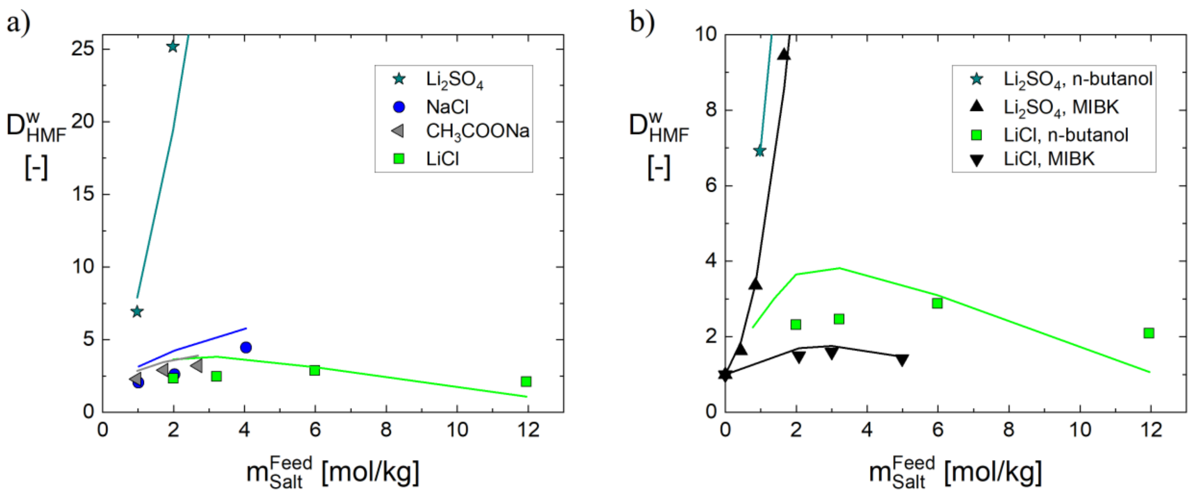

Figure V.40. $D^{w}(HMF)$ values in quaternary water/organic solvent/HMF/salt systems depending on the salt feed molality at constant HMF molality (m(HMF) = 4 mol/kg), 298.15 K and 1 bar. Symbols represent experimental data and lines are ePC-SAFT modelling results. –a) Organic solvent (n-butanol); (🟩) LiCl, (★) Li_2SO_4, (●) NaCl and (◁) CH_3COONa. –b) Comparison of $D^{w}(HMF)$ values obtained with two different organic solvents (n-butanol and MIBK); (🟩) LiCl & n-butanol, (★) Li_2SO_4 & n-butanol, (▼) LiCl & MIBK and (▲) Li_2SO_4 & MIBK.

V.3.8 Discussion

From modelling results, it was concluded that the tendency of electrolytes to form ion pairs in water promotes the salting-out effect on HMF. This proposition is contrary to the salting-out theory of preferential hydration of the ions (water withdrawal), because ion pair formation releases water molecules, which would then be available as solvent for the non-electrolyte. It is less established to deduce the salting-out effects to indirect effects like alteration of the solvent structure or the formation of ion pairs. In case of macromolecules like proteins, it is the direct interaction between ions and the peptide backbone as well as the interaction between ions and the water molecules from the first hydration shell of the macromolecule, which are decisive for a salting-in or a salting-out effect, as discussed in section II.2.4. For the salting-out of small hydrophobic solutes (like benzene or methane) the preferential hydration of the ions is still an established notion. In this context, the general question arises why LiCl is a weaker salting-out agent than NaCl and KCl, although Li^+ exhibits a higher charge density and is more strongly hydrated than Na^+ and K^+.

Theoretical studies about the salting-out process of benzene in aqueous alkali chloride solutions applying KB theory and MD simulations revealed that benzene can penetrate the first hydration shell of Li^+ without perturbing it significantly. This energetically favourable arrangement does not change the coordination number (4) of water oxygens around Li^+ compared to that in the bulk. In addition, water-mediated interaction of Li^+ with benzene was found in terms of π-electrons of benzene acting as acceptor for a hydrogen bond from water molecules of the hydration shell of Li^+. Consequently, the calculated benzene-LiCl KBIs are higher than those obtained with the other alkali chloride salts due to the water bridging interactions between the hydrated Li^+ and the benzene ring, which can be interpreted as the reason for the less pronounced salting-out effect of LiCl compared to other alkali chlorides[528]. Similar findings, were reported for interactions between hydrated Li^+ and the non-electrolytes methane and neopentane[529], although in the latter two cases, the interaction mechanisms are not identical to that observed for hydrated Li^+ and benzene.

This effect probably changes for different counteranions, e.g. for the sulphate anion. In the latter case, there will be a more pronounced competition between Li^+ and SO_4^{2-} ions for water molecules compared to Li^+ and Cl^-, which is apparent regarding the effective hydration numbers of Li^+ in aqueous solutions of LiCl ($Z_{ib}(Li^+) = 12 \pm 2$) and Li_2SO_4 ($Z_{ib}(Li^+) = 7.8 \pm 2.6$)[518]. Z_{ib} is not strictly a coordination number, but rather a measure of the influence of ions on the dynamics of the surrounding solvent molecules. Coordination numbers (water molecules in the first hydration shell) of Li^+ in aqueous LiCl solutions were found to be 4.3, 4.9 and 4.8 at LiCl molalities of 6, 3, and 1 mol/kg, respectively, and in Li_2SO_4 solutions, the coordination number at 1.5 mol/kg was found to be 5.0. These coordination numbers were inferred from neutron scattering experiments[530]. A further interesting observation of that study is the independence of the Li^+ hydration number on the ion molality up to 3m. This reflects the strong interaction between Li^+ and the first hydration shell providing a repulsive mean force between Li^+ and Cl^-, which prevents the direct ion-counterion contact due to electrostatic attraction.

Thus, in the very special case of LiCl, the strong hydration of Li^+, which hinders ion pair formation (small association constant, $K_A^0(LiCl) = 1.5\ M^{-1} \pm 1.2$), leads to a reduced salting-out effect (compared to NaCl and KCl) due to interactions of the hydrated Li^+ with the non-electrolyte, which would not be possible if ion pairing would occur. In case of Li_2SO_4, the strong salting-out effect is still reasonably explained by the strong hydration of its ions or ion pairs. The ion pairing process of Li_2SO_4 is reported to be also weakly pronounced, but higher than that of LiCl ($K_A^0(LiSO_4^-) \sim 6.4\ M^{-1} \pm 1.4$), corresponding to the formation of 2SIPs and SIPs[518]. It is therefore assumed that the less pronounced effective hydration of Li^+ and the higher tendency of ion pair formation in case of Li_2SO_4 compared to LiCl in aqueous solution are reasons for a passivation of Li^+ to interact with non-electrolytes. The association constant of $LiSO_4^-$ is basically equal to that of $NaSO_4^-$ (see section V.3.4.1.2), but the effective hydration number, extrapolated to zero electrolyte concentration, of Li_2SO_4 ($Z_{ib}^0(Li_2SO_4) = 25.5 \pm 4.6$) is higher than that of Na_2SO_4 ($Z_{ib}^0(Na_2SO_4) = 19 \pm 0.3$), which may be a reason for the higher salting-out effect of Li_2SO_4 on HMF compared to Na_2SO_4 for both extractive solvents MIBK and n-butanol at 25°C and supports the assumption of passivated Li^+ in the system containing Li_2SO_4.

This discussion above is in line with the conclusions drawn from ePC-SAFT modelling and experimentally determined *D(HMF)* values, but is contrary to the conclusions drawn from osmotic coefficients of binary water/HMF and ternary water/HMF/LiCl mixtures, for which only a small influence of the electrolytes on the HMF behaviour (chemical potential) was stated for salt molalities equal to 1m and 3m.

The difference between *D(HMF)* values obtained with LiCl and NaCl is increasing with salt molality, especially upon salt molalities higher than 3m (for both organic solvents MIBK and n-butanol), which may indicate that the effect of the hydrated Li^+ on HMF becomes increasingly significant at higher LiCl concentrations. To use the *D(HMF)* value as indicator for processes in aqueous solution is, however, only of limited significance, because of the different distribution of components, especially in case of the quaternary LLE water/n-butanol/HMF/LiCl.

The semi-ideal mixing behaviour found for ternary water/HMF/LiCl mixtures implies that the solute 1-solute 2 interactions are negligible or are mutually self-cancelling. The latter case must be true to coincide with the ability of hydrated Li^+ to interact with HMF. Following this scenario, HMF serves as a hydrogen bond acceptor from water molecules within the hydration sphere of Li^+, similar to the process described for benzene[528]. In case of HMF, even more hydrogen bond acceptor sites are present (π-electrons, oxygen free electron pairs in the ether, aldehyde and hydroxyl group). The occurrence of interactions between hydrated Li^+ and HMF must in turn reduce the interactions between HMF molecules, which is confirmed regarding correlation functions obtained from DLS measurements of ternary water/HMF/LiCl mixtures at m(HMF) = 4 mol/kg and 25°C, see Figure III.8. Here, it can be observed that the correlation functions are decreasing with increasing LiCl concentration from zero molality up to m(LiCl) = 12 mol/kg. This indicates a decreased HMF self-association with increasing LiCl concentration, as is expected for semi-ideal mixing behaviour for self-cancelling interactions.

For the explanation of the decreasing salting-out effect on HMF with increasing LiCl concentration (>6m for n-butanol) and the salting-in effect on HMF (>6m for MIBK), a different scenario must be conceived. As already discussed in section V.3.1.6, structural changes of the solution are occuring at very high salt concentrations in terms of a transition from water-electrolyte to electrolyte-water solvent[521]. Recent MD and reversed Monte Carlo (RMC) simulations[531] revealed that the Li^+ cation is surrounded by 4 oxygen atoms from water molecules in the nearest environment at a LiCl concentration of 3.74 mol/kg, which could be fitted without respecting ion pairing. But, with increasing LiCl concentration, the number of cation-anion pairs is increasing and the number of surrounding water molecules is decreasing, while the total number of neighbouring atoms around Li^+ remains 4 (oxygen and Cl^- anions together) independent of concentration. The Cl^- anions are surrounded by about 7 hydrogen atoms (from different water molecules) at low concentrations. With increasing concentration, two hydrogen atoms are replaced by one Li^+ cation. The teratrahedral structure in pure water and its hydrogen bond structure is globally broken down. Close to the solubility limit, almost all water molecules bind to two Cl^- anions *via* the hydrogen atoms and one Li^+ cation. Similar structural features were discovered by Petit et al.[532] using Car-Parrinello MD simulations at a LiCl molarity of 14 mol/L. They also found a tetrahedral configuration of the Li^+ solvation shell and observed three stable clusters: Li^+-$4H_2O$, Li^+-$(H_2O)_3Cl^-$ and Li^+-$(H_2O)_2(Cl^-)_2$. The hydration sphere around Cl^- anions was also found to be formed by strong bonds to hydrogen atoms from surrounding water molecules, but with a different coordination number of 4.4. Retrieving Collins concept of matching water affinities, Li^+ is considered as kosmotrope (water structure-maker) and Cl^- as chaotrope (water structure-breaker) and accordingly both ions avoid direct contact unless their concentration is very high. As already pointed out in the review of Yizhak Marcus and Glenn Hefter about ion pairing[533], the near surroundings of an ion at high electrolyte concentrations (e.g in molten salt hydrates) must include both water molecules and at least one counterion resulting in ion pair formation. SIPs and CIPs are present merely due to geometrical causes, before any consideration of electrostatic attraction. Although Harsányi and Pusztai[534] claimed that no ion pairs are present in LiCl solutions even at high concentrations based on investigations using RMC, in a more recent study[535] of the same researchers, it was shown that water oxygen and anions partially occupy sites in the environment of the cation, which indicates the occurrence of CIPs and possibly the formation of clusters in highly concentrated LiCl solutions. Experimental evidence for LiCl ion pairs are given by neutron scattering[536], dieletric relaxation spectroscopy[518] and raman spectroscopy[537]. At such high LiCl concentrations discussed here, the intermolecular water structure is certainly affected, which was shown e.g. by neutron diffraction in LiCl solution[538]. It was reported that in 10m LiCl solution, the number of hydrogen bonds is about 70% lower than in pure water. Consequently, physical properties of the solution will change, such as the static dielectric constant (ε_0), which was found to decrease from 79.2 at zero LiCl molality down to 21.4 at LiCl molality of 13.4 mol/kg[539]. In the frequency range of 45MHz to 20 GHz, the dielectric response is due to free water molecules and the response of bound water occurs at lower frequencies and is not observed. A model, which describes the liquid, composed of free water, hydrated single ions and hydrated ion pairs is used to analyse the static dielectric data and is appropriate for concentrations below 5.1m. Dielectric properties below 5.1m are dominated by free water molecules and water molecules within the hydration shells were assumed not to contribute. Consequently, with increasing ion concentration, as more and more water molecules form hydration shells, ε_0 decreases due to the loss of free water. Above 5.1m, the solution can no longer be seen as multicomponent liquid but has rather glasslike properties, in which the free water molecules no longer interact dominantly with each other. The solution at high LiCl concentration was considered to be a network of interpenetrating cages of ions, ion pairs and water molecules. Lyashchenko[521] suggested a model for the structural and molecular-kinetic changes from dilute to concentrated electrolyte solutions. In the first concentration region, ions and complexes are present in the normal water structure. In a narrow transition region, ionic ion-water clusters and at very high concentrations polymeric melt structures are assumed. The structural transitions are attributed to a decrease in electrostatic hydration and an abrubt decrease of ε_0 at high electrolyte concentrations. Such a strong decrease in ε_0 is connected with a decrease in polarity of the solvent. These suggested changes in the solvent structure are quite similar to what was found and thus confirmed later by MD simulations of Pethes[531] and Petit et al.[532] described above.

The decreased *D(HMF)* values observed above 6m LiCl may thus be attributed to the altered structure and property (decreased ε_0 and polarity) of the aqueous phase combined with the ability of hydrated Li^+ to interact with HMF. If no more free water molecules are present in the aqueous phase, it is conceivable that HMF molecules participate to the clusters formed at high LiCl concentration in water and partition back from the organic to the “aqueous phase”. In this regard, the conclusions made from ePC-SAFT modelling must not be generalised, because the mechanism for the decreasing salting-out or even salting-in effect on HMF with increasing salt concentration depends on the nature of the electrolyte and the related solvent properties of the electrolyte solution. Such an atypical behaviour was observed only in the very special case of LiCl.

For further investigations, it would be interesting to study the effect of $MgCl_2$ on *D(HMF)* values depending on the salt concentration. Mg^{2+} has even a higher charge density than Li^+ and also exhibits a second hydration shell. A relatively high effective hydration number of Mg^{2+} at infinite dilution ($Z_{ib}^0(Mg^{2+}) = 20 \pm 1$) and a small association constant ($\log K_A^0(MgCl^+) = 0.5\ M^{-1} \pm 0.2$) were found for $MgCl_2$ in water[540]. In addition and also similarly to LiCl, glasslike behaviour as well as a strong decrease of ε_0 were observed in aqueous $MgCl_2$ solution at high concentrations[541]. Maybe similar effects to those observed for LiCl at high concentrations become apparent using $MgCl_2$ as salting-out agent for HMF.

To verify whether ion pair formation promotes the salting-out effect on HMF from the aqueous phase, $ZnCl_2$ could be tested as salting-out agent. Pronounced ion pair formation between Zn^{2+} and Cl^- in terms of very stable CIPs with partly covalent character was reported for $ZnCl_2$ in aqueous solutions[542].

V.3.9 Influence of Solvent on the HMF Distribution

As already mentioned in the introduction of this chapter, different LLE data of ternary and quaternary systems containing HMF are obtainable from literature. Here, only the influence of solvents on the HMF extraction perfomance from the aqueous phase is evaluated in absence of salts. The limitation to ternary systems is justified by qualitatively similar salt-effects found in quaternary systems with different organic solvents. Another reason is that in other works no feed concentrations or no uniform salt concentrations were chosen for the investigation of quaternary systems. In Figure V.41, $D^w(HMF)$ and $\alpha^w(HMF, water)$ values of ternary water/organic solvent/HMF systems are compared, depending on the HMF feed molality. The values were calculated from LLE data obtainable from literature. $D^w(HMF)$ values are decreasing with increasing HMF content, as already described in section V.3.3.1, except for n-butanol (Dalmolin et al.[502]) and n-hexanol (Cavalcanti et al.[505]), for which maxima are observed. Neglecting data for n-butanol (doubted) and 2-butanol (low maximum HMF feed concentration), both from Dalmolin et al., the series for the solvents driving to the highest $D^w(HMF)$ values is: n-pentanol > n-butanol > 2-pentanol > MIBK > n-hexanol > n-heptanol. Accordingly, the series for $\alpha^w(HMF, water)$ values is: MIBK > n-pentanol > n-hexanol > 2-pentanol > n-heptanol > n-butanol. This presentation shows that $D^w(HMF)$ and $\alpha^w(HMF, water)$ values are opposed to a certain extent. E.g., MIBK shows low $D^w(HMF)$ values, but very high $\alpha^w(HMF, water)$ values, which is due to the very low solubility of water in MIBK. Another advantage of MIBK is the large biphasic area in the ternary phase diagram water/MIBK/HMF[419], providing a high maximum HMF feed concentration in the extraction system. On the other hand, n-butanol shows quite high $D^w(HMF)$ values, but very low $\alpha^w(HMF, water)$ values, which is due to the relatively high solubility of water in n-butanol (~ 20 wt%). In this context, n-pentanol seems to be a good compromise, providing high $D^w(HMF)$ values, combined with high $\alpha^w(HMF, water)$ values. This indicates that n-pentanol is superior to n-butanol for HMF extraction from the aqueous phase. Higher alcohols than n-pentanol bear no benefits, due to low $D^w(HMF)$ as well as low $\alpha^w(HMF, water)$ values. Similarly, secondary alcohols are less effective extractive solvents for HMF. This solvent evaluation highlights n-pentanol, showing good extraction performance in terms of capacity and selectivity. Thus, studies of the salt effects in the ternary water/n-pentanol/HMF system would be an interesting contribution.

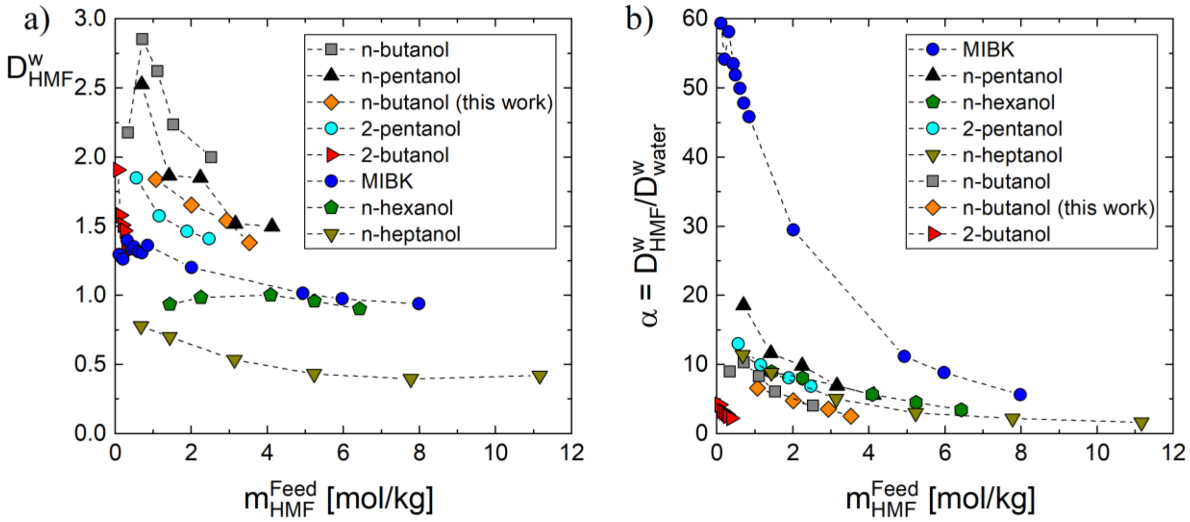

Figure V.41. –a) $D^{w}(HMF)$ values and –b) $\alpha^{w}(HMF,water)$ values of ternary water/organic solvent/HMF systems depending on the HMF feed molality at 298.15 K and 1 bar. Organic solvents: (■) n-butanol[502], (▲) n-pentanol[505], (◆) n-butanol (this work), (●) 2-pentanol[502], (▶) 2-butanol[502], (●) MIBK[419], (⬟) n-hexanol[505], (▼) n-heptanol[505].

V.4 Conclusion

In this chapter, LLE data of biphasic ternary water/n-butanol/salt, water/n-butanol/HMF and water/n-butanol/glycerol as well as quaternary water/n-butanol/HMF/salt and quaternary water/n-butanol/glycerol/salt systems were experimentally determined at 298.15 K and 1 bar. In addition, LLE data of the quaternary system water/n-butanol/HMF/Na_2SO_4 were determined also at 303.15 K and 1 bar.

For the investigation of ternary LLE data of water/n-butanol/salt systems, the following salts were used: NaCl, KCl, Na_2SO_4, Li_2SO_4, $LiNO_3$, NH_4NO_3, CH_3OOLi, CH_3COONa, C_2H_5COONa and C_3H_7COONa. The gained LLE data were applied to construct salting-out diagrams for n-butanol. By comparing chloride, sulphate, nitrate and acetate salts in molality scale, the salting-out effect on n-butanol from the aqueous phase increases in the following order: $NH_4^+ < Li^+ < Na^+$. For chloride salts, K^+ has an effect similar to that of Na^+. The salting-out effect of C_1 to C_3 carboxylates decreases with a higher number of carbon atoms. For C_2H_5COONa, even a salting-in effect was detected at a high salt concentration. If salts with equal cations are compared (e.g. for lithium or sodium salts), it turns out that the influence of anions on the n-butanol solubility in the aqueous phase is more pronounced than that of the cations. The anions are therefore dominating the salt effects in mixed aqueous organic solvent systems with added salt. For the numerical comparison of the salting-out effects of the different salts, a modified *Setchenov* correlation was applied on mole fraction scale. Calculated *Setchenov* constants K_s for the aqueous phase were considered for the evaluation of the strength of salting-out effect on n-butanol from the aqueous phase. The most detailed anion series is obtained for sodium salts, which is more or less transferrable to the other cations. In mole fraction scale the strength of the salting-out effect of anions is detected in the following order: $NO_3^- < C_3H_7COO^- < C_2H_5COO^- < CH_3COO^- < Cl^- \leq Br^- < SO_4^{2-}$ with the most salting-out anion on the right. For sodium salts, this trend of K_s values matches with the *Setchenov* constants reported for the salting-out of benzene from water[276], except for NaBr. The influence of salts on the binary LLE of water/n-butanol was further investigated by the evolution of the TLLs. Salt addition leads to extended tie-lines and similar trends are obtained as for *Setchenov* plots in the corresponding aqueous phases. For the TLLs of lithium salts, also very similar curves to those obtained by the *Setchenov* plots in the corresponding organic phases are observed.

The ternary system water/n-butanol/HMF exhibits a relatively small biphasic region for the LLEx application. At an HMF concentration of approximately 20 wt%, the miscibility gap between water and n-butanol disappears. HMF distributes, however preferably to the organic phase indicated by $D^w(HMF)$ values higher than unity and positive TLSs. With increasing HMF concentration, TLSs increase, while $D^w(HMF)$ values decrease. The affinity of HMF towards the n-butanol-rich phase may be enhanced due to the relatively large amount of water in the organic branch of the binodal curve. Higher $D^w(HMF)$ values were reported from Dalmolin et al.[502], compared to those measured in this work. Own values are recommended due to multiple experimental confirmation. The critical point was found at the composition of w(n-butanol) = 0.26, w(HMF) = 0.19, w(water) = 0.55. The LLE of the ternary system water/HMF/n-butanol were reasonably reproduced by COSMO-RS calculations with renormalisation of LLE (correction factor) using the COSMO*therm*X 17 and COSMObase-1701.

Quaternary LLE of water/n-butanol/HMF/salt systems were investigated using the following salts: LiCl, NaCl, KCl, Na_2SO_4, Li_2SO_4, $Al_2(SO_4)_3$, NH_4NO_3, CH_3COONa and C_2H_5COONa. Additional $D^w(HMF)$ values were measured for C_3H_7COONa and (Phy^{5-}, $5Na^+$). Salt addition to the ternary water/n-butanol/HMF system leads to an enlargement of the biphasic region (increased TLLs), which is related to the salting-out effect on n-butanol. At a constant salt molality, also the TLSs and $D^w(HMF)$ values are increasing for all salts, except NH_4NO_3, for which reduced $D^w(HMF)$ values and almost horizontally aligned tie-lines were observed. Reduced $D^w(HMF)$ values were also measured for C_3H_7COONa. At m(salt) = 3 mol/kg, the strength of the salting-out effect, rated by the $D^w(HMF)$ values, increases in the order: LiCl < KCl < CH_3COONa ≈ NaCl, which is again in accordance to the *Setchenov* constants found for benzene[276]. For these salts, the $D^w(HMF)$ values are enhanced, compared to the ternary without salts, but remain rather constant with increasing HMF content. In contrast, $D^w(HMF)$ values increase with increasing HMF content in case of a constant sulphate salt concentration, which indicates a very strong salting-out effect. The series for the sulphate salts is: Na_2SO_4 < $Al_2(SO_4)_3$ < Li_2SO_4 with Li_2SO_4 driving to the highest $D^w(HMF)$ values. The organic salt, (Phy^{5-}, $5Na^+$) shows also a very strong salting-out effect on HMF, as $D^w(HMF)$ values also increase with increasing HMF concentration, but at a constant salt concentration. At a constant HMF molality of 4 mol/kg and varying salt concentrations, the overall series for the salting-out efficiency, rated by the highest achieved $D^w(HMF)$ value independently of the

salt concentration scale, can be written as:
NH_4NO_3 < LiCl < KCl < CH_3COONa ≈ NaCl < Na_2SO_4 < $Al_2(SO_4)_3$ < Li_2SO_4 < (Phy^{5-}, $5Na^+$). Regarding sodium salts, the anion series: CH_3COO^- ≈ Cl^- < SO_4^{2-} can be observed, which is in line with the *Setchenov* constants reported for e.g. benzene[276] and more or less with the *direct* Hofmeister series. A specific salt-effect was observed for LiCl, for which an increasing salting-out behaviour up to m(salt) = 6 mol/kg was observed and, upon higher salt concentration, the strength of the salting-out effect was reduced. In general, the influence of salts on D^w*(HMF)* values is qualitatively equal to that observed on α^w*(HMF,water)* values. The LLE data of the quaternary system water/n-butanol/HMF/Na_2SO_4 determined at 303.15 K, revealed D^w*(HMF)* and α^w*(HMF,water)* values, which are even superior to those obtained with Li_2SO_4 at 298.15 K.

Glycerol preferably distributes to the aqueous phase in ternary water/n-butanol/glycerol mixtures and thus, n-butanol is not an appropriate solvent for glycerol separation from the aqueous phase. Quaternary LLE of water/n-butanol/glycerol/salt systems were investigated using NaCl and Li_2SO_4 as salt. Further, D^w*(glycerol)* values were measured for $Na_5P_3O_{10}$, $K_4P_2O_7$ and (Phy^{5-}, $5Na^+$). In case of constant salt molality m(NaCl) = 3 mol/kg and m(Li_2SO_4) = 2 mol/kg, decreased D^w*(glycerol)* values were detected, compared to the ternary system without salt, which stay rather constant with increasing glycerol concentration. Higher D^w*(glycerol)* values were obtained with (Phy^{5-}, $5Na^+$) at m(salt) = 0.8 mol/kg and m(HMF) = 1 and 2 mol/kg. At constant glycerol molality m(glycerol) = 4 mol/kg, D^w*(glycerol)* was found to decrease with increasing NaCl or Li_2SO_4 molality. In contrast, D^w*(glycerol)* increased with increasing salt molality for $Na_5P_3O_{10}$, $K_4P_2O_7$ and (Phy^{5-}, $5Na^+$). Due to the highest water solubility, addition of $K_4P_2O_7$ allowed for the highest D^w*(glycerol)* values. Although a salting-out effect on glycerol of the latter three salts was observed, the D^w*(glycerol)* values remained far below unity.

Modelling results with ePC-SAFT for the ternary systems water/n-butanol/salts, water/n-butanol/HMF and the quaternary systems water/n-butanol/HMF/salts were in quantitative agreement with the experimental data. The results for the ternary systems water/n-butanol/salts were considered to be semi-predictive, because the binary parameters between n-butanol and ions are ion-specific and applicable to different salts, independently of the ion combination in the individual salts. For the ternary water/n-butanol/HMF system, ePC-SAFT slightly overestimated the miscibility gap at HMF weight fractions higher than

0.15. The LLE of quaternary water/n-butanol/HMF/salts systems were modelled by ePC-SAFT using binary parameters of the subsystems. No parameter fitting to experimental LLE data of the quaternary systems were performed. It could be concluded that ePC-SAFT allows for prediction of the quaternary LLE data and thus for predictions of the salt influence on the distribution behaviour of HMF in these systems. These are promising results, as the binary HMF/ion parameters are transferrable to systems with other organic extractive solvents, are valid for all salts of arbitrarily combined ions and they are independent of the salt concentration. Modelling results revealed that salts, which have a propensity to from ion pairs in aqueous solution like sulphates and acetates, show a pronounced salting-out effect on HMF. In contrast, salts, which contain strongly hydrated ions like Li^+ in aqueous LiCl solutions, reduce the strength of the salting-out effect or even lead to a salting-in effect at high salt concentrations. The strong hydration of Li^+ results in LiCl dissociation even at high salt concentrations and thus prevents the formation of ion pairs.

However, the conclusions from modelling results must not be generalised, because the decreasing salting-out or even salting-in effect on HMF with increasing LiCl concentration may be caused by interactions between the hydrated Li^+ and the non-electrolyte as well as by changes of the solvent properties (decreased ε_0 and polarity) at high salt concentrations. LiCl is thus a very special case, which is not suitable to derive general conclusions. Further studies on the distribution behaviour of HMF between two separated liquid phases with $MgCl_2$ and $ZnCl_2$ as salting-out agents are suggested.

The best combination (in thermodynamic sense) of organic solvent and salt for HMF extraction from the aqueous phase can be predicted. The combination of n-butanol and Li_2SO_4 was suggested, due to very high distribution ratios obtained by this combination. However, separation factors matter as well. In this regard, the extractive solvents MIBK and n-pentanol seem to be favourable.

Chapter VI

Summary and Outlook

This work was subdivided in three main parts: properties and characterisation of aqueous HMF mixtures in Chapter III, salting-in and salting-out effects in water/DPnP and water/ethanol mixtures in Chapter IV and liquid-liquid equilibrium in Chapter V.

In Chapter III, the focus was set on osmotic coefficients in binary water/HMF and ternary water/HMF/salt mixtures (salt = LiCl or NaCl). Osmometric data were used to calculate activity coefficients of HMF in binary and ternary mixtures as well as of salts in ternary mixtures. The isodesmic asscociation model was applied to calculate an association constant for HMF in water. Osmotic coefficents in binary mixtures decrease with increasing HMF concentration. Although this negative deviation from ideal behaviour indicates molecular association of HMF in water, the association tendency is not very pronounced. This statement is based on the high HMF concentrations, at which the decrease of the osmotic coefficients gets significant, the low association constant, calculated from the isodesmic model and the low correlation functions obtained from DLS. Osmotic coefficents in ternary mixtures decrease also with increasing HMF concentration and increase with increasing salt concentration. For LiCl, the increase is higher than for NaCl. A good approximation of osmotic coefficents in ternary systems was realised by the ZSR-mixing rule, which is based on semi-ideal mixture behaviour. Concurrently, it was shown that the osmolalities of the corresponding binary solutions are additive. For ternary water/HMF/LiCl mixtures, it is assumed that interactions between LiCl and HMF are occurring on the cost of HMF self-interactions.

The activity coefficents of HMF in water are low and decrease exponentially with increasing HMF concentration. In the presence of electrolytes (NaCl, LiCl), activity coefficents of HMF decrease nearly linearly, which is in accordance to the Long-McDevit equation. A small influence of electrolytes on the HMF activity coefficents in aqueous solution was observed, which is conform to the ZSR-mixing rule. MIACs of LiCl and NaCl increase at a background salt molality of 1 mol/kg and decrease at a background salt molality of 3 mol/kg with increasing HMF content. The MIACs of LiCl are higher than those of NaCl and are similar to those in the corresponding binary water/salt systems. The higher MIACs of LiCl and the increase with increasing salt concentration are related to a pronounced hydration of the Li^+ cation.

The calculation of activity coefficents in ternary systems was perfomed with a relatively low amount of data points. For a more robust fitting procedure and enhanced accuracy, the number of data points should be increased by investigation of an extended concentration range of HMF and especially of the salt. An independent method for the determination of MIACs in ternary mixtures, e.g., conductivity measurements, would also support the studies.

Further investigations of aqueous HMF mixtures were DR-13 solubilisation experiments and surface tension measurements. Results of both studies indicate a co-solvent character of HMF. Low signals from DLS point to only weak association, which is conform to the co-solvent character. To clearly distinguish between co-solvents and hydrotropes, the investigation of the structuring in the ternary mixtures (e.g. water/HMF/DR-13) would be required.

In Chapter IV, salting-in and salting-out effects of different inorganic and organic compounds on the LST in water/DPnP were presented. A salting-out effect was observed for inorganic sulphate and phosphate salts, short carboxylate sodium salts, amino-acids, quaternary ammonium salts and typical sugars, whereas a salting-in effect was observed for short organic acids, sweeteners and the antagonistic salt (Ph_4PCl). Independently of a salting-in or salting-out effect, a nearly linear relationship between the evolution of the LST and the additive concentration was detected. Among the organic additives, pentasodium phytate (Phy^{5-}, $5Na^+$) showed the most pronounced salting-out, while Ph_4PCl showed the most pronounced salting-in effect. The strength of the salting-out effect for sulphate salts decreased in the order: $Al_2(SO_4)_3 > Na_2SO_4 > Li_2SO_4 > (NH_4)_2SO_4$ and for phosphate salts in the order: $Na_4P_2O_7 > Na_5P_3O_{10} > K_4P_2O_7$. These series are in accordance with S*etchenov* constants found for sulphate salts and for individual cations with other organic solutes ($CHCl_3$, benzene and chlorobenzene) to be salted-out from the aqueous phase. A similar salting-out effect could be noted for $Al_2(SO_4)_3$ and $Na_4P_2O_7$.

The strengths of the salting-in effect of short organic acids and that of the salting-out effect of short organic carboxylate salts were related to the number of functional groups within the molecular structures. The most salting-in acid (citric acid) corresponds to the most salting-out carboxylate salt (trisodium citrate).

The salting-out effect of amino acids is weakly specific, except that of monosodium L-glutamate, which is most pronounced due to its two carboxylic functions and that of L-cysteine, which is least pronounced due the thiol group within its chemical structure.

The effects found for quaternary ammonium salts were of similar magnitude, compared to those of amino-acids and they were also only slightly specific. TMAO was most effective in decreasing the LST, while triethylphenylammonium chloride was least effective.

Sweetners caused a non-specific salting-in effect. The decrease of the LST by the addition of sugars was related to the "sugaring-out" effect. The strength of the sugaring-out effect was deduced to the number of OH-groups being present in the sugar molecules. For glucose, fructuose, xylitol and sorbitol, similar effects were noted, while a pronounced sugaring-out effect was observed for isomalt with its nine alcoholic functions. The six phosphate functions within (Phy^{5-}, $5Na^+$) lead to the most pronounced salting-out effect of all tested organic additives in the water/DPnP mixtures.

Ethanol separation from water using $(NH_4)_2SO_4$ showed the best performance at low concentrations. (Phy^{5-}, $5Na^+$) and $K_4P_2O_7$ are more soluble in water than $(NH_4)_2SO_4$ and allowed an enhanced separation of ethanol from water at higher salt concentrations. The most water-soluble agent $K_4P_2O_7$ turned out to be even more efficient than (Phy^{5-}, $5Na^+$).

Generally, the strengths of the salting-out effects in the water/DPnP and water/ethanol systems were deduced to the ability of the additive to bind water molecules (hydration).

It is conceivable to use the water/DPnP mixture as hydrotropic cloud-point extraction (HCPE) system for the separation of HMF from water. If this strategy is pursued, the co-solvent properties of HMF in the water/DPnP system have to be investigated. This could be done by monitoring the evolution of the LST by the addition of different amounts of HMF. In a next step, salting-out compounds could be added to influence the distribution behaviour of HMF between the water-rich and the DPnP-rich phase. In HCPE systems, the extraction process can additionally be controlled by the temperature, e.g. mixing could be applied at lower temperature, at which the system is monophasic, while phase separation and settling could be achieved at higher temperatures (but still moderate). However, the high boiling point of DPnP (bp = 213°C) is unfavourable for solvent regeneration.

In Chapter V, LLE data of various ternary and quaternary systems have been determined. These systems contain interesting product molecules for white biotechnology, which are n-butanol, HMF and glycerol. Ternary systems were water/n-butanol/salt, water/n-butanol/HMF and water/n-butanol/glycerol and quaternary systems were water/n-butanol/HMF/salt and water/n-butanol/glycerol/salt. All LLE data were determined at 298.15 K and 1 bar and for the quaternary system water/n-butanol/HMF/Na_2SO_4 additional LLE data were determined at 303.15 K.

For the investigation of ternary water/n-butanol/salt LLE data, the following salts: NaCl, KCl, Na_2SO_4, Li_2SO_4, $LiNO_3$, NH_4NO_3, CH_3OOLi, CH_3COONa, C_2H_5COONa and C_3H_7COONa

were used. The influence of anions on the n-butanol solubility in water was more pronounced compared to that of the cations. A modified *Setchenov* correlation was applied to evaluate the salt effects on mole fraction scale and for sodium salts, the strength of the salting-out effects followed the anions series: $NO_3^- < C_3H_7COO^- < C_2H_5COO^- < CH_3COO^- < Cl^- \leq Br^- < SO_4^{2-}$. Similar trends were found by the evaluation of the TLLs.

The ternary system water/n-butanol/HMF gets monophasic at an HMF concentration of approximately 20 wt%. $D^w(HMF)$ values are higher than unity, but decrease with increasing HMF content. Similarly, the TLLs are decreasing with increasing HMF content. The high water content in the organic phases may be a reason for the affinity of HMF towards the organic phase. The critical point was found at w(n-butanol) = 0.26, w(HMF) = 0.19, w(water) = 0.55. The LLE of the ternary system water/HMF/n-butanol were reasonably predicted by COSMO-RS calculations.

Quaternary LLE of water/n-butanol/HMF/salt systems were investigated using the following salts: LiCl, NaCl, KCl, Na_2SO_4, Li_2SO_4, $Al_2(SO_4)_3$, NH_4NO_3, CH_3COONa and C_2H_5COONa. Additional $D^w(HMF)$ values were reported for C_3H_7COONa and (Phy^{5-}, $5Na^+$). At m(salt) = 3 mol/kg, the strength of the salting-out effect on HMF increases in the order: LiCl < KCl < $CH_3COONa \approx$ NaCl. For sulphate salts at constant concentration, $D^w(HMF)$ values increase with increasing HMF content, which indicates a very strong salting-out effect.The series for the sulphate salts is: $Na_2SO_4 < Al_2(SO_4)_3 < Li_2SO_4$. A very strong salting-out effect on HMF was also detected for (Phy^{5-}, $5Na^+$).

At m(HMF) = 4 mol/kg, the salting-out effect on HMF increased in the following order: $NH_4NO_3 < LiCl < KCl < CH_3COONa \approx NaCl < Na_2SO_4 < Al_2(SO_4)_3 < Li_2SO_4 < (Phy^{5-}, 5Na^+)$. A maximum of $D^w(HMF)$ was detected for LiCl at m(salt) = 6 mol/kg. Upon higher salt concentration, the strength of the salting-out effect was reduced. The same trends observed for $D^w(HMF)$ were found for $\alpha^w(HMF,water)$. At 303.15 K, Na_2SO_4 was even more effective than Li_2SO_4 at 298.15 K.

In most cases the observed salting-out trends match very well with reported *Setchenov* constants for the salting-out of benzene[276] and the anion series is more or less conform to the *direct* anion Hofmeister series.

In ternary water/n-butanol/glycerol mixtures, $D^w(glycerol)$ values were far below unity and even decreased by NaCl or Li_2SO_4 addition, i.e. the salts have a salting-in effect on glycerol. In contrast, phosphate salts induced a salting-out effect on glycerol with (Phy^{5-}, $5Na^+$) being most effective. Due to a higher water solubility of $K_4P_2O_7$, even higher $D^w(glycerol)$ values could be achieved, compared to those obtained with (Phy^{5-}, $5Na^+$). The use of $Na_5P_3O_{10}$ was limited due to its low solubility. Despite a salting-out effect on glycerol, $D^w(glycerol)$ values remain far below unity. The only opportunity to separate glycerol *via* LLEx from the aqueous phase is its derivatisation into a more hydrophobic molecule. An alternative to LLEx for glycerol separation is the membrane separation method.

Modelling results with ePC-SAFT were in quantitative agreement with the experimental data. Results for water/n-butanol/salts were considered to be semi-predictive, due to ion-specific binary n-butanol/ion parameters, which are applicable to different salts. The miscibility gap in the ternary water/n-butanol/HMF was slightly overestimated by ePC-SAFT. Quaternary water/n-butanol/HMF/salts systems were modelled by ePC-SAFT with parameters of the subsystems and no fitting to experimental LLE data of the quaternary systems was done. In this respect, ePC-SAFT allowed the prediction of quaternary LLE data. This result is very useful, as binary HMF/ion parameters could be applied for other extraction systems with other organic solvents and arbitrary salts, for which ion parameters are available. In addition, the parameters were independent of the salt concentration. From the modelling results it appeared that salts, which form ion pairs in aqueous solution like sulphates and acetates, show a pronounced salting-out effect on HMF, while salts, which contain strongly hydrated ions like Li^+ in aqueous LiCl solutions, reduce the strength of the salting-out effect or even lead to a salting-in effect at high salt concentrations. LiCl is, however, a very special case, because interactions between the hydrated Li^+ and HMF are assumed to influence the salting-out effect. In addition, changes of the solvent properties at very high LiCl concentrations certainly affect the distribution behaviour of HMF between both phases. LiCl is thus not a suitable candidate to derive general rules for salts regarding their salting-out or salting-in effects. To prove the conclusions made from ePC-SAFT modelling, the salting-out agents $MgCl_2$ and $ZnCl_2$ are suggested for further investigations.

The best combination of organic solvent and salt for HMF extraction from the aqueous phase could be predicted. The combination of n-butanol and Li_2SO_4 was suggested due to very high distribution ratios obtained by this combination. However, separation factors matter as well. In this regard, the extractive solvents MIBK and n-pentanol seem to be favourable. In this regard, it would be interesting to systematically study the salt effects on the LLE of the ternary water/n-pentanol/HMF system.

The ePC-SAFT model and the corresponding model-parameters were used to develop a LLE-calculation tool, which could then be provided to companies. That work was done by Ulrich Westhaus (DECHEMA) and by the company *Supren*. The software package is useful for solvent and salt screening. To compare performance differences of extractions with and without salt, three performance indicators were defined for each scenario. These were the theoretical stages, the solvent and the primary energy requirement. With the exemplary system water/n-butanol/HMF/NaCl, it was shown that a significant reduction of solvent (38%) and primary energy (39%) requirement relative to the system without salt (100%) could be achieved by salt addition. The number of the theoretical stages however remained constant (n = 3).

Appendix

A Aqueous HMF Mixtures

Osmotic data of binary water/HMF and ternary water/HMF/salt systems

Table A-1. HMF molalities m_1, associated isopiestic NaCl molalities m_{Ref} from reference [344], water activities a_s and osmotic coefficients ϕ_1^0 of the binary system water/HMF at 298.15 K and 975 hPa. Relative standard deviations were used to account for the confidence intervals of m_{Ref}, a_s and ϕ_1^0.

m_1^0 [mol/kg]	m_{Ref} [mol/kg]	a_s	ϕ_1^0
0.496	0.228 ± 0.003	0.992 ± 0.014	0.850 ± 0.012
0.991	0.392 ± 0.005	0.987 ± 0.013	0.730 ± 0.010
1.483	0.511 ± 0.007	0.983 ± 0.013	0.635 ± 0.009
1.980	0.613 ± 0.008	0.980 ± 0.013	0.572 ± 0.008
2.473	0.696 ± 0.009	0.977 ± 0.013	0.522 ± 0.007
2.967	0.739 ± 0.010	0.976 ± 0.013	0.462 ± 0.006
3.459	0.823 ± 0.011	0.973 ± 0.013	0.442 ± 0.006
3.950	0.841 ± 0.011	0.972 ± 0.013	0.396 ± 0.005
4.444	0.900 ± 0.012	0.970 ± 0.013	0.378 ± 0.005
4.935	0.977 ± 0.013	0.968 ± 0.013	0.370 ± 0.005

u(T) = $1*10^{-3}$ K, u(p) = 7 hPa, u(m_1^0) = 0.001 mol/kg

Table A-2. Activity Coefficients of HMF in water at 298.15 K and 975 hPa.

m_1^0 [mol/kg]	γ_1^0
0.5	0.712 ± 0.016
1.0	0.549 ± 0.014
1.5	0.443 ± 0.013
2.0	0.368 ± 0.012
2.5	0.314 ± 0.011
3.0	0.273 ± 0.010
3.5	0.242 ± 0.010
4.0	0.217 ± 0.010
4.5	0.198 ± 0.009
5.0	0.182 ± 0.009

u(T) = $1*10^{-3}$ K, u(p) = 7 hPa, u(m_1^0) = 0.001 mol/kg

Table A-3. HMF molalities m_1, salt molalities m_2, associated isopiestic NaCl molalities m_{Ref} from reference[344] water activities a_s and osmotic coefficients $\phi_{1,2}$ of the ternary systems water/HMF/NaCl and water/HMF/LiCl at 298.15 K and 975 hPa. Relative standard deviations were used to account for the confidence intervals of m_{Ref}, a_s and ϕ_1^0.

m_1 [mol/kg]	m_2 [mol/kg]	m_{Ref} [mol/kg]	a_s	$\phi_{1,2}$
NaCl background molality m_2 = 1 mol/kg				
0.990	0.9985	1.318 ± 0.013	0.956 ± 0.009	0.838 ± 0.008
1.980	0.9983	1.527 ± 0.015	0.949 ± 0.009	0.737 ± 0.007
2.967	0.9975	1.725 ± 0.017	0.942 ± 0.009	0.674 ± 0.007
3.950	0.9955	1.905 ± 0.018	0.935 ± 0.009	0.628 ± 0.006
4.933	0.9946	1.980 ± 0.019	0.932 ± 0.009	0.562 ± 0.005
NaCl background molality m_2 = 3 mol/kg				
0.992	2.9970	3.075 ± 0.030	0.890 ± 0.009	0.924 ± 0.009
1.980	2.9929	3.329 ± 0.032	0.880 ± 0.008	0.891 ± 0.009
2.967	2.9909	3.458 ± 0.033	0.875 ± 0.008	0.831 ± 0.008
3.951	2.9864	3.739 ± 0.036	0.863 ± 0.008	0.825 ± 0.008
4.935	2.9848	3.808 ± 0.037	0.860 ± 0.008	0.768 ± 0.007
LiCl background molality m_2 = 1 mol/kg				
0.991	0.9989	1.439 ± 0.014	0.952 ± 0.009	0.920 ± 0.009
1.979	0.9979	1.723 ± 0.017	0.942 ± 0.009	0.840 ± 0.008
2.966	0.9974	1.901 ± 0.018	0.935 ± 0.009	0.750 ± 0.007
3.950	0.9958	1.970 ± 0.019	0.933 ± 0.009	0.651 ± 0.006
4.929	0.9940	2.049 ± 0.020	0.930 ± 0.009	0.584 ± 0.006
LiCl background molality m_2 = 3 mol/kg				
0.991	2.9965	3.816 ± 0.037	0.8595 ± 0.008	1.203 ± 0.012
1.979	2.9930	3.970 ± 0.038	0.8530 ± 0.008	1.108 ± 0.011
2.967	2.9910	4.133 ± 0.040	0.8459 ± 0.008	1.038 ± 0.010
3.950	2.9864	4.122 ± 0.040	0.8464 ± 0.008	0.933 ± 0.009
4.927	2.9799	4.175 ± 0.040	0.8441 ± 0.008	0.864 ± 0.008
u(T) = 1*10^{-3} K, (u)p = 7 hPa, u(m_1) = 0.001 mol/kg, u(m_2) = 0.0002 mol/kg				

Table A-4. Approximation of $D = \Delta/(m_1 m_2)$ with Eq. (III-28), N = 10, for ternary systems water/HMF/NaCl or LiCl at 298.15 K and 975 hPa.

m_1 [mol/kg]	m_2 [mol/kg]	D^{obs}	D^{calc}	$(x-x_i)^2$	$\sum(x-x_i)^2$ / St. dev.
		NaCl			
0.990	0.9985	-0.0908	-0.10420	0.00018	
1.980	0.9983	-0.0362	-0.01796	0.00033	
2.967	0.9975	0.0279	0.03567	0.00006	
3.950	0.9955	0.0685	0.05222	0.00026	
4.933	0.9946	0.0463	0.05009	0.00002	
0.992	2.9970	-0.1782	-0.16601	0.00015	
1.980	2.9929	-0.0475	-0.06842	0.00044	
2.967	2.9909	-0.0223	-0.01514	0.00005	
3.951	2.9864	0.0307	0.03034	0.00000	
4.935	2.9848	0.0234	0.02550	0.00000	0.00149 / 0.013
		LiCl			
0.991	0.9989	-0.0017	-0.01470	0.00027	
1.979	0.9979	0.0925	0.06791	0.00061	
2.966	0.9974	0.1027	0.09718	0.00003	
3.950	0.9958	0.0647	0.08435	0.00039	
4.929	0.9940	0.0457	0.04007	0.00003	
0.991	2.9965	-0.0052	-0.01673	0.00013	
1.979	2.9930	0.0023	0.02224	0.00040	
2.967	2.9910	0.0248	0.01439	0.00011	
3.950	2.9864	0.0002	0.00721	0.00005	
4.927	2.9799	-0.0019	-0.00691	0.00003	0.00205 / 0.015

Table A-5. Activity coefficients of HMF (γ_1) and NaCl (γ_2) in ternary water/HMF/NaCl solutions with NaCl background molality of m_2 = 1 and 3 mol/kg at 298.15 K and 975 hPa.

m_1 [mol/kg]	γ_1, m_2 = 1 mol/kg	γ_1, m_2 = 3 mol/kg	γ_2, m_2 = 1 mol/kg	γ_2, m_2 = 3 mol/kg
1.0	n.s.	0.381	0.613	0.636
2.0	n.s.	0.322	0.597	0.584
3.0	n.s.	0.276	0.603	0.546
4.0	n.s.	0.234	0.622	0.515
5.0	n.s.	0.191	0.646	0.481

Table A-6. Activity coefficients of HMF (γ_1) and LiCl (γ_2) in ternary water/HMF/LiCl solutions with LiCl background molality of m_2 = 1 and 3 mol/kg at 298.15 K and 975 hPa.

m_1 [mol/kg]	γ_1, m_2 = 1 mol/kg	γ_1, m_2 = 3 mol/kg	γ_2, m_2 = 1 mol/kg	γ_2, m_2 = 3 mol/kg
1.0	n.s.	0.533	0.764	1.108
2.0	n.s.	0.393	0.782	1.051
3.0	n.s.	0.292	0.816	0.972
4.0	n.s.	0.213	0.855	0.863
5.0	n.s.	0.150	0.886	0.725

Density Data

Table A-7. Densities of binary water/HMF mixtures at 298.15 K and 1 bar.

m [mol/kg]	ρ [g/cm^3]	
0	0.9970	[419]
0.0200	0.9976	[419]
0.0498	0.9984	[419]
0.0997	0.9998	[419]
0.1996	1.0025	[419]
0.2972	1.0048	[419]
0.4298	1.0087	[419]
0.4994	1.0105	[419]
1.9867	1.0435	this work
2.9681	1.0613	this work
4.0121	1.0760	this work
4.9931	1.0889	this work

DR-13 Solubilisation Data

Table A-8. Relative optical densities (O.D.) of ternary water/HMF/DR-13 mixtures and calculated amounts of solubilised DR-13 in ppm (w/w).

m(HMF) [mol/kg]	c(HMF) [mol/L]	relative O.D.	ppm (w/w) of solubilised DR-13
0.1034	0.1020	0.0198	0.25
0.2513	0.2444	0.0656	0.82
0.5082	0.4824	0.1643	2.06
0.9996	0.9071	0.5769	7.23
2.0228	1.6824	2.4510	30.70
2.9976	2.3090	5.4506	68.28
4.0309	2.8771	10.1595	127.27
4.9822	3.3269	14.5480	182.25

Surface Tension Data

Table A-9. Experimentally determined surface tensions of aqueous HMF solutions at 296 ± 1 K. HMF concentrations are given in molality and molarity.

m(HMF) [mol/kg]	c(HMF) [mol/L]	σ [mN/m]
0.0000	0.0000	72.40
0.0214	0.0212	70.36
0.0259	0.0258	69.96
0.0518	0.0514	69.91
0.0854	0.0844	69.23
0.1040	0.1026	68.68
0.1716	0.1682	67.41
0.2099	0.2050	67.10
0.3510	0.3382	63.49
0.4316	0.4127	61.93
0.7327	0.6812	59.88
0.9051	0.8283	57.23
1.5832	1.3657	52.68
1.9762	1.6498	50.00
3.7573	2.7353	41.78
4.9115	3.2957	37.68

B LLE Data

LLE of ternary water/n-butanol/salt systems

Table B-1. Experimental equilibrium weight fractions in the ternary systems water/n-butanol/salt at 298.15 K and 1 bar for the salts NaCl, KCl, $LiNO_3$, NH_4NO_3, Li_2SO_4, Na_2SO_4, CH_3COOLi, CH_3COONa, C_2H_5COONa and C_3H_7COONa.

aqueous phase			n-butanol-rich phase			TLL	TLS
water	n-butanol	salt	water	n-butanol	salt	0.7223	0
NaCl							
0.9173	0.0629	0.0198	0.1817	0.8179	0.0005	0.7552	-2.56%
0.8966	0.0462	0.0572	0.1572	0.8419	0.0009	0.7977	-7.07%
0.8854	0.0434	0.0655	0.1527	0.8462	0.0011	0.8054	-8.03%
0.8498	0.0260	0.1242	0.1240	0.8745	0.0015	0.8573	-14.46%
0.8151	0.0178	0.1671	0.1071	0.8954	0.0016	0.8931	-18.87%
0.7746	0.0107	0.2200	0.0861	0.9122	0.0018	0.9275	-24.21%
0.7517	0.0092	0.2391	0.0798	0.9184	0.0019	0.9396	-26.09%
KCl							
0.9025	0.0545	0.0419	0.1672	0.8298	0.0008	0.7764	-5.30%
0.8788	0.0437	0.0775	0.1506	0.8468	0.0012	0.8068	-9.50%
0.8295	0.0278	0.1426	0.1261	0.8723	0.0016	0.8562	-16.70%
0.7537	0.0127	0.2359	0.0963	0.9010	0.0017	0.9186	-26.36%
$LiNO_3$							
0.8582	0.0578	0.0788	0.1748	0.8160	0.0092	0.7614	-9.18%
0.7876	0.0425	0.1699	0.1605	0.8103	0.0292	0.7805	-18.33%
0.7146	0.0321	0.2533	0.1520	0.7949	0.0531	0.7887	-26.25%
0.6482	0.0235	0.3235	0.1429	0.7774	0.0798	0.7922	-32.33%
NH_4NO_3							
0.8755	0.0643	0.0602	0.1766	0.8234	0.0000	0.7615	-7.93%
0.6824	0.0362	0.2814	0.1203	0.8712	0.0085	0.8786	-32.69%
0.5382	0.0207	0.4412	0.0940	0.8900	0.0160	0.9678	-48.91%
0.4536	0.0136	0.5328	0.0745	0.9002	0.0253	1.0216	-57.23%

Continued

Li_2SO_4							
0.9060	0.0344	0.0549	0.1613	0.8339	0.0002	0.8013	-6.84%
0.8615	0.0191	0.1186	0.1417	0.8582	0.0002	0.8474	-14.11%
0.7897	0.0057	0.2144	0.1108	0.8891	0.0001	0.9090	-24.26%
Na_2SO_4							
0.8877	0.0300	0.0823	0.1691	0.8308	0.0001	0.8050	-10.25%
0.8700	0.0231	0.1060	0.1613	0.8369	0.0002	0.8206	-13.01%
0.8563	0.0189	0.1251	0.1546	0.8452	0.0002	0.8357	-15.12%
0.8347	0.0138	0.1514	0.1492	0.8506	0.0001	0.8504	-18.08%
CH_3COOLi							
0.8446	0.0374	0.1180	0.1327	0.8674	0.0054	0.8376	-13.56%
0.8032	0.0295	0.1632	0.1224	0.8694	0.0081	0.8542	-18.47%
0.6912	0.0181	0.2932	0.0955	0.8924	0.0178	0.9166	-31.50%
CH_3COONa							
0.8713	0.0425	0.0863	0.1655	0.8330	0.0015	0.7952	-10.89%
0.8262	0.0306	0.1431	0.1367	0.8612	0.0024	0.8424	-16.95%
0.7861	0.0233	0.1906	0.1188	0.8787	0.0033	0.8757	-21.89%
0.7385	0.0194	0.2420	0.1073	0.8886	0.0041	0.9011	-27.37%
C_2H_5COONa							
0.8583	0.0462	0.0955	0.1578	0.8382	0.0040	0.7973	-11.55%
0.7949	0.0349	0.1702	0.1454	0.8427	0.0119	0.8232	-19.60%
0.6130	0.1527	0.2343	0.3849	0.4572	0.1579	0.3139	-25.09%
C_3H_7COONa							
0.9102	0.0668	0.0230	0.1926	0.8060	0.0015	0.7394	-2.91%
0.8901	0.0644	0.0454	0.1920	0.8041	0.0038	0.7409	-5.63%
0.8748	0.0582	0.0670	0.1983	0.7944	0.0073	0.7386	-8.11%
0.8589	0.0566	0.0845	0.2028	0.7844	0.0128	0.7313	-9.85%

Standard uncertainties u are u(w^{aq}(water)) = 0.0044, u(w^{org}(water)) = 0.0012), u(w^{aq}(n-butanol) = 0.0001, u(w^{org}(n-butanol)) = 0.0040, u(w^{aq}(salt)) = 0.0006, u(w^{org}(salt)) = 0.0001 and the combined expanded uncertainty Uc is Uc(w) = 0.0097 (for 0.95 level of confidence).

LLE of ternary water/n-butanol/HMF and water/n-butanol/glycerol systems

Table B-2. Experimental equilibrium weight fractions in the ternary system water/n-butanol/HMF at 298.15 K and 1 bar.

aqueous phase			n-butanol-rich phase			TLL	TLS
water	n-butanol	HMF	water	n-butanol	HMF	0.7223	0
Water/n-Butanol/HMF (for PC-SAFT modelling)							
0.8908	0.0831	0.0261	0.1814	0.7702	0.0484	0.6875	3.25%
0.8638	0.0982	0.0380	0.1877	0.7400	0.0723	0.6427	5.34%
0.8317	0.1093	0.0590	0.2245	0.6730	0.1025	0.5654	7.72%
0.8235	0.0989	0.0777	0.2552	0.6127	0.1321	0.5167	10.59%
0.7753	0.1277	0.0970	0.2796	0.5758	0.1446	0.4506	10.62%
0.7418	0.1342	0.1240	0.3038	0.5077	0.1886	0.3790	17.30%
0.7173	0.1448	0.1379	0.3531	0.4470	0.1999	0.3085	20.52%
Water/n-Butanol/HMF							
0.8778	0.0825	0.0414	0.2454	0.6788	0.0761	0.5974	5.83%
0.8296	0.0951	0.0767	0.2890	0.5799	0.1269	0.4874	10.35%
0.7767	0.1180	0.1087	0.3391	0.4944	0.1675	0.3810	15.63%
0.7206	0.1413	0.1326	0.3933	0.4214	0.1834	0.2847	18.14%

Standard uncertainties u are $u(w^{aq}(\text{water})) = 0.0068$, $u(w^{org}(\text{water})) = 0.0037)$, $u(w^{aq}(\text{n-butanol}) = 0.0011$, $u(w^{org}(\text{n-butanol})) = 0.0050$, $u(w^{aq}(\text{HMF})) = 0.0000$, $u(w^{org}(\text{HMF})) = 0.0001$ and the combined expanded uncertainty U_c is $U_c(w) = 0.0136$ (for 0.95 level of confidence).

Table B-3. Experimental equilibrium weight fractions in the ternary system water/n-butanol/glycerol at 298.15 K and 1 bar.

aqueous phase			n-butanol-rich phase			TLL	TLS
water	n-butanol	glycerol	water	n-butanol	glycerol	0.7223	0
Water/n-Butanol/Glycerol							
0.8369	0.0711	0.0920	0.1844	0.8016	0.0140	0.7347	-10.68%
0.7246	0.0657	0.2097	0.1738	0.7922	0.0340	0.7474	-24.18%
0.6909	0.0632	0.2459	0.1650	0.7945	0.0405	0.7596	-28.09%
0.5952	0.0595	0.3253	0.1557	0.7913	0.0595	0.7786	-36.32%
0.5402	0.0672	0.3928	0.1448	0.7764	0.0788	0.7756	-44.28%

Standard uncertainties u are $u(w^{aq}(\text{water})) = 0.0055$, $u(w^{org}(\text{water})) = 0.0024)$, $u(w^{aq}(\text{n-butanol}) = 0.0009$, $u(w^{org}(\text{n-butanol})) = 0.0045$, $u(w^{aq}(\text{glycerol})) = 0.0002$, $u(w^{org}(\text{glycerol})) = 0.0001$ and the combined expanded uncertainty U_c is $U_c(w) = 0.0110$ (for 0.95 level of confidence).

LLE of quaternary water/n-butanol/HMF/salt systems

Table B-4. Experimental equilibrium weight fractions for the quaternary systems water/n-butanol/HMF/salt at 298.15 K and 1 bar for the salts LiCl, NaCl, KCl, Li_2SO_4, Na_2SO_4, $Al_2(SO_4)_3$, CH_3COONa, C_2H_5COONa and for water/n-butanol/HMF/Na_2SO_4 at 303.15 K and 1 bar.

aqueous phase				n-butanol-rich phase			
water	n-butanol	HMF	salt	water	n-butanol	HMF	salt
LiCl, m(HMF) = 4 mol/kg							
0.7368	0.0429	0.1089	0.1113	0.1939	0.5202	0.2678	0.0189
0.7005	0.0302	0.0981	0.1712	0.1718	0.5154	0.2818	0.0397
0.6011	0.0198	0.1070	0.2704	0.1680	0.5110	0.2237	0.0950
LiCl, m(Salt) = 3 mol/kg							
0.8205	0.0323	0.0360	0.1112	0.1349	0.7744	0.0807	0.0100
0.7983	0.0354	0.0598	0.1065	0.1547	0.6846	0.1487	0.0120
0.7549	0.0441	0.1009	0.1001	0.1937	0.5481	0.2404	0.0177
NaCl, m(HMF) = 4 mol/kg							
0.7602	0.0550	0.1199	0.0650	0.2253	0.5359	0.2457	0.0066
0.7523	0.0326	0.1001	0.1151	0.1774	0.5603	0.2615	0.0075
0.7208	0.0146	0.0660	0.1987	0.1234	0.5934	0.2933	0.0082
NaCl, m(Salt) = 3 mol/kg							
0.8008	0.0197	0.0243	0.1558	0.1174	0.7971	0.0827	0.0028
0.7580	0.0212	0.0659	0.1549	0.1486	0.6292	0.2188	0.0065
0.7249	0.0231	0.0958	0.1561	0.1695	0.4824	0.3558	0.0122
KCl, m(HMF) = 4 mol/kg							
0.7330	0.0653	0.1199	0.0818	0.2275	0.5292	0.2351	0.0081
0.7234	0.0377	0.1021	0.1368	0.1796	0.5699	0.2418	0.0088
0.6540	0.0387	0.0886	0.2188	0.1366	0.6021	0.2519	0.0094
KCl, m(Salt) = 3 mol/kg							
0.7581	0.0217	0.0293	0.1909	0.1214	0.7957	0.0799	0.0029
0.7280	0.0210	0.0505	0.2005	0.1288	0.7228	0.1435	0.0049
0.6922	0.0247	0.0896	0.1935	0.1510	0.5885	0.2510	0.0095
0.6628	0.0292	0.1253	0.1827	0.1802	0.4740	0.3298	0.0159

Continued

Li_2SO_4, m(HMF) = 4 mol/kg							
0.8094	0.0163	0.0412	0.1291	0.1868	0.5276	0.2853	0.0003
0.7642	0.0041	0.0124	0.2194	0.1416	0.5467	0.3115	0.0001
0.7451	0.0027	0.0086	0.2470	0.1279	0.5740	0.3085	0.0001
Li_2SO_4, m(Salt) = 2 mol/kg							
0.7841	0.0055	0.0068	0.1975	0.1212	0.7709	0.1079	0.0001
0.7724	0.0047	0.0094	0.2067	0.1292	0.6885	0.1822	0.0001
0.7658	0.0040	0.0124	0.2126	0.1411	0.5649	0.2939	0.0001
Na_2SO_4, m(HMF) = 4 mol/kg							
0.8011	0.0598	0.0930	0.0462	0.2711	0.4898	0.2382	0.0010
0.8023	0.0409	0.0587	0.0982	0.2338	0.5135	0.2520	0.0008
0.7975	0.0197	0.0370	0.1458	0.2126	0.5299	0.2570	0.0005
Na_2SO_4, m(Salt) = 0.5 mol/kg							
0.8617	0.0329	0.0241	0.0813	0.1841	0.7316	0.0841	0.0002
0.8388	0.0324	0.0409	0.0880	0.2012	0.6459	0.1525	0.0003
0.8223	0.0329	0.0529	0.0919	0.2164	0.5757	0.2073	0.0005
0.8023	0.0409	0.0587	0.0982	0.2338	0.5135	0.2520	0.0008
$Al_2(SO_4)_3$, m(Salt) = 0.5 mol/kg							
0.8042	0.0133	0.0140	0.1684	0.1910	0.6730	0.1359	0.0001
0.7923	0.0114	0.0187	0.1776	0.2098	0.5723	0.2178	0.0001
0.7782	0.0108	0.0203	0.1906	0.2217	0.4921	0.2861	0.0002
0.7709	0.0079	0.0198	0.2014	0.2305	0.4241	0.3452	0.0002
CH_3COONa, m(HMF) = 4 mol/kg							
0.7511	0.0627	0.1041	0.0820	0.2416	0.5100	0.2385	0.0099
0.7362	0.0451	0.0893	0.1294	0.2007	0.5267	0.2603	0.0123
0.7014	0.0341	0.0886	0.1726	0.1747	0.5395	0.2838	0.0159
CH_3COONa, m(Salt) = 1.75 mol/kg							
0.8101	0.0352	0.0288	0.1277	0.1480	0.7675	0.0824	0.0039
0.7831	0.0383	0.0459	0.1251	0.1629	0.6954	0.1324	0.0064
0.7583	0.0402	0.0697	0.1300	0.1809	0.5978	0.2177	0.0097
0.7368	0.0433	0.0907	0.1292	0.1933	0.5592	0.2290	0.0118

Continued

CH_3COONa, m(Salt) = 3 mol/kg							
0.7364	0.0230	0.0252	0.2154	0.1223	0.7896	0.0853	0.0027
0.7258	0.0254	0.0452	0.2037	0.1337	0.7044	0.1524	0.0095
0.7186	0.0279	0.0622	0.1913	0.1470	0.6360	0.2118	0.0051
0.7001	0.0294	0.0748	0.1957	0.1557	0.5758	0.2540	0.0144
C_2H_5COONa, m(Salt) = 1 mol/kg							
0.8147	0.0521	0.0329	0.1003	0.1889	0.7305	0.0742	0.0064
0.7770	0.0610	0.0620	0.1000	0.2201	0.6436	0.1341	0.0022
0.7481	0.0777	0.0931	0.0810	0.2645	0.5430	0.1838	0.0086
0.6797	0.1102	0.1295	0.0806	0.3243	0.4429	0.2137	0.0190
NH_4NO_3, m(HMF) = 4 mol/kg							
0.5465	0.0678	0.1431	0.2426	0.1971	0.5503	0.2036	0.0490
0.4443	0.0394	0.1386	0.3777	0.1335	0.5890	0.2146	0.0629
0.3719	0.0291	0.1372	0.4618	0.1127	0.5962	0.2378	0.0533
NH_4NO_3, m(Salt) = 5 mol/kg							
0.6323	0.0390	0.0392	0.2895	0.1389	0.7152	0.0729	0.0730
0.6004	0.0463	0.0773	0.2760	0.1536	0.6443	0.1054	0.0967
0.5784	0.0546	0.1113	0.2557	0.1744	0.5562	0.1542	0.1152
0.5465	0.0678	0.1431	0.2426	0.1971	0.5503	0.2036	0.0490
Na_2SO_4, m(HMF) = 4 mol/kg, T = 303.15 K							
0.8065	0.0234	0.0581	0.1120	0.2153	0.5216	0.2631	0.0000
0.8001	0.0128	0.0274	0.1597	0.1892	0.5309	0.2799	0.0000
0.7232	0.0028	0.0084	0.2656	0.1547	0.5527	0.2926	0.0000

Standard uncertainties u are u(w^{aq}(water)) = 0.0049, u(w^{org}(water)) = 0.0017), u(w^{aq}(n-butanol) = 0.0005, u(w^{org}(n-butanol)) = 0.0033, u(w^{aq}(salt)) = 0.0012, u(w^{org}(salt)) = 0.0002, u(w^{aq}(HMF)) = 0.0001, u(w^{org}(HMF)) = 0.0003 and the combined expanded uncertainty U_c is U_c(w) = 0.0097 (for 0.95 level of confidence).

LLE of quaternary water/n-butanol/glycerol/salt systems

Table B-5. Experimental equilibrium weight fractions in the quaternary systems water/n-butanol/glycerol/salt at 298.15 K and 1 bar for the salts NaCl, Li_2SO_4.

aqueous phase				n-butanol-rich phase			
water	n-butanol	glycerol	salt	water	n-butanol	glycerol	salt
NaCl, m(Glycerol) = 4 mol/kg							
0.6607	0.0412	0.2548	0.0433	0.1319	0.8322	0.0339	0.0019
0.6068	0.0221	0.2531	0.1180	0.0944	0.8818	0.0219	0.0018
0.5683	0.0126	0.2377	0.1815	0.0720	0.9096	0.0160	0.0024
NaCl, m(Salt) = 3 mol/kg							
0.7591	0.0195	0.0857	0.1357	0.1064	0.8827	0.0092	0.0017
0.6903	0.0206	0.1641	0.1250	0.1030	0.8793	0.0159	0.0019
0.6320	0.0215	0.2298	0.1144	0.0954	0.8831	0.0197	0.0018
0.5589	0.0230	0.3100	0.1082	0.0932	0.8764	0.0285	0.0019
Li_2SO_4, m(Glycerol) = 4 mol/kg							
0.6843	0.0386	0.2384	0.0387	0.1377	0.8288	0.0335	0.0000
0.6668	0.0231	0.2331	0.0771	0.1170	0.8528	0.0301	0.0000
0.6214	0.0112	0.2181	0.1493	0.0947	0.8778	0.0275	0.0000
Li_2SO_4, m(Salt) = 2 mol/kg							
0.7517	0.0074	0.0624	0.1785	0.1007	0.8918	0.0074	0.0000
0.7089	0.0082	0.1267	0.1563	0.0944	0.8910	0.0146	0.0000
0.6366	0.0111	0.2242	0.1281	0.0908	0.8820	0.0272	0.0000
0.5755	0.0122	0.2945	0.1177	0.0851	0.8783	0.0366	0.0000

Standard uncertainties u are $u(w^{aq}(\text{water})) = 0.0061$, $u(w^{org}(\text{water})) = 0.0020)$, $u(w^{aq}(\text{n-butanol}) = 0.0004$, $u(w^{org}(\text{n-butanol})) = 0.0037$, $u(w^{aq}(\text{salt})) = 0.0015$, $u(w^{org}(\text{salt})) = 0.0003$, $u(w^{aq}(\text{glycerol})) = 0.0002$, $u(w^{org}(\text{glycerol})) = 0.0004$ and the combined expanded uncertainty U_c is $U_c(w) = 0.0097$ (for 0.95 level of confidence).

Distribution Ratios and Separation Factors

Table B-6. Distribution ratios D^w*(HMF)* and separation factors α^w*(HMF, water)* of HMF and glycerol in ternary water/n-butanol/product systems without salt at 298.15 K and 1 bar.

Water/n-Butanol/HMF		
m(HMF) [mol/kg]	D^w(HMF)	α^w(HMF, water)
1.0705	1.8382	6.5751
2.0104	1.6545	4.7494
2.9339	1.5409	3.5295
3.5295	1.3831	2.5341

Water/n-Butanol/Glycerol		
m(glycerol) [mol/kg]	D^w(glycerol)	α^w(glycerol, water)
1.1210	0.1524	0.6918
2.9296	0.1623	0.6768
3.9339	0.1648	0.6901
5.7843	0.1831	0.6998
7.7552	0.2006	0.7482

Table B-7. HMF distribution ratios $D^w(HMF)$, HMF separation factors $\alpha^w(HMF, water)$, TLL and TLS for the quaternary water/n-butanol/HMF/salt systems at m(HMF) = 4 mol/kg, 298.15 K and 1 bar and for the water/n-butanol/HMF/Na_2SO_4 system at m(HMF) = 4 mol/kg, 303.15 K and 1 bar.

m(salt) [mol/kg]	D^w(HMF)	α^w(HMF, water)	TLL	TLS
LiCl				
3.2175	2.4586	9.3409	0.6689	-14.99%
5.9937	2.8718	11.707	0.6889	-20.02%
11.954	2.0897	7.4738	0.6631	-28.33%
NaCl				
1.0134	2.0488	6.9122	0.6389	-10.27%
2.0330	2.6130	11.080	0.7254	-16.47%
4.0425	4.4425	25.950	0.8278	-25.09%
KCl				
1.0339	1.9607	6.3162	0.6231	-13.32%
1.9637	2.3686	9.6446	0.7236	-19.65%
3.0112	2.8016	12.845	0.7846	-26.35%
3.9669	2.8439	13.615	0.7956	-29.83%
Li_2SO_4				
0.9734	6.9188	29.986	0.7356	-18.64%
1.9779	24.113	130.12	0.8231	-28.00%
2.4740	35.739	207.17	0.8521	-30.56%
Na_2SO_4				
0.1987	2.5617	7.5699	0.5791	-8.60%
0.4876	4.2950	14.740	0.6513	-16.06%
0.7761	6.9456	26.061	0.7089	-21.75%
CH_3COONa				
0.9692	2.2906	7.1206	0.6049	-13.11%
1.7336	2.9149	10.693	0.6744	-18.94%
2.6891	3.2049	12.870	0.7214	-24.00%

Continued

NH_4NO_3				
4.9500	1.4229	3.9446	0.6508	-36.22%
10.0836	1.5487	5.1557	0.7901	-50.88%
14.8875	1.7330	5.7167	0.8814	-62.18%
Na_2SO_4, T = 303.15 K				
0.4967	4.5274	16.9568	0.6933	-17.42%
1.0001	10.2015	43.1408	0.7425	-22.67%
1.9850	34.8966	163.1015	0.8232	-34.41%

Table B-8. HMF distribution ratios $D^{w}(HMF)$, HMF separation factors $\alpha^{w}(HMF, water)$, TLL and TLS for the quaternary water/n-butanol/HMF/salt systems at a constant salt molality, 298.15 K and 1 bar.

m(HMF) [mol/kg]	D^{w}(HMF)	α^{w}(HMF, water)	TLL	TLS
LiCl, m(Salt) = 3 mol/kg				
1.0354	2.2431	13.641	0.7470	5.50%
2.0257	2.4868	12.832	0.6586	12.79%
3.9424	2.3837	9.2893	0.5260	26.07%
NaCl, m(Salt) = 3 mol/kg				
1.0019	3.4091	23.254	0.7779	6.99%
3.0695	3.3205	16.934	0.6225	23.35%
5.9776	3.7126	15.877	0.5109	53.07%
KCl, m(Salt) = 3 mol/kg				
0.9389	2.7323	17.057	0.7725	5.71%
2.0218	2.8418	16.069	0.7048	11.58%
4.0221	2.8016	12.845	0.5813	25.25%
5.7680	2.6320	9.6782	0.4816	40.77%
Li_2SO_4, m(Salt) = 2 mol/kg				
1.0641	15.778	102.07	0.7705	12.99%
2.0222	19.309	115.34	0.7035	24.94%
3.9501	23.747	128.72	0.6251	49.68%
Na_2SO_4, m(Salt) = 0.5 mol/kg				
0.9945	3.4887	16.327	0.6983	8.32%
2.0006	3.7329	15.559	0.6201	17.65%
3.0060	3.9162	14.880	0.5600	27.63%
3.8864	4.2950	14.740	0.5045	39.94%

Continued

$Al_2(SO_4)_3$, m(Salt) = 0.5 mol/kg				
1.0162	9.6893	40.798	0.6677	18.12%
1.9889	11.6236	43.891	0.5916	34.92%
2.9621	14.0672	49.386	0.5453	54.52%
3.9671	17.4371	58.318	0.5238	77.36%
CH_3COONa, m(Salt) = 1.75 mol/kg				
0.9077	2.8588	15.646	0.7305	6.81%
1.7799	2.8847	13.870	0.6627	12.28%
2.8795	3.1232	13.089	0.5706	24.96%
3.6126	2.5247	9.6233	0.5358	24.84%
CH_3COONa, m(Salt) = 3 mol/kg				
1.0104	3.3833	20.370	0.7644	7.01%
1.9666	3.3740	18.315	0.6862	14.30%
3.0152	3.4066	16.650	0.6199	22.49%
3.9869	3.3963	15.269	0.5719	30.08%
C_2H_5COONa, m(Salt) = 1 mol/kg				
0.9961	2.2556	9.7280	0.6784	5.63%
1.9787	2.1623	7.6345	0.5810	11.35%
2.9845	1.9741	5.5830	0.4708	18.15%
3.9529	1.6505	3.4590	0.3405	23.22%
NH_4NO_3, m(Salt) = 5 mol/kg				
1.0102	1.8585	8.4599	0.7170	3.27%
1.9836	1.3639	5.3325	0.6495	1.53%
2.9886	1.3856	4.5966	0.5559	4.46%
3.9301	1.4229	3.9446	0.4898	5.14%

Table B-9. Glycerol distribution ratios D^w*(glycerol),* glycerol separation factors α^w*(glycerol, water),* TLL and TLS in quaternary water/n-butanol/glycerol/salt systems at m(glycerol) = 4 mol/kg, 298.15 K and 1 bar for the salts NaCl, Li_2SO_4.

m(salt) [mol/kg]	D^w(glycerol)	α^w(glycerol, water)	TLL	TLS
NaCl				
0.9893	0.1332	0.6671	0.8081	-6.96%
2.9743	0.0867	0.5572	0.8859	-17.90%
5.0663	0.0675	0.5326	0.9380	-25.95%
Li_2SO_4				
0.4828	0.1404	0.6981	0.8085	-6.29%
1.0129	0.1292	0.7360	0.8552	-11.84%
1.9799	0.1259	0.8254	0.9086	-21.50%

Table B-10. Glycerol distribution ratios D^w*(glycerol),* glycerol separation factors α^w*(glycerol, water),* TLL and TLS in quaternary water/n-butanol/glycerol/salt systems at constant salt molality, 298.15 K and 1 bar for the salts NaCl, Li_2SO_4.

m(glycerol) [mol/kg	D^w(glycerol)	α^w(glycerol, water)	TLL	TLS
NaCl, m(Salt) = 3 mol/kg				
1.1970	0.1077	0.7687	0.8663	-10.44%
2.6577	0.0968	0.6489	0.8744	-20.02%
3.6880	0.0857	0.5672	0.8933	-27.95%
5.7014	0.0919	0.5512	0.9101	-37.43%
Li_2SO_4, m(Salt) = 2 mol/kg				
0.9832	0.1193	0.8903	0.8854	-7.76%
2.0501	0.1153	0.8660	0.8917	-15.38%
4.3562	0.1214	0.8510	0.8992	-26.45%
5.9613	0.1242	0.8401	0.9141	-34.39%

Initial Mixture Compositions

Table B-11. Initial (or global) mixture compositions (in grams) and the salt feed (aqua)molality of the ternary systems water/n-butanol/salt for the salts NaCl, KCl, $LiNO_3$, NH_4NO_3, Li_2SO_4, Na_2SO_4, CH_3COOLi, CH_3COONa, C_2H_5COONa and C_3H_7COONa at 298.15 K and 1 bar.

water	n-butanol	Salt	m(salt) [mol/kg]
	NaCl		
4.4451	3.4460	0.0816	0.3141
4.3585	3.4155	0.2410	0.9462
4.0034	4.4587	0.2404	1.0275
4.007	3.4563	0.5207	2.2236
4.0251	4.0112	0.7319	3.1115
3.4494	3.678	0.8778	4.3545
4.0107	3.9957	1.1677	4.9820
	KCl		
3.9468	4.0040	0.1492	0.5071
4.0141	3.9894	0.2980	0.9958
3.9818	3.9966	0.5956	2.0064
3.9919	4.0442	1.1928	4.0081
	$LiNO_3$		
4.0114	3.9668	0.3649	1.3194
4.0366	4.0098	0.8653	3.1092
4.0007	4.0891	1.4320	5.1916
4.0246	4.0154	2.084	7.5104
	NH_4NO_3		
3.9805	3.9939	0.3279	1.0292
4.0716	4.0260	1.5946	4.8930
4.0620	4.0003	3.1890	9.8086
4.0408	3.9800	4.8216	14.9079

Continued

Li_2SO_4			
4.0114	3.9668	0.2252	0.5106
4.0366	4.0098	0.4537	1.0223
4.0007	4.0891	0.9182	2.0876
Na_2SO_4			
3.9867	4.0037	0.2957	0.5222
4.0828	4.0844	0.4059	0.6999
4.2796	3.9240	0.5078	0.8354
4.1561	4.1516	0.6219	1.0535
CH_3COOLi			
4.0888	3.9613	0.5378	1.9932
4.0585	4.0843	0.7840	2.9273
4.0377	4.0122	1.6004	6.0064
CH_3COONa			
4.1765	4.0838	0.3372	0.9843
4.2989	4.0824	0.6501	1.8436
4.4152	3.9449	0.9852	2.7203
4.5101	3.9331	1.2702	3.4334
C_2H_5COONa			
4.0220	4.0106	0.3851	0.9968
3.9996	4.0361	0.7702	2.0047
3.9878	4.0000	1.5374	4.0134
C_3H_7COONa			
3.9802	4.0326	0.0860	0.1963
4.0026	3.9826	0.1756	0.3985
3.9819	4.0439	0.2692	0.6141
3.9826	3.9658	0.3613	0.8240

Table B-12. Initial (or global) mixture compositions (in grams) and the HMF feed (aqua)molality of the ternary systems water/n-butanol/HMF at 298.15 K and 1 bar.

Water/n-Butanol/HMF			
water	n-butanol	HMF	m(HMF) [mol/kg]
3.0044	3.0074	0.4056	1.0705
3.0032	3.0316	0.7614	2.0104
3.0076	3.0045	1.1128	2.9339
3.0168	3.0517	1.3428	3.5295

Table B-13. Initial (or global) mixture compositions (in grams) and the glycerol feed molality of the ternary systems water/n-butanol/glycerol at 298.15 K and 1 bar.

Water/n-Butanol/Glycerol			
water	n-butanol	Glycerol	m(glycerol) [mol/kg]
3.9911	4.0310	0.4120	1.1210
4.0629	4.0710	1.0961	2.9296
4.0318	3.9725	1.4606	3.9339
4.1718	3.9856	2.2222	5.7843
4.3475	4.0150	3.1049	7.7552

Table B-14. Initial (or global) mixture compositions (in grams), HMF and salt feed (aqua)molalities of the quaternary systems water/n-butanol/HMF/salt for the salts LiCl, NaCl, KCl, Li_2SO_4, Na_2SO_4, $Al_2(SO_4)_3$, CH_3COONa, C_2H_5COONa and NH_4NO_3 at 298.15 K and 1 bar and of the quaternary systems water/n-butanol/HMF/Na_2SO_4 at 303.15 K and 1 bar.

water	n-butanol	HMF	salt	m(HMF) [mol/kg]	m(salt) [mol/kg]
LiCl, m(HMF) = 4 mol/kg					
3.9834	3.6771	2.0860	0.5433	4.1525	3.2175
3.9898	3.4886	2.1267	1.0137	4.2267	5.9937
4.0549	3.6015	2.0348	2.0548	3.9792	11.954
LiCl, m(Salt) = 3 mol/kg					
3.4746	3.4569	0.4537	0.4615	1.0354	3.1333
3.5176	3.4057	0.8986	0.4477	2.0257	3.0025
3.5794	3.4232	1.7796	0.4474	3.9424	2.9486
NaCl, m(HMF) = 4 mol/kg					
3.4935	3.6639	1.7795	0.2069	4.0391	1.0134
3.4468	3.4843	1.7671	0.4095	4.0653	2.0330
3.4261	3.4991	1.7508	0.8094	4.0522	4.0425
NaCl, m(Salt) = 3 mol/kg					
4.0872	3.8990	0.5164	0.7087	1.0019	2.9671
4.0341	3.8632	1.5616	0.7150	3.0695	3.0328
4.0035	3.8924	3.0180	0.7012	5.9776	2.9970
KCl, m(HMF) = 4 mol/kg					
3.8987	4.0746	2.0460	0.3005	4.1614	1.0339
4.0705	4.0226	2.0108	0.5959	3.9172	1.9637
4.0303	4.0183	2.0140	1.1919	3.9625	3.9669
KCl, m(Salt) = 3 mol/kg					
4.2794	4.0700	0.5067	0.8969	0.9389	2.8113
3.9318	4.1099	1.0025	0.8950	2.0218	3.0533
3.9722	4.0503	2.0148	0.8917	4.0221	3.0112
4.2289	3.8990	3.0761	0.8915	5.7680	2.8277

Continued

Li_2SO_4, m(HMF) = 4 mol/kg					
4.0695	4.0045	2.0770	0.4355	4.0471	0.9734
4.0589	4.0220	2.0977	0.8826	4.0981	1.9779
4.0292	3.9838	2.0498	1.0959	4.0341	2.4740
Li_2SO_4, m(Salt) = 2 mol/kg					
4.1553	4.0444	0.5576	0.8778	1.0641	1.9215
3.9743	3.9502	1.0135	0.8801	2.0222	2.0143
4.1508	4.0519	2.0677	0.8784	3.9501	1.9249
Na_2SO_4, m(HMF) = 4 mol/kg					
4.0003	4.0554	2.0574	0.1129	4.0783	0.1987
4.0858	3.9892	2.0025	0.2830	3.8864	0.4876
4.0076	4.0694	2.0101	0.4418	3.9773	0.7761
Na_2SO_4, m(Salt) = 0.5 mol/kg					
3.9986	3.9476	0.5015	0.2819	0.9945	0.4963
3.9633	3.9488	0.9999	0.2820	2.0006	0.5009
3.9878	3.9756	1.5117	0.2827	3.0060	0.4991
$Al_2(SO_4)_3$, m(salt) = 0.5 mol/kg					
4.8262	3.0077	0.6185	0.8218	1.0162	0.4977
4.8557	3.0832	1.2179	0.8279	1.9889	0.4983
4.8033	3.0278	1.7943	0.8237	2.9621	0.5012
4.8601	3.0706	2.4315	0.8256	3.9671	0.4965
CH_3COONa, m(HMF) = 4 mol/kg					
4.2520	3.9173	2.1295	0.3381	3.9713	0.9692
4.3771	3.8305	2.1207	0.6225	3.8419	1.7336
4.6177	3.5765	2.1247	1.0186	3.6485	2.6891

Continued

CH_3COONa, m(HMF) = 4 mol/kg					
4.2520	3.9173	2.1295	0.3381	3.9713	0.9692
4.3771	3.8305	2.1207	0.6225	3.8419	1.7336
4.6177	3.5765	2.1247	1.0186	3.6485	2.6891
CH_3COONa, m(salt) = 1.75 mol/kg					
4.4806	3.8316	0.5129	0.6418	0.9077	1.7462
4.4721	3.7049	1.0038	0.6388	1.7799	1.7413
4.3937	3.7786	1.5955	0.6531	2.8795	1.8122
4.4573	3.9444	2.0307	0.6489	3.6126	1.7748
CH_3COONa, m(salt) = 3 mol/kg					
3.9821	4.0498	0.5074	1.0051	1.0104	3.0770
4.0822	4.0304	1.0124	0.9980	1.9666	2.9803
3.9727	3.9879	1.5106	1.0008	3.0152	3.0711
4.0182	4.0898	2.0203	1.0055	3.9869	3.0505
C_2H_5COONa, m(salt) 1 mol/kg					
2.9925	2.9648	0.3759	0.2891	0.9961	1.0057
3.0112	3.0695	0.7514	0.2902	1.9787	1.0033
2.9917	3.0185	1.1260	0.2878	2.9845	1.0015
3.0126	3.0263	1.5018	0.2896	3.9529	1.0007
NH_4NO_3, m(HMF) = 4 mol/kg					
4.0476	4.0106	2.0061	1.6037	3.9301	4.9500
3.9703	2.9943	2.0082	3.2045	4.0108	10.084
4.0415	2.0300	2.0020	4.8160	3.9280	14.888
NH_4NO_3, m(salt) = 5 mol/kg					
3.9736	3.9987	0.5062	1.6057	1.0102	5.0484
4.0115	4.0266	1.0035	1.6032	1.9836	4.9930
4.0102	4.0138	1.5114	1.6074	2.9886	5.0077
Na_2SO_4, m(HMF) = 4 mol/kg, T = 303.15 K					
4.0583	4.0505	2.0100	0.2863	3.9274	0.4967
4.0204	4.0124	2.0097	0.5711	3.9638	1.0001
4.0302	4.0105	2.0131	1.1363	3.9609	1.9850

Table B-15. Initial (or global) mixture compositions (in grams) and the glycerol and salt feed molalities of the quaternary systems water/n-butanol/glycerol/salt for the salts NaCl and Li_2SO_4 at 298.15 K and 1 bar.

water	n-butanol	glycerol	salt	m(glycerol) [mol/kg]	m(salt) [mol/kg]
NaCl, m(Glycerol) = 4 mol/kg					
4.0579	3.8398	1.4660	0.2346	3.9230	0.9893
4.0468	3.7974	1.5028	0.7034	4.0325	2.9743
3.9375	4.0344	1.4835	1.1658	4.0912	5.0663
NaCl, m(NaCl) = 3 mol/kg					
4.1839	3.9795	0.4612	0.7072	1.1970	2.8923
4.0724	4.0518	0.9967	0.7034	2.6577	2.9556
4.0774	4.0147	1.3848	0.7107	3.6880	2.9826
4.0374	3.9545	2.1198	0.7079	5.7014	3.0003
Li_2SO_4, m(Glycerol) = 4 mol/kg					
4.1072	3.9790	1.4665	0.2180	3.8772	0.4828
3.9414	4.0244	1.5010	0.4389	4.1354	1.0129
4.0230	3.9389	1.4988	0.8757	4.0456	1.9799
Li_2SO_4, m(Li_2SO_4) = 2 mol/kg					
4.0601	3.7755	0.3676	0.8774	0.9832	1.9656
3.9795	4.0291	0.7513	0.8777	2.0501	2.0061
4.1275	3.9753	1.6558	0.8787	4.3562	1.9364
4.1129	4.0058	2.2579	0.8813	5.9613	1.9490

C Equation Set according to Gibbard et al.

$$\phi = 1 - \frac{S\mathrm{Z}}{\mathrm{a}} + \sum_{\mathrm{j}=1}^{4} D_{\mathrm{j}} m^{\mathrm{j}} \tag{C-1}$$

$$\begin{aligned} S = {} & 1.17284 - \frac{6202.357\tau}{\mathrm{T_s^2}\left(1 + \frac{\tau}{\mathrm{T_s}}\right)} + 54.4251 \ln\left(1 + \frac{\tau}{\mathrm{T_s}}\right) \\ & -0.161993\tau + 8.59609 * 10^{-5}(2\mathrm{T_s}\tau + \tau^2)\,, \end{aligned} \tag{C-2}$$

where $\mathrm{Z} = \{1 + \mathrm{X} - [1/(1 + \mathrm{X})\,] - 2\ln(1 + \mathrm{X})\}/\mathrm{X}^2$; $\tau = \mathrm{T} - \mathrm{T_s}$; $\mathrm{X} = \mathrm{a}\sqrt{\mathrm{m}}$; $\mathrm{T_s} = 298.15$ K; a = 1.5.

$$D_{\mathrm{j}} = D_{\mathrm{j}}^{(\mathrm{s})} - 0.2516103 \sum_{\mathrm{k}=0}^{3} \frac{D_{\mathrm{j}}^{(\mathrm{k})}}{\mathrm{k}!} \int_0^{\tau} \frac{\mathrm{t^k}}{(\mathrm{t} + \mathrm{T_s})} \mathrm{dt} \tag{C-3}$$

The coefficients $D_j^{(s)}$ and $D_j^{(k)}$ are based on precise measurements, which are given in the paper of Gibbard and Scatchard [344].

D Contributions to the Helmholtz Energy in ePC-SAFT

The hard-chain contribution (a^{hc}) as reference system was introduced by Chapman et al.[543] and describes the formation of chains out of m_{seg} free spherical segments

$$a^{hc} = \bar{m}_{seg} a^{hs} - \sum_{i} x_i \left(m_{seg,i} - 1\right) ln g_{ii}^{hs}(\sigma_{ii}), \tag{D-4}$$

where $\bar{m}_{seg}$ is the mean segment number ($\bar{m}_{seg} = \sum_i x_i m_i$) in the mixture and g_{ij}^{hs} is the radial pair-distribution function, which reflects the probability to find a segment j next to segment i and reads:

$$g_{ij}^{hs}\left(\sigma_{ij}\right) = \frac{1}{(1-\zeta_3)} + \left(\frac{\sigma_i \sigma_j}{\sigma_i + \sigma_j}\right) \frac{3\zeta_2}{(1-\zeta_3)^2} + \left(\frac{\sigma_i \sigma_j}{\sigma_i + \sigma_j}\right)^2 \frac{2\zeta_2^2}{(1-\zeta_3)^3} \tag{D-5}$$

The repulsive energy of spherical molecules (a^{hs}) in Eq. (D-4) is given by:

$$a^{hs} = \frac{1}{\zeta_0}\left[\frac{3\zeta_1\zeta_2}{1-\zeta_3} + \frac{{\zeta_2}^3}{\zeta_3(1-\zeta_3)^2} + \left(\frac{{\zeta_2}^3}{{\zeta_3}^2} - \zeta_0\right) \ln(1-\zeta_3)\right], \tag{D-6}$$

where ζ_n are the moments of the temperature-dependent segment diameter:

$$\zeta_n = \frac{\pi}{6} \rho_N \sum_{i} x_i d_i^n \qquad n = 1, 2, 3 \tag{D-7}$$

and ρ_N being the density number:

$$\rho_N = \rho N_A \tag{D-8}$$

The temperature-dependent segment diameter (d_i) is defined according to Eq. (II-59).

The dispersion contribution (a^{disp}) reads:

$$\begin{aligned} a^{disp} = \frac{A^{disp}}{N k_B T} &= -2\pi \rho_N I_1\left(\zeta, \bar{m}_{seg}\right) \sum_{i} \sum_{j} x_i x_j m_{seg,i} m_{seg,j} \left(\frac{u_{ij}}{k_B T}\right)^2 \sigma_{ij}^3 \\ &\quad - \pi \rho_N \bar{m}_{seg} C_1 I_2\left(\zeta, \bar{m}_{seg}\right) \sum_{i} \sum_{j} x_i x_j m_{seg,i} m_{seg,j} \left(\frac{u_{ij}}{k_B T}\right)^2 \sigma_{ij}^3 , \end{aligned} \tag{D-9}$$

where C_1 is defined as:

$$C_1 = \left(1 + Z^{hc} + \rho \frac{\partial Z^{hc}}{\partial \rho}\right)^{-1}, \tag{D-10}$$

with the power series I_1 and I_2, which are depending on the density and the mean segment number:

$$I_1(\zeta, \bar{m}_{seg}) = \sum_{i=o}^{6} r_i(\bar{m}_{seg})\zeta^i \tag{D-11}$$

$$I_2(\zeta, \bar{m}_{seg}) = \sum_{i=o}^{6} s_i(\bar{m}_{seg})\zeta^i \tag{D-12}$$

Here, the interactions between different segments in a chain are described by r_i and s_i, which were determined by fitting model constants to the alkane homologous series[186].

The association contribution (a^{assoc}) to the free energy can be calculated from:

$$a^{assoc} = \frac{A^{assoc}}{Nk_BT} = \sum_i x_i \sum_{A_i} \left(\ln X^{A_i} - \frac{X^{A_i}}{2} + \frac{1}{2}\right), \tag{D-13}$$

where X^{A_i}, the mole fraction of molecules of type i that are **not** bonded at the association site A, is given below:

$$X^{A_i} = \left(1 + \rho_N \sum_j x_j \sum_{B_j} X^{B_j} \Delta^{A_i B_j}\right)^{-1} \tag{D-14}$$

The association strength ($\Delta^{A_i B_j}$) is the extent of the interaction between the association sites A_i and B_j:

$$\Delta^{A_i B_j} = g_{ij}^{hs}(\sigma_{ij}) \kappa^{A_i B_j} \sigma_{ij}^3 \left(exp\left(\frac{\varepsilon^{A_i B_j}}{k_B T}\right) - 1\right) \tag{D-15}$$

E List of Figures

F List of Tables

G Abbreviations

(Phy^{5-}, $5Na^+$)	Pentasodium phytate
1,3-PDO	1,3-Propandiol
2,5-DMF	2,5 Dimethylfuran
2SIP	Double-Solvent-Shared Ion Pair
ACN	Acetonitrile
AES	Atomic Emission Spectroscopy
AMF	5-Acetoxymethylfurfural
BHMF	2,5 Bishydroxymethylfurfural
CAC	Critical Aggregation Concentration
CAF	Caffeine
CIP	Contact Ion Pair
CMC	Critical Micelle Concentration
COSMO	COnductor like Screening MOdel
COSMO-RS	COnductor like Screening MOdel for Real Solvation
COSMO-RS-ES	COnductor like Screening MOdel for Real Solvation in Electrolyte Solutions
DH	Debye-Hückel
DLS	Dynamic Light Scattering
DMF	N,N Dimethylformamide
DMSO	Dimethylsulfoxide
DPnP	Dipropylene glycol n-Propyl ether
DR-13	Disperse Red 13
EHS	Environmental, Health and Safety
EMF	5-Ethoxymethylfurfural
EoS	Equation of State
ePC-SAFT	electrolyte Perturbed-Chain Statistical Association Fluid Theory
FDCA	2,5 Furandicarboxylic acid
FID	Flame Ionisation Detector
GC	Gas Chromatography
G^E	Gibbs-Excess Energy
GVL	γ-Valerolactone
HMF	5-Hydroxymethylfurfural
HPLC	High-Performance-Liquid-Chromatography
HTC	Hydrothermal Carbonisation
IC	Anion-Exchange Chromatography
ILs	Ionic Liquids
IUPAC	International Union of Pure and Applied Chemistry
KB	Kirkwood Buff

KF-Titration	Karl Fischer-Titration
LA	Levulinic Acid
LLE	Liquid-Liquid Equilibrium
LLEx	Liquid-Liquid Extraction
LMWA	Law of Matching Water Affinities
LR	Long-Range
LST	Lower Solution Temperature
MAC	Minimum Aggregation Concentrations
MD	Molecular Dynamics
MHC	Minimum Hydrotrope Concentration
MIAC	Mean Ionic Activity Coefficient
MIBK	Methyl Isobutyl Ketone
MMF	5-Methoxymethylfurfural
MSA	Mean Spherical Approximation
MTHF	2-Methyltetrahydrofuran
NA	Nicotinamide
NMP	N-methyl-2-pyrrolidone
NRTL	Non-Random-Two-Liquid
PC-SAFT	Perturbed-Chain Statistical Association Fluid Theory
PDH	Pitzer-Debye-Hückel
PEF	Polyethylene Furanoate
PEG	Polyethylene Glycol
PET	Polyethylene Terephtalate
PMF	Potential Mean Force
PnP	Propylene glycol n Propyl ether
PR	Peng-Robinson
PVP	Poly(1-vinyl-2-pyrrolidone)
RBF	Riboflavin
RI	Refractive Index
RMC	Reversed Monte Carlo
SAFT	Statistical Association Fluid Theory
SAM	Self-Assembled Monolayers
SB	Sodium Benzoate
SCS	Sodium Cumene Sulfonate
SDS	Sodium Dodecylsulphate
SFME	Surfactant-free microemulsion
SIP	Solvent-Shared Ion Pair
SMF	5-Sulfoxymethylfurfural
SR	Short-Range

SRK	Soave-Redlich-Kwong
SXS	Sodium Xylene Sulfonate
THF	Tetrahydrofuran
TLL	Tie-Line Length
TLS	Tie-Line Slope
TPA	Terephtalic Acid
UCST	Upper Critical Solubility Temperature
UNIFAC	UNIversal Functional group Activity Coefficient
UNIQUAC	UNIversal QUasi-Chemical model
VLE	Vapour-Liquid Equilibria
VPO	Vapour Pressure Osmometry
ZSR	Zdanovskii-Stokes-Robinson

References

(1) BP. *Full report – BP Statistical Review of World Energy 2019*.

(2) Stottmeister, U.; Aurich, A.; Wilde, H.; Andersch, J.; Schmidt, S.; Sicker, D. *J. Ind. Microbiol. Biotechnol.* **2005**, *32*, 651–664.

(3) Glaser, J. A. *Clean. Techn. Environ. Policy* **2005**, *7*, 233–235.

(4) Frazzetto, G. *EMBO Rep.* **2003**, *4*, 835–837.

(5) Ulber, R.; Sell, D. *White Biotechnology* 105; Springer Berlin Heidelberg: Berlin, Heidelberg, 2007.

(6) Barcelos, M. C. S.; Lupki, F. B.; Campolina, G. A.; Nelson, D. L.; Molina, G. *FEMS microbiol. lett.* **2018**, *365*.

(7) Li, H.; Bhadury, P. S.; Riisager, A.; Yang, S. *Catal. Sci. Technol.* **2014**, *4*, 4138–4168.

(8) Yinghuai, Z.; Oh, A.; Siwei, X.; S, N.; A., J. Ionic Liquids in Catalytic Biomass Transformation. In *Applications of ionic liquids in science and technology*; Handy, S. T., Ed.; InTech: Rijeka, Croatia, 2011.

(9) Carole, T. M.; Pellegrino, J.; Paster, M. D. *ABAB* **2004**, *115*, 871–886.

(10) Bozell, J. J.; Petersen, G. R. *Green Chem.* **2010**, *12*, 539.

(11) Bozell, J. J. *Clean Soil Air Water* **2008**, *36*, 641–647.

(12) Bozell, J. J.; Patel, M. K. *Feedstocks for the Future* 921; American Chemical Society: Washington, DC, 2006.

(13) Chheda, J. N.; Huber, G. W.; Dumesic, J. A. *Angew. Chem. Int Ed. Engl.* **2007**, *46*, 7164–7183.

(14) van Putten, R.-J.; van der Waal, J. C.; Jong, E. de; Rasrendra, C. B.; Heeres, H. J.; Vries, J. G. de. *Chem. Rev.* **2013**, *113*, 1499–1597.

(15) Werpy, T.; Petersen, G. *Top Value Added Chemicals from Biomass: Volume I -- Results of Screening for Potential Candidates from Sugars and Synthesis Gas*, 2004.

(16) Holladay, J. E.; White, J. F.; Bozell, J. J.; Johnson, D. *Top Value-Added Chemicals from Biomass - Volume II—Results of Screening for Potential Candidates from Biorefinery Lignin*, 2007.

(17) Choi, S.; Song, C. W.; Shin, J. H.; Lee, S. Y. *Metab. Eng.* **2015**, *28*, 223–239.

(18) Moreau, C.; Belgacem, M. N.; Gandini, A. *Top. Catal.* **2004**, *27*, 11–30.

(19) Gandini, A. *Prog. Polym. Sci.* **1997**, *22*, 1203–1379.

(20) Kröger, M.; Prüße, U.; Vorlop, K. ‐ D. *Top. Catal.* **2000**, *13*, 237–242.

(21) Yoshida, N.; Kasuya, N.; Haga, N.; Fukuda, K. *Polym. J.* **2008**, *40*, 1164–1169.

(22) Buntara, T.; Noel, S.; Phua, P. H.; Melián-Cabrera, I.; Vries, J. G. de; Heeres, H. J. *Angew. Chem. Int. Ed. Engl.* **2011**, *50*, 7083–7087.

(23) Gandini, A.; Lacerda, T. M.; Carvalho, A. J. F.; Trovatti, E. *Chem. Rev.* **2016**, *116*, 1637–1669.

(24) Zhang, D.; Dumont, M.-J. *J. Polym. Sci. Part A: Polym. Chem.* **2017**, *55*, 1478–1492.

(25) Huber, G. W.; Chheda, J. N.; Barrett, C. J.; Dumesic, J. A. *Science* **2005**, *308*, 1446–1450.

(26) Román-Leshkov, Y.; Barrett, C. J.; Liu, Z. Y.; Dumesic, J. A. *Nature* **2007**, *447*, 982–985.

(27) Abraham, K.; Gürtler, R.; Berg, K.; Heinemeyer, G.; Lampen, A.; Appel, K. E. *Mol. Nutr. Food Res.* **2011**, *55*, 667–678.

(28) Lewkowski, J. *Arkivoc* **2005**, *2001*, 17–54.

(29) Shapla, U. M.; Solayman, M.; Alam, N.; Khalil, M. I.; Gan, S. H. *Chem. Cent. J.* **2018**, *12*, 35.

(30) Murkovic, M.; Pichler, N. *Mol. Nutr. Food Res.* **2006**, *50*, 842–846.

(31) Louis Camille Maillard. *Comptes Rendus* **1912**, *154*, 66–68.

(32) Meyer-Eppler. Deutscher Imkerbund e. V. | Echter Deutscher Honig Qualitaetsrichtlinien. https://deutscherimkerbund.de/229-Echter_Deutscher_Honig_Qualitaetsrichtlinien (accessed February 28, 2020).

(33) Severin, I.; Dumont, C.; Jondeau-Cabaton, A.; Graillot, V.; Chagnon, M.-C. *Toxicol. Lett.* **2010**, *192*, 189–194.

(34) Lee, Y. C.; Shlyankevich, M.; Jeong, H. K.; Douglas, J. S.; Surh, Y. J. *Biochem. Biophys. Res. Commun.* **1995**, *209*, 996–1002.

(35) Hardt-Stremayr, M.; Mattioli, S.; Greilberger, J.; Stiegler, P.; Matzi, V.; Schmid, M. G.; Wintersteiger, R. *J. Sep. Sci.* **2013**, *36*, 670–676.

(36) Morales, F. J. Hydroxymethylfurfural (HMF) and Related Compounds. In *Process-induced food toxicants: Occurrence, formation, mitigation, and health risks*; Stadler, R. H., Lineback, D. R., Eds.; Wiley-Blackwell: Oxford, 2008; pp 135–174.

(37) Rapp, K. M.; Daub, J. *Herstellung und Derivatisierung von 5-Hydroxymethylfurfural. In: Manfred Eggersdorfer und Siegried Warwall (Hg.): Nachwachsende Rohstoffe. Perspektiven für die Chemie.*; Weinheim:VCH, 1993.

(38) Zhang, Z.; Deng, K. *ACS Catal.* **2015**, *5*, 6529–6544.

(39) Krawielitzki, S.; Kläusli, T. M. *Ind. Biotechnol.* **2015**, *11*, 6–8.

(40) Xia, H.; Xu, S.; Hu, H.; An, J.; Li, C. *RSC Adv.* **2018**, *8*, 30875–30886.

(41) https://bioplasticsnews.com/2019/06/08/avantium-moving-forward-on-bio-based-plastics-plant/.

(42) Pang, J.; Zheng, M.; Sun, R.; Wang, A.; Wang, X.; Zhang, T. *Green Chem.* **2016**, *18*, 342–359.

(43) Tuck, C. O.; Pérez, E.; Horváth, I. T.; Sheldon, R. A.; Poliakoff, M. *Science* **2012**, *337*, 695–699.

(44) Zhong, S.; Daniel, R.; Xu, H.; Zhang, J.; Turner, D.; Wyszynski, M. L.; Richards, P. *Energy Fuels* **2010**, *24*, 2891–2899.

(45) Xu, H.; Wang, C. A Comprehensive Review of 2,5-Dimethylfuran as a Biofuel Candidate. In *Biofuels from lignocellulosic biomass: Innovations beyond bioethanol*; Boot, M., Ed.; Wiley-VCH: Weinheim, 2016; pp 105–129.

(46) Wettstein, S. G.; Alonso, D. M.; Gürbüz, E. I.; Dumesic, J. A. *Curr. Opin. Chem. Eng.* **2012**, *1*, 218–224.

(47) Mullen, B. D.; Yontz, D. J.; Leiblig, C. M. Process to prepare levulinic acid, Mar 21, 2017.

(48) Li, Y.-X.; Li, Y.; Qian, Z. J.; Kim, M.-M.; Kim, S.-K. *J. Microbiol. Biotechnol.* **2009**, *19*, 1319–1327.

(49) Zhao, L.; Chen, J.; Su, J.; Li, L.; Hu, S.; Li, B.; Zhang, X.; Xu, Z.; Chen, T. *J. Agric. Food Chem.* **2013**, *61*, 10604–10611.

(50) Zhang, J.-H.; Di, Y.; Wu, L.-Y.; He, Y.-L.; Zhao, T.; Huang, X.; Ding, X.-F.; Wu, K.-W.; Fan, M.; Zhu, L.-L. *Free Radic. Res.* **2015**, *49*, 86–94.

(51) Oder, E.; Safo, M. K.; Abdulmalik, O.; Kato, G. J. *Br. J. Haematol.* **2016**, *175*, 24–30.

(52) Ding, X.; Wang, M.-Y.; Yao, Y.-X.; Li, G.-Y.; Cai, B.-C. *J. Ethnopharmacol.* **2010**, *128*, 373–376.

(53) Li, W.; Qu, X.-N.; Han, Y.; Zheng, S.-W.; Wang, J.; Wang, Y.-P. *Int. J. Mol. Sci.* **2015**, *16*, 2446–2457.

(54) Wang, M.-Y.; Zhao, F.-M.; Peng, H.-Y.; Lou, C.-H.; Li, Y.; Ding, X.; Yu, X.-Y.; Yang, G.-M.; Xu, D.-Q.; Jiang, L.-H.*; et al. J. Ethnopharmacol.* **2010**, *130*, 424–428.

(55) Kuster, B. F. M. *Starch/Stärke* **1990**, *42*, 314–321.

(56) Rosatella, A. A.; Simeonov, S. P.; Frade, R. F. M.; Afonso, C. A. M. *Green Chem.* **2011**, *13*, 754.

(57) Corma, A.; Iborra, S.; Velty, A. *Chem. Rev.* **2007**, *107*, 2411–2502.

(58) Cottier, L. and Descotes, G. *Trends. Heterocycl. Chem.* **1991**, *2*, 233–248.

(59) Saha, B.; Abu-Omar, M. M. *Green Chem.* **2014**, *16*, 24–38.

(60) Román-Leshkov, Y.; Dumesic, J. A. *Top. Catal.* **2009**, *52*, 297–303.

(61) Antal, M. J.; Mok, W. S.L.; Richards, G. N. *Carbohydr. Res.* **1990**, *199*, 91–109.

(62) Rapp, K. M. Verfahren zur Herstellung von 5-Hydroxymethylfurfural einschliesslich eines kristallinen Produktes unter ausschliesslicher Verwendung von Wasser als Lösungsmittel. EP 0230250 A2, Jan 13, 1987.

(63) Kunz, M.; Haji Begli, A.; Kröner, C.; Wach, W.; Graf, A. M.; Kraus, W. HMF Production Method. US 20200002300 A1, Jan 2, 2020.

(64) Brown, D. W.; Floyd, A. J.; Kinsman, R. G.; RoshanhyphenAli, Y. *J. Chem. Technol. Biotechnol.* **1982**, *32*, 920–924.

(65) Bicker, M.; Kaiser, D.; Ott, L.; Vogel, H. *J. Supercrit. Fluids* **2005**, *36*, 118–126.

(66) Gruter, G.J.M.; Dautzenberg, F. Method for the Synthesis of 5-Alkoxymethyl Furfural Ethers and their use. US 2011/0082304 A1, Apr 7, 2011.

(67) Reichert, D.; Sarich, M.; Merz, F. Process for preparing 5-hydroxymethylfurfural via 5-acyloxymethylfurfural as an intermediate. EP 1958944 B1, Feb 7, 2008.

(68) Seri, K.; Inoue, Y.; Ishida, H. *Chem. Lett.* **2000**, *29*, 22–23.

(69) Wang, F.; Shi, A.-W.; Qin, X.-X.; Liu, C.-L.; Dong, W.-S. *Carbohydr. Res.* **2011**, *346*, 982–985.

(70) Jeong, J.; Antonyraj, C. A.; Shin, S.; Kim, S.; Kim, B.; Lee, K.-Y.; Cho, J. K. *J. Ind. Eng. Chem.* **2013**, *19*, 1106–1111.

(71) Gruter, G. J. M.; Dautzenberg, F. Method for the synthesis of organic acid esters of 5-hydroxymethylfurfural. EP 2105439 B1, Oct 19, 2011.

(72) Amarasekara, A. S.; Williams, L. D.; Ebede, C. C. *Carbohydr. Res.* **2008**, *343*, 3021–3024.

(73) Nakamura, Y.; Morikawa, S. *BCSJ* **1980**, *53*, 3705–3706.

(74) Szmant, H. H.; Chundury, D. D. *J. Chem. Technol. Biotechnol.* **1981**, *31*, 135–145.

(75) Musau, R. M.; Munavu, R. M. *Biomass* **1987**, *13*, 67–74.

(76) Sanborn, A. J. Processes for the preparation and purification of hydroxymethylfurfuraldehyde and derivatives. US 7,317,116 B2, Jan 8, 2008.

(77) Binder, J. B.; Raines, R. T. *J. Am. Chem. Soc.* **2009**, *131*, 1979–1985.

(78) Gallo, J. M. R.; Alonso, D. M.; Mellmer, M. A.; Dumesic, J. A. *Green Chem.* **2013**, *15*, 85–90.

(79) Román-Leshkov, Y.; Chheda, J. N.; Dumesic, J. A. *Science* **2006**, *312*, 1933–1937.

(80) Klamt, A. *J. Phys. Chem.* **1995**, *99*, 2224–2235.

(81) Blumenthal, L. C.; Jens, C. M.; Ulbrich, J.; Schwering, F.; Langrehr, V.; Turek, T.; Kunz, U.; Leonhard, K.; Palkovits, R. *ACS Sustain. Chem. Eng.* **2016**, *4*, 228–235.

(82) Qi, X.; Watanabe, M.; Aida, T. M.; Smith, R. L. *Ind. Eng. Chem. Res.* **2008**, *47*, 9234–9239.

(83) Gaset, A.; Rigal, L.; Paillassa, G.; J.-P., S.; Flèche, G. Process for manufacturing 5-hydroxymethylfurfural. U.S. 4,590,283, May 20, 1986.

(84) Chheda, J. N.; Román-Leshkov, Y.; Dumesic, J. A. *Green Chem.* **2007**, *9*, 342–350.

(85) Qi, X.; Watanabe, M.; Aida, T. M.; Smith, J. R. L. *Green Chem.* **2008**, *10*, 799.

(86) Bicker, M.; Hirth, J.; Vogel, H. *Green Chem.* **2003**, *5*, 280–284.

(87) Motagamwala, A. H.; Huang, K.; Maravelias, C. T.; Dumesic, J. A. *Energy Environ. Sci.* **2019**, *12*, 2212–2222.

(88) Chen, J.-D.; Kuster, B. F.M.; van der Wiele, K. *Biomass and Bioenerg.* **1991**, *1*, 217–223.

(89) Kuster, B. F.M. *Carbohydr. Res.* **1977**, *54*, 177–183.

(90) Tschirner, S.; Weingart, E.; Teevs, L.; Prüße, U. *Molecules* **2018**, *23*.

(91) Weingart, E.; Tschirner, S.; Teevs, L.; Prüße, U. *Molecules* **2018**, *23*.

(92) Gogoi, G.; Hazarika, S. *Korean J. Chem. Eng.* **2019**, *36*, 1626–1636.

(93) Mäki-Arvela, P.; Anugwom, I.; Virtanen, P.; Sjöholm, R.; Mikkola, J. P. *Ind. Crops Prod.* **2010**, *32*, 175–201.

(94) Zakrzewska, M. E.; Bogel-Łukasik, E.; Bogel-Łukasik, R. *Chem. Rev.* **2011**, *111*, 397–417.

(95) Ståhlberg, T.; Fu, W.; Woodley, J. M.; Riisager, A. *ChemSusChem* **2011**, *4*, 451–458.

(96) V M Chernyshev; O A Kravchenko; V P Ananikov. *Russ. Chem. Rev.* **2017**, *86*, 357–387.

(97) Kuster, B. F. M.; van Steen, H. J. C. D. *Starch/Stärke* **1977**, *29*, 99–103.

(98) Chheda, J. N.; Dumesic, J. A. *Catal. Today* **2007**, *123*, 59–70.

(99) Esteban, J.; Vorholt, A. J.; Leitner, W. *Green Chem.* **2020**, *107*, 2411.

(100) Peniston, P. Q. Manufacture of 5-hydroxymethyl-2-furfural. U.S. 2,750,394, Jun 12, 1956.

(101) McNeff, C. V.; Nowlan, D. T.; McNeff, L. C.; Yan, B.; Fedie, R. L. *Appl. Catal. A-Gen.* **2010**, *384*, 65–69.

(102) Nikolla, E.; Román-Leshkov, Y.; Moliner, M.; Davis, M. E. *ACS Catal.* **2011**, *1*, 408–410.

(103) Yang, F.; Liu, Q.; Yue, M.; Bai, X.; Du, Y. *Chem. commun. (Camb)* **2011**, *47*, 4469–4471.

(104) Cope, A. C. Production and recovery of furans. U.S. 2,917,520, Dec 15, 1959.

(105) Moreau, C.; Durand, R.; Razigade, S.; Duhamet, J.; Faugeras, P.; Rivalier, P.; Ros, P.; Avignon, G. *Appl. Catal. A-Gen.* **1996**, *145*, 211–224.

(106) Shimanouchi, T.; Kataoka, Y.; Yasukawa, M.; Ono, T.; Kimura, Y. *Solvent Extr. Res. Dev.* **2013**, *20*, 205–212.

(107) Dibenedetto, A.; Aresta, M.; Di Bitonto, L.; Pastore, C. *ChemSusChem* **2016**, *9*, 118–125.

(108) Sindermann, E. C.; Holbach, A.; Haan, A. de; Kockmann, N. *Chem. Eng. J.* **2016**, *283*, 251–259.

(109) Lima, S.; Antunes, M. M.; Fernandes, A.; Pillinger, M.; Ribeiro, M. F.; Valente, A. A. *Molecules* **2010**, *15*, 3863–3877.

(110) Dumesic, J. A.; Roman-Leshkov Y.; Chheda, J. N. Catalytic process for producing furanderivatives in a biphasic reactor, Aug 11, 2009.

(111) Gupta, D.; Ahmad, E.; Pant, K. K.; Saha, B. *RSC Adv.* **2017**, *7*, 41973–41979.

(112) Hansen, T. S.; Mielby, J.; Riisager, A. *Green Chem.* **2011**, *13*, 109–114.

(113) Jiang, N.; Qi, W.; Huang, R.; Wang, M.; Su, R.; He, Z. *J. Chem. Technol. Biotechnol.* **2014**, *89*, 56–64.

(114) Xu, S.; Yan, X.; Bu, Q.; Xia, H. *RSC Adv.* **2016**, *6*, 8048–8052.

(115) Yang, L.; Yan, X.; Xu, S.; Chen, H.; Xia, H.; Zuo, S. *RSC Adv.* **2015**, *5*, 19900–19906.

(116) Xu, S.; Pan, D.; Hu, F.; Wu, Y.; Wang, H.; Chen, Y.; Yuan, H.; Gao, L.; Xiao, G. *Fuel Process. Technol.* **2019**, *190*, 38–46.

(117) Cao, Z.; Fan, Z.; Chen, Y.; Li, M.; Shen, T.; Zhu, C.; Ying, H. *Appl. Catal. B-Environ.* **2019**, *244*, 170–177.

(118) Xiong, H.; Wang, T.; Shanks, B. H.; Datye, A. K. *Catal. Lett.* **2013**, *143*, 509–516.

(119) Pagán-Torres, Y. J.; Wang, T.; Gallo, J. M. R.; Shanks, B. H.; Dumesic, J. A. *ACS Catal.* **2012**, *2*, 930–934.

(120) Muranaka, Y.; Nakagawa, H.; Masaki, R.; Maki, T.; Mae, K. *Ind. Eng. Chem. Res.* **2017**, *56*, 10998–11005.

(121) Atanda, L.; Silahua, A.; Mukundan, S.; Shrotri, A.; Torres-Torres, G.; Beltramini, J. *RSC Adv.* **2015**, *5*, 80346–80352.

(122) Weingart, E.; Teevs, L.; Krieg, R.; Prüße, U. *Energy Technol.* **2018**, *6*, 432–440.

(123) Wrigstedt, P.; Keskiväli, J.; Repo, T. *RSC Adv.* **2016**, *6*, 18973–18979.

(124) Dhamole, P. B.; Mahajan, P.; Feng, H. *J. Chem. Eng. Data* **2010**, *55*, 3803–3806.

(125) Wang, B.; Ezejias, T.; Feng, H.; Blaschek, H. *Chem. Eng. Sci.* **2008**, *63*, 2595–2600.

(126) Wettstein, S. G.; Alonso, D. M.; Chong, Y.; Dumesic, J. A. *Energy Environ. Sci.* **2012**, *5*, 8199.

(127) Moity, L.; Durand, M.; Benazzouz, A.; Pierlot, C.; Molinier, V.; Aubry, J.-M. *Green Chem.* **2012**, *14*, 1132.

(128) Zhou, J.; Xia, Z.; Huang, T.; Yan, P.; Xu, W.; Xu, Z.; Wang, J.; Zhang, Z. C. *Green Chem.* **2015**, *17*, 4206–4216.

(129) Thananatthanachon, T.; Rauchfuss, T. B. *Angew. Chem. Int Ed. Engl.* **2010**, *49*, 6616–6618.

(130) Takagaki, A.; Takahashi, M.; Nishimura, S.; Ebitani, K. *ACS Catal.* **2011**, *1*, 1562–1565.

(131) Vyskocil J., K. A. Verfahren zur Extraktion von Furfuralen aus Biomasse. DE102011053034A1, Feb 28, 2013.

(132) Consult, S. Press Release: AVALON Industries Takes Over All Bio-based Chemistry Activities From AVA-CO2. https://www.sustainabilityconsult.com/news/229-press-release-avalon-industries-takes-over-all-bio-based-chemistry-activities-from-ava-co2 (accessed March 11, 2020).

(133) Patel, A. N. *J. Chem. Technol. Biotechnol.* **1979**, *29*, 51–55.

(134) Quispe, C. A.G.; Coronado, C. J.R.; Carvalho Jr., J. A. *Renew. Sust. Energ. Rev.* **2013**, *27*, 475–493.

(135) Ciriminna, R.; Della Pina, C.; Rossi, M.; Pagliaro, M. *Eur. J. Lipid Sci. Technol.* **2014**, *116*, 1432–1439.

(136) Samudrala, S. P.; Kandasamy, S.; Bhattacharya, S. *Sci. Rep.* **2018**, *8*, 7484.

(137) Yang, F.; Hanna, M. A.; Sun, R. *Biotechnol. Biofuels* **2012**, *5*, 13.

(138) Xiao, Y.; Xiao, G.; Varma, A. *Ind. Eng. Chem. Res.* **2013**, *52*, 14291–14296.

(139) Moity, L.; Benazzouz, A.; Molinier, V.; Nardello-Rataj, V.; Elmkaddem, M. K.; Caro, P. de; Thiébaud-Roux, S.; Gerbaud, V.; Marion, P.; Aubry, J.-M. *Green Chem.* **2015**, *17*, 1779–1792.

(140) Research, G. V. *Glycerol Market From Biodiesel, Fatty Acids, Fatty Alcohols For Personal Care, Alkyd Resins, Polyether Polyols Applications, Downstream Opportunities And Segment Forecasts To 2020*; Grand View Research: San Francisco, 2014.

(141) Harvey, B. G.; Meylemans, H. A. *J. Chem. Technol. Biotechnol.* **2011**, *86*, 2–9.

(142) Jin, C.; Yao, M.; Liu, H.; Lee, C.-f. F.; Ji, J. *Renew. Sust. Energ. Rev.* **2011**, *15*, 4080–4106.

(143) Mascal, M. *Biofuels, Bioprod. Bioref.* **2012**, *6*, 483–493.

(144) Oudshoorn, A.; van der Wielen, L. A. M.; Straathof, A. J. J. *Ind. Eng. Chem. Res.* **2009**, *48*, 7325–7336.

(145) Liu, Z.; Ying, Y.; Li, F.; Ma, C.; Xu, P. *J. Ind. Microbiol. Biotechnol.* **2010**, *37*, 495–501.

(146) Karimi, K.; Tabatabaei, M.; Sárvári Horváth, I.; Kumar, R. *Biofuel Res. J.* **2015**, *2*, 301–308.

(147) Lee, S.; Monnappa, A. K.; Mitchell, R. J. *BMB Rep.* **2012**, *45*, 265–274.

(148) Rosales-Calderon, O.; Arantes, V. *Biotechnol. Biofuels* **2019**, *12*, 240.

(149) Visioli, L. J.; Enzweiler, H.; Kuhn, R. C.; Schwaab, M.; Mazutti, M. A. *Sustain. Chem. Process.* **2014**, *2*, 15.

(150) Oudshoorn, A.; Peters, M. C. F. M.; van der Wielen, L. A. M.; Straathof, A. J. J. *J. Chem. Technol. Biotechnol.* **2011**, *86*, 714–718.

(151) Abdehagh, N.; Tezel, F. H.; Thibault, J. *Biomass and Bioenerg.* **2014**, *60*, 222–246.

(152) Abdehagh, N.; Dai, B.; Thibault, J.; Handan Tezel, F. *J. Chem. Technol. Biotechnol.* **2017**, *92*, 245–251.

(153) Harmsen, P. F. H.; Hackmann, M. M.; Bos, H. L. *Biofuels, Bioprod. Bioref.* **2014**, *8*, 306–324.

(154) Cantero, C.; Lopez, G.; Alvarado, V.; Jimenez, R.; Morales, J.; Coronado, E. *Energies* **2017**, *10*, 1276.

(155) Nishi, Y. *J. Chem. Eng. Japan / JCEJ* **1975**, *8*, 187–191.

(156) Rydberg, J.; Cox, M.; Musikas, C. *Solvent Extraction Principles and Practice*; Marcel Dekker Inc: Hoboken, 2004.

(157) Behr, A.; Agar, D. W.; Jörissen, J. *Einführung in die Technische Chemie*; Spektrum Akademischer Verlag: Heidelberg, 2010.

(158) Schmidt, A.; Strube, J. Application and Fundamentals of Liquid-Liquid Extraction Processes: Purification of Biologicals, Botanicals, and Strategic Metals. In *Encyclopedia of chemical technology*; Kirk, R. E., Othmer, D. F., Eds.; Wiley: New York, NY, 2003; pp 1–52.

(159) Kiezyk, P. R.; Mackay, D. *Can. J. Chem. Eng.* **1971**, *49*, 747–752.

(160) Schügerl, K. *Solvent Extraction in Biotechnology: Recovery of Primary and Secondary Metabolites*; Springer Berlin Heidelberg: Berlin, Heidelberg, s.l., 1994.

(161) John M. Prausnitz, Rudiger N. Lichtenthaler, Edmundo Gomes de Azevedo. *Molecular Thermodynamics of Fluid-Phase Equilibria (3rd Edition)*-; Prentice Hall: Upper Saddle River, New Jersey, 1998.

(162) Rice, N. M.; Irving, H. M. N. H.; Leonard, M. A. *Pure Appl. Chem.* **1993**, *65*, 2373–2396.

(163) Berthod, A.; Carda-Broch, S. *J. Chromatogr. A* **2004**, *1037*, 3–14.

(164) Hampe, M. J. *Chem.-Ing.-Tech.* **1985**, *57*, 669–681.

(165) Gaikar, V. G.; Sharma, M. M. *Solvent Extr. Ion Exc.* **1986**, *4*, 839–846.

(166) Gmehling, J.; Schedemann, A. *Ind. Eng. Chem. Res.* **2014**, *53*, 17794–17805.

(167) Saravanan, G.; Srinivasan, D. *J. Chem. Eng. Data* **1985**, *30*, 166–171.

(168) Marcilla A; Ruiz F; Olaya MM. *Fluid Phase Equilib.* **1995**, *105*, 71–91.

(169) Machatha, S. G.; Yalkowsky, S. H. *Int. J. Pharm.* **2005**, *294*, 185–192.

(170) Scheytt, T.; Mersmann, P.; Lindstädt, R.; Heberer, T. *Water Air Soil Pollut.* **2005**, *165*, 3–11.

(171) Pinsuwan, S.; Li, A.; Yalkowsky, S. H. *J. Chem. Eng. Data* **1995**, *40*, 623–626.

(172) Sangster, J. *Octanol-water partition coefficients: Fundamentals and physical chemistry*; Wiley series in solution chemistry 2; Wiley: Chichester, 1997.

(173) D. Cronin, M. *CAD* **2006**, *2*, 405–413.

(174) Arnott, J. A.; Planey, S. L. *Expert Opin Drug Discov* **2012**, *7*, 863–875.

(175) Treybal, R. E. *Extracción en fase líquida*. 1º Ed. UTEHA, 1968.

(176) Campbell, J. A. *Ind. Eng. Chem.* **1944**, *36*, 1158–1161.

(177) Brancker, A. V.; Hunter, T. G.; Nash, A. W. *Ind. Eng. Chem. Anal. Ed.* **1940**, *12*, 35–37.

(178) Bachman, I. *Ind. Eng. Chem. Anal. Ed.* **1940**, *12*, 38–39.

(179) Othmer, D. F.; Tobias, P. E. *Ind. Eng. Chem.* **1942**, *34*, 690–692.

(180) Hand, D. B. *J. Phys. Chem.* **1930**, *34*, 1961–2000.

(181) Eisen, E. O.; Joffe, J. *J. Chem. Eng. Data* **1966**, *11*, 480–484.

(182) Chemat, F.; Strube, J. *Green Extraction of Natural Products*; Wiley-VCH Verlag GmbH & Co. KGaA: Weinheim, Germany, 2015.

(183) DDBST - DDBST GmbH. http://www.ddbst.com/ (accessed March 30, 2020).

(184) DIPPR | Design Institute for Physical Properties. https://www.aiche.org/dippr (accessed March 30, 2020).

(185) Reaxys. https://www.reaxys.com/ (accessed March 30, 2020).

(186) Gross, J.; Sadowski, G. *Ind. Eng. Chem. Res.* **2001**, *40*, 1244–1260.

(187) Klamt, A.; Eckert, F. *Fluid Phase Equilib.* **2000**, *172*, 43–72.

(188) Gmehling, J.; Kolbe, B.; Kleiber, M.; Rarey, J. R. *Chemical thermodynamics for process simulation*; Wiley-VCH-Verl.: Weinheim, 2012.

(189) Hildebrand, J. H.; Scott, R. L. *The solubility of nonelctrolytes*; Reinhold Pub. Corp.: New York, N.Y., 1950.

(190) Hansen, C. M. *Hansen solubility parameters: A user's handbook*, 2nd ed.; Taylor & Francis: Boca Raton, 2007.

(191) Hofmeister, F. *Archiv fuer experimentelle Pathologie und Pharmakologie* **1888**, *24*, 247–260.

(192) Poiseuille Jl. *Ann. Chim. Phys.* **1847**, 76–110.

(193) Kunz, W.; Henle, J.; Ninham, B. W. *Curr. Opin. Colloid Interface Sci.* **2004**, *9*, 19–37.

(194) Kunz, W. *Specific ion effects*; World Scientific: Singapore, Hackensack NJ, 2010.

(195) Schwierz, N.; Horinek, D.; Netz, R. R. *Langmuir* **2013**, *29*, 2602–2614.

(196) Kunz, W.; Lo Nostro, P.; Ninham, B. W. *Curr. Opin. Colloid Interface Sci.* **2004**, *9*, 1–18.

(197) Collins, K. D.; Washabaugh, M. W. *Q. Rev. Biophys.* **1985**, *18*, 323–422.

(198) Traube, J. *J. Phys. Chem.* **1909**, *14*, 452–470.

(199) Schwierz, N.; Horinek, D.; Netz, R. R. *Langmuir* **2010**, *26*, 7370–7379.

(200) Zhang, Y.; Cremer, P. S. *Proc. Natl. Acad. Sci. U.S.A.* **2009**, *106*, 15249–15253.

(201) Komsa-Penkova, R.; Koynova, R.; Kostov, G.; Tenchov, B. G. *Biochim. Biophys. Acta* **1996**, *1297*, 171–181.

(202) Lyklema, J. *Adv. Colloid Interface Sci.* **2003**, *100-102*, 1–12.

(203) Lyklema, J. *Chem. Phys. Lett.* **2009**, *467*, 217–222.

(204) Schwierz, N.; Horinek, D.; Netz, R. R. *Langmuir* **2015**, *31*, 215–225.

(205) Boström, M.; Tavares, F. W.; Finet, S.; Skouri-Panet, F.; Tardieu, A.; Ninham, B. W. *Biophys. Chem.* **2005**, *117*, 217–224.

(206) Salis, A.; Monduzzi, M. *Curr. Opin. Colloid Interface Sci.* **2016**, *23*, 1–9.

(207) Schwierz, N.; Horinek, D.; Sivan, U.; Netz, R. R. *Curr. Opin. Colloid Interface Sci.* **2016**, *23*, 10–18.

(208) Kunz, W. *Curr. Opin. Colloid Interface Sci.* **2010**, *15*, 34–39.

(209) Leontidis, E. *Curr. Opin. Colloid Interface Sci.* **2002**, *7*, 81–91.

(210) Zhang, Y.; Cremer, P. S. *Curr. Opin. Chem. Biol.* **2006**, *10*, 658–663.

(211) Marcus, Y. *Chem. Rev.* **2009**, *109*, 1346–1370.

(212) Cox, W. M.; Wolfenden, J. H. *P. Roy. Soc. A-Math. Phy.* **1934**, *145*, 475–488.

(213) Jenkins, H. D. B.; Marcus, Y. *Chem. Rev.* **1995**, *95*, 2695–2724.

(214) Jones, G.; Dole, M. *J. Am. Chem. Soc.* **1929**, *51*, 2950–2964.

(215) Gurney, R. W. *Ionic processes in solution*; McGraw-Hill: New York, 1953.

(216) Krestov, G. A. *Thermodynamics of solvation: Solution and dissolution, ions and solvents, structure and energetics*; Ellis Horwood series in physical chemistry; Horwood: New York, 1991.

(217) Robinson, J. B.; Strottmann, J. M.; Stellwagen, E. *Proc. Natl. Acad. Sci. U.S.A.* **1981**, *78*, 2287–2291.

(218) Zwanzig, R. *J. Chem. Phys.* **1963**, *38*, 1603–1605.

(219) Zwanzig, R. *J. Chem. Phys.* **1970**, *52*, 3625.

(220) Franks, F. *Water: a comprehensive treatise, Vol. 3*; Plenum Press: London, 1973.

(221) Bakker, H. J. *Chem. Rev.* **2008**, *108*, 1456–1473.

(222) Zangi, R. *J. Phys. Chem. B* **2010**, *114*, 643–650.

(223) Okur, H. I.; Hladílková, J.; Rembert, K. B.; Cho, Y.; Heyda, J.; Dzubiella, J.; Cremer, P. S.; Jungwirth, P. *J. Phys. Chem. B* **2017**, *121*, 1997–2014.

(224) Omta, A. W.; Kropman, M. F.; Woutersen, S.; Bakker, H. J. *Science* **2003**, *301*, 347–349.

(225) Omta, A. W.; Kropman, M. F.; Woutersen, S.; Bakker, H. J. *J. Chem. Phys.* **2003**, *119*, 12457–12461.

(226) Kropman, M. F.; Bakker, H. J. *J. Am. Chem. Soc.* **2004**, *126*, 9135–9141.

(227) Wachter, W.; Kunz, W.; Buchner, R.; Hefter, G. *J. Phys. Chem. A* **2005**, *109*, 8675–8683.

(228) Stirnemann, G.; Wernersson, E.; Jungwirth, P.; Laage, D. *J. Am. Chem. Soc.* **2013**, *135*, 11824–11831.

(229) O'Brien, J. T.; Prell, J. S.; Bush, M. F.; Williams, E. R. *J. Am. Chem. Soc.* **2010**, *132*, 8248–8249.

(230) Marcus, Y. *J. Solution Chem.* **2009**, *38*, 513–516.

(231) Marcus, Y. *Pure Appl. Chem.* **2010**, *82*, 1889–1899.

(232) Kropman, M. F.; Bakker, H. J. *Chem. Phys. Lett.* **2003**, *370*, 741–746.

(233) Ball, P.; Hallsworth, J. E. *Phys. Chem. Chem. Phys.* **2015**, *17*, 8297–8305.

(234) Hamaguchi, K.; Geiduschek, E. P. *J. Am. Chem. Soc.* **1962**, *84*, 1329–1338.

(235) Tielrooij, K. J.; Garcia-Araez, N.; Bonn, M.; Bakker, H. J. *Science* **2010**, *328*, 1006–1009.

(236) Tielrooij, K. J.; van der Post, S. T.; Hunger, J.; Bonn, M.; Bakker, H. J. *J. Phys. Chem. B* **2011**, *115*, 12638–12647.

(237) Collins, K. D. *Biophys. J.* **1997**, *72*, 65–76.

(238) Collins, K. D. *Methods* **2004**, *34*, 300–311.

(239) Collins, K. D. *Biophys. Chem.* **2006**, *119*, 271–281.

(240) Collins, K. D.; Neilson, G. W.; Enderby, J. E. *Biophys. Chem.* **2007**, *128*, 95–104.

(241) Collins, K. D. *Biophys. Chem.* **2012**, *167*, 43–59.

(242) Washabaugh, M. W.; Collins, K. D. *J. Biol. Chem.* **1986**, *261*, 12477–12485.

(243) Collins, K. D. *Proc. Natl. Acad. Sci. U.S.A.* **1995**, *92*, 5553–5557.

(244) Kuhn, L. A.; Siani, M. A.; Pique, M. E.; Fisher, C. L.; Getzoff, E. d.; Tainer, J. A. *J. Mol. Biol.* **1992**, *228*, 13–22.

(245) Enderby, J. E. *Chem. Soc. Rev.* **1995**, *24*, 159.

(246) Salis, A.; Ninham, B. W. *Chem. Soc. Rev.* **2014**, *43*, 7358–7377.

(247) Morris, D. F. C. Ionic radii and enthalpies of hydration of ions. In *Structure and Bonding*; Jørgensen, C. K., Neilands, J. B., Nyholm, R. S., Reinen, D., Williams, R. J. P., Eds.; Structure and Bonding 4; Springer: Berlin, Heidelberg, 1968; pp 63–82.

(248) Lee, J. d. *Concise inorganic chemistry*, 4. ed., rev. ed.; Chapman & Hall: London, 1991.

(249) Robinson, R. A.; Stokes, R. H. *Electrolyte solutions*, 2., rev. ed.; Dover Publ: Mineola, NY, 2002.

(250) Vlachy, N.; Jagoda-Cwiklik, B.; Vácha, R.; Touraud, D.; Jungwirth, P.; Kunz, W. *Adv. Colloid Interface Sci.* **2009**, *146*, 42–47.

(251) Renoncourt, A.; Vlachy, N.; Bauduin, P.; Drechsler, M.; Touraud, D.; Verbavatz, J.-M.; Dubois, M.; Kunz, W.; Ninham, B. W. *Langmuir* **2007**, *23*, 2376–2381.

(252) Vlachy, N.; Drechsler, M.; Verbavatz, J.-M.; Touraud, D.; Kunz, W. *J. Colloid Interface Sci.* **2008**, *319*, 542–548.

(253) Vlachy, N.; Drechsler, M.; Touraud, D.; Kunz, W. *C. R. Chim.* **2009**, *12*, 30–37.

(254) Chen, X.; Yang, T.; Kataoka, S.; Cremer, P. S. *J. Am. Chem. Soc.* **2007**, *129*, 12272–12279.

(255) Jungwirth, P.; Tobias, D. J. *J. Phys. Chem. B* **2001**, *105*, 10468–10472.

(256) Jungwirth, P.; Tobias, D. J. *Chem. Rev.* **2006**, *106*, 1259–1281.

(257) Jarvis, N. L.; Scheiman, M. A. *J. Phys. Chem.* **1968**, *72*, 74–78.

(258) Weissenborn, P. K.; Pugh, R. J. *J. Colloid Interface Sci.* **1996**, *184*, 550–563.

(259) Onsager, L.; Samaras, N. N. T. *J. Chem. Phys.* **1934**, *2*, 528–536.

(260) Ghosal, S.; Hemminger, J. C.; Bluhm, H.; Mun, B. S.; Hebenstreit, E. L. D.; Ketteler, G.; Ogletree, D. F.; Requejo, F. G.; Salmeron, M. *Science* **2005**, *307*, 563–566.

(261) Padmanabhan, V.; Daillant, J.; Belloni, L.; Mora, S.; Alba, M.; Konovalov, O. *Phys. Rev. Lett.* **2007**, *99*, 86105.

(262) Viswanath, P.; Motschmann, H. *J. Phys. Chem. C* **2007**, *111*, 4484–4486.

(263) Horinek, D.; Mamatkulov, S. I.; Netz, R. R. *J. Chem. Phys.* **2009**, *130*, 124507.

(264) López-León, T.; Santander-Ortega, M. J.; Ortega-Vinuesa, J. L.; Bastos-González, D. *J. Phys. Chem. C* **2008**, *112*, 16060–16069.

(265) Horinek, D.; Netz, R. R. *Phys. Rev. Lett.* **2007**, *99*, 226104.

(266) Horinek, D.; Serr, A.; Bonthuis, D. J.; Boström, M.; Kunz, W.; Netz, R. R. *Langmuir* **2008**, *24*, 1271–1283.

(267) Dishon, M.; Zohar, O.; Sivan, U. *Langmuir* **2009**, *25*, 2831–2836.

(268) Morag, J.; Dishon, M.; Sivan, U. *Langmuir* **2013**, *29*, 6317–6322.

(269) Long, F. A.; McDevit, W. F. *Chem. Rev.* **1951**, 119–169.

(270) Kunz, W.; Belloni, L.; Bernard, O.; Ninham, B. W. *J. Phys. Chem. B* **2004**, *108*, 2398–2404.

(271) Setchenov, J. *Z. Phys. Chem.* **1889**, *4*, 117–128.

(272) Pytkowicz, R. M., Ed. *Activity coefficients in electrolyte solutions*; CRC Press: Boca Raton, Fla., 1979.

(273) Endo, S.; Pfennigsdorff, A.; Goss, K.-U. *Environ. Sci. Technol.* **2012**, *46*, 1496–1503.

(274) Gross, P. M. *Chem. Rev.* **1933**, *13*, 91–101.

(275) Robinson, D. R. [16] The determination of activity coefficients from distribution measurements. In *Enzyme structure*; Hirs, C. H. W., Ed.; Methods in Enzymology 26; Acad. Press: New York, NY, 1972; pp 365–380.

(276) Wen-Hui, X.; Jing-Zhe, S.; Xi-Ming, X. *Thermochim. Acta* **1990**, *169*, 271–286.

(277) Görgényi, M.; Dewulf, J.; van Langenhove, H.; Héberger, K. *Chemosphere* **2006**, *65*, 802–810.

(278) Debye, P., McAulay, J. *Phys. Z.* **1925**, *26*, 22–29.

(279) Conway, B.E., Desnoyers, J.E., Smith, A. C. *Phil. Trans. R. Soc. Lond. A* **1964**, *256*, 389–437.

(280) Masterton, W. L.; Lee, T. P. *J. Phys. Chem.* **1970**, *74*, 1776–1782.

(281) Xie, W.H., Yang, W.T. *Acta Physicochim. Sin.* **1987**, *3*, 258–264.

(282) Xie, W. H., Ji, H.W., Li, W.J. *Acta Physicochim. Sin.* **1985**, *1*, 304–307.

(283) Ni, N.; Yalkowsky, S. H. *Int. J. Pharm.* **2003**, *254*, 167–172.

(284) Dai, J.-Y.; Sun, Y.-Q.; Xiu, Z.-L. *Eng. Life Sci.* **2014**, *14*, 108–117.

(285) Stevens, M. J.; Rempe, S. L. B. *J. Phys. Chem. B* **2016**, *120*, 12519–12530.

(286) Ohtaki, H.; Radnai, T. *Chem. Rev.* **1993**, *93*, 1157–1204.

(287) Shimizu, S. *Food Funct.* **2015**, *6*, 3228–3235.

(288) Zangi, R.; Hagen, M.; Berne, B. J. *J. Am. Chem. Soc.* **2007**, *129*, 4678–4686.

(289) Graziano, G. *Chem. Phys. Lett.* **2010**, *491*, 54–58.

(290) Balasubramanian, D.; Shaikh, R. *Biopolymers* **1973**, *12*, 1639–1650.

(291) Bjerrum, J.; Ryhl, T.; Åsen, S.; Halvarson, H.; Nilsson, L. *Acta Chem. Scand.* **1964**, *18*, 843–857.

(292) Hyde, A. M.; Zultanski, S. L.; Waldman, J. H.; Zhong, Y.-L.; Shevlin, M.; Peng, F. *Org. Process Res. Dev.* **2017**, *21*, 1355–1370.

(293) Willauer, H. D.; Huddleston, J. G.; Rogers, R. D. *Ind. Eng. Chem. Res.* **2002**, *41*, 1892–1904.

(294) Gerlach, T.; Smirnova, I. *J. Chem. Eng. Data* **2016**, *61*, 3548–3558.

(295) Ingram, T.; Gerlach, T.; Mehling, T.; Smirnova, I. *Fluid Phase Equilib.* **2012**, *314*, 29–37.

(296) Neuberg, C. *Biochem. Z.* **1916**, *76*, 107–176.

(297) Saleh, A. M.; El-Khordagui, L. K. *Int. J. Pharm.* **1985**, *24*, 231–238.

(298) Balasubramanian, D.; Srinivas, V.; Gaikar, V. G.; Sharma, M. M. *J. Phys. Chem.* **1989**, *93*, 3865–3870.

(299) Bauduin, P.; Renoncourt, A.; Kopf, A.; Touraud, D.; Kunz, W. *Langmuir* **2005**, *21*, 6769–6775.

(300) Williams, R. O. *J. Am. Chem. Soc.* **2000**, *122*, 9882.

(301) Bauduin, P. Characterization of short polypropylene glycol monoalkylethers and design of enzymatic reaction media. Dissertation, Universität, Regensburg, 2005.

(302) Sokolowski, A.; Chlebicki, J. *Tenside Detergents* **1982**, *19*, 282–286.

(303) Sokołowski, A.; Burczyk, B. *J. Colloid Interface Sci.* **1983**, *94*, 369–379.

(304) Bauduin, P.; Basse, A.; Touraud, D.; Kunz, W. *Colloids Surf. A Physicochem. Eng. Asp.* **2005**, *270-271*, 8–12.

(305) Stig E Friberg. *Curr. Opin. Colloid Interface Sci.* **1997**, 490–494.

(306) Srinivas, V.; Rodley, G. A.; Ravikumar, K.; Robinson, W. T.; Turnbull, M. M. *Langmuir* **1997**, *13*, 3235–3239.

(307) Gaikar, V. G.; Sharma, M. M. *Separations Technology* **1993**, *3*, 2–11.

(308) Srinivas, V.; Balasubramanian, D. *Langmuir* **1998**, *14*, 6658–6661.

(309) Kunz, W.; Holmberg, K.; Zemb, T. *Curr. Opin. Colloid Interface Sci.* **2016**, *22*, 99–107.

(310) da Silva, R. C.; Spitzer, M.; da Silva, L. H.M.; Loh, W. *Thermochim. Acta* **1999**, *328*, 161–167.

(311) Horváth-Szabó, G.; Yin, Q.; Friberg, S. E. *J. Colloid Interface Sci.* **2001**, *236*, 52–59.

(312) Queste, S.; Bauduin, P.; Touraud, D.; Kunz, W.; Aubry, J.-M. *Green Chem.* **2006**, *8*, 822–830.

(313) Strey, R.; Viisanen, Y.; Aratono, M.; Kratohvil, J. P.; Yin, Q.; Friberg, S. E. *J. Phys. Chem. B* **1999**, *103*, 9112–9116.

(314) Durand, M.; Zhu, Y.; Molinier, V.; Féron, T.; Aubry, J.-M. *J. Surfactants Deterg.* **2009**, *12*, 371–378.

(315) Bauduin, P.; Wattebled, L.; Schrödle, S.; Touraud, D.; Kunz, W. *J. Mol. Liq.* **2004**, *115*, 23–28.

(316) Charman, W. N.; Lai, C. S.; Finnin, B. C.; Reed, B. L. *Pharm. Res.* **1991**, *8*, 1144–1150.

(317) Coffman, R. E.; Kildsig, D. O. *J. Pharm. Sci.* **1996**, *85*, 848–853.

(318) Coffman, R. E.; Kildsig, D. O. *Pharm. Res.* **1996**, *13*, 1460–1463.

(319) Charman, W. N.; Lai, C. S.C.; Craik, D. J.; Finnin, B. C.; Reed, B. L. *Aust. J. Chem.* **1993**, *46*, 377.

(320) Cui, Y.; Xing, C.; Ran, Y. *J. Pharm. Sci.* **2010**, *99*, 3048–3059.

(321) Cui, Y. *Int. J. Pharm.* **2010**, *397*, 36–43.

(322) Shimizu, S.; Matubayasi, N. *J. Phys. Chem. B* **2014**, *118*, 10515–10524.

(323) Shimizu, S.; Booth, J. J.; Abbott, S. *Phys. Chem. Chem. Phys.* **2013**, *15*, 20625–20632.

(324) Booth, J. J.; Abbott, S.; Shimizu, S. *J. Phys. Chem. B* **2012**, *116*, 14915–14921.

(325) Wagle, V. B.; Kothari, P. S.; Gaikar, V. G. *J. Mol. Liq.* **2007**, *133*, 68–76.

(326) Coffman, R. E.; Kildsig, D. O. *J. Pharm. Sci.* **1996**, *85*, 951–954.

(327) Frank, H. S.; Franks, F. *J. Chem. Phys.* **1968**, *48*, 4746–4757.

(328) Abbott, S.; Booth, J. J.; Shimizu, S. *Green Chem.* **2017**, *19*, 68–75.

(329) Sanghvi, R.; Evans, D.; Yalkowsky, S. H. *Int. J. Pharm.* **2007**, *336*, 35–41.

(330) Booth, J. J.; Omar, M.; Abbott, S.; Shimizu, S. *Phys. Chem. Chem. Phys.* **2015**, *17*, 8028–8037.

(331) Schnell, E.; Touraud, D.; Gick, R.; Kunz, W. *Int. J. Cosmet. Sci.* **2008**, *30*, 347–351.

(332) Bauduin, P.; Testard, F.; Zemb, T. *J. Phys. Chem. B* **2008**, *112*, 12354–12360.

(333) Bauduin, P.; Testard, F.; Berthon, L.; Zemb, T. *Phys. Chem. Chem. Phys.* **2007**, *9*, 3776–3785.

(334) Hatzopoulos, M. H.; Eastoe, J.; Dowding, P. J.; Rogers, S. E.; Heenan, R.; Dyer, R. *Langmuir* **2011**, *27*, 12346–12353.

(335) Eastoe, J.; Hatzopoulos, M. H.; Dowding, P. J. *Soft Matter* **2011**, *7*, 5917.

(336) Schöttl, S.; Marcus, J.; Diat, O.; Touraud, D.; Kunz, W.; Zemb, T.; Horinek, D. *Chem. Sci.* **2014**, *5*, 2949–2954.

(337) Klossek, M. L.; Touraud, D.; Zemb, T.; Kunz, W. *Chemphyschem* **2012**, *13*, 4116–4119.

(338) Diat, O.; Klossek, M. L.; Touraud, D.; Deme, B.; Grillo, I.; Kunz, W.; Zemb, T. *J. Appl. Crystallogr.* **2013**, *46*, 1665–1669.

(339) Marcus, J.; Touraud, D.; Prévost, S.; Diat, O.; Zemb, T.; Kunz, W. *Phys. Chem. Chem. Phys.* **2015**, *17*, 32528–32538.

(340) Onuki, A.; Okamoto, R. *Curr. Opin. Colloid Interface Sci.* **2011**, *16*, 525–533.

(341) Onuki, A.; Yabunaka, S.; Araki, T.; Okamoto, R. *Curr. Opin. Colloid Interface Sci.* **2016**, *22*, 59–64.

(342) Buchecker, T.; Krickl, S.; Winkler, R.; Grillo, I.; Bauduin, P.; Touraud, D.; Pfitzner, A.; Kunz, W. *Phys. Chem. Chem. Phys.* **2017**, *19*, 1806–1816.

(343) Niels Bjerrum. *Z. Elektrochem.* **1918**, *24*, 321–328.

(344) Gibbard, H. F.; Scatchard, G.; Rousseau, R. A.; Creek, J. L. *J. Chem. Eng. Data* **1974**, *19*, 281–288.

(345) Zdanovskii, A. B. *Trudy Solyanoi Laboratorii Akad SSSR, No.6* **1936**, 5–70.

(346) Robinson, R. A.; Stokes, R. H. *J. Phys. Chem.* **1966**, *70*, 2126–2131.

(347) Kirgintsev, A.; Luk'yanov, A. V. *Russ. J. Phys. Chem.* **1966**, *40*, 953–956.

(348) Chen, H.; Sangster, J.; Teng, T. T.; Lenzi, F. *Can. J. Chem Eng.* **1973**, *51*, 234–241.

(349) Sangster, J.; Lenzi, F. *Can. J. Chem. Eng.* **1975**, *53*, 1410–1413.

(350) Clegg, S. L.; Seinfeld, J. H. *J. Phys. Chem. A* **2004**, *108*, 1008–1017.

(351) Königsberger, E.; Königsberger, L.-C.; Hefter, G.; May, P. M. *J. Solution Chem.* **2007**, *36*, 1619–1634.

(352) Dahneke, B. E. *Measurement of suspended particles by quasi-elastic light scattering: Edited by Barton E. Dahneke*; Wiley: New York, 1983.

(353) Pecora, R., Ed. *Dynamic Light Scattering: Applications of Photon Correlation Spectroscopy*; Springer US: Boston, MA, 1985.

(354) Du Noüy, P. L. *J. Gen. Physiol.* **1925**, *7*, 625–631.

(355) Berry, J. D.; Neeson, M. J.; Dagastine, R. R.; Chan, D. Y. C.; Tabor, R. F. *J. Colloid Interface Sci.* **2015**, *454*, 226–237.

(356) Hernández-Baltazar, E.; Gracia-Fadrique, J. *J. Colloid Interface Sci.* **2005**, *287*, 213–216.

(357) Rotenberg, Y.; Boruvka, L.; Neumann, A.W. *J. Colloid Interface Sci.* **1983**, *93*, 169–183.

(358) Hefter, G. T.; Tomkins, R. P. T., Eds. *The experimental determination of solubilities*; Wiley series in solution chemistry 6; Wiley: Chichester, 2003.

(359) Gomis, V.; Ruíz, F.; Asensi, J. C.; Saquete, M. D. *Fluid Phase Equilib.* **1997**, *129*, 15–19.

(360) Fischer, K. *Angew. Chem.* **1935**, *48*.

(361) Gaspar, E. M. S. M.; Lopes, J. F. *J. Chromatogr. A* **2009**, *1216*, 2762–2767.

(362) Hájek, M.; Skopal, F.; Machek, J. *Eur. J. Lipid Sci. Technol.* **2006**, *108*, 666–669.

(363) Bondioli, P.; Della Bella, L. *Eur. J. Lipid Sci. Technol.* **2005**, *107*, 153–157.

(364) Debye, P., Hückel, E. *Phys. Z.* **1923**, *24*, 185–206.

(365) Waisman, E.; Lebowitz, J. L. *J. Chem. Phys.* **1970**, *52*, 4307–4309.

(366) Held, C. *Measuring and modeling thermodynamic properties of biological solutions*. Zugl.: Dortmund, Techn. Univ., Diss., 2011, 1. Aufl.; Schriftenreihe Thermodynamik 2; Verl. Dr. Hut: München, 2012.

(367) Lüdecke, C.; Lüdecke, D. *Thermodynamik: Physikalisch-chemische Grundlagen der thermischen Verfahrenstechnik*; Springer-Lehrbuch; Springer: Berlin, Heidelberg, 2000.

(368) Margules, M. *Sitzungsber. Akad. Wiss. Wien, math.-naturwiss. Klasse, 104 Abt. IIa* **1895**, 1243–1278.

(369) van Laar, J. J. *Z. Phys. Chem.* **1910**, *72U*.

(370) Wilson, G. M. *J. Am. Chem. Soc.* **1964**, *86*, 127–130.

(371) Renon, H.; Prausnitz, J. M. *AIChE J.* **1968**, *14*, 135–144.

(372) Abrams, D. S.; Prausnitz, J. M. *AIChE J.* **1975**, *21*, 116–128.

(373) Fredenslund, A.; Jones, R. L.; Prausnitz, J. M. *AIChE J.* **1975**, *21*, 1086–1099.

(374) Gmehling, J. *Fluid Phase Equilib.* **1998**, *144*, 37–47.

(375) Weidlich, U.; Gmehling, J. *Ind. Eng. Chem. Res.* **1987**, *26*, 1372–1381.

(376) Klamt, A.; Schüürmann, G. *J. Chem. Soc., Perkin Trans. 2* **1993**, 799–805.

(377) Klamt, A.; Jonas, V.; Bürger, T.; Lohrenz, J. C. W. *J. Phys. Chem. A* **1998**, *102*, 5074–5085.

(378) Eckert, F.; Klamt, A. *AIChE J.* **2002**, *48*, 369–385.

(379) Chen, C.-C.; Britt, H. I.; Boston, J. F.; Evans, L. B. *AIChE J.* **1982**, *28*, 588–596.

(380) Chen, C.-C.; Evans, L. B. *AIChE J.* **1986**, *32*, 444–454.

(381) Pitzer, K. S. *J. Phys. Chem.* **1973**, *77*, 268–277.

(382) Nass, K. K. *AIChE J.* **1988**, *34*, 1257–1266.

(383) Liu, Y.; Watanasiri, S. *Fluid Phase Equilib.* **1996**, *116*, 193–200.

(384) Zerres, H.; Prausnitz, J. M. *AIChE J.* **1994**, *40*, 676–691.

(385) Papaiconomou, N.; Simonin, J.-P.; Bernard, O.; Kunz, W. *Phys. Chem. Chem. Phys.* **2002**, *4*, 4435–4443.

(386) Archer, D. G. *J. Phys. Chem. Ref. Data* **1991**, *20*, 509–555.

(387) Nasirzadeh, K.; Neueder, R.; Kunz, W. *Ind. Eng. Chem. Res.* **2005**, *44*, 3807–3814.

(388) Chen, H.; Dou, M.; Nan, S. *Fluid Phase Equilib.* **2011**, *305*, 83–87.

(389) Pirahmadi, F.; Dehghani, M. R.; Behzadi, B.; Seyedi, S. M.; Rabiee, H. *Fluid Phase Equilib.* **2010**, *299*, 122–126.

(390) Pirahmadi, F.; Behzadi, B.; Dehghani, M. R. *Fluid Phase Equilib.* **2011**, *307*, 39–44.

(391) Pirahmadi, F.; Dehghani, M. R.; Behzadi, B. *Fluid Phase Equilib.* **2012**, *325*, 1–5.

(392) Kuramochi, H.; Noritomi, H.; Hoshino, D.; Nagahama, K. *J. Chem. Eng. Data* **1997**, *42*, 470–474.

(393) Kuramochi, H.; Noritomi, H.; Hoshino, D.; Nagahama, K. *Fluid Phase Equilib.* **1997**, *130*, 117–132.

(394) Gerlach, T.; Müller, S.; Smirnova, I. *AIChE J.* **2018**, *64*, 272–285.

(395) Mohammad, S.; Held, C.; Altuntepe, E.; Köse, T.; Gerlach, T.; Smirnova, I.; Sadowski, G. *Fluid Phase Equilib.* **2016**, *416*, 83–93.

(396) Dahl, S., Macedo, E.A. *Ind. Eng. Chem.* **1992**, *31*, 1195–1201.

(397) Myers, J. A.; Sandler, S. I.; Wood, R. H. *Ind. Eng. Chem. Res.* **2002**, *41*, 3282–3297.

(398) Zuo, J. Y.; Zhang, D.; Fürst, W. *Fluid Phase Equilib.* **2000**, *175*, 285–310.

(399) Khoshkbarchi, M. K.; Vera, J. H. *Ind. Eng. Chem. Res.* **1998**, *37*, 3052–3057.

(400) Chapman, W. G.; Gubbins, K. E.; Jackson, G.; Radosz, M. *Fluid Phase Equilib.* **1989**, *52*, 31–38.

(401) Wertheim, M. S. *J. Stat. Phys.* **1984**, *35*, 19–34.

(402) Wertheim, M. S. *J. Stat. Phys.* **1984**, *35*, 35–47.

(403) Schreckenberg, J. M.A.; Dufal, S.; Haslam, A. J.; Adjiman, C. S.; Jackson, G.; Galindo, A. *Mol. Phys.* **2014**, *112*, 2339–2364.

(404) Cameretti, L. F.; Sadowski, G.; Mollerup, J. M. *Ind. Eng. Chem. Res.* **2005**, *44*, 3355–3362.

(405) Gross, J.; Sadowski, G. *Ind. Eng. Chem. Res.* **2002**, *41*, 5510–5515.

(406) Wolbach, J. P.; Sandler, S. I. *Ind. Eng. Chem. Res.* **1998**, *37*, 2917–2928.

(407) Chen, S. S.; Kreglewski, A. *Ber. Bunsen Phys. Chem.* **1977**, *81*, 1048–1052.

(408) Held, C.; Prinz, A.; Wallmeyer, V.; Sadowski, G. *Chem. Eng. Sci.* **2012**, *68*, 328–339.

(409) Reschke, T.; Brandenbusch, C.; Sadowski, G. *Fluid Phase Equilib.* **2014**, *375*, 306–315.

(410) Held, C.; Cameretti, L. F.; Sadowski, G. *Fluid Phase Equilib.* **2008**, *270*, 87–96.

(411) Held, C.; Sadowski, G. *Fluid Phase Equilib.* **2009**, *279*, 141–148.

(412) Held, C.; Reschke, T.; Mohammad, S.; Luza, A.; Sadowski, G. *Chem. Eng. Res. Des.* **2014**, *92*, 2884–2897.

(413) Nann, A.; Held, C.; Sadowski, G. *Ind. Eng. Chem. Res.* **2013**, *52*, 18472–18481.

(414) Fuchs, D.; Fischer, J.; Tumakaka, F.; Sadowski, G. *Ind. Eng. Chem. Res.* **2006**, *45*, 6578–6584.

(415) Tihic, A.; Kontogeorgis, G. M.; Solms, N. von; Michelsen, M. L. *Fluid Phase Equilib.* **2006**, *248*, 29–43.

(416) Huang, S. H.; Radosz, M. *Ind. Eng. Chem. Res.* **1990**, *29*, 2284–2294.

(417) Cameretti, L. F.; Sadowski, G. *Chem. Eng. Process.* **2008**, *47*, 1018–1025.

(418) Kleiner, M.; Sadowski, G. *Fluid Phase Equilib.* **2007**, *260*, 190–194.

(419) Mohammad, S.; Held, C.; Altuntepe, E.; Köse, T.; Sadowski, G. *J. Phys. Chem. B* **2016**, *120*, 3797–3808.

(420) Tsurko, E. N.; Neueder, R.; Kunz, W. *J. Solution Chem.* **2007**, *36*, 651–672.

(421) Tsurko, E. N.; Neueder, R.; Kunz, W. *J. Solution Chem.* **2008**, *37*, 421–431.

(422) Tsurko, E. N.; Neueder, R.; Kunz, W. *Acta Chim. Slov.* **2009**, *56*, 58–64.

(423) Tsurko, E. N.; Neueder, R.; Kunz, W. *J. Chem. Eng. Data* **2012**, *57*, 3123–3127.

(424) Tsurko, E. N.; Neueder, R.; Müller, R.; Kunz, W. *J. Chem. Eng. Data* **2014**, *59*, 2741–2749.

(425) Held, C.; Tsurko, E. N.; Neueder, R.; Sadowski, G.; Kunz, W. *J. Chem. Eng. Data* **2016**, *61*, 3190–3199.

(426) Held, C.; Reschke, T.; Müller, R.; Kunz, W.; Sadowski, G. *J. Chem. Thermodyn.* **2014**, *68*, 1–12.

(427) Plesiewicz, E.; Stępień, E.; Bolewska, K.; Wierzchowski, K. L. *Biophys. Chem.* **1976**, *4*, 131–141.

(428) Żółkiewski, M. *J. Solution Chem.* **1987**, *16*, 1025–1034.

(429) Wagle, V. B.; Gaikar, V. G. *J. Chem. Eng. Data* **2006**, *51*, 886–891.

(430) Wagle, V. B.; Gaikar, V. G. *J. Chem. Eng. Data* **2009**, *54*, 1775–1781.

(431) Bower, V. E.; Robinson, R. A. *J. Phys. Chem.* **1963**, *67*, 1524–1527.

(432) Szyszkowski, B. von. *Z. Phys. Chem.* **1908**, *64U*.

(433) Rosen, M. J. *Surfactants and Interfacial Phenomena*; John Wiley & Sons, Inc: Hoboken, NJ, USA, 2004.

(434) Hey, M. J.; Kippax, P. G. *Colloids Surf. A Physicochem. Eng. Asp.* **2005**, *262*, 198–203.

(435) Barthel, J.; Neueder, R. *GIT Fachz. Lab.* **1984**, *28*, 1002–1012.

(436) Widera, B.; Neueder, R.; Kunz, W. *Langmuir* **2003**, *19*, 8226–8229.

(437) Lavi, P.; Marmur, A. *J. Colloid Interface Sci.* **2000**, *230*, 107–113.

(438) Connors, K. A.; Wright, J. L. *Anal. Chem.* **1989**, *61*, 194–198.

(439) Grote, F.; Ermilova, I.; Lyubartsev, A. P. *J. Phys. Chem. B* **2018**, *122*, 8416–8428.

(440) Gibbard, H. F.; Scatchard, G. *J. Chem. Eng. Data* **1973**, *18*, 293–298.

(441) Ts'o, P. O. P.; Melvin, I. S.; Olson, A. C. *J. Am. Chem. Soc.* **1963**, *85*, 1289–1296.

(442) Paul O. P. Ts'o and Sunney I. Chan **1964**.

(443) Kim, J. Y.; Kim, S.; Papp, M.; Park, K.; Pinal, R. *J. Pharm. Sci.* **2010**, *99*, 3953–3965.

(444) Schellman, J. A. *C. R. Trav. Lab. Carlsberg Ser. Chim.* **1955**, *29*, 223–229.

(445) Kelly, F. J.; Robinson, R. A.; Stokes, R. H. *J. Phys. Chem.* **1961**, 1958–1960.

(446) Wen, W.-Y.; Chen, C.-M. L. *J. Phys. Chem.* **1969**, *73*, 2895–2901.

(447) Robinson, R. A.; Stokes, R. H.; Marsh, K. N. *J. Chem. Thermodyn.* **1970**, *2*, 745–750.

(448) Robinson, R. A.; Stokes, R. H. *J. Phys. Chem.* **1961**, 1954–1958.

(449) Smidovich, L. S.; Tsurko, E. N. *Kharkov Univ. Bull. Chem. Ser.* **1999**, *4*, 173–179.

(450) Rankin, D. W.H. *Crystallogr. Rev.* **2009**, *15*, 223–224.

(451) Vazquez, G.; Alvarez, E.; Navaza, J. M. *J. Chem. Eng. Data* **1995**, *40*, 611–614.

(452) Khattab, I. S.; Bandarkar, F.; Fakhree, M. A. A.; Jouyban, A. *Korean J. Chem. Eng.* **2012**, *29*, 812–817.

(453) Glinski, J.; Chavepeyer, G.; Platten, J.‐K. *J. Chem. Phys.* **1996**, *104*, 8816–8820.

(454) Gliński, J.; Chavepeyer, G.; Platten, J.‐K. *J. Chem. Phys.* **1995**, *102*, 2113–2117.

(455) Habrdová, K.; Hovorka, Š.; Bartovská, L. *J. Chem. Eng. Data* **2004**, *49*, 1003–1007.

(456) Yano, Y. F. *J. Colloid Interface Sci.* **2005**, *284*, 255–259.

(457) Lunkenheimer, K.; Schrödle, S.; Kunz, W. *Prog. Colloid Polym. Sci.* **2004**, *126*, 14–20.

(458) Kahlweit, M.; Lessner, E.; Strey, R. *J. Phys. Chem.* **1983**, *87*, 5032–5040.

(459) Pérez, M. M.; Salager, J.-L.; Miñana-Pérez, M.; Graciaa, A.; Lachaise, J. *Prog. Colloid Polym. Sci.* **1995**, *98*, 177–179.

(460) Bauduin, P.; Wattebled, L.; Touraud, D.; Kunz, W. *Z. Phys. Chem.* **2004**, *218*, 631–641.

(461) Schrödle, S.; Buchner, R.; Kunz, W. *Fluid Phase Equilib.* **2004**, *216*, 175–182.

(462) Holtzscherer, C.; Candau, F. *J. Colloid Interface Sci.* **1988**, *125*, 97–110.

(463) Schott. *J. Colloid Interface Sci.* **1998**, *205*, 496–502.

(464) Laughlin, R. G. *The aqueous phase behavior of surfactants*; Colloid Science 6; Academic Press: London, 1996.

(465) Lebeuf, R.; Illous, E.; Dussenne, C.; Molinier, V.; Silva, E. D.; Lemaire, M.; Aubry, J.-M. *ACS Sustain. Chem. Eng.* **2016**, *4*, 4815–4823.

(466) Chirife, J.; Fontan, C. F. *J. Food Sci.* **1980**, *45*, 802–804.

(467) Abdoh, A. A.; Zughul, M. B.; Badwan, A. A. *J. Disper. Sci. Technol.* **2002**, *23*, 759–768.

(468) Jeköné, B. Z. *Acta Pharm. Hung.* **1998**, *68*, 133–136.

(469) Roy, S. D.; Flynn, G. L. *Pharm. Res.* **1989**, *6*, 147–151.

(470) Lo, S. C.; Ramanan, R. N.; Tey, B. T.; Ling, T. C.; Show, P. L.; Ooi, C. W. *J. Chem. Eng. Data* **2015**, *60*, 2848–2857.

(471) Bellisle, F. *Neurosci. Biobehav. Rev.* **1999**, *23*, 423–438.

(472) Eiberweiser, A.; Nazet, A.; Kruchinin, S. E.; Fedotova, M. V.; Buchner, R. *J. Phys. Chem. B* **2015**, *119*, 15203–15211.

(473) Shaukat, S.; Fedotova, M. V.; Kruchinin, S. E.; Bešter-Rogač, M.; Podlipnik, Č.; Buchner, R. *Phys. Chem. Chem. Phys.* **2019**, *21*, 10970–10980.

(474) Hunger, J.; Tielrooij, K.-J.; Buchner, R.; Bonn, M.; Bakker, H. J. *J. Phys. Chem. B* **2012**, *116*, 4783–4795.

(475) Desnoyers, J. E.; Pelletier, G. E.; Jolicoeur, C. *Can. J. Chem.* **1965**, *43*, 3232–3237.

(476) Graf, E. *J. Am. Oil Chem. Soc.* **1983**, *60*, 1861–1867.

(477) Uedaira, H.; Uedaira, H. *J. Chem. Thermodyn.* **1985**, *17*, 901–902.

(478) Uedaira, H.; Ishimura, M. *BCSJ* **1989**, *62*, 574–575.

(479) Uedaira, H.; Uedaira, H. *J. Solution Chem.* **1985**, *14*, 27–34.

(480) Uedaira, H.; Ikura, M.; Uedaira, H. *BCSJ* **1989**, *62*, 1–4.

(481) Sato, Y.; Miyawaki, O. *Food Chem.* **2016**, *190*, 594–598.

(482) Miyawaki, O.; Saito, A.; Matsuo, T.; Nakamura, K. *Biosci. Biotech. Bioch.* **1997**, *61*, 466–469.

(483) Burakowski, A.; Gliński, J. *Chem. Rev.* **2012**, *112*, 2059–2081.

(484) Winkler, R.; Buchecker, T.; Hastreiter, F.; Touraud, D.; Kunz, W. *Phys. Chem. Chem. Phys.* **2017**, *19*, 25463–25470.

(485) Bhupesh C. Roy; Awual M. R.; Goto M. *J. Appl. Sci.* **2007**, *7*, 1053–1060.

(486) Naoki Hirayama; Takaaki Higo; Hisanori Imura. *Solvent Extr. Res. Dev.* **2014**, *21*, 71–76.

(487) Xie, Y.; Yu, F.; Wang, Y.; He, X.; Zhou, S.; Cui, H. *Fluid Phase Equilib.* **2019**, *493*, 137–143.

(488) Gomis, V.; Ruiz, F.; Asensi, J. C.; Cayuela, P. *Fluid Phase Equilib.* **1996**, *119*, 191–195.

(489) Gomis, V.; Ruiz, F.; Vera, G. de; López, E.; Saquete, M.D. *Fluid Phase Equilib.* **1994**, *98*, 141–147.

(490) Chung, N.; Tabata, M. *Talanta* **2002**, *58*, 927–933.

(491) Sólimo, H. N.; Bonatti, C. M.; Zurita, J.; Gramajo de Doz, M. B. *Fluid Phase Equilib.* **1997**, *137*, 163–172.

(492) Santis, R. de; Marrelli, L.; Muscetta, P. N. *J. Chem. Eng. Data* **1976**, *21*, 324–327.

(493) Santis, R. de; Marrelli, L.; Muscetta, P. N. *Chem. Eng. J.* **1976**, *11*, 207–214.

(494) Li, Z.; Tang, Y.; Liu, Y.; Li, Y. *Fluid Phase Equilib.* **1995**, *103*, 143–153.

(495) Gomis, V.; Ruiz, F.; Asensi, J. C.; Saquete, M. D. *J. Chem. Eng. Data* **1996**, *41*, 188–191.

(496) Al-Sahhaf, T. A.; Kapetanovic, E. *J. Chem. Eng. Data* **1997**, *42*, 74–77.

(497) Lintomen, L.; Pinto, R. T. P.; Batista, E.; Meirelles, A. J. A.; Maciel, M. R. W. *J. Chem. Eng. Data* **2000**, *45*, 1211–1214.

(498) Olaya, M. M.; Conesa, J. A.; Marcilla, A. *J. Chem. Eng. Data* **1997**, *42*, 858–864.

(499) Marcilla, A.; Ruiz, F.; García, A. N. *Fluid Phase Equilib.* **1995**, *112*, 273–289.

(500) Tan, T.C.; Aravinth, S. *Fluid Phase Equilib.* **1999**, *163*, 243–257.

(501) Malinowski, J. J.; Daugulis, A. J. *AIChE J.* **1994**, *40*, 1459–1465.

(502) Dalmolin, I.; Pinto, R. R.; Oliveira, L. H. de; Follegatti-Romero, L. A.; Costa, A. C.; Aznar, M. *J. Chem. Thermodyn.* **2017**, *111*, 80–87.

(503) Altway, S.; Pujar, S. C.; Haan, A. B. de. *Fluid Phase Equilib.* **2018**, *475*, 100–110.

(504) Zhang, Y.; Guo, X.; Xu, J.; Wu, Y.; Lu, M. *J. Chem. Eng. Data* **2018**, *63*, 2775–2782.

(505) Cavalcanti, K. V.M.; Follegatti-Romero, L. M.; Dalmolin, I.; Follegatti-Romero, L. A. *J. Chem. Thermodyn.* **2019**, *138*, 59–66.

(506) Gomis, V.; Ruiz, F.; Boluda, N.; Saquete, M.D. *Fluid Phase Equilib.* **1999**, *155*, 241–249.

(507) El-Dossoki, F. I. *Fluid Phase Equilib.* **2011**, *305*, 161–168.

(508) Tang, Y.; Li, Z.; Li, Y. *Fluid Phase Equilib.* **1995**, *105*, 241–258.

(509) Gomis, V.; Ruiz, F.; Boluda, N.; Saquete, M. D. *J. Chem. Eng. Data* **1999**, *44*, 918–920.

(510) Boluda, N.; Gomis, V.; Ruiz, F.; Saquete, M.D.; Barnes, N. *Fluid Phase Equilib.* **2001**, *179*, 269–276.

(511) Gomis, V.; Ruiz, F.; Boluda, N.; Saquete, M. D. *Fluid Phase Equilib.* **2004**, *215*, 79–83.

(512) Feng, Z.; Li, J. Q.; Sun, X.; Sun, L.; Chen, J. *Fluid Phase Equilib.* **2012**, *317*, 1–8.

(513) Hansén, O.; Rosenholm, J. B. *J. Chem. Soc., Faraday Trans. 1* **1986**, *82*, 77.

(514) http://gestis.itrust.de/nxt/gateway.dll/gestis_de/491033.xml?f=templates$fn=default.htm$3.0.

(515) http://www.enzolifesciences.com/ALX-270-301/sodium-butyrate/.

(516) Li, M.-Y.; Wang, L.-S.; Wang, K.-P.; Jiang, B.; Gmehling, J. *Fluid Phase Equilib.* **2011**, *307*, 104–109.

(517) Gomis, V.; Ruiz, F.; Boluda, N.; Saquete, M. D. *J. Chem. Eng. Data* **2008**, *53*, 2851–2853.

(518) Wachter, W.; Fernandez, S.; Buchner, R.; Hefter, G. *J. Phys. Chem. B* **2007**, *111*, 9010–9017.

(519) Liu, S.; Jia, G.-Z.; Liu, F.-H. *Phys. Chem. Liq.* **2016**, *54*, 155–164.

(520) Buchner, R.; Hölzl, C.; Stauber, J.; Barthel, J. *Phys. Chem. Chem. Phys.* **2002**, *4*, 2169–2179.

(521) Lyashchenko, A. K. *J. Mol. Liq.* **2001**, *91*, 21–31.

(522) Gabra, G. G.; Torma, A. E. *Hydrometallurgy* **1978**, *3*, 23–33.

(523) Matsumoto, K.; Sone, S. *Yakugaku Zasshi* **1957**, *77*, 1151–1152.

(524) Buchner, R.; Capewell, S. G.; Hefter, G.; May, P. M. *J. Phys. Chem. B* **1999**, *103*, 1185–1192.

(525) Schrödle, S.; Rudolph, W. W.; Hefter, G.; Buchner, R. *Geochim. Cosmochim. Acta* **2007**, *71*, 5287–5300.

(526) Plessen, H. von. Sodium Sulfates. *Ullmann's encyclopedia of industrial chemistry*; Wiley: Chichester, 2010; p 28.

(527) Bharmoria, P.; Gehlot, P. S.; Gupta, H.; Kumar, A. *J. Phys. Chem. B* **2014**, *118*, 12734–12742.

(528) Ganguly, P.; Hajari, T.; van der Vegt, N. F. A. *J. Phys. Chem. B* **2014**, *118*, 5331–5339.

(529) Thomas, A. S.; Elcock, A. H. *J. Chem. Theory Comput.* **2011**, *7*, 818–824.

(530) Mason, P. E.; Ansell, S.; Neilson, G. W.; Rempe, S. B. *J. Phys. Chem. B* **2015**, *119*, 2003–2009.

(531) Pethes, I. *J. Mol. Liq.* **2018**, *264*, 179–197.

(532) Petit, L.; Vuilleumier, R.; Maldivi, P.; Adamo, C. *J. Chem. Theory Comput.* **2008**, *4*, 1040–1048.

(533) Marcus, Y.; Hefter, G. *Chem. Rev.* **2006**, *106*, 4585–4621.

(534) Harsányi, I.; Pusztai, L. *J. Chem. Phys.* **2005**, *122*, 124512.

(535) Harsányi, I.; Pusztai, L. *J. Chem. Phys.* **2012**, *137*, 204503.

(536) Copestake, A. P.; Neilson, G. W.; Enderby, J. E. *J. Phys. C: Solid State Phys.* **1985**, *18*, 4211–4216.

(537) Rudolph, W.; Brooker, M. H.; Pye, C. C. *J. Phys. Chem.* **1995**, *99*, 3793–3797.

(538) Tromp, R. H.; Neilson, G. W.; Soper, A. K. *J. Chem. Phys.* **1992**, *96*, 8460–8469.

(539) Wei, Y. ‐ Z.; Sridhar, S. *J. Chem. Phys.* **1990**, *92*, 923–928.

(540) Friesen, S.; Hefter, G.; Buchner, R. *J. Phys. Chem. B* **2019**, *123*, 891–900.

(541) Turton, D. A.; Hunger, J.; Hefter, G.; Buchner, R.; Wynne, K. *J. Chem. Phys.* **2008**, *128*, 161102.

(542) Duboué-Dijon, E.; Mason, P. E.; Fischer, H. E.; Jungwirth, P. *J. Phys. Chem. B* **2018**, *122*, 3296–3306.

(543) Chapman, W. G.; Gubbins, K. E.; Jackson, G.; Radosz, M. *Ind. Eng. Chem. Res.* **1990**, *29*, 1709–1721.

Declaration

Hereby, I declare that I have composed this work on my own and using exclusively the quoted references and resources. Literally or correspondingly adapted material has been marked accordingly.

Erklärung

Hiermit erkläre ich, dass ich die vorliegende Arbeit selbstständig und nur mit den angegebenen Quellen und Hilfsmitteln angefertigt habe. Wörtlich oder sinngemäß übernommenes Gedankengut habe ich als solches kenntlich gemacht.